

**Liquid Crystalline Hexabenzocoronenes as
Organic Molecular Materials –
Synthesis, Characterization and Application**

Dissertation zur Erlangung des Grades
“Doktor der Naturwissenschaften”
am Fachbereich Chemie und Pharmazie
der Johannes Gutenberg-Universität in Mainz

Andreas Fechtenkötter

geb. in Georgsmarienhütte

Mainz 2001

Dekan:

1. Berichterstatter:

2. Berichterstatter:

Tag der mündlichen Prüfung: 18.10.2001

Die vorliegende Arbeit wurde in der Zeit von Mai 1998 bis Mai 2001 am Max-Planck-Institut für Polymerforschung in Mainz unter Anleitung von Herrn Professor Dr. K. Müllen durchgeführt.

Herrn Professor Dr. K. Müllen danke ich für seine wissenschaftliche und persönliche Unterstützung sowie für zahlreiche motivierende Diskussionen.

Contents

1	INTRODUCTION	1
1.1	Molecular Electronic Devices	1
1.2	Discotic Liquid Crystals	2
1.3	Synthesis and Properties of Hexabenzocoronenes	7
1.4	Mesophase Characterization	10
1.5	Solid State NMR Spectroscopy	12
1.6	Charge Carrier Mobility	15
1.7	STM Investigations	17
1.8	Functionalized Hexabenzocoronenes	19
1.9	“Superbenzene” Chemistry	23
2	MOTIVATION AND OBJECTIVE	27
2.1	Motivation	27
2.2	Objective	27
3	NOVEL HBC DERIVATIVES WITH C₆ SYMMETRY	31
3.1	Introduction	31
3.2	Hexaphenyl HBC – A New Material	31
3.2.1	Attempts Towards Direct Functionalization of Hexabromo-hexaphenylbenzene	31
3.2.2	Synthesis of Hexaphenylhexabenzocoronene (HBC-PhC ₁₂)	36
3.2.3	Mesophase Characterization of HBC-PhC ₁₂ : TGA, DSC, and POLMIC Analysis	39
3.2.4	Solid State NMR and X-Ray Investigations	41
3.2.5	Charge carrier mobility	46
3.2.6	HBC-PhC ₁₂ as a semiconductor in high efficiency photovoltaics	52
3.2.7	HBC-PhC ₁₂ as a semiconductor in organic field effect transistors	61
3.3	Chiral and racemic branched-alkyl substituted HBCs – Synthesis and properties	66
3.3.1	Synthesis and preparation of the chiral HBC-C ₈ *	66

Contents

3.3.2	Synthesis and preparation of the racemic HBC-C ₈	69
3.3.3	Mesophase characterization of HBC-C ₈ * and HBC-C ₈ : TGA, DSC, and POLMIC analysis	71
3.3.4	Characterization of the chiral superstructure exhibited by HBC-C ₈ * 48	74
3.4	Combination of branched-alkyl chain substitution and phenyl-ring insertion – Two new HBC derivatives with C₆-symmetry	84
3.4.1	Synthesis and preparation of the chiral HBC-PhC ₈ * 61 and the racemic HBC-PhC ₈ 62	84
3.4.2	Mesophase Characterization of HBC-PhC ₈ * 61 and HBC-PhC ₈ 62: TGA and DSC analysis	88
3.4.3	Circular dichorism studies for HBC-PhC ₈ * 61	89
3.5	HBC-C₁₆: A room temperature liquid crystal with a lowered isotropization temperature	93
3.5.1	Synthesis and preparation of HBC-C ₁₆	93
3.5.2	Mesomorphic properties: DSC and optical microscopy of HBC-C ₁₆ 68	95
3.6	The influence of heteroatoms on liquid crystals	99
3.7	STM investigations of HBCs with C₆ symmetry	105
3.8	¹H-NMR investigation of the aromatic p-stacking of hexabenzocoronene in solution	118
3.8.1	Introduction and previous work	118
3.8.2	Application of self-association models to experimental data	120
3.8.3	Models using nearest neighbors:	121
3.8.4	Models using next nearest neighbors:	122
3.8.5	Results of experimental data and applied models	122
3.8.6	Concentration dependant UV/Vis measurements	129
4	FUNCTIONALIZED HBC DERIVATIVES	133
4.1	Introduction	133
4.2	Towards single columns of HBC	134
4.3	Thiophene substituted HBCs	141
4.3.1	Synthesis and characterization of α-thiophene substituted HBCs	142
4.3.2	Mesophase characterization of thiophene substituted HBC derivatives 83, 84 and 85	147
4.3.3	Synthesis and characterization of β-thiophene substituted HBC	149
4.4	Ultrafast excitation energy transfer in covalently linked donor-acceptor systems	151
4.4.1	Syntheses of novel donor-acceptor systems	152
4.4.2	Absorption properties	157
4.4.3	Fluorescence properties	158
4.4.4	Time resolved fluorescence experiments	159
4.5	Synthesis and characterization of aryl amine substituted HBC derivatives and attempted oxidation towards diimines	161
4.5.1	Synthesis of dodecylaniline substituted HBCs	161

Contents

4.5.2	Attempt to oxidize amino substituted HBC 97 to the quinoid diimine	166
4.5.3	A novel HBC derivative with a triarylamine moiety	170
4.6	HBC as a building block for supramolecular chemistry	173
4.7	Towards hexa anthracene substituted HBC	179
5	SUMMARY	183
6	EXPERIMENTAL SECTION	189
6.1	General Methods	189
6.2	Materials	189
6.3	Syntheses	190
6.3.1	4,4'-Bis(4- <i>n</i> -dodecylphen-1-yl)diphenylacetylene (41)	190
6.3.2	Hexa(4- <i>n</i> -dodecylbiphen-1-yl)benzene (42)	191
6.3.3	Hexa(4- <i>n</i> -dodecylphen-1-yl)hexa- <i>peri</i> -hexabenzocoronene (43)	192
6.3.4	4,4'-Bis((<i>S</i>)-3,7-dimethyloctanyl)diphenylacetylene (46)	193
6.3.5	Hexa-4-((<i>S</i>)-3,7-dimethyloctanyl)hexaphenylbenzene (47)	194
6.3.6	Hexa((<i>S</i>)-3,7-dimethyloctanyl)hexa- <i>peri</i> -hexabenzocoronene (48)	195
6.3.7	4,4'-Bis(3,7-dimethyloctanyl)diphenylacetylene (49):	196
6.3.8	Hexa-4-(3,7-dimethyloctanyl)hexaphenylbenzene (50)	197
6.3.9	Hexa(3,7-dimethyloctanyl)hexa- <i>peri</i> -hexabenzocoronene (51)	198
6.3.10	(<i>S</i>)-1-(3,7-dimethyloctanyl)-4-trimethylsilybenzene (53)	199
6.3.11	1-(3,7-dimethyloctanyl)-4-trimethylsilybenzene (54)	200
6.3.12	(<i>S</i>)-1-(3,7-dimethyloctanyl)-4-iodobenzene (55)	200
6.3.13	1-(3,7-dimethyloctanyl)-4-iodobenzene (56)	201
6.3.14	Bis((<i>S</i>)-4-(3,7-dimethyloctanyl)biphenyl)acetylene (57)	202
6.3.15	Bis(4-(3,7-dimethyloctanyl)biphenyl)acetylene (58)	203
6.3.16	Hexa((<i>S</i>)-4-(3,7-dimethyloctanyl)biphenyl)benzene (59)	204
6.3.17	Hexa(4-(3,7-dimethyloctanyl)biphenyl)benzene (60)	205
6.3.18	Hexa((<i>S</i>)-4-(3,7-dimethyloctanyl)phenyl)hexa- <i>peri</i> -hexabenzocoronene (61)	206
6.3.19	Hexa(4-(3,7-dimethyloctanyl)phenyl)hexa- <i>peri</i> -hexabenzocoronene (62)	207
6.3.20	4,4'-Bis(3,7,11,15-tetramethylhexadecenyl)diphenylacetylene (66)	208
6.3.21	Hexa(4-(3,7,11,15-tetramethylhexadecenyl)phen-1-yl)benzene (67)	209
6.3.22	Hexa-(3,7,11,15-tetramethylhexadecanyl)hexa- <i>peri</i> -hexabenzocoronene (68)	210
6.3.23	4,4'-Bis(4- <i>n</i> -dodecyloxyphen-1-yl)diphenylacetylene (74)	211
6.3.24	Hexa(4- <i>n</i> -dodecyloxybiphenyl)benzene (75)	212
6.3.25	2,11-Di-(hex-5-enyl)-5,8,14,17-tetradodecyl-hexa- <i>peri</i> -hexabenzocoronene (80)	213
6.3.26	2-(Thien-2-yl)-5,8,14,11,17-pentadodecyl-hexa- <i>peri</i> -hexabenzocoronene (83)	214
6.3.27	2,11-Di-(thien-2-yl)-5,8,14,17-tetradodecyl-hexa- <i>peri</i> -hexabenzocoronene (84)	215
6.3.28	2-Di-(5-dodecyl-thien-2-yl)-5,8,14,17-tetradodecyl-hexa- <i>peri</i> -hexabenzocoronene (85)	217

Contents

6.3.29	2,11-Di-(thien-3-yl)-5,8,14,17-tetradodecyl-hexa- <i>peri</i> -hexabenzocoronene (86)	218
6.3.30	2,11-Di[<i>N</i> -(2,6-diisopropylphenyl)-perylene-9-yl-3,4-dicarboxiimide]-5,8,14,17-tetradodecyl-hexa- <i>peri</i> -hexabenzocoronene (88)	219
6.3.31	2-((4-Dodecylphenyl)amino)-5,8,11,14,17-pentadodecyl-hexa- <i>peri</i> -hexabenzocoronene (96)	220
6.3.32	2,11-Di-((4-dodecylphenyl)amino)-5,8,14,17-tetradodecyl-hexa- <i>peri</i> -hexabenzocoronene (97)	222
6.3.33	2,11-Di-(diphenylamino)-5,8,14,17-tetradodecyl-hexa- <i>peri</i> -hexabenzocoronene (99)	223
6.3.34	2,11-Di-[<i>trans</i> -Pd(PPh ₃) ₂ -Br]-5,8,14,17-tetradodecyl-hexa- <i>peri</i> -hexabenzocoronene (102)	224
6.3.35	9-(3,7-Dimethyloctanyl)anthracene (104)	225
6.3.36	9-Bromo-10-(3,7-dimethyloctanyl)anthracene (105)	226
6.3.37	4,4'-Bis(10-(3,7-dimethyloctanyl)anthracen-9-yl)diphenylacetylene (107)	227
6.3.38	Hexakis(4-(10-(3,7-dimethyloctanyl)anthracen-9-yl)phen-1-yl)benzene (108)	228

7 LITERATURE

231

1 Introduction

1.1 Molecular Electronic Devices

The development of materials and devices such as tools or machines has been one of the most important driving forces for humanity and mankind. The development process, from the actual invention to the real application, often took centuries. In 1839, the French experimental physicist Edmund Becquerel, discovered the photovoltaic effect while experimenting with an electrolytic cell made up of two metal electrodes placed in an electrically conducting solution; the current increased when exposed to light.^[1] In 1905, Albert Einstein speculated that light could penetrate atoms. The collision of photons and atoms could force atoms to leave their orbit. This would allow for the creation of an electric current. Nevertheless, it was not until 1954 when the first solar cell was developed in the USA by scientists at Bell Labs.^[2]

It was the development of smaller and smaller growing integrated circuits that, *e.g.*, made it possible to build faster and more compact computers. Shockley, Brattain, and Bardeen were awarded the Nobel Prize in 1956 for their research on Field Effect Transistors (FETs).^[3-5] Many of today's leading scientists agree that the invention of the transistor is probably one of the most important achievements of the 20th century. The raw material that is most often used for building these devices, *i.e.*, photovoltaic cells and Field Effect Transistor, is silicon. Silicon is the second most abundant element on earth (after oxygen) but does not occur in its pure state in nature. Therefore, extensive efforts have to be made in order to obtain the material in its crystalline form.

Within the last two decades, research interest has focused more and more on devices built from polymers or other organic materials. Around 1980, Cohen and co-workers reported the first solar cell using conducting polymers^[6-8] and it was in 1989 that two groups reported the utilization of polymers in FETs^[9, 10]. In addition, organic materials have found a number of other potential applications such as sensors, batteries, switching devices, and optical data storage. Unlike inorganic materials that consist of covalent or ionic lattices in three dimensions,

organic materials are based on individual molecules which are linked together via weak intermolecular forces such as van der Waals hydrogen bonds, or π - π interactions. Alternately, mesophase (self-assembling) molecules show great promise since they are easier to process, and self-healing. It is because of these self-assembling forces that organic materials have led to so much research interest in the past. Due to the nature of these forces, the design of the material can be made on the level of the individual molecule. Therefore, the amount of synthetic work is considerably lower than in the case of inorganic materials such as crystalline silicon. When organic materials are used in electronic or optoelectronic devices, they are usually in the form of thin films, due to which mesophase forming liquid crystals are being intensively studied.

1.2 Discotic Liquid Crystals

Mesophases (liquid crystals and plastic crystals) represent states of order between crystals and liquids. They have imperfect long range orders of orientation and/or position. Thus, they can be fluid like a liquid and also have anisotropic properties like crystals. Whereas plastic crystals have a predominant positional order, liquid crystals have a predominant orientational order (Figure 1).

The main reasons for the formation of liquid crystalline phases are:

- a simple geometrical form of the molecule: rods, discs or balls, which allow a closer packing in a mesophase,
- an intramolecular contrast, which causes microseparation of different parts of the molecules

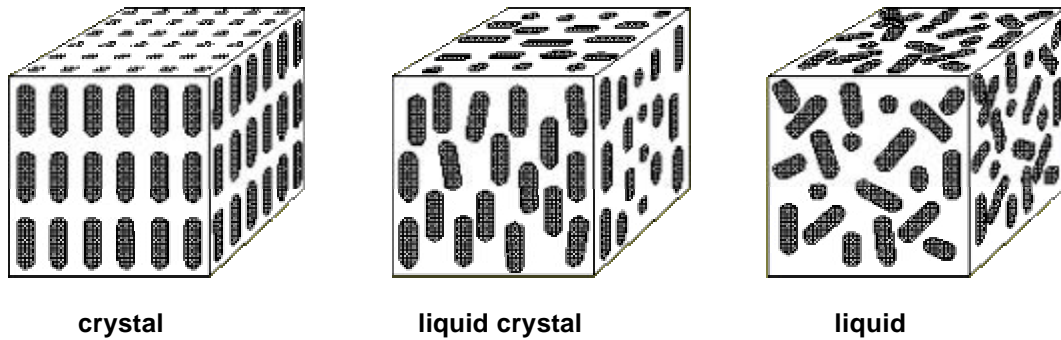


Figure 1: **Illustration of crystal-, liquid crystal-, and liquid-phase**

On the basis of their appearance, liquid crystals are divided into two different classes: calamitic mesogens, which are rod-like molecules, and discotic mesogens, characterized by a disc-like core of the molecule. Since Reinitzer^[11] discovered the state of liquid crystallinity in 1888, immense efforts in research and development have pushed this field to where it now stands. With the discovery of liquid crystals from disc shaped molecules, or discotic liquid crystals, in 1977 by Chandrasekhar^[12], a demanding and challenging door was opened for many of today's research groups.^[13]

The mesophases exhibited by these disk-like structures can be classified into three distinct types (Figure 2): columnar (col), discotic-nematic (N_d), and discotic-lamellar, where the structure of the latter has not yet been completely elucidated.^[13]

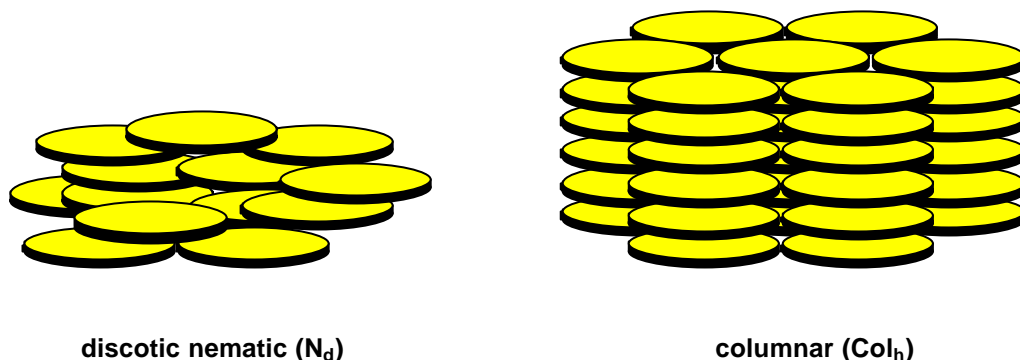


Figure 2: **Illustration of the two different mesophases of discotic liquid crystals**

The columnar phase consists of discs stacked one on top of the other to form columns, the different columns constituting a two-dimensional lattice. Several variations of the columnar structure have been identified (Figure 3): i.e. columns with a hexagonal lattice (Col_h), rectangular lattice (Col_r), and an oblique lattice (Col_{ob}), , etc.

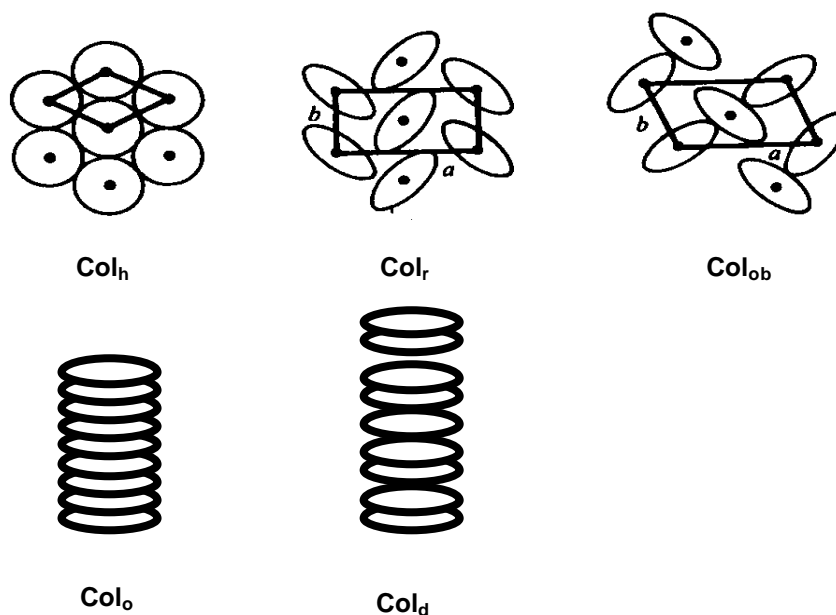


Figure 3: **Structures of columnar mesophases**

Additionally, the suffix “o” (for ordered) and “d” (for disordered) can indicate the degree of established organization in the system as depicted in Figure 3, bottom.

Apart from a few exceptions, these discotic mesogens have a flat or nearly flat core which is surrounded by four, six, or eight alkyl chains. In Figure 4 some of the most prominent discotic liquid crystals are displayed. These range from the first reported discotic liquid crystal namely the hexakis-alkanoyloxy-benzenes **1**, to phthalocyanines **2**^[14, 15], perylenes **3**^[16-18], triphenylenes **4**^[19-23], dibenzopyrenes **5**^[21, 24, 25], and hexabenzocoronenes **6**^[26-37] (henceforth referred to as HBC), with the most extended aromatic core of the above. The latter four belong to the class of large polyaromatic hydrocarbons (PAHs).^[38]

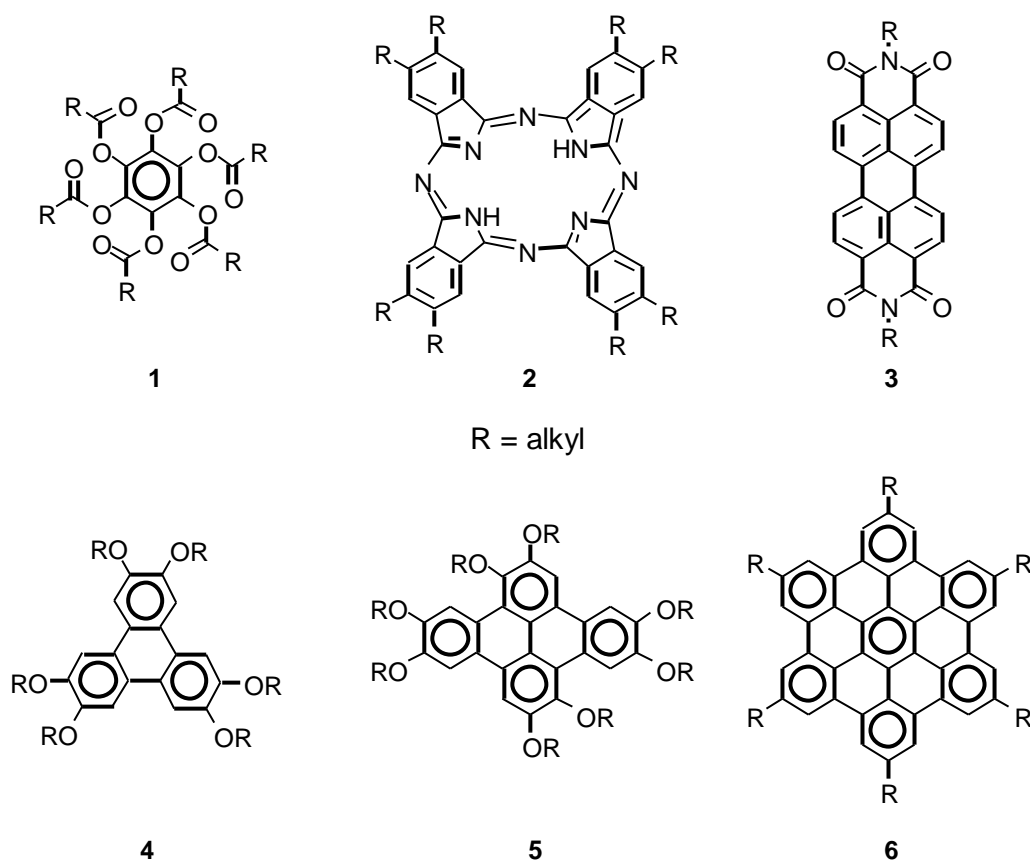


Figure 4: **Variety of some of the most prominent discotic liquid crystals**

Perylene is a well known chromophore which displays high extinction coefficients and nearly quantitative fluorescence quantum yields with outstanding photochemical and thermal stability.^[17, 18] However, it suffers from its low processability. This was overcome with the introduction of solubilizing side groups, also yielding perylene derivatives that exhibit discotic liquid crystallinity over temperature ranges of up to 200 °C.^[17] These materials combine several target properties: a) stable mesophases over large temperature ranges, b) high thermal and photochemical stability, and c) intense absorption at long wavelengths.^[17]

Among the above-mentioned liquid-crystalline PAHs, triphenylenes are the ones that have been studied most extensively in view of their mechanism of charge transport^[39-41], one-dimensional energy transport^[42, 43], photoconductivity^[44-49], ordering of multilayers (investigated by using Langmuir-Blodgett techniques)^[50],

orientation of two-dimensional crystals^[51, 52] (investigated using scanning tunneling microscopy (STM)) and their alignment under the influence of a magnetic field^[53]. Further, liquid crystalline polymers with triphenylenes both in the main and in the side chain have been prepared and analyzed.^[21, 54-57]

Photophysical properties of several different alkoxy substituted dibenzopyrene derivatives have been determined to study the phase transitions with the help of absorption and fluorescence spectroscopy.^[25] Two switchable ferroelectric phases of a columnar dibenzopyrene derivative have been reported by Bock *et al.*^[24] Here, the co-existence of different columnar phases depends on the strength of an applied electric field, thus opening possible applications for electro-optical displays. From the examples given above, it can be seen that by varying the size and geometry of the aromatic core of discotic liquid crystals, the properties change dramatically. Increasing the size of the core results in enhanced π - π overlap, thus giving rise to larger phase widths and more stable mesophases. Vast differences in the mesoscopic properties are also seen by changing the periphery, e.g. a hexahexylthiotriphenylene^[45] exhibits a helical columnar phase and was the previous record holder for charge carrier mobilities of organic materials other than in single crystals.^[45] Simmerer *et al.* showed that by changing the substituents on the perimeter of the triphenylene disc from pentyloxy to butyloxy, one does not only proceed from a columnar hexagonal packing to the formation of a so-called plastic discotic phase, but one also increases the mobilities by an order of magnitude.^[46] Two different alignments in a magnetic field were observed when the triphenylene core was substituted with six 4-*n*-octyloxybenzoate groups.^[53] And finally, Langmuir-Blodgett films of an asymmetrically substituted triphenylene derivative carrying hydrophobic and hydrophilic side chains were obtained and investigated.^[50]

This ample variety of functions, properties and applications also provided impetus for the development of new and improved syntheses of triphenylenes. Since Bachmann synthesized the first triphenylene^[58] and Destrade *et al.* the first liquid crystalline derivative^[59] in 1979, numerous improvements in the synthesis and processing of triphenylenes have been reported.

Initially, hexaalkyloxy triphenylenes with groups larger than methyl had to be prepared by a three-step route comprised of oxidative trimerization of veratrole

with chloranil, demethylation of the hexamethoxy triphenylene, and then alkylation of the resulting hexahydroxy compound. It was later shown that various hexaalkoxy derivatives could be prepared directly from dialkoxy benzenes using suspended FeCl_3 as oxidizing agent, followed by reductive workup with methanol.^[60] Recently, Kumar and co-workers reported that VOCl_3 performs the same oxidation in high yield in very short reaction times (10 minutes), which was attributed to the high solubility of the oxidizing agent.^[61] Further, unsymmetrically substituted triphenylenes were desired and a number of routes have been developed for the synthesis of these.^[14]

1.3 Synthesis and Properties of Hexabenzocoronenes

The very promising properties of alkyl-substituted hexabenzocoronenes (HBCs) **6a-d** (Figure 5) prompted the group of Professor Müllen to begin systematic investigations of various functionalized derivatives. Hexabenzocoronenes belong to the class of polycyclic aromatic hydrocarbons that possess an all-benzenoid configuration of fused benzene rings.^[38] This is in itself quite unique considering the fact that from the total of roughly 20.600 possible alternating hydrocarbons having between 4 and 10 fused benzene rings, only 17 are all-benzenoid.^[38, 62] The „benzene-like behavior“ can adequately be described in terms of Clar’s model of the aromatic sextet.^[63] In this qualitative, although highly successful concept, the π -electrons are assigned to specific six-membered rings in such a way that the largest possible number of π -electron sextets is formed. If, according to the Clar formula, all π -electrons are distributable in closed sextets, the number of carbon atoms necessary is an integral multiple of six.

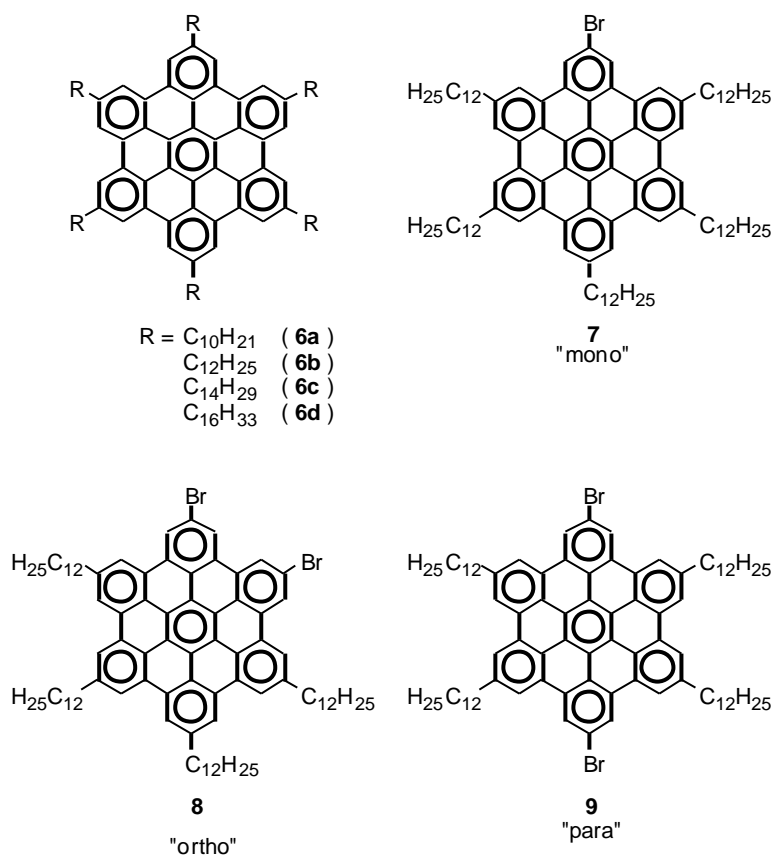
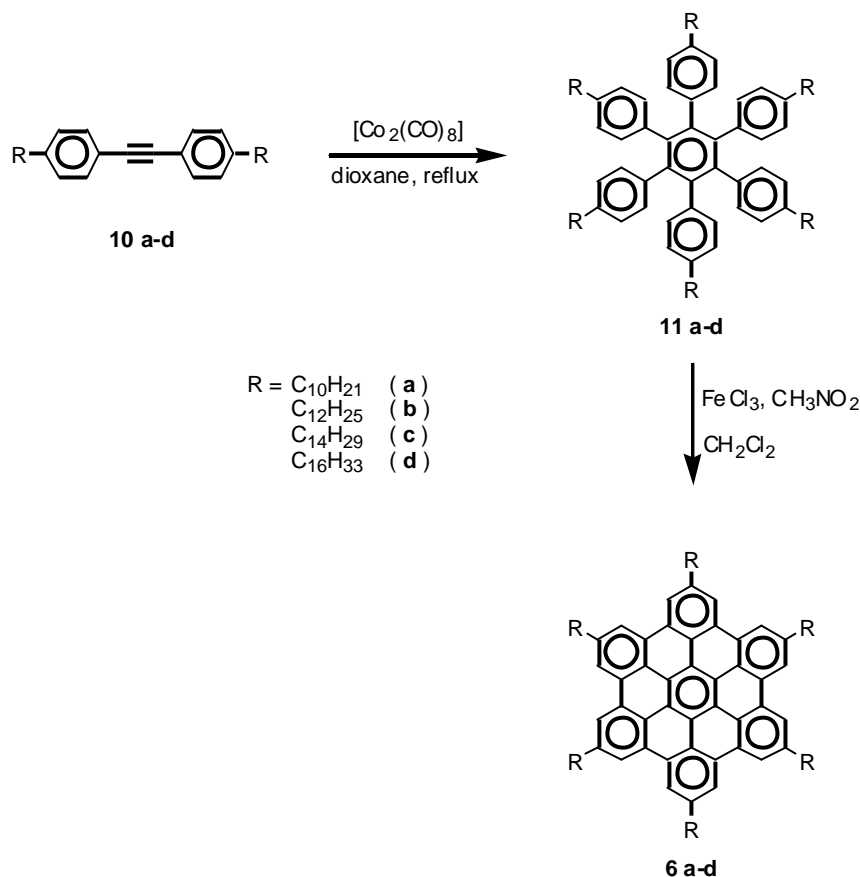


Figure 5: **Alkyl substituted and bromo functionalized HBCs**

Alkyl-substituted hexabenzocoronenes **6a-6d** and their functionalized derivatives **7-9** (Figure 5) are discotic liquid crystalline materials with one of the largest PAH cores (approximately three times the size of triphenylene).^[26-37] This class of mesogen is being well recognized for its extremely large phase widths (up to 250 °C)^[27] and its record charge carrier mobilities along the columnar axis ($1.13 \text{ cm}^2\text{V}^{-1}\text{s}^{-1}$)^[30, 35].

It was Herwig who reported the first synthesis of an alkyl substituted HBC (**6b**) in 1995.^[26] Scheme 1 depicts the reaction sequence that was designed to synthesize the first soluble HBC, since hexabenzocoronene^[64-67] without any alkyl substitution (**6**: $R = \text{H}$) is completely insoluble in any common organic solvent. The alkyl substituted diphenylacetylene **10b** was synthesized in a four step procedure from commercially available 4-dodecylaniline. In a cobalt octacarbonyl catalyzed cyclotrimerization 4,4'-didodecyldiphenylacetylene (**10b**)

was transformed to hexaphenylbenzene **11b**. Hexa(4-dodecylphen-1-yl)benzene is very soluble in many organic solvents and could be obtained analytically pure after column chromatography, on multigram scale. The next step in the reaction cycle is the cyclodehydrogenation, which is the most crucial step for the synthesis of hexabenzocoronenes. Clar and co-workers reported the synthesis of unsubstituted HBC (**6**: R = H) via the evolution of hydrogen from the precursor at temperatures of 482 °C.^[66] Naturally, this procedure was not applicable to the alkylated precursor **11**. It was Kovacic^[68] who reported the utilization of a Lewis-acid (aluminum(III)trichloride) and an oxidant (copper(II)chloride) for the improved oxidative polymerization of benzene to yield poly(*para*-phenylene) with molecular weights between 900 and 1000.^[69-71] Herwig modified these conditions slightly by replacing the copper(II)chloride with copper(II)trifluoromethanesulfonate and this system afforded the alkyl substituted hexabenzocoronenes **6a-6d** in moderate yields (ca. 50%).^[26, 27] Brand altered these cyclodehydrogenation conditions slightly, and was able to achieve higher yields and a wider tolerance of other functionalities other than simple alkyl chains.^[34, 72] Here, iron(III)chloride dissolved in nitromethane was used as the Lewis-acid and the oxidant. A detailed history and description of the development of the above dehydrogenation methods was discussed by Dötz in 2000.^[73]

Scheme 1: **Synthesis of alkyl substituted hexabenzocoronenes**

1.4 Mesophase Characterization

All alkyl substituted HBC derivatives **6a-d** exhibit liquid crystalline mesophases. This has been demonstrated by means of polarized optical microscopy studies (polmic), differential scanning calorimetry (DSC), and X-Ray studies. Temperature gravimetric analysis (TGA) analysis revealed that the compounds are stable up to temperatures of 300 °C, at which point decomposition of the molecules starts. Decomposition is characterized by two steps in the TGA curve. At first the alkyl chains are cleaved at temperatures between 300 and 490 °C. After that, the unsubstituted HBC disc (**6**: R = H), which is stable at temperatures up to 700 °C, sublimates between 500 and 600 °C.^[72, 74] Figure 6 shows a DSC heating and cooling cycle that is typical for the alkyl substituted HBCs.

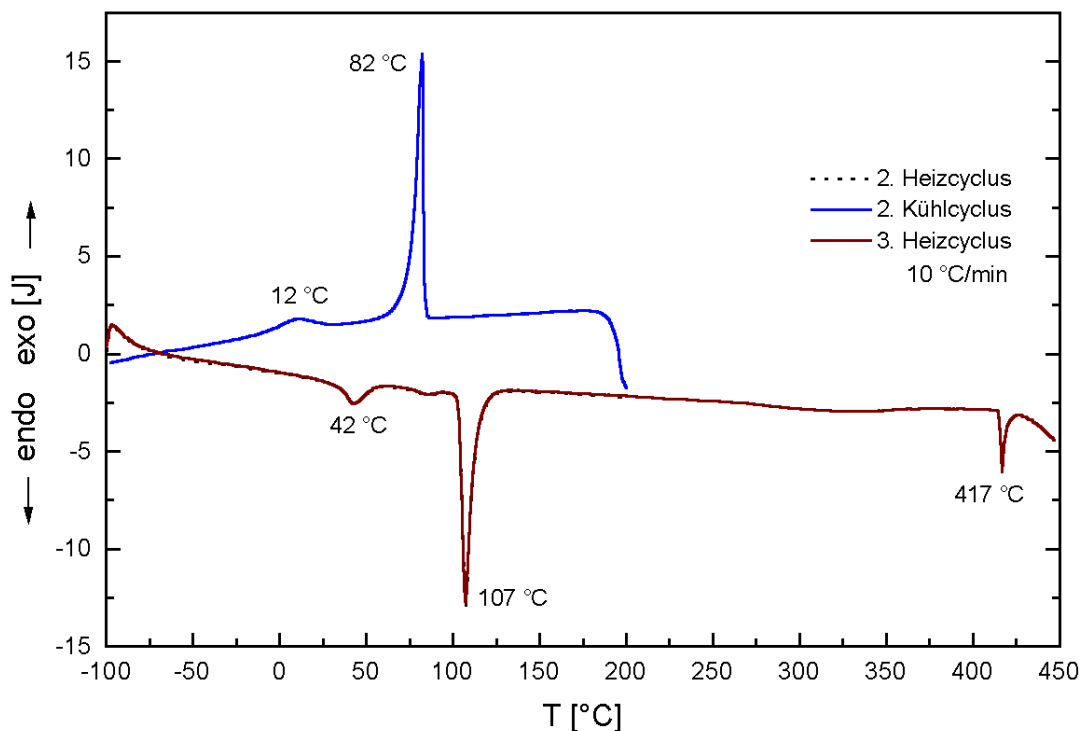


Figure 6: **DSC heating and cooling cycle of HBC-C₁₂ (@ 10 °C / min)**

The peaks can be assigned as follows: upon heating to 42 °C, a crystalline to crystalline transition takes place ($K_1 \rightarrow K_2$), This is attributed to a change in conformation of the mobile alkyl chains. Then, the transition into the mesophase at 107 °C ($K_2 \rightarrow D_h$) is characterized by the melting of the alkyl chains and the onset of uni-axial rotation of the aromatic cores. A detailed investigation of this phenomenon utilizing solid-state NMR technique will be discussed later. At 417 °C the isotropization temperature is reached and the compound enters the liquid state. These DSC results point out that HBC-C₁₂ (**6b**) has a remarkable phase width of 310 °C, which is among the largest ever reported for columnar discotics.^[27, 75-77] The combination of TGA and DSC results unfortunately demonstrate that an annealing process, which is sometimes very important for optimum film formation when an application in devices is desired, can not be accomplished. This is because annealing at the isotropization temperature of 417 °C is well above the beginning of the decomposition process at around 300 °C. From polarization microscopy, a fan-like texture, characteristic for columnar discotic mesophases was observed.^[27] X-Ray analysis executed in the liquid

crystalline mesophase of the material disclosed the real nature of the structure. Figure 7 shows an example of a X-Ray diffractogram recorded at 150 °C with Cu-K α radiation.

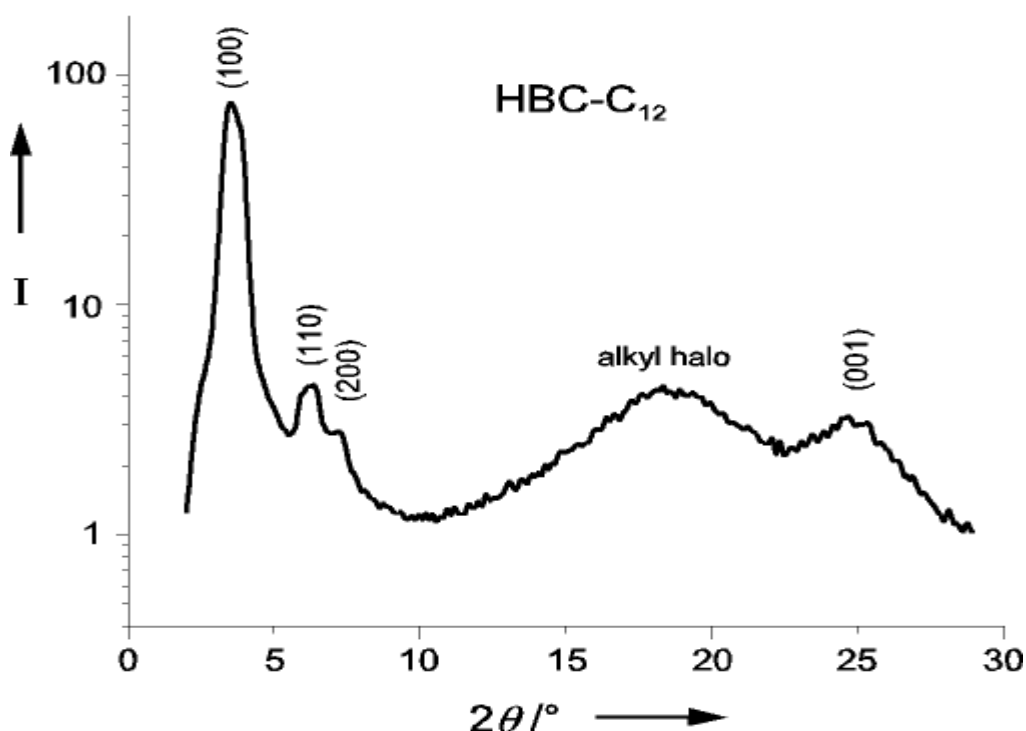


Figure 7: *X-Ray diffractogram of HBC-C₁₂ in the mesophase*

The most prominent reflections are marked and confirm that the assumed discotic columnar structure is present and that the superstructure has a hexagonal lattice.^[27] Their reciprocal spacing follow the ratio $1:\sqrt{3}:\sqrt{4}:\sqrt{7}:\sqrt{9}$. The intercolumnar distance determined from the (100) reflection is 25.2 Å whereas the (001) reflection resolves the intracolumnar (face-to-face) distance to be 3.55 Å. The hexagonal superstructure finds support in the presence of the (110) reflection.

1.5 Solid State NMR Spectroscopy

As mentioned above, solid-state NMR spectroscopy is a powerful tool for the investigation of aromatic packing behaviors and dynamical processes in liquid crystals.^[34, 78-81] Using these techniques, the bulk properties and the solid state

characteristics of a material can be studied. In the case of the alkyl substituted HBC derivative **6b**, a structural isomer in which the α -CH₂ protons were replaced by deuterium (**6b** _{α -d₁₂}), was synthesized for these studies.^[27, 34] Extreme high-field shifts of $\delta = 5.6$ ppm, have been recorded^[34] for the aromatic protons in the solid state phase indicative of the pronounced intermolecular deshielding interaction present in the bulk. Fast magic-angle spinning (MAS) and double-quantum ¹H solid-state NMR spectroscopy have been used to further investigate the π - π packing in the columnar structures formed by hexabenzocoronenes and triphenylenes.^[81] In the crystalline phase of the former **6b** _{α -d₁₂}, three distinct aromatic signals (Figure 8 (I)) are found in the single-quantum MAS spectrum, in spite of the hexagonal molecular symmetry.^[34]

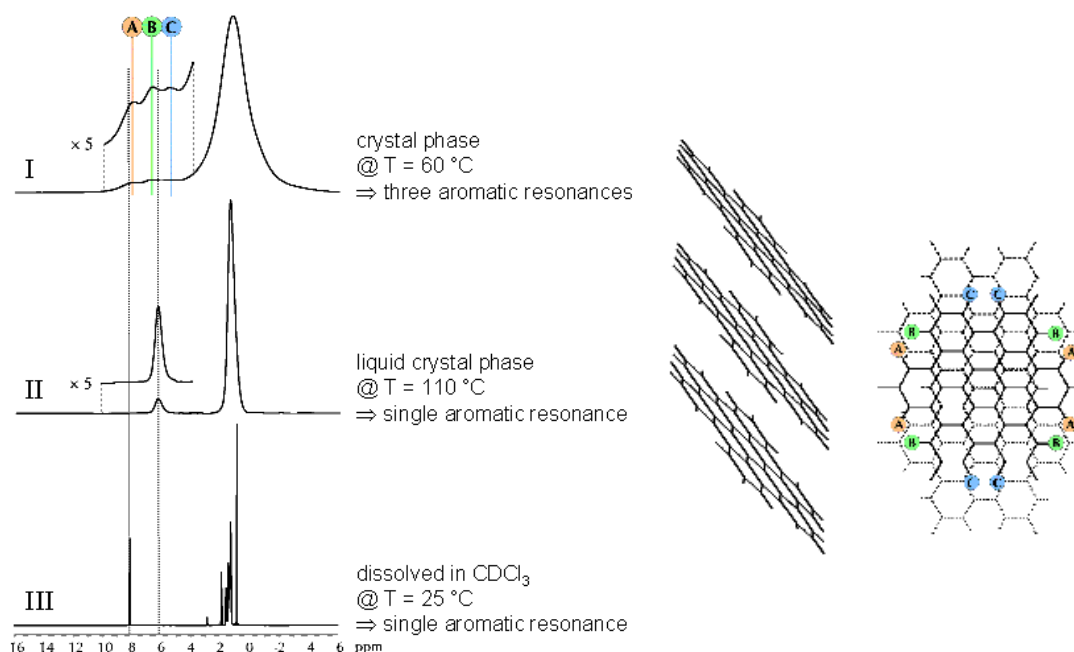


Figure 8: **Solid state NMR spectra of HBC at different temperatures and herringbone-type arrangement in the crystal phase**

These three distinguishable peaks are explained in terms of different ring current influences of adjacent layers which the aromatic core protons experience since they are stacked in a columnar-rectangular herringbone-type fashion as demonstrated in Figure 8. These observations are in agreement with the crystal structures obtained from substituted^[31, 81] and unsubstituted^[82] HBCs.

However, upon increasing the temperature, so that the liquid crystalline phase is entered, the three aromatic signals merge into a single resonance (Figure 8 (II)). This can be attributed to the transformation into the columnar hexagonal mesophase and fast axial motion of the HBC discs around the columnar axis.

Quantum chemical *ab initio* calculations conducted are in agreement with the solution and solid-state experimental data presented above.^[83, 84] The theoretical proton resonance frequency of an isolated HBC **6** (R = H) disc was calculated to be $\delta = 9.3$ ppm. Computation of a trimeric aggregate system also revealed three different high field ¹H-NMR signals for the aromatic core as has been experimentally found with solid-state NMR techniques.^[34, 83, 84]

In addition to the data concerning the behavior of aromatic packing and dynamical processes, solid-state NMR can reveal information about the degree of order that is present in the hexagonally arranged columns formed by these discotic materials. The order parameter S, which is defined by Equation 1.0, determines how perfect the columns that are formed in the mesophase are organized.

$$S = \frac{\Delta n_{LC}}{\frac{1}{2} \Delta n_{solid}} \quad (1.0)$$

ν = NMR frequency in kHz

With $S = 1$ a perfectly ordered column would be defined and $S = 0$ would circumscribe a totally random arrangement of discs. For example, the glass-forming (2S,3S)-2-chloro-3-methylpentanoyloxypentakis(pentoxy) triphenylene has an order parameter of $S = 0.95$, close to the maximum for a perfectly ordered column.^[75] In the case of the alkyl substituted HBC-C₁₂ **6b**, S was determined to be 0.84 which is substantially lower than the one reported for discotic phaseforming triphenylenes.^[27, 75] Herwig and co-workers^[27] attribute this to the fact that the area of the core of hexabenzocoronene is approximately three times the size of triphenylene and therefore the overlap of the aromatic core can be very well sustained even without “perfect” π - π overlap, thus still exhibiting the extremely large phase widths reported above. However, it would

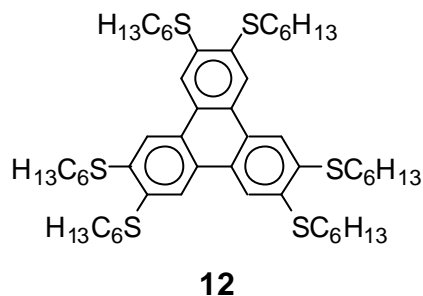
be desirable to improve the order in the columns, since charge carrier mobility strongly depends on order and orientation of the columns.^[85]

1.6 Charge Carrier Mobility

It is obvious that organic materials which exhibit a high intramolecular charge carrier mobility are particularly suitable for the implementation in devices such as Field Effect Transistors (FETs) or photovoltaic cells. However, it is not only the value of the charge carrier mobility that is the decisive factor but also the availability, stability, and most importantly, processability for the decision: Ordinary compound or material?^[19, 47, 86, 87] Since, discotic liquid crystals such as triphenylenes and phthalocyanines meet most or all of the above criteria they have been studied for their application in devices ever since they have been synthesized.^[87, 88]

In considering the bulk electrical properties of discotics, one must consider the possibility of the molecules acting as nanowires where transport processes occur strictly intermolecularly through the overlapping π -systems as opposed to the situation of conducting polymers.^[88] These channels of π -systems are coaxially insulated by the substituents attached to the periphery of the aromatic core, thus the designation of nanowires. Transport processes in discotic liquid crystals have been studied extensively in recent years.^[19, 39-41, 47, 88] A recent paper summarizes some the important concepts of this situation including considerations of band gaps of such ensembles and charge injection.^[88] Mechanisms for charge transport in a triphenylene dimer^[41] have been proposed after combining Pulse Radiolysis Time Resolved Microwave Conductivity (PR-TRMC) measurements and Time of Flight (TOF) experimental techniques, as well as simulations.^[39, 41] PR-TRMC utilizes a rapidly oscillating electric field to probe charge carrier motion without the need for electrodes, which are required in the case of TOF measurements. In 1994, Adam and co-workers reported the highest charge carrier mobility ($\mu = 0.1 \text{ cm}^2/\text{Vs}$) in the helical columnar phase formed by 2,3,6,7,10,11-hexahexylthiotriphenylene (**12**), which at that time was higher than for any organic material other than single

crystal phases.^[45] Since then, many publications investigating the behavior of this material have appeared.^[39, 40, 46]



It was A. van de Craats who reported the new record charge carrier mobility for organic phase forming materials in excess of ($\mu = 1 \text{ cm}^2/\text{Vs}$) in an alkyl substituted hexabenzocoronene derivative^[30, 35], Figure 9 depicts the temperature dependant one-dimensional charge carrier mobility reported for HBC-C₁₂ **6b**.

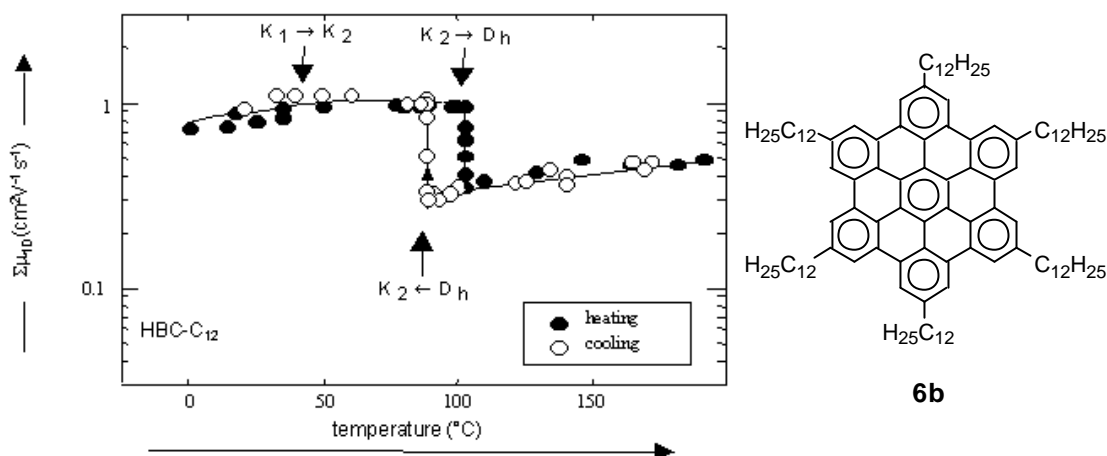


Figure 9: **Temperature dependant charge carrier mobility of HBC-C₁₂ 6b**

Upon heating, μ_{K1} remains almost constant at $0.96 \text{ cm}^2/\text{Vs}$ up to approximately $105 \text{ }^\circ\text{C}$, where an abrupt decrease in charge carrier mobility down to $0.38 \text{ cm}^2/\text{Vs}$ occurs within a few degrees Celsius. After this, no further change in μ_{Dh} is observed up to the maximum temperature of $200 \text{ }^\circ\text{C}$ attainable in the PR-TRMC measurements. Upon cooling, the same behavior is detected with a slight hysteresis.^[30, 35] The drastic changes in the mobility occur at temperatures

at which the HBC-C₁₂ **6b** transforms from the crystalline phase into the columnar hexagonal mesophase. In the case of substituted HBCs, both crystal structures and solid state NMR measurements indicate that in the crystalline form the disks are stacked with an overlap much like that in graphite giving optimum π - π overlap. The drop in charge carrier mobility upon entering the mesophase, associated with increase in mobility and onset of uniaxial rotation, is therefore attributed to a decrease in order. A similar temperature dependant behavior was reported for the charge carrier mobility of mesomorphic triphenylenes^{[40] [41]} and also for phase forming phthalocyanines^[89, 90]. Mobilities in the crystalline phases of some triphenylenes are more sensitive to temperature changes, which is attributed to the smaller π - π overlap creating greater susceptibility of the stacks to perturbation by the side chains.

1.7 STM Investigations

Columns built from hexabenzocoronenes with a face-to-face arrangement have been described as typical supramolecular patterns of these benzene-based macromolecules.^[27, 28, 34] Such ordered arrays of molecules are important for understanding many electrical and electrooptical properties. Further, they document the need for a more general view upon electronic structures which includes both intra- and intermolecular π - π -interaction. When dealing with supramolecular architectures an immediate question concerns the persistence length of the prevailing motif and the spatial extension of the particular patterns. Such a view establishes a structural hierarchy which includes the initial formation of aggregates of a few molecules and proceeds to increasingly complex structures. The logical starting point of such considerations is the visualization of single molecules in real space. Scanning probe techniques, e.g. scanning tunneling microscopy^[23, 26, 28, 29, 91-95] and atomic force microscopy^[91], are now available which allow such visualization in real space. In many instances such experiments require the immobilization of the single molecules in a matrix or at a surface for which the above principles of self-organization are important.

Substituted and unsubstituted PAHs can be made to self assemble in 2 and 3 dimensions as a result of intermolecular interactions and interactions with surfaces or templates (Figure 10). Self-assembled monolayers may be deposited on a variety of surfaces to yield, in essence, 2-dimensional crystals.^[26, 28, 52, 93, 96] The electron-rich cores are particularly amenable to visualization by scanning tunneling microscopy (STM), giving bright spots which provide a clear map of the 2D lattice.^[52] The findings of these endeavors include characterization of the molecule and insight into packing behavior.

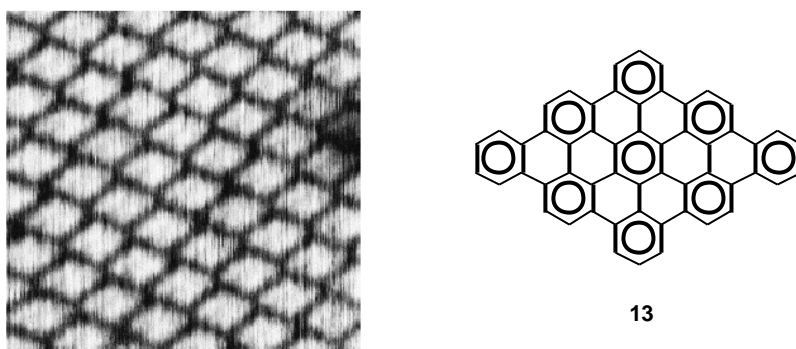


Figure 10: **STM image of 13**

The high thermal stability of large unsubstituted PAHs such as route shaped compound **13**^[96, 97] permits fractional sublimation at 550-650 °C under ultrahigh vacuum conditions. The self-organization of the sublimed molecules leads to epitaxial growth of monomolecular adsorption layers on substrates such as molybdenum sulfide and HOPG as depicted in Figure 10. Using desorption spectroscopy it was even possible to determine the binding energy of the molecule to the surface.^[96, 97]

HBC **6** (R = H) forms a hexagonal lattice, indicated by earlier low-energy electron diffraction (LEED) measurements and later confirmed by STM.^[95, 98] The coincidence of substrate and adsorbate symmetries is crucial for the ordering, i.e. for the formation of 2D crystals. Additionally, the HBC **6** (R = H) molecule, which itself resembles a graphite segment, is oriented along the HOPG lattice in the same way as a (second) imposed graphite layer.^[95] This concludes that the substrate rules the orientation of the molecules. Ordered

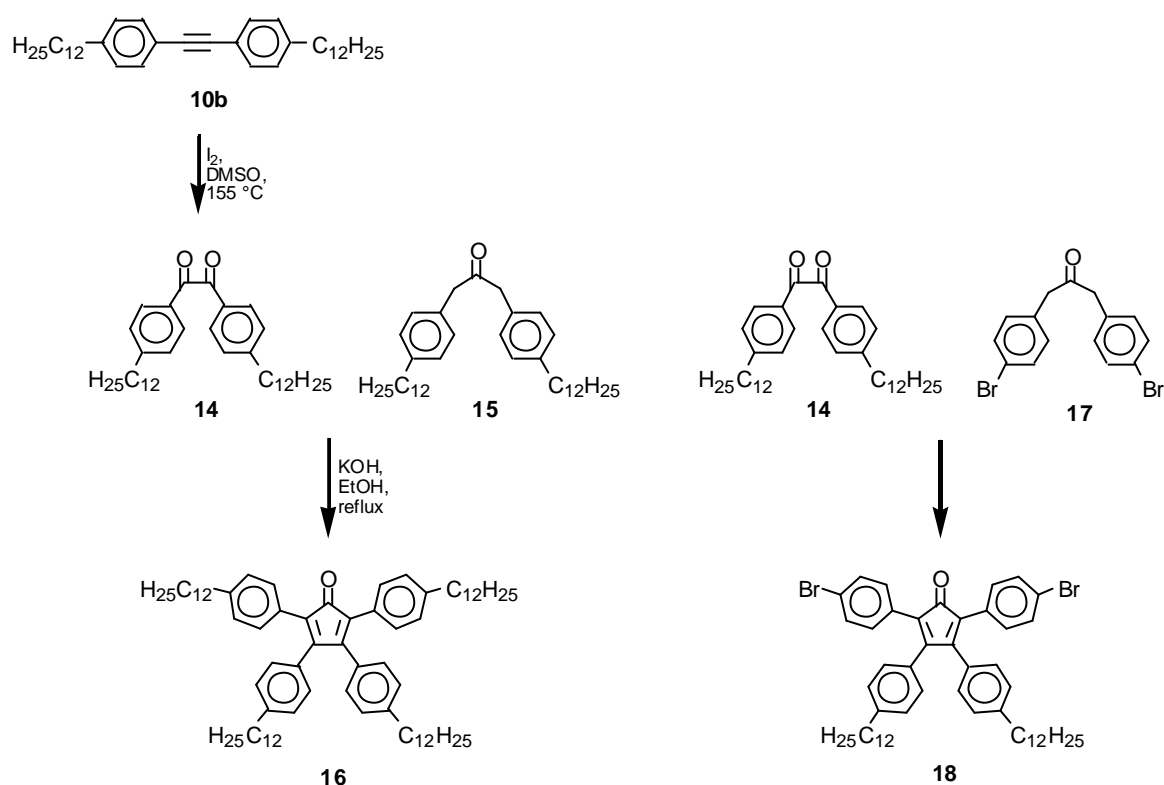
monolayers of HBC could also be used as a ground floor for deposition of a second layer of a perylenetetracarboxylic dianhydride.^[95] This resulted in true organic-organic heterostructures with interfaces flat on a molecular level, presenting the first example of ordered growth of layers (from two different planar molecules) in a heteroepitaxially stacked film.^[95]

When the HBCs are substituted with flexible alkyl chains they can be deposited on the surface by physisorption from solution.^[26-28] STM images obtained at the solid-liquid interface exhibit lower resolution due to a constant equilibration between adsorbate molecules and molecules in solution as well as conformational mobilities faster than the STM scanning rate. Visualization by STM offers support to conclusions which might be drawn from 3D measurements (X-Ray) such as interdigitation of side chains, interaction of heteroatoms, hydrogen bonding, etc.^[92] Regularly ordered monolayers are formed, where the flexible alkyl chains fill the space between the aromatic cores. In the case of HBC-C₁₂ **6b**, two co-existing packing patterns were observed; one rhombic lattice and one where dimers orient in parallel rows.^[26, 28] In all STM images presented here, the areas of higher tunneling current (bright spots in the STM) correspond to the aromatic part of the molecule, whereas the areas of lower current (dark spots) are attributed to the alkyl side chains. Higher resolution for the aliphatic side chains could not be achieved due to their fast dynamics at the solid liquid interface.

1.8 Functionalized Hexabenzocoronenes

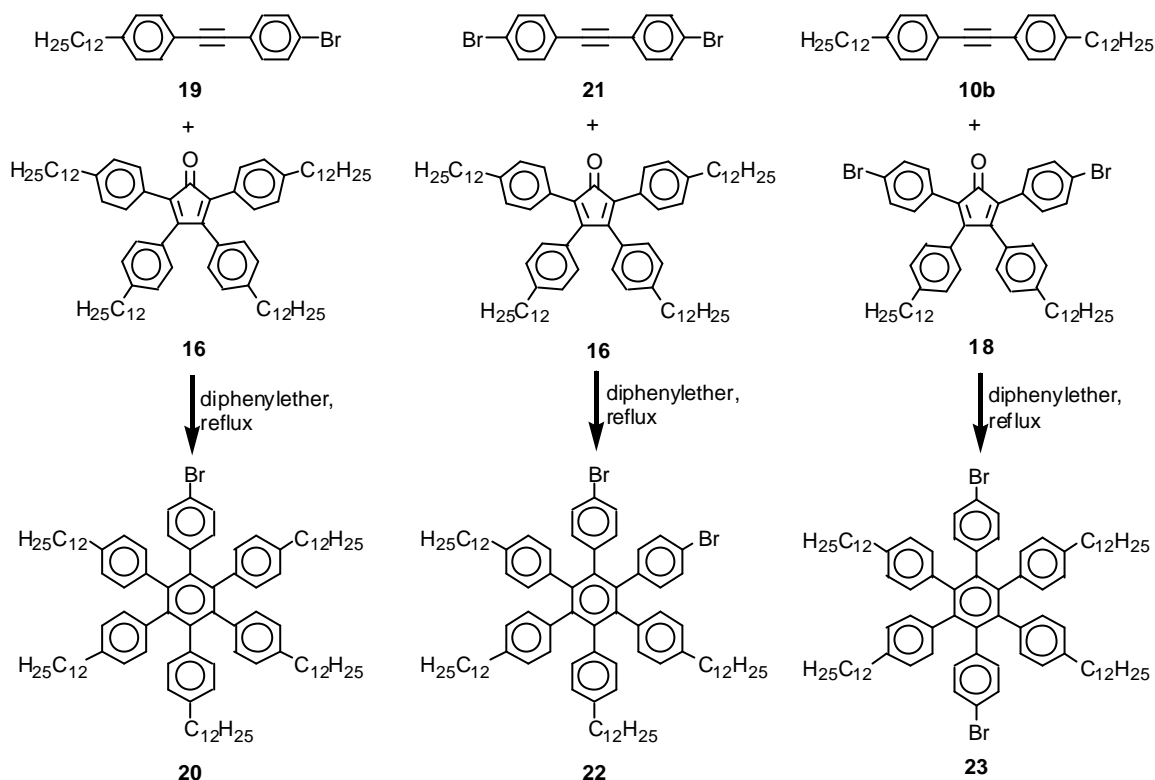
Consideration of the molecular structure of HBC, with its hexagonal symmetry, suggests its description as a “superbenzene”, where each peripheral benzene ring is equal to one sp²-carbon of benzene. In this fashion, benzene-analogous nomenclature is used to denote substitution patterns, e.g. HBCs functionalized in the positions “ortho” **8** and “para” **9** as depicted in Figure 5.^[28] Alternative procedures to synthesize any “meta” derivatives have yet to be implemented. (This scheme becomes more complicated when substituents are placed in the bay positions)

These functionalized HBC derivatives were synthesized on a different route, since the reaction sequence presented above (Scheme 1) can only produce hexabenzocoronenes with a C_6 symmetry. The corresponding bromo-hexaphenylbenzene precursors that were required for the build-up of the bromo-functionalized HBCs were synthesized as depicted in Scheme 2 and Scheme 3.^[28]



Scheme 2: **Synthesis of cyclopentadienones 16 and 18**

Twofold Aldol condensation of **14** and **15** (as well as **14** and **17**) in refluxing ethanol yielded the tetracyclopentadienones building blocks **16** and **18** respectively (Scheme 2).



Scheme 3: **Synthesis of functionalized hexaphenylbenzenes**

[4+2] Diels-Alder reaction of diarylacetylenes (**19**, **21**, and **10b**) with tetraarylcyclopentadienones (**16** and **18**) in refluxing diphenylether with *in situ* decarbonylation afforded the targeted bromo functionalized hexaphenylbenzenes **20**, **22**, and **23**. The hexaphenylbenzenes were obtained in good yields and were very soluble in many organic solvents, all were fully characterized by NMR spectroscopy, mass spectrometry, and elemental analysis.^[28]

Transformation of these hexaphenylbenzenes (**20**, **22**, and **23**) to the desired hexabenzocoronenes (**7-9**, Figure 5) using aluminum(III)chloride and copper(II)trifluoromethanesulfonate did not however, result in the HBC compounds. According to mass spectrometry data, only partially cyclized product were formed.^[28] This problem was overcome by utilizing the same methods that were earlier described by Brand, i.e. using iron(III)chloride dissolved in nitromethane as the oxidizing agent for the cyclodehydrogenation

reaction. Implementing this method, bromo functionalized HBCs **7-9** were isolated in excellent yields.^[28]

By benzene-analogous transition-metal catalyzed chemistry, HBC derivatives with cyano, ether, ester, amino, etc. functionality were prepared^[28] from the functionalized HBCs (**7-9**). Their mesoscopic behavior as well as their packing in two and three dimensions was studied. The direct visualization of two-dimensional crystals and liquid crystals of hexabenzocoronene derivatives on surfaces such as HOPG (highly oriented pyrolytic graphite) and molybdenum sulfide was achieved by STM techniques.^[26, 28, 29, 94] In the case of the *mono* bromo-substituted HBC **7**, a particularly interesting lattice structure was observed^[28] with two types of arrangements: molecules associated in trimers (bromine atoms located in the center) and single molecules. The supramolecular arrangement reveals a hexagonal lattice in which single molecules fill positions in the center of an ensemble of six trimers as depicted in Figure 11.^[28]

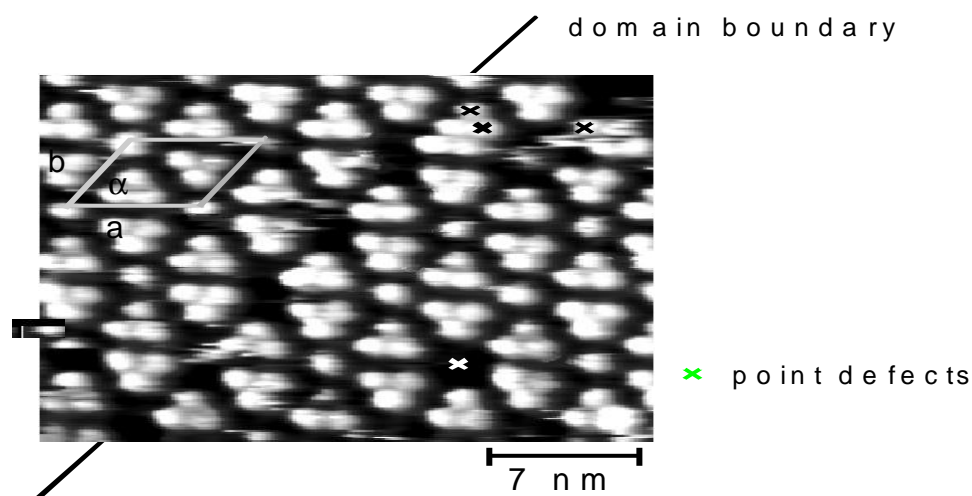


Figure 11: **STM image of mono bromo HBC-C₁₂ 7**

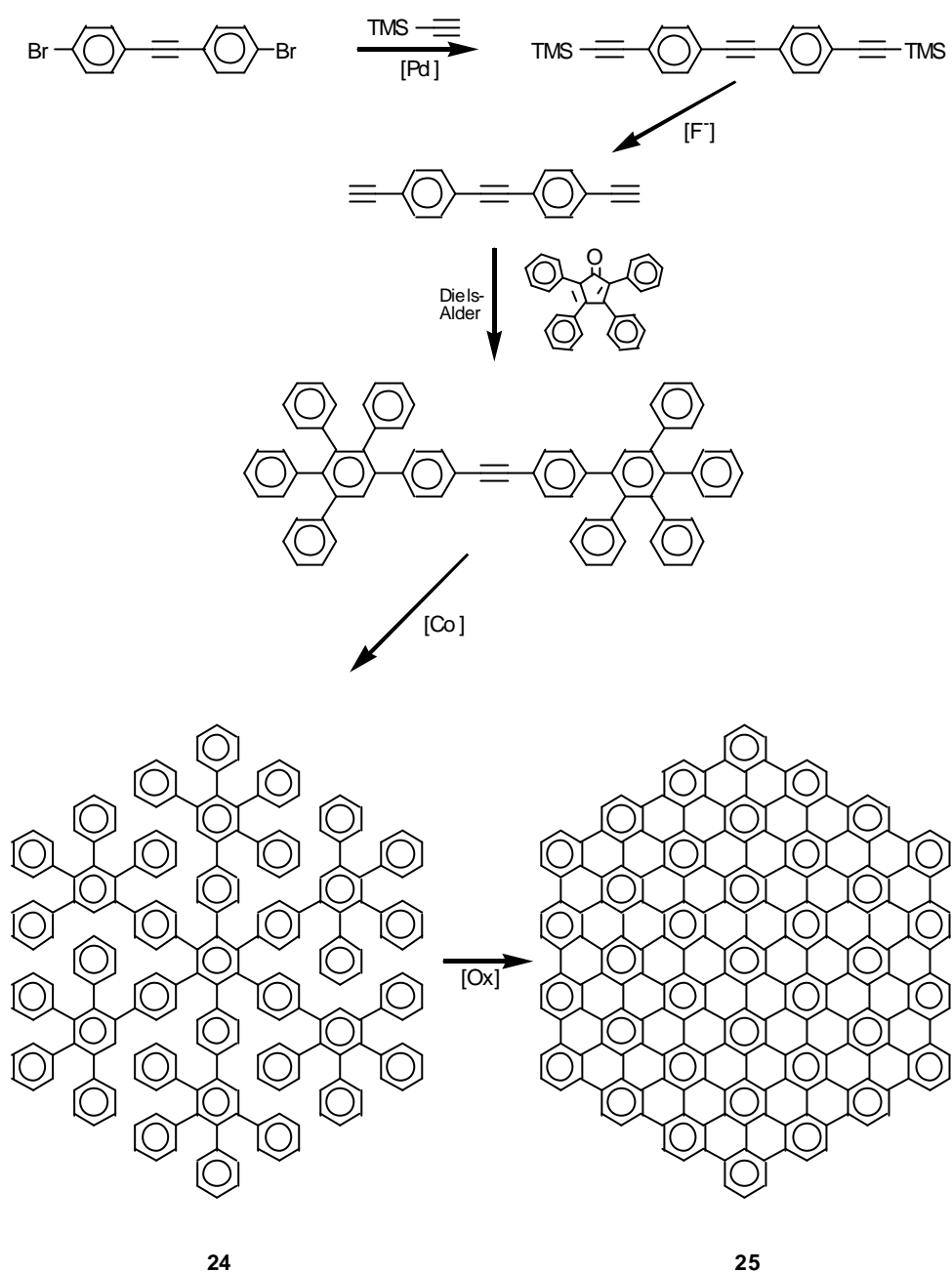
The *mono* bromo-substituted HBC was also used as a starting material for a surface active HBC with a tethered carboxylic acid group. This derivative was then complexed with amino functionalized polysiloxane and polyethyleneimine resulting in remarkably long columns essentially free of defects.^[32, 33] The surface activity of this HBC was exploited to prepare LB films at the air-water interface.^[99] These few examples taken together with the already existing vast

number of triphenylene derivatives emphasize the wide horizon facing the field of discotic liquid crystalline PAHs.

1.9 “Superbenzene” Chemistry

The number of possible large PAHs which have been prepared, and/or strictly isolated, is relatively small compared to other classes of hydrocarbons.^[38, 100] One limiting factor is the harsh synthetic conditions which are often employed. A particularly mild and reasonably well-defined synthetic method has been recently developed,^[38, 100] by which Clar-type PAHs of unprecedented size become available Scheme 4.^[97]

The synthetic route taken is surprisingly simple and allows a systematic variation not only of the size, but also of the symmetry and the type of periphery.^[28] The first phase of the sequence includes the synthesis of 3-dimensional oligophenylene precursors, which, due to the twisting among the benzene rings, are non-colored and nicely soluble. The second phase which is the fusing of the benzene rings can be accomplished by the same mild oxidative cyclodehydrogenation at room temperature that was described above.^[34, 73] The requisite 3D-oligophenylenes are available by transition-metal catalyzed cyclotrimerization of suitable diarylacetylenes or by the Diels-Alder reaction of such diarylacetylenes with tetraarylcyclopentadienones and *in situ* decarbonylation.^[28] The repetition of these reactions and the use of oligomeric starting compounds with multiple acetylene (dienophile) and cyclopentadienone (diene) functions leads to a remarkable structural manifold.^[101] One example is, C₂₂₂ **25**, which is the largest PAH that has been synthesized so far (Scheme 4).^[102] MALDI-TOF spectrometry proves that, indeed, 108 hydrogens are removed upon transition from **24** to **25** and that the resulting organic material is 99% pure.^[103]



Scheme 4: **Reaction sequence for the synthesis of C_{222} 25**

The topology of the oligophenylenes is designed such that the previously mentioned intramolecular dehydrogenation leads to a flattening of the molecule and the transition from an oligophenylene to a Clar-type PAH.

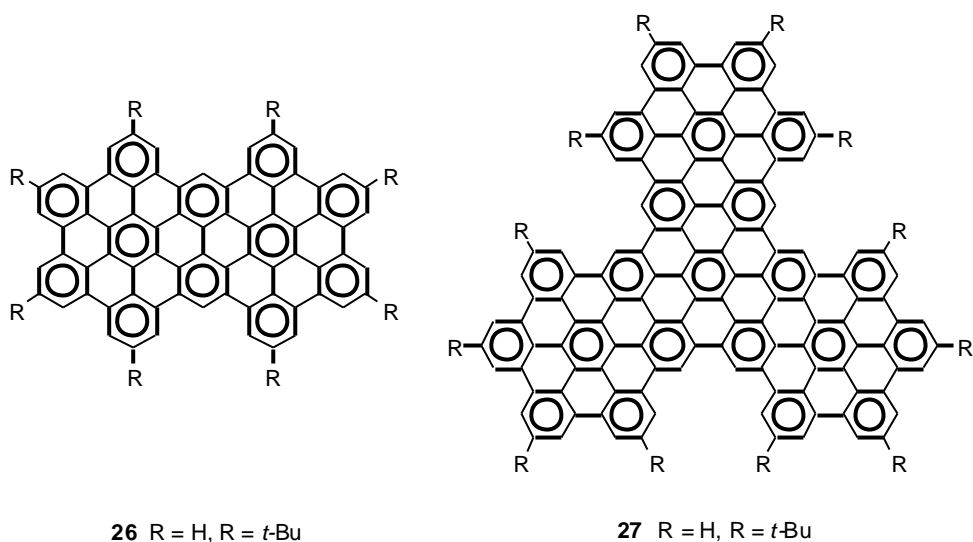


Figure 12: **Structures of “supernaphthalene” 26 and supertriphenylene 27**

The role of HBC as “superbenzene” as a repeat unit of giant fused PAHs is analogous to using benzene as a building block to produce fused homologues. This is clear in the naming of the “supernaphthalene” **26**^[102] and supertriphenylene **27**^[102], in which 2 and 3 “superbenzenes” (HBCs) are fused, respectively (Figure 12).

Functionalization of “superbenzene” as described above, permits covalent linking leading to, e.g. “superbiphenyl” **28**^[29], and the “supertolane” **29**^[29], prepared by transition-metal catalyzed coupling reactions starting from the monobromo derivatives.

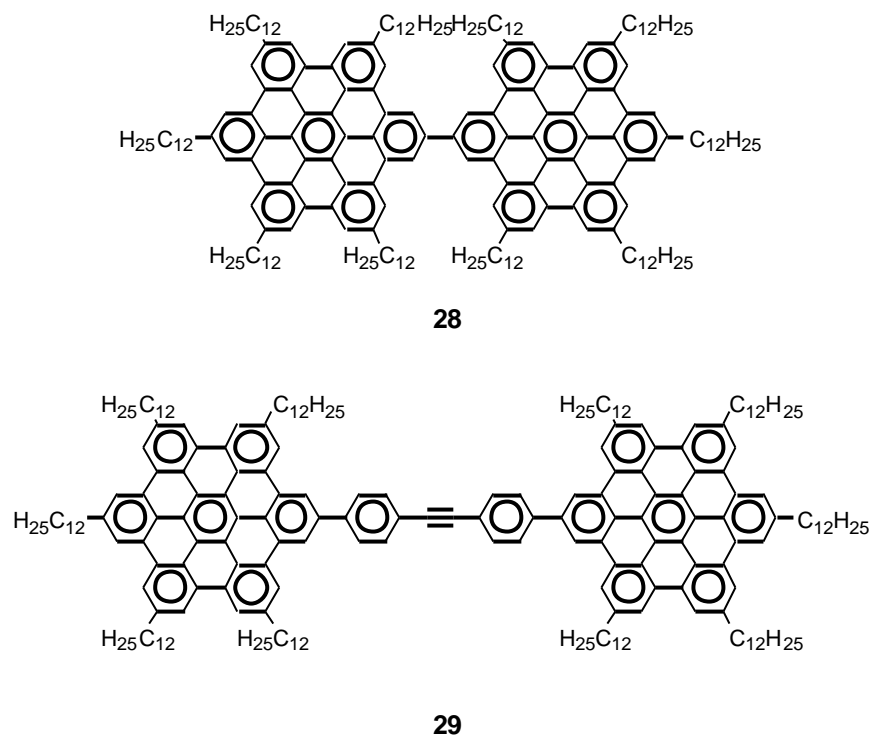


Figure 13: **Structures “superbiphenyl” 28, and the “supertolane” 29**

Superbenzene as a building block of more complex macromolecular architectures, becomes particularly obvious from the fact that a benzene-like chemistry originates from the synthesis of mono-, *ortho*-di- and *para*-disubstituted species mentioned above. Keeping in mind the versatile role of functionalized benzene derivatives in polymerization and polycondensation chemistry, it now becomes possible to design an analogous chemistry of superbenzene.

2 Motivation and Objective

2.1 Motivation

Once a chemical substance crosses the border from being simply a new compound to the stage where its materials properties become most dominant and relevant for its application in devices, one has to think of designing the synthesis to be as easy, inexpensive and efficient as possible. For one class of compounds this border has been crossed some time ago. Discotic liquid crystalline hexabenzocoronenes are being recognized for their potential applications in molecular electronics as already presented in the Introduction^[35]. However, more thorough understanding of the potential of HBCs as materials will require a library of derivatives, enhanced solubility and processability, and improved synthetic routes to facilitate their preparation. Soluble conjugated organic materials such as HBC combine the electronic properties of semiconductors and the mechanical processing properties of polymeric materials. This makes them suitable for commercial applications in optoelectronic technologies where the adaptability and simplicity and low cost of manufacture make them extremely attractive. In the field of photovoltaics where the output vs. cost ratio ultimately defines the viability of a technology, solution-processible organics have a unique advantage.

2.2 Objective

Recently published routes to prepare substituted hexabenzocoronenes relied on multistep syntheses and long term planning of the substitution pattern in cases with reduced symmetry and/or functionalized derivatives. It was the aim of this work to improve procedures for preparing the building blocks needed for HBC synthesis with symmetric six-fold alkyl substitution where a variety of different substituents can be introduced as late in the reaction sequence as possible.^[28] Further, improvement of the solubility and processability of hexabenzocoronenes is desired since up to this point all alkyl substituted HBCs

6a-d are only soluble in organic solvents at elevated temperatures and re-precipitate completely out of solution after cooling to room temperature. Improved solubility will not only widen the range of feasible reactions but also influence the processability in terms of spincoating from solution or the use of printing techniques to produce homogeneous thin films that might find application in devices. This task is targeted with the idea of using longer or branched alkyl chains in combination with additional aryl groups as substituents for the periphery of hexabenzocoronenes. Another outcome of this systematical investigation of substituents could be the discovery of a HBC derivative that has an isotropization temperature below the beginning of decomposition. This would permit annealing and thus, give additional control for manipulating the material. Since these substituted HBCs form columnar liquid crystals, the aromatic cores undergo rapid axial rotation on the μs timescale in the mesophase. As a result of this, the order parameter of the discs (for HBC-C₁₂ **6b**), $S = 0.84$, is found to be considerably lower than in other columnar discotics.^[27] Since high mobility and low order limit the charge carrier mobility, it was also the aim to synthesize a less mobile mesogen, which at the same time should improve hexagonal columnar ordering (Figure 14).

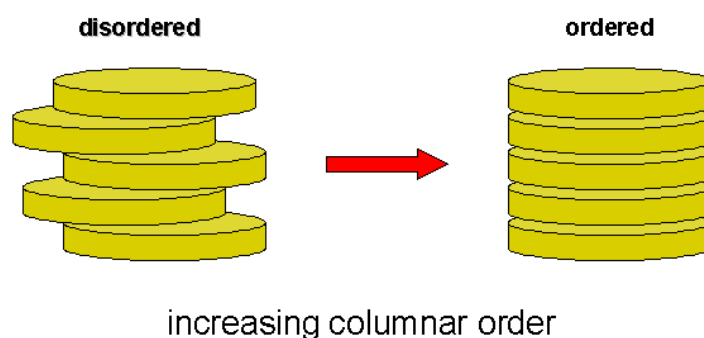


Figure 14: **Illustration of targeted orientation**

Increase of intracolumnar order as depicted in Figure 14 can also be tackled by the introduction of chiral substituents, demonstrated by the increased one-dimensional charge carrier mobility which was reported for the helical mesophase of a hexa hexylthiotriphenylene derivative.^[39, 45] Before the introduction of liquid-crystalline hexabenzocoronenes, this material was the

previous record holder for the mobility of charge carriers in organic liquid crystals.^[35] The influence of chiral substituents is also an attractive task for the visualization of HBC derivatives with an STM at the solid-liquid interface on surfaces such as HOPG. This influence could lead to interesting new architectures of PAHs on defined surfaces.

In this context, “surface-induced chirality” was noted in monolayers of nonchiral triphenylenes on the nonchiral surface HOPG. The disks were ordered in a 2D hexagonal array as in the 3D mesophase, although with smaller intermolecular distances. The appearance of a super-lattice in derivatives with longer alkyl chains, as evidenced by differing contrasts, was attributed to “chiral domains”. Bromo substituted HBCs **7-9** were earlier synthesized and characterized by Brand and Wehmeier in the group of Professor Müllen.^[28] With benzene-analog chemistry a variety of functionalized derivatives were reported.^[28] Following up on this subject, the functionalization of hexabenzocoronenes was carried out in such a manner that subsequent reactions towards the formation of dimers or oligomers resulting in stabilized columns of HBC were envisaged.

3 Novel HBC Derivatives with C₆ Symmetry

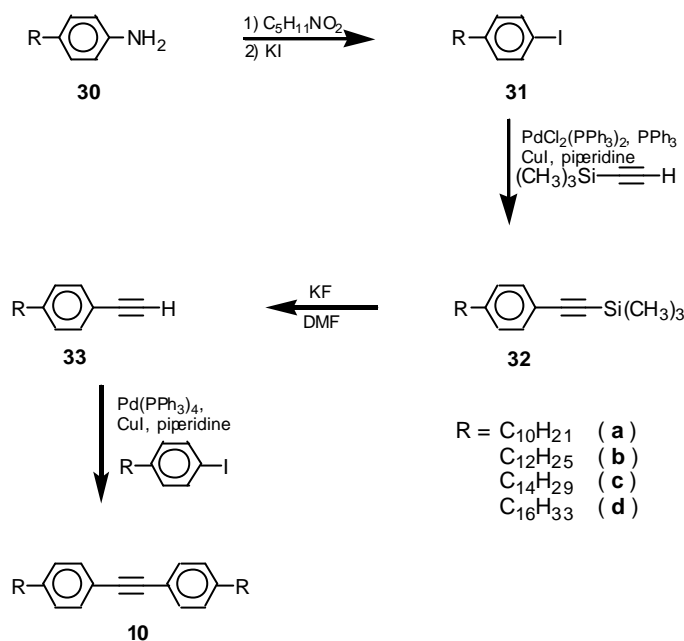
3.1 Introduction

A more thorough understanding of the potential of HBCs as materials will require a library of derivatives and improved synthetic routes to facilitate their preparation. Recently published routes to prepare substituted hexabenzocoronenes relied on multistep syntheses and long term planning of the substitution pattern in cases with reduced symmetry and/or functionalized derivatives.^[26, 27] Here, improved procedures for preparing the building blocks needed for HBC synthesis with symmetric six-fold alkyl and aryl substitution will be discussed. Detailed characterization of the materials properties by means of X-Ray and solid-state NMR experiments will be presented.^[104] Further, the advantageous combination of room temperature liquid crystallinity and high intramolecular charge carrier mobility^[30] proved to be very important and was utilized in a photovoltaic cell with high external quantum efficiencies.^[105] A detailed scanning tunneling microscopy (STM) investigation revealed that the functionalization of the HBC core with chiral alkyl and chiral alkylphenyl substituents^[37] resulted in a fascinating staircase topology on the surface of highly oriented pyrolytic graphite.^[106]

3.2 Hexaphenyl HBC – A New Material

3.2.1 Attempts Towards Direct Functionalization of Hexabromo-hexaphenylbenzene

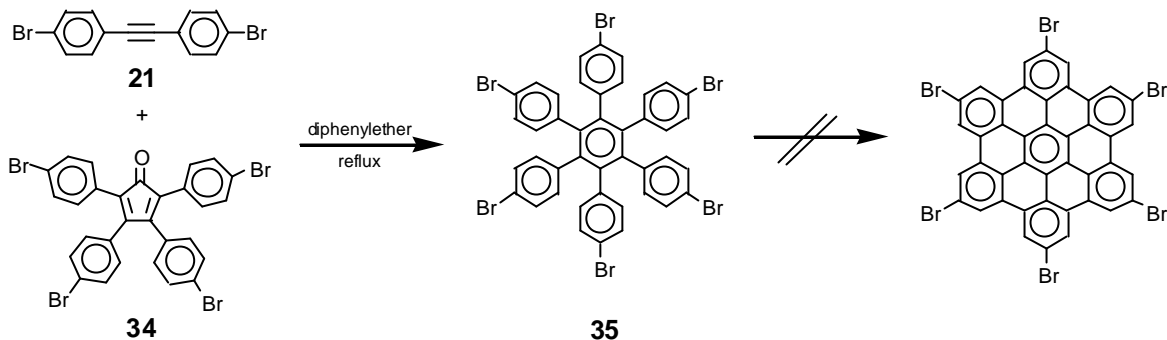
As reported by Herwig and co-workers in 1995^[26], a four-step synthetic sequence was utilized to prepare alkyl substituted 4,4'-diphenylacetylenes, the crucial building block for the hexafold-substituted HBC derivatives as depicted in Scheme 5.^[27]

Scheme 5: **Synthesis of alkyl substituted 4,4'-diphenylacetylenes**

The synthesis started with commercially available 4-alkylaniline (**30**), which was transformed via Sandmeyer reaction^[107] to the corresponding 1-iodo-4-alkylbenzene (**31**). Trimethylsilylacetylene and 1-iodo-4-alkylbenzene (**31**) are then coupled under classical Hagihara^[108] conditions to yield compound **33**. After deprotection of the acetylene with potassium fluoride in DMF, another Hagihara coupling was carried out under slightly different conditions as described before.^[108] This last step finally afforded the desired 4,4'-dialkyldiphenyl acetylene (**10a-d**) which is the precursor needed for the cyclotrimerization discussed in the introduction.

Two disadvantages of this synthesis easily come to mind: a) two of the four steps are catalyzed by expensive palladium catalysts, and b) the introduction of a different substituent can not be accomplished on the level of the 4,4'-diphenylacetylene, but must be introduced right at the beginning of the reaction sequence. This of course is hard to tolerate in view of fast and easy excess to an ample variety of different substituents necessary for the screening of potential materials application. To overcome this problem, direct functionalization of the hexabenzocoronene core is required. It was already in 1968 that Broser et al^[109] reported the synthesis of hexakis-(4-bromphen-1-

yl)benzene (**35**) (Scheme 6). Here, the synthesis was accomplished via [4+2] Diels-Alder reaction in refluxing diphenylether with *in situ* decarbonylation of 4,4'-dibromodiphenylacetylene (**21**) and tetra-(4-bromophenyl)cyclopentadienone (**34**).



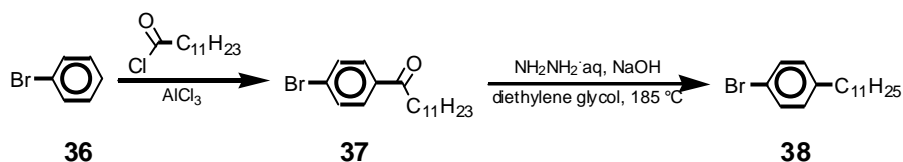
Scheme 6: **Synthesis of hexakis-(4-bromophen-1-yl)benzene**

Following this procedure, it was possible to synthesize hexakis-(4-bromophen-1-yl)benzene (**35**) on a multi-gram scale. Unfortunately, this hexa-functionalized hexaphenylbenzene could not be transferred to the corresponding HBC derivative, with six bromo atoms on the periphery, due to the very low solubility of the resulting product.^[72] Since the synthesis of a hexa-functionalized HBC failed, it was instead attempted to use the available hexakis-(4-bromophen-1-yl)benzene (**35**) for further reactions.

As mentioned in the Introduction, the overall goal is not only to improve the reaction pathways for the synthesis of substituted HBC derivatives but also to improve solubility, processability and the materials properties for the class of hexabenzocoronenes. Herwig^[27] and others in our group synthesized a variety of HBCs with different alkyl substitution. However, the materials that were obtained were only soluble in organic solvents such as THF or toluene at elevated temperatures, upon cooling precipitation was almost complete.

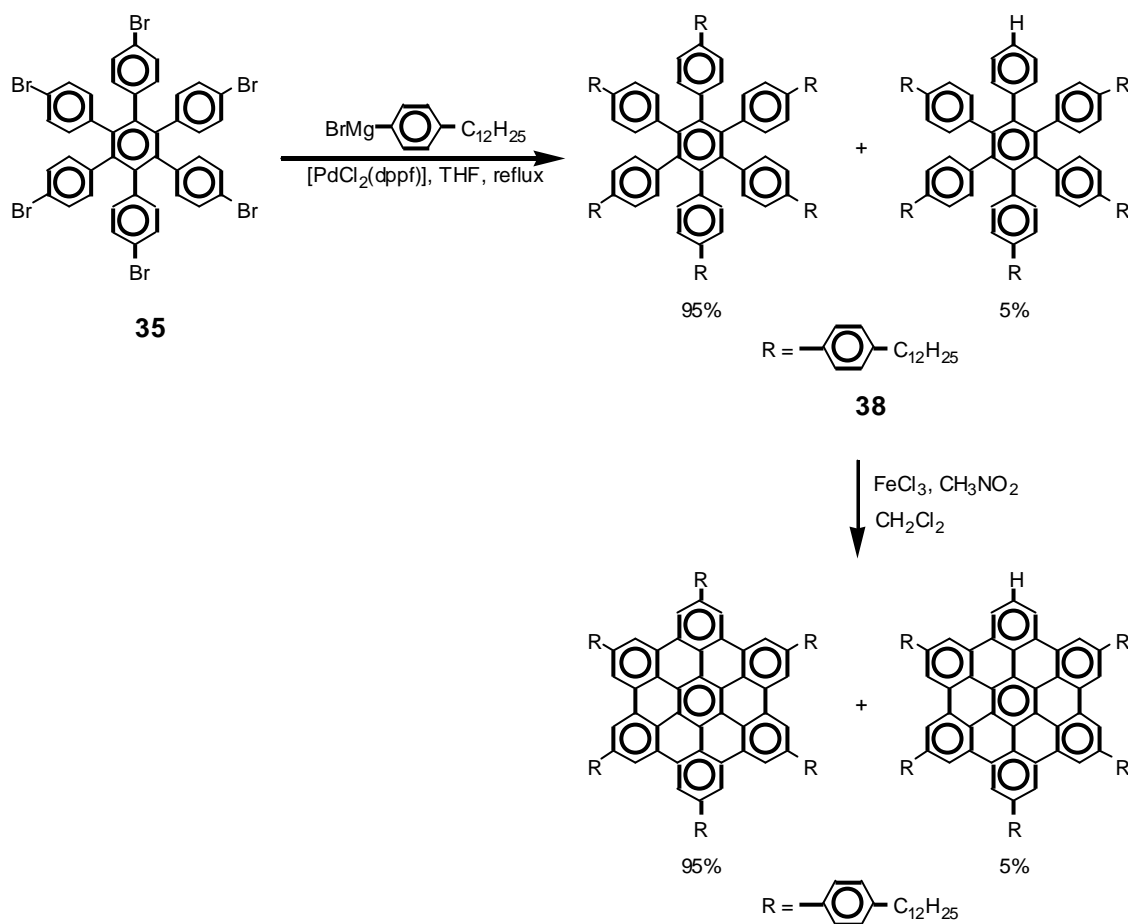
Since high mobility and low order limit the charge carrier mobility, the synthesis of a less mobile mesogen, which at the same time should improve hexagonal columnar ordering, was targeted. With this in mind, additional phenyl rings were thought to be ideal for the insertion between the planar HBC discs and the pendent alkyl chains. As outlined in Scheme 7 the reaction of bromobenzene

with dodecanoyl chloride afforded 1-(4-bromophenyl)dodecan-1-one (**37**).^[110] Then the reduction of the carbonyl functionality was carried out with hydrazine hydrate and sodium hydroxide in diethylene glycol at 185 °C to afford compound **38** as a colorless oil in good yields.^[111]



Scheme 7: *Synthesis of 1-bromo-4-dodecylbenzene (38)*

Having the right precursor in hand, the next step was to decide on an appropriate coupling reaction, since a six-fold functionalization of hexakis-(4-bromophen-1-yl)benzene (**35**) had to be attempted. In 1981 Hayashi et al.^[112] reported that palladium dichloro[1,1'-bis(diphenylphosphino)-ferrocene], henceforth referred to as [PdCl₂(dppf)], is an effective catalyst for the reaction of secondary and primary alkyl Grignard and alkyl-zinc reagents with organic halides to give the corresponding coupling products selectively in exceedingly high yields. Since extremely high yields and selectivity are the prerequisites for a six-fold coupling reaction it was decided to try to functionalize hexakis-(4-bromophen-1-yl)benzene (**35**) under Kumada-type^[112] coupling conditions. At first, a one molar solution of 4-dodecylphenylmagnesiumbromide was prepared under classical Grignard conditions.^[107] Then this solution was added dropwise to a degassed suspension of hexakis-(4-bromophen-1-yl)benzene (**35**) in dry THF (Scheme 8). An inert atmosphere and the use of absolutely dry solvents are crucial for this reaction, since even traces of water will jeopardize the complete coupling of all six bromo functionalities with the corresponding Grignard reagent.



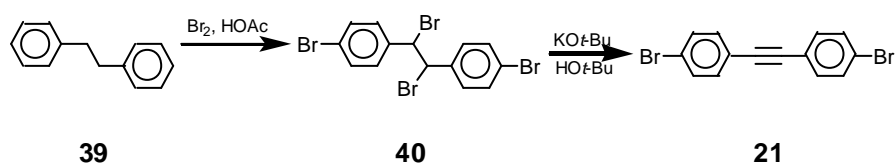
Scheme 8: Attempted reaction sequence for the synthesis of dodecylphenyl substituted HBC

After refluxing the reaction mixture overnight and purification of the crude product, $^1\text{H-NMR}$ spectroscopy mass spectrometry analysis revealed that two products had formed. The major percentage of the analyzed fraction could be attributed to the desired product. However, around five percent of a side product had formed where one of the six peri positions was not substituted with a phenyl-alkyl side chain. Debromination had occurred and was attributed to high temperatures or to the fact that not all of the starting material (hexakis-(4-bromophen-1-yl)benzene (**35**)) was dissolved at the beginning of the reaction. Nevertheless, it was inspiring that 95% of desired product had formed. During the course of the following experiments, the temperature, concentration of starting material and amount of catalyst was varied. Unfortunately, it was not possible to run the reaction without the formation of by-products. On the other

hand, attempts to purify the mixture also failed due to the similar chemical and physical properties of the products. After having tried different reaction conditions and methods of purification, it was considered possible that separation of the two products could be feasible after the mixture of products was subjected to the next step in the reaction pathway. Cyclodehydrogenation using iron trichloride dispersed in nitromethane was selected as the method of choice for the oxidative removal of the twelve hydrogen atoms.^[34] While the experiment was carried out under the optimized and tuned cyclodehydrogenation conditions developed in our group the proceeding of the ongoing reaction was monitored by means of FD-mass spectrometry. After taking a sample every 5 minutes it became obvious that after 45 minutes the reaction was complete. Quenching of the mixture followed by analysis of the obtained product revealed again the presence of the impurity described above. Again, attempts to separate the two compounds by column chromatography or methods of fractional re-precipitation failed. It was clear that a different reaction sequence had to be chosen to obtain the desired product.

3.2.2 Synthesis of Hexaphenylhexabenzocoronene (HBC-PhC₁₂)

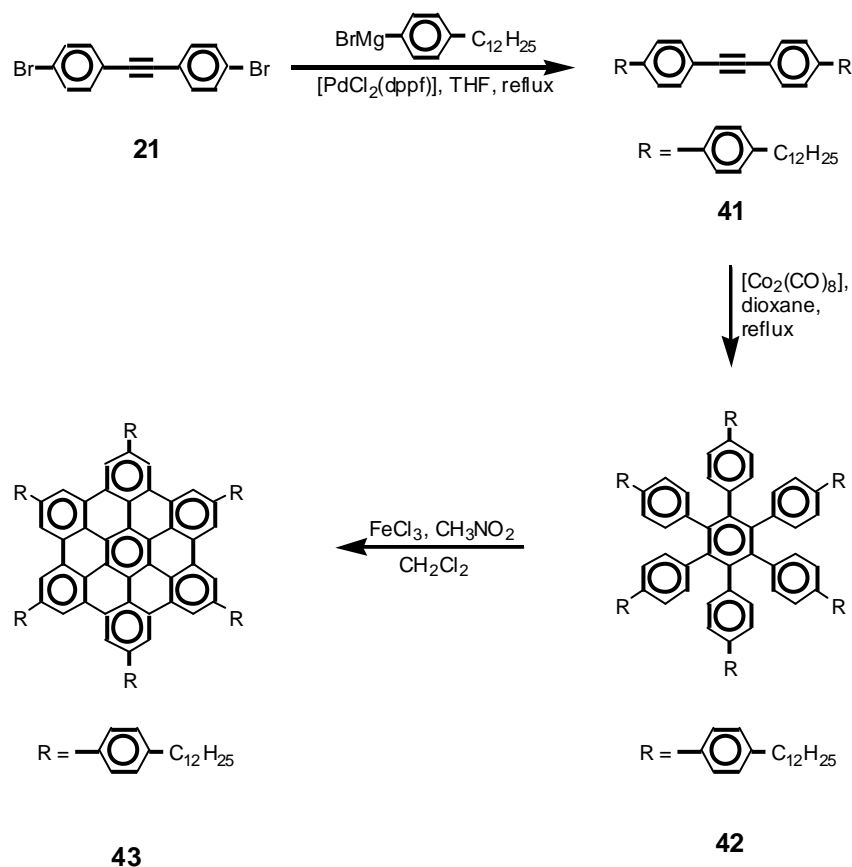
Since the direct hexa-functionalization of hexakis-(4-bromphen-1-yl)benzene (**35**) could not be achieved, it was the goal to target the next nearest precursor in the reaction sequence. The material best suited for this new attempt is 4,4'-dibromodiphenylacetylene (**21**). Scheme 9 outlines the synthesis of 4,4'-dibromodiphenylacetylene (**21**), which can be prepared in a two step synthesis, according to literature procedures^[28, 72, 113, 114], on several hundred gram scale.



Scheme 9: **Synthesis of 4,4'-dibromodiphenylacetylene (21)**

However, previous attempts^[28] to functionalize **21** under common Grignard coupling conditions using $\text{NiCl}_2(\text{dppf})$, $\text{NiCl}_2(\text{dppp})$, or $\text{Pd}(\text{PPh}_3)_4$ were unsatisfactory. Encouraged by the high conversion rates of the new $[\text{PdCl}_2(\text{dppf})]$ catalyst, the functionalization of 4,4'-dibromodiphenylacetylene was the next experiment to be conducted on the way to a faster and easier route towards the synthesis of liquid crystalline hexabenzocoronenes.

The new synthesis is outlined in Scheme 10. First, in a Kumada-type coupling reaction catalyzed with $[\text{PdCl}_2(\text{dppf})]$ ^[112] 4,4'-dibromotoluene (**21**) reacts with 4-dodecylphenylmagnesiumbromide to give di(4-dodecylbiphenyl) acetylene (**41**) with a yield of 75%. Cyclotrimerization of **41**, catalyzed by $[\text{Co}_2(\text{CO})_8]$, in dioxane then afforded hexa(4-dodecylbiphenyl)benzene (**42**) with 70% yield after workup.



Scheme 10: **Reaction sequence for the synthesis of HBC-PhC₁₂ 43**

The key step for the synthesis of HBCs is the oxidative cyclodehydrogenation. Here, hexa(4-dodecylbiphenyl)benzene (**42**) was dissolved in CH_2Cl_2 and

flushed with argon for several minutes, before adding FeCl_3 dissolved in CH_3NO_2 . Precipitation with MeOH after 45 minutes and workup finally afforded hexa(4-n-dodecylphen-1-yl)hexa-peri-hexabenzocoronene **43**, henceforth referred to as HBC-PhC₁₂ **43**, with 80% yield.^[104]

As indicated by Scheme 10, the reaction afforded the desired product analytically pure and in good yields. This is the first example in our group and in the literature showing that it is feasible to directly functionalize 4,4'-dibromotoluene (**21**). The discovery of the $[\text{PdCl}_2(\text{dppf})]$ catalyst for this reaction sequence is a milestone for faster excess and multiple convertibility towards new hexabenzocoronenes.

When HBC-PhC₁₂ **43** became available in larger quantities, it was obvious that the material would have different properties than HBC-C₁₂ **6b** which is the parent case for all comparisons.

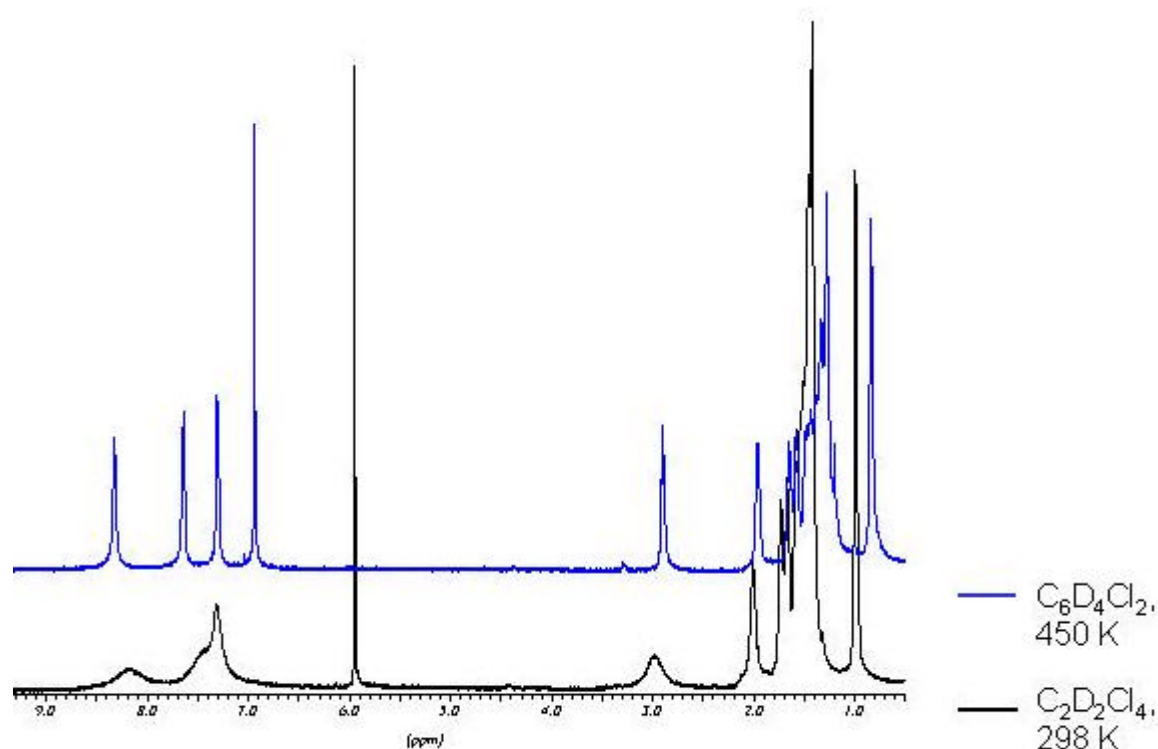


Figure 15: *High resolution* ¹H-NMR spectra of HBC-PhC₁₂ **43** at different temperatures

During the workup of HBC-PhC₁₂ **43** and sample preparation, it was most striking to notice the dramatically increased solubility of this new HBC derivative. However, upon measuring a ¹H-NMR spectra only very low resolution was achieved (Figure 15, bottom).^[104]

It is well known in the literature, that a major obstacle in the NMR-spectroscopic description of PAHs, related to the limited solubility, is the strong tendency of the disc-type structures to form aggregates in solution^[115, 116], which causes significant line broadening and shielding. The shielding in this case is of course intermolecular, versus the diatropic effects^[117] which are normally considered when looking at single aromatic molecules. Figure 15 shows, however, that by increasing the temperature from 298 K to 450 K one can obtain ¹H-NMR signals with sufficiently narrow line widths.^[104]

This simple experiment already indicates that strong intermolecular forces such as π - π interactions and interlocking of the pending phenyl rings must be present. More detailed studies such as polarized optical microscopy (POLMIC), differential scanning calorimetry (DSC), X-Ray, and solid state NMR spectroscopy will be described in the following chapters.

3.2.3 Mesophase Characterization of HBC-PhC₁₂: TGA, DSC, and POLMIC Analysis

DSC measurements were performed to study the phase behavior of HBC-PhC₁₂ **43**. The DSC curve is shown in Figure 16, whereas the phase transition temperatures and enthalpy changes are given in Table 1.

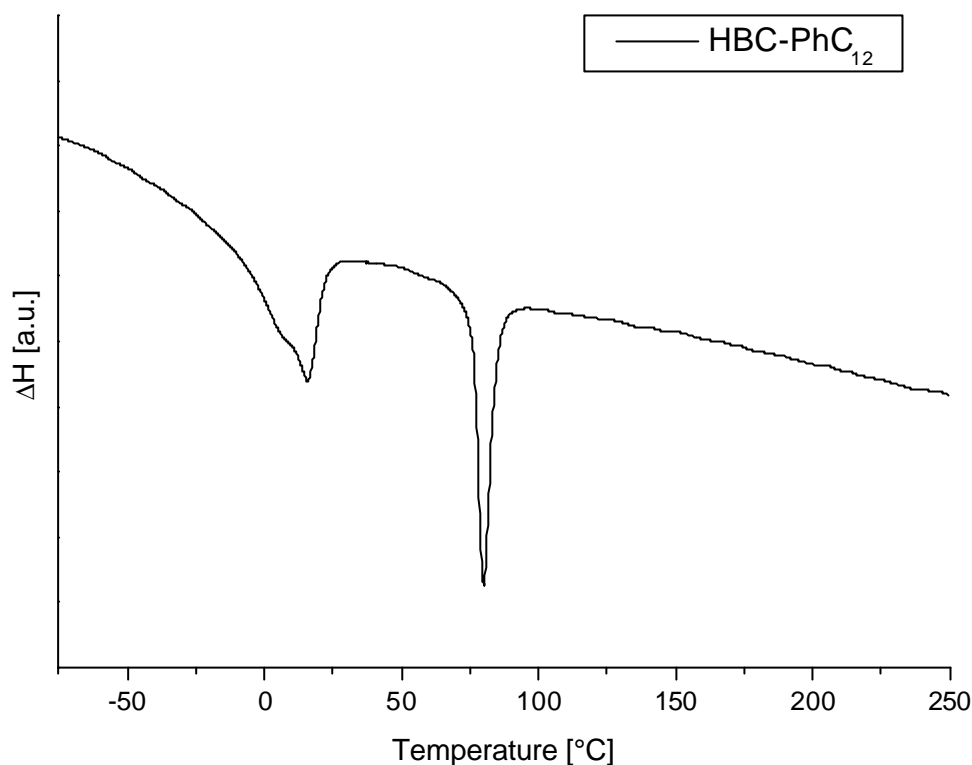


Figure 16: **DSC trace for the third heating trajectory of HBC-PhC₁₂ at 10 °C/min**

At temperatures below -10 °C, HBC-PhC₁₂ **43** is a solid but exhibits a first broad liquid crystalline phase transition, K→D₁, in the room temperature area between -6 °C and 28 °C, with a maximum at 15.3 °C. The endothermic enthalpy change that is correlated to this peak is in the order of 30 kJ/mol and thus in the range of characteristic enthalpy changes reported for other mesophase forming hexabenzocoronenes such as **6a-d**.^[27, 28] On further heating a second sharp transition, D₁→D₂, was found at 79.8 °C. The energy change that corresponds to this transition is 16.6 kJ/mol. The transition from the mesophase into the isotropic liquid, D₂→I, at around 420 °C is accompanied by a small change in enthalpy of about 5 J/g but was measured only as an exception, since it occurs at temperatures above 350 °C where decomposition slowly starts. On cooling the sample to temperatures below 350 °C, reversible phase transitions with supercooling in the range of 20 °C were observed.

	T [°C]	ΔH [J/mol]	Transition
HBC-PhC ₁₂ 43	15.3	30	K→D ₁
	79.8	16.6	D ₁ →D ₂

Table 1: *Phase transition temperatures, enthalpy changes, and structural assignments for HBC-PhC₁₂ (K = crystalline phase, D₁ = first mesophase, D₂ = second mesophase)*

To further study the thermal behavior of HBC-PhC₁₂ by optical microscopy studies, a drop cast film was prepared from a chloroform solution. At room temperature, the film already showed birefringence supporting the findings that HBC-PhC₁₂ forms a mesophase at room temperature. On heating the material under an nitrogen atmosphere, HBC-PhC₁₂ underwent only one phase transition at around 420 °C where the material becomes isotropic. The other phase transitions at 15.3 and 79.8 °C were not observed due to the fact that compound **43** is already liquid crystalline at room temperature and the experimental setup does not allow studies which require cooling below room temperature. The textures observed in the POLMIC experiment were not well developed domains and did not show any ribbon- or fan-like structures typical for columnar mesophases.^[14, 118, 119] Owing to this fact, no mesophase superstructure was assigned to HBC-PhC₁₂ at this point.

3.2.4 Solid State NMR and X-Ray Investigations

The fact that solid state NMR methods are a great tool to investigate the behavior and properties of discotic liquid crystals can be concluded from the Introduction. The results^[104] that are presented below were obtained from of a collaboration with Dr. Kai Saalwächter in the group of Prof. Dr. Spiess.

For both HBC-C₁₂ **6b** and HBC-PhC₁₂ **43**, WAXS patterns demonstrated that the high-temperature LC mesophases exist as ordered columnar hexagonal (Col_{h0}) superstructures (Figure 17).^[27, 104] For a perfect hexagonal lattice, reflections at small angles with relative spacings of $1:\sqrt{3}:\sqrt{4}:\sqrt{7}:\sqrt{9}$ are expected, where the intensities depend on the perfection of the lattice and the order

parameter. As shown in Figure 17, only the first three peaks, i.e. (100), (110), and (200), are observed for HBC-C₁₂ while the fourth peak, (210), is apparent for HBC-PhC₁₂ above the noise level, indicating improved long-range packing of the columns to form a hexagonal arrangement. In addition, the packing of the cores within the columns is improved, as indicated by the sharp (001) reflection at $2\theta \approx 25.6^\circ$. This corresponds to an intermolecular distance of 0.350 nm between the aromatic cores, which should be compared to a spacing of about 0.355 nm in the LC phase of HBC-C₁₂, where the (001) reflection is significantly broader.^[27, 104]

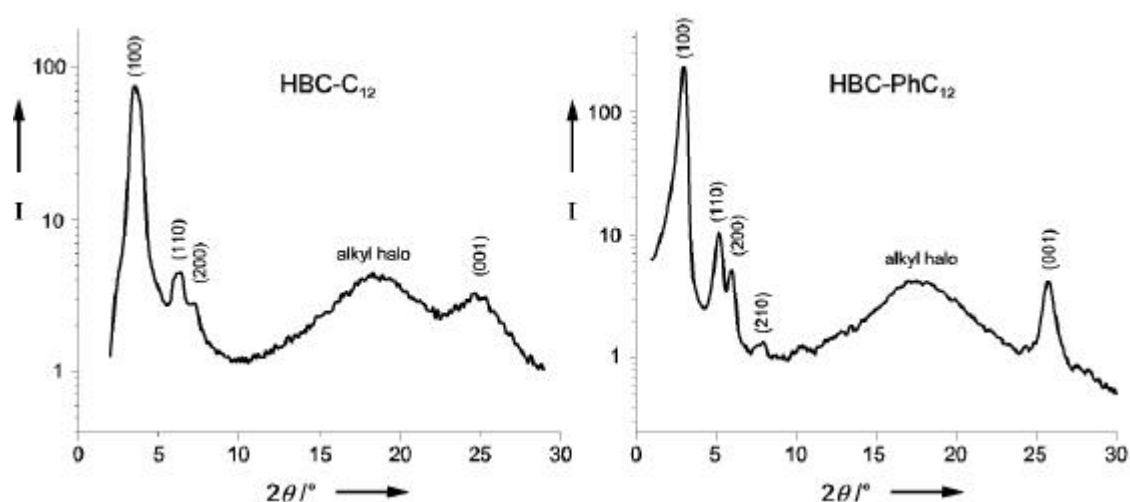


Figure 17: *X-Ray diffractograms of HBC-C₁₂ and HBC-PhC₁₂ in the mesophase*

Structure and dynamics on a molecular level can be probed in detail by advanced solid-state NMR spectroscopy.^[120] For the high-temperature LC phase, the rapid rotation of the disc-shaped molecules about the columnar axis has been confirmed by ²H NMR,^[27] and more recently by ¹H double-quantum (DQ) magic-angle spinning (MAS) NMR.^[34] This rotation leads to an averaging of the respective interaction tensors, i.e. the quadrupolar coupling tensor in the case of ²H NMR, and the homonuclear dipolar coupling tensor in the case of ¹H DQ spectroscopy. Thus, fast motional processes can be quantified by measuring the reduction of the coupling constants. If the symmetry axes of the tensors (the CH-bond vector and the H-H internuclear vector of the two core-CH

protons) lie in a plane perpendicular to the rotational axis, the coupling constants are reduced by a factor of 0.5. With the two methods, reduction factors of 0.40 and 0.42 have been observed, corresponding to order parameters^[121] for the discs of 0.80 and 0.84, respectively, indicating additional out-of-plane or librational motions.

The application of both methods mentioned above is limited. ²H-NMR spectroscopy requires specifically isotopically labeled samples, which represents a considerable synthetic challenge, while ¹H DQ MAS NMR is unsuitable in the case of HBC-PhC₁₂ **43**, since the core-CH and the exo-phenyl-CH ¹H resonances cannot be differentiated. Both limitations are overcome by a recently developed heteronuclear multiple-quantum correlation method. REPT-HMQC (**R**ecoupled **P**olarization-**T**ransfer **H**eteronuclear **M**ultiple-**Q**uantum **C**orrelation)^[120] is a two-dimensional correlation experiment for solids under very-fast MAS, which exploits the concept of a 'separated local field' spectroscopy.^[122] An advantage of this technique is the enhanced site-resolution, made available by the observation of ¹³C resonances, rather than ¹H. As in ¹H solid-state DQ MAS spectra, the signal in the MQ dimension can be distributed over several orders of spinning sidebands, with intensities depending on the dipolar coupling and the spinning frequency.^[123, 124] These sideband intensities can then be used to quantitatively evaluate the heteronuclear dipolar coupling of site-resolved carbons to their neighboring protons. The sensitivity of the technique to dipolar couplings of different magnitudes can be chosen by simply changing the so-called recoupling time, τ_{rcpl} , which corresponds to the number of rotor periods, τ_{R} , used to excite the MQ modes.

By measuring the dipolar coupling within a CH moiety, one can use such 2D spectra to obtain site-resolved dynamical information in complex molecules without the need for isotopic labeling. It should be emphasized that the REPT-HMQC method is applicable to samples naturally abundant in ¹³C, and only requires small amounts of sample, typically 10-15 mg. Both the heteronuclear dipolar and the quadrupolar coupling tensor of a C-¹H and a C-²H group, respectively, exhibit the same symmetry, such that the results from the experiments described here can be seen as being analogous to those obtained

by ^2H -NMR spectroscopy, the latter being a well-established method for the investigation of liquid crystals.^[121]

In Figure 18, MQ spinning sideband patterns corresponding to the core-CH signals of HBC- C_{12} and HBC- PhC_{12} are displayed for different temperatures and different recoupling times. In the latter case, as shown in the ^{13}C CP MAS spectra, the exo-phenyl-CH are resolved from the core-CH signals. For very-fast MAS,^[125, 126] the sideband pattern is that of an isolated spin pair, i.e. being composed of odd-order sidebands only, with the observed intensity distribution depending on the product of the recoupling time and the dipolar coupling constant.^[120, 123]

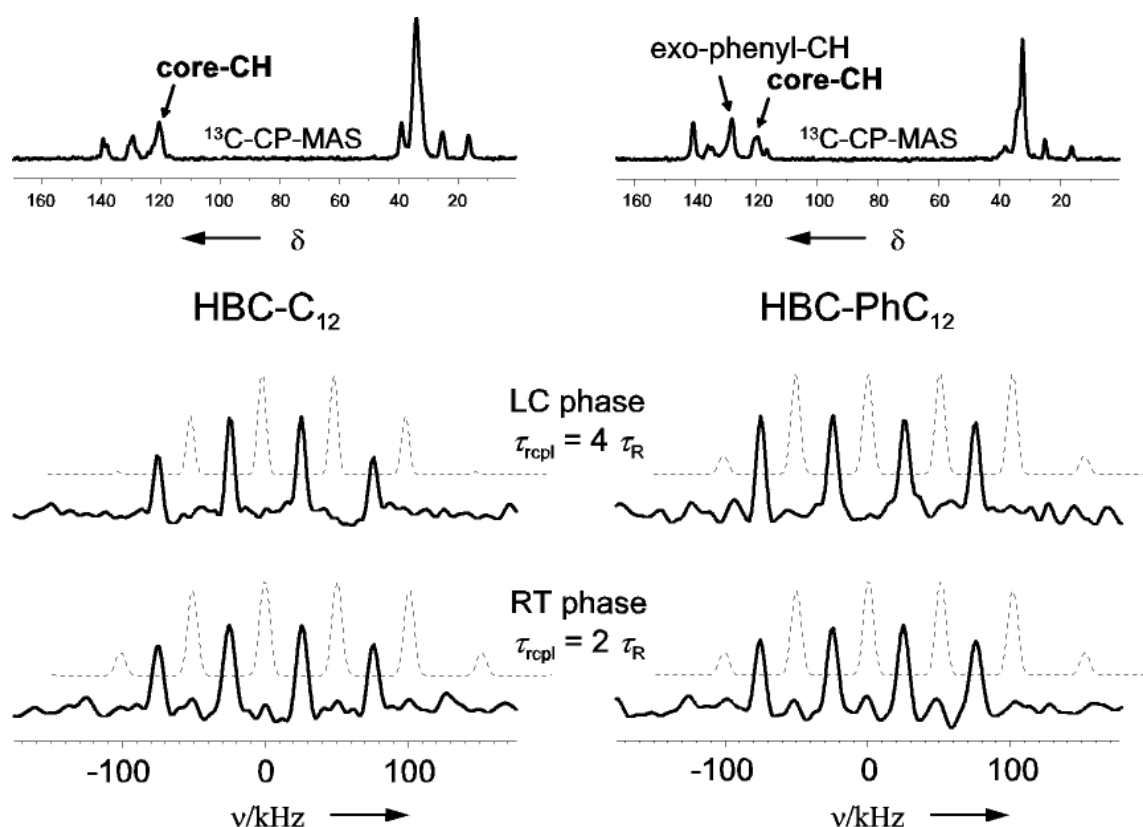


Figure 18: **Solid-state ^1H - ^{13}C heteronuclear multiple-quantum spinning side-band patterns, obtained at a spinning frequency of 25 kHz using the REPT-HMQC pulse sequence**

The shown sideband patterns for the room-temperature and high-temperature LC phases of both materials are similar, but the recoupling times are $2 \tau_{\text{R}}$ and $4 \tau_{\text{R}}$ for the RT and LC phases, respectively. This means that the dipolar coupling

are reduced by approximately 50%. A closer inspection reveals that the sideband pattern for the LC phase of HBC-C₁₂ exhibits less intense third-order sidebands, indicating a weaker coupling than in HBC-PhC₁₂.

The dipolar coupling constants were evaluated quantitatively by numerically fitting the sideband patterns to the analytical solution for the case of a heteronuclear spin pair; such best-fit spectra are shown as dotted lines in Figure 18. From various independent measurements, the average dipolar coupling constant for a rigid aromatic CH group - as found in the RT phase of both materials - was determined to be 20.9 ± 0.5 kHz, which corresponds to an internuclear distance of 113 ± 1 pm, while the motionally reduced coupling constants for the LC phases were determined to be 8.2 ± 0.9 kHz and 9.7 ± 0.9 kHz for HBC-C₁₂ and HBC-PhC₁₂, respectively. Thus, one calculates reduction factors of 0.39 ± 0.04 and 0.46 ± 0.04 for the motional processes in the two materials, corresponding to order parameters of 0.78 ± 0.09 and 0.93 ± 0.09 . Within the limits of experimental error, the value for HBC-C₁₂ agrees with the earlier findings.^[27, 34] In contrast, for HBC-PhC₁₂ the order parameter for the discs has increased by 15 %, which means that the rotational motion is better defined and that additional out-of-plane motions are suppressed more effectively. It should be emphasized that the increase in the order parameter is better defined than its absolute value, which is subject to systematic deviations. It may further be noted that the MQ measurements were carried out at 120°C, such that the motional processes in both HBC samples are assured to be fast on the NMR timescale, i.e. at least in the μ s range. In this respect, from the decrease of ¹H MAS linewidths upon heating, it became clear that for HBC-PhC₁₂, despite its lower calorimetric phase transition temperature of 79.8 °C, the degree of motional averaging still increases up to about 110°C. One should keep in mind that these thermally activated motions, though fast on an NMR timescale, are not expected to interfere with the dynamics of the hopping process of charge transport, which takes place on a timescale of less than 1 ns. These NMR findings strongly support the conclusion of high intracolumnar order drawn from the X-ray data, and thus we can state that order phenomena in the LC phase of HBC-PhC₁₂ not only extend to longer ranges - as detected by scattering experiments - but also manifest themselves in a well-defined packing

of the rotating discs on a molecular level. We also note that preliminary results concerning motional processes in the sidechains at different temperatures indicate an initially surprising higher mobility in HBC-PhC₁₂ as compared to HBC-C₁₂, indicating that a higher order of the HBC cores does not necessarily lead to an overall reduction of mobility in the system. Since the charge carrier transport properties in such systems are limited by the degree of long-range order within the columns, the possibility of the system to undergo molecular reorientations due to this motional freedom, thus allowing for self-healing, is highly desirable.

In summary, the design, synthesis and mesophase characterization of a hexaphenyl substituted HBC has indicated that symmetric substitution can inhibit out-of-plane mesogen mobility without interrupting the columnar hexagonal superstructure. Both MQ NMR results and X-ray diffraction indicate higher inter- and intracolumnar ordering in the mesophase.

3.2.5 Charge carrier mobility

The results presented in this section are the direct outcome of a strong collaboration with Dr. Anick van de Craats in the group of Professor Warman, TU Delft.

Increasing attention is being paid to the possible application of discotic materials as conducting layers in organic molecular electronic devices. These compounds such as HBCs **6a-d** and **43** self-organize into columnar stacks with aromatic macrocyclic cores surrounded by a saturated hydrocarbon mantle. This insulated, coaxial structure results in the one-dimensional transport of charge within the core. Furthermore, their liquid-crystalline properties offer the possibility of obtaining extensive, well-organized layers in which the columnar orientation can be controlled and self-healing of structural defects can occur. For optimum performance, compounds are sought which display high charge carrier mobilities and extensive temperature regimes over which they have liquid-crystalline mesophases.

Mesomorphic derivatives of hexabenzocoronene **6a-d** and HBC-PhC₁₂ **43** display this combination of advantageous properties.^[30, 35] For the first time for

discotic materials, a charge carrier mobility in excess of $1 \text{ cm}^2/\text{Vs}$ was observed in the crystalline solid phase of these materials, and a value as high as $0.5 \text{ cm}^2/\text{Vs}$ was found even in their hexagonal columnar liquid crystalline phase. In addition, one of the compounds was liquid crystalline at room temperature and, because of its high solubility in organic solvents, can be readily spin-coated thus making it an ideal candidate for device applications.^[30, 35]

The molecular structures of the hexabenzocoronene derivatives studied are shown in Figure 19. Their phase transitions as monitored by differential scanning calorimetry (DSC) are given in Table 2 and indicated in Figure 19.

	T [°C]	ΔH [J/mol]	Transition
HBC-C ₁₀ 6a	69	9	K ₁ →K ₂
	124	64	K ₂ →D _h
HBC-C ₁₂ 6b	42	10	K ₁ →K ₂
	105	78	K ₂ →D _h
HBC-C ₁₄ 6c	52	13	K ₁ →K ₂
	107	99	K ₂ →D _h
HBC-PhC ₁₂ 43	15.3	30	K ₁ →D ₁
	79.8	16.6	D ₁ →D ₂

Table 2: **Phase transition temperatures, enthalpy changes, and structural assignments for HBCs 6a-c and HBC-PhC₁₂ 43 (K = crystalline phase, D_h = hexagonal mesophase, D₁ = first mesophase, D₂ = second mesophase)**

The sum of the one-dimensional charge carrier mobilities, $\Sigma\mu_{1D}$, has been derived from the pulse-radiolysis time-resolved microwave conductivity technique (PR-TRMC). The values of $\Sigma\mu_{1D}$ are plotted as a function of temperature in Figure 19.

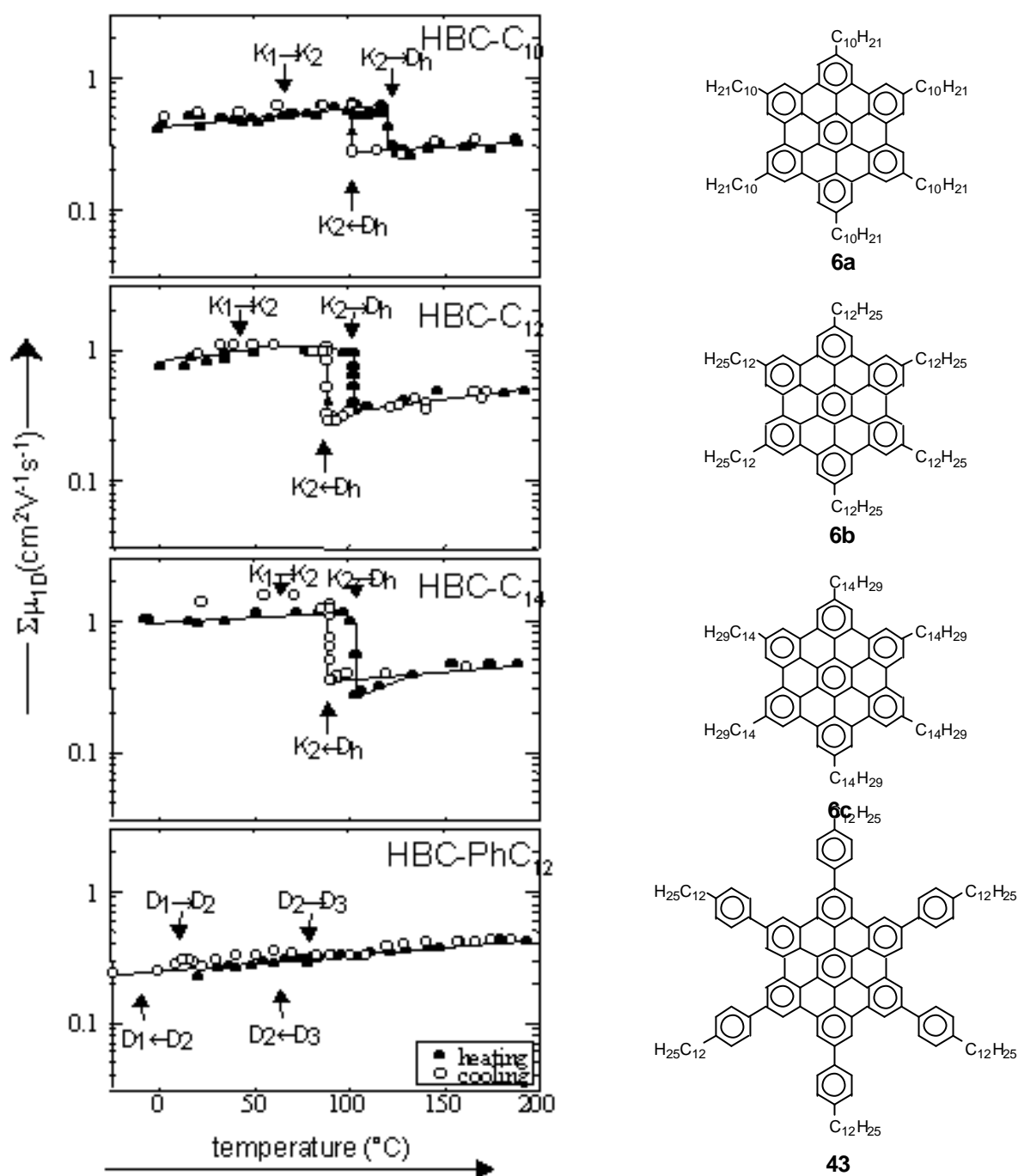


Figure 19: **Temperature dependence of the intracolumnar charge carrier mobilities.** Phase transitions as indicated by DSC are depicted by vertical arrows.

The temperature-dependence for the three directly linked n-alkyl derivatives, **6a-c**, is seen to be very similar: the mobility increased slightly on heating in the crystalline solid phase, K, with no abrupt changes observed at the solid-solid transitions found in DSC measurements. On entering the D_h-mesophase

however, an abrupt decrease in the mobility occurred after which it increased again gradually on further heating. On cooling, the mobility values were reproduced with a hysteresis of approximately 20 °C at the reverse $D_h \rightarrow K$ phase transition. The drastic changes in the mobility occur at temperatures at which the HBC **6a-c** transform from the crystalline phase into the columnar hexagonal mesophase. In the case of substituted HBCs, both crystal structures and solid state NMR measurements indicate that in the crystalline form the disks are stacked with an overlap much like that in graphite giving optimum π - π overlap. The drop in charge carrier mobility upon entering the mesophase, associated with increase in mobility and onset of uniaxial rotation, is therefore attributed to a decrease in order. The behavior observed was similar to that found previously for n-alkoxy-substituted phthalocyanines,^[90] for which the decrease at the $K \rightarrow D_h$ transition was attributed to the greater motional freedom and resulting increased structural disorder with the columns in the mesophase. The mobilities measured at 10 degrees below and above the $K \rightarrow D_h$ transition temperatures are listed in Table 3.

	T [°C]	Phase	$\sum m_D$ [°C]	$t_{1/2}$ [ns]
HBC-C ₁₀ 6a	115	K ₂	0.55	180
	133	D _h	0.26	142
HBC-C ₁₂ 6b	98	K ₂	0.96	360
	110	D _h	0.38	180
HBC-C ₁₄ 6c	98	K ₂	1.13	1840
	116	D _h	0.31	120
HBC-PhC ₁₂ 43	-78	K ₁	0.17	1800
	22	D ₁	0.22	1000
	192	D ₂	0.46	540

Table 3: *Intracolumnar charge carrier mobilities $\sum m_D$, and first half-lives $t_{1/2}$*

The values for the K phase increased with increasing alkyl chain length up to a value slightly in excess of $1 \text{ cm}^2/\text{V s}$ for the HBC-C₁₄ compound. The values for the D_h or D₂ phase varied only slightly with the majority of the data for all four compounds lying within the range $0.4 \pm 0.1 \text{ cm}^2/\text{Vs}$, which is well within the experimental error of the experiments.

For HBC-PhC₁₂, in which the alkyl chains are coupled to the core via a phenylene moiety, no evidence was found for an abrupt change in $\Sigma\mu_{1D}$ at any temperature within the range studied. Even on cooling to $-78 \text{ }^\circ\text{C}$ no abrupt increase in $\Sigma\mu_{1D}$, indicative of the formation of a crystalline solid phase, was observed. The values of $\Sigma\mu_{1D}$, determined at room temperature and at the lowest and highest temperatures measured, are listed in Table 3. In view of the fact that no abrupt transition was observed, and the absolute values of the mobility at elevated temperatures were very close to those for the D_h phases of the HBC **6a-c** compounds, it is further confirmation that HBC-PhC₁₂ was in fact liquid-crystalline (Col_{h0}) at all temperatures studied and thus does not undergo the transformation from the typical Herringbone (Col_{ro}) arrangement in the crystalline phase to the Col_{h0} orientation in the LC phase, resulting in generally lower values for the charge carrier mobility at temperatures below 100°C (see also further discussion in the X-Ray section). In support of this conclusion, the compound was found to be malleable even at room temperature and could be readily compressed by hand to a density of 0.95 g/cm^3 , which is considerably higher than can be achieved with polycrystalline solids. The relatively broad DSC peaks observed at ca. 15 and $80 \text{ }^\circ\text{C}$ are therefore attributed to conformational changes within the mesophase and addressed as D₁ and D₂.^[30, 34, 104]

The mobility values for the liquid-crystalline phases of the present compounds are the highest ever found for discotic materials, and are well in excess of the value of ca. $0.1 \text{ cm}^2/\text{V s}$ found by both PR-TRMC and time-of-flight techniques for the H (helical) phase of hexakis-hexylthio-triphenylene (**12**), a previous record holder.^[39, 45] The values are in fact comparable with the room-temperature mobilities determined for single crystals of aromatic compounds^[127]

and approach the value of ca. $3 \text{ cm}^2/\text{V s}$ found for the inter-sheet mobility in graphite.^[128]

Also listed in Table 3 are the first half-lives, $t_{1/2}$, of the mobile charge carriers in the present materials. As was previously found for the K phase of n-alkoxy-substituted phthalocyanines, $t_{1/2}$ for the HBC **6a-c** compounds increased dramatically with increasing alkyl chain length in the solid.^[90, 129] This was taken as evidence that the decay process involves charge recombination via intercolumnar tunneling through the saturated hydrocarbon mantle. The shorter life-times in the mesophase for the longer chain compounds were attributed to the occurrence of an additional pathway for recombination when the alkyl chains melt, involving intercolumnar diffusion of charged macrocyclic units. It is interesting in this regard that $t_{1/2}$ for the HBC-PhC₁₂ material is considerably longer than for the D_h phase of the HBC **6a-c** compounds. This indicates that the columnar structure in the mesophase of the former is much more stable with respect to intercolumnar diffusion. It also indicates that electronic cross-talk between the columns for this material should be much less, which would further increase the one-dimensional anisotropy of charge transport.

In conclusion, it was demonstrated that charge-carrier mobilities in mesomorphic derivatives of hexabenzocoronene are larger than any mobility value previously found for liquid-crystalline discotic materials. In addition, it was found that the liquid-crystalline properties can be preserved even at sub-ambient temperatures by incorporating a phenylene group as the coupling element between the core and the peripheral alkyl chains. The resulting combination of high mobility, room-temperature liquid-crystallinity, and very high solubility in organic solvents makes the HBC-PhC₁₂ compound a particularly attractive candidate for applications as a conducting layer in molecular electronic devices, which will be demonstrated in the following section.

3.2.6 HBC-PhC₁₂ as a semiconductor in high efficiency photovoltaics

All the results presented in this section are the direct outcome of a strong collaboration with Lukas Schmidt-Mende in the group of Professor Friend, University of Cambridge.

High efficiency organic photovoltaic devices derive their performance from two basic elements: The dissociation of photo-excitons and the transport of the resulting separated charge out of the devices. Blends of soluble conjugated polymers and dyes which phase separate into interpenetrating networks of polymers which exhibit photoinduced charge separation have been used to create devices with external quantum efficiencies (EQE) of 5-10%.^[130, 131] The high degree of photoluminescence quenching in these systems suggests that transport, not exciton dissociation, limits performance. By using lamination to create a multilayer device with an idealized charge transport structure from spin-coated films soluble in a common solvent, external quantum efficiencies (EQE) as high as 29% were demonstrated.^[132] However, yield and scaling difficulties limit the commercial application of a lamination technique. Impressive efficiencies have also been demonstrated with small molecule devices relying on either carefully controlled layer deposition of charge transfer pairs or the use of extrinsic dopant-mediated charge transfer in a high mobility molecular matrix.^[133-135] However, both of these approaches suffer from the need for UHV processing.

In the following passages it will be demonstrated that phase-separated blends of soluble, small molecule materials have been utilized in such a way as to produce self-organized photovoltaic structures with maximum EQEs of >34% and power efficiencies of 1.7%. Microscopy, spectral characteristics and basic modeling indicate that a nearly ideal, vertically segregated structure, with a high interfacial area between the electron accepting perylene and hole-accepting hexabenzocoronene, HBC-PhC₁₂ **43**, components has been attained. In this way, multicomponent self-organization, inducing a high interfacial surface area morphology and a vertically segregated composition, has been applied to organic photodiodes in such a way that complex ideally-ordered structures can be realized in a potentially manufacturable technique. It is uniquely different

from other extrinsic approaches that rely on multiple evaporation, lamination or spinning steps to create stratified organic structures.

The materials used in this study include commercially available perylene N,N'-Bis(1-ethylpropyl)-3,4,9,10-perylenebis(dicarboximide) (perylene diimide **44**, Figure 20) and the discotic, liquid crystalline hexaphenyl-substituted hexabenzocoronene (HBC-PhC₁₂ **43**).^[104]

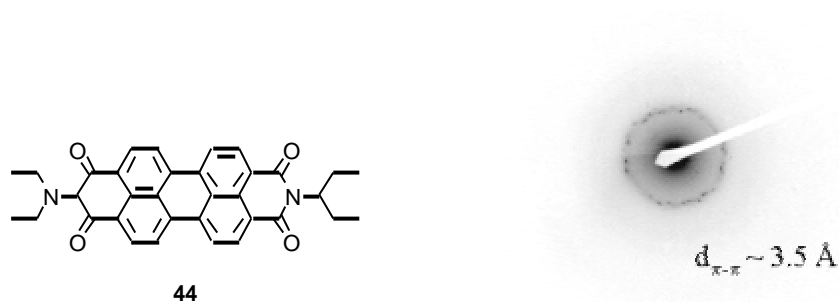


Figure 20: **Structure of perylene diimide 44 and electron diffraction image of a spin coated film**

Perylene diimides are known to possess high electron mobilities^[16, 136] and have been utilized previously as an electron acceptor and transport material in small molecules and dye-polymer blend devices^[133, 137, 138]. Electron diffraction has been used to show the high crystallinity of the perylene in spin-coated films. The perylene dye and the HBC-PhC₁₂ are both soluble in chloroform. As already outlined in the above sections HBC-PhC₁₂ is discotic liquid crystalline (LC) at room temperature. In the LC phase columns of disc-shaped molecules are formed, which give rise to a quasi-one-dimensional transport of charge carriers and excitons along the columns with high carrier mobility. Mobilities as high as $\Sigma\mu_{1D} = 0.22\text{cm}^2/\text{Vs}$ have been measured for intracolumnar charge carrier motion in HBC PhC₁₂.^[30]

Figure 20 shows the structure of the perylene molecule and an electron diffraction image taken from a spin-coated xylene film. The most dense ring of diffraction spots from perylene crystallites corresponds to a spacing of approximately 3.5 Å which is similar to the π - π stacking direction spacing

observed in many conjugated molecules.^[139] Cyclic voltammetry indicates a HOMO-level of 5.25 eV and a LUMO-level of 2.64 eV for HBC-PhC₁₂ which has a relatively large bandgap of 2.61 eV as demonstrated in Figure 21. Relative to the perylene, which has a high electron affinity as a result of the electron-withdrawing diimide bridges, there is 0.65 eV LUMO step and 0.07 eV HOMO step which promotes exciton dissociation and charge transfer, verified by photoluminescence quenching.

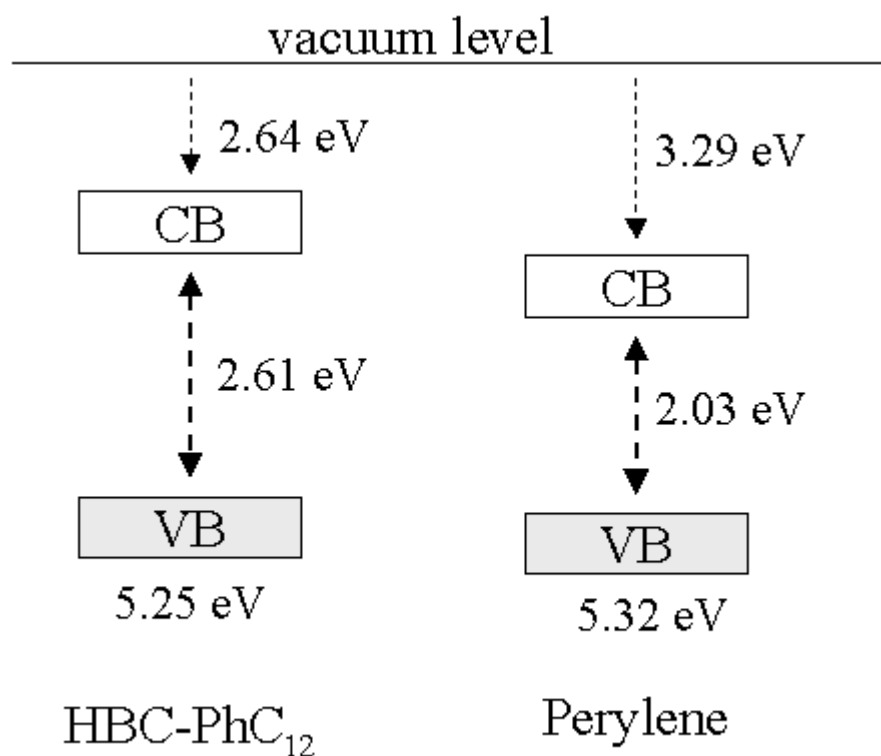


Figure 21: *HOMO- and LUMO-levels of HBC-PhC₁₂ 43 and perylene diimide 44 (CB = conduction band (LUMO), VB = valence band (HOMO))*

Both the hexabenzocoronene and the perylene exhibit characteristic thin film morphologies upon spin coating from 15 g/l solutions. Figure 22 (a, left) shows the tapping mode AFM image of a pure HBC-PhC₁₂ on 5 μm and 20 μm (inset) scales which shows a smooth, textured surface with a RMS surface roughness of <10 nm. Polarized light microscopy indicates the presence of large domains with typical in-plane lengthscales of hundreds of microns.

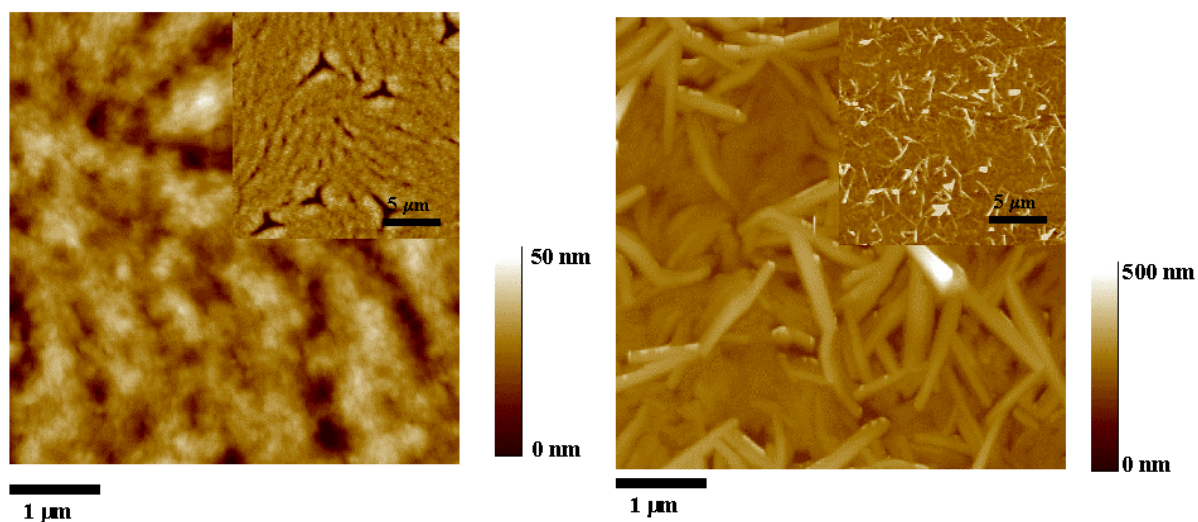


Figure 22: *Tapping mode AFM image of pure HBC-PhC₁₂ (a, left) and pure perylene (b, right) on 5 μm and 20 μm (inset) scales*

In contrast, the pure perylene surface is considerably rougher with characteristic micron-scale elongated crystallites as shown in Figure 22 (b, right). The RMS of a typical perylene film was >40nm with some crystals protruding 100's of nanometers from the surface.

Spin coating of blend solutions of close to equal parts HBC PhC₁₂ and perylene resulted in a markedly different surface morphology indicating the presence of a nearly continuous surface coverage of shortened perylene crystallites. This can be seen in the AFM micrograph presented in Figure 23.

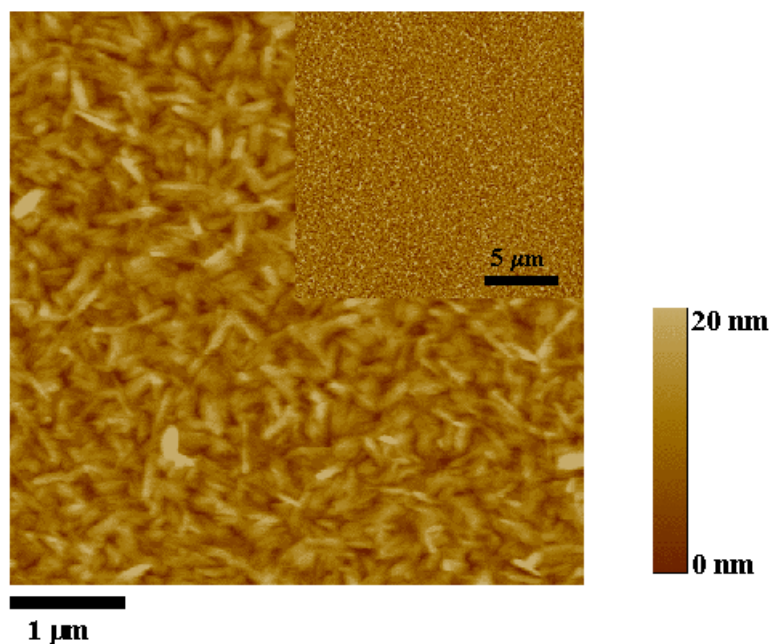


Figure 23: **AFM image of a spin coated film from a 40:60 HBC-PhC₁₂ / perylene mixture**

Cross sections of blend films spin-coated on a Si (100) wafer were prepared by cleaving after immersion in liquid N₂. The films were then imaged in a field emission scanning electron microscope (SEM) capable of high resolution, low accelerating voltage operation.

Figure 24 shows an electron micrograph of 40% HBC PhC₁₂ blend sample imaged with the cleaved surface tilted 15 degrees from normal to the incident electron beam. A stratification is clearly visible in the cross-section with a characteristic polycrystalline perylene sheet extending down the top surface of the film. Between the crystalline top surface and the substrate, a less-featured intermediate layer, possibly HBC-PhC₁₂, can be seen at the cleaved edge. Perylene crystallites with a cross-section resembling that of the long crystallites observed by AFM in the pure perylene film as in Figure 22 (b, right), can be seen dispersed through the intermediate layer in SEM the image. Blends with more than a 20% imbalance in binary composition produced more complex morphologies which suggested that continuous layers were stable only within composition or thickness limits.

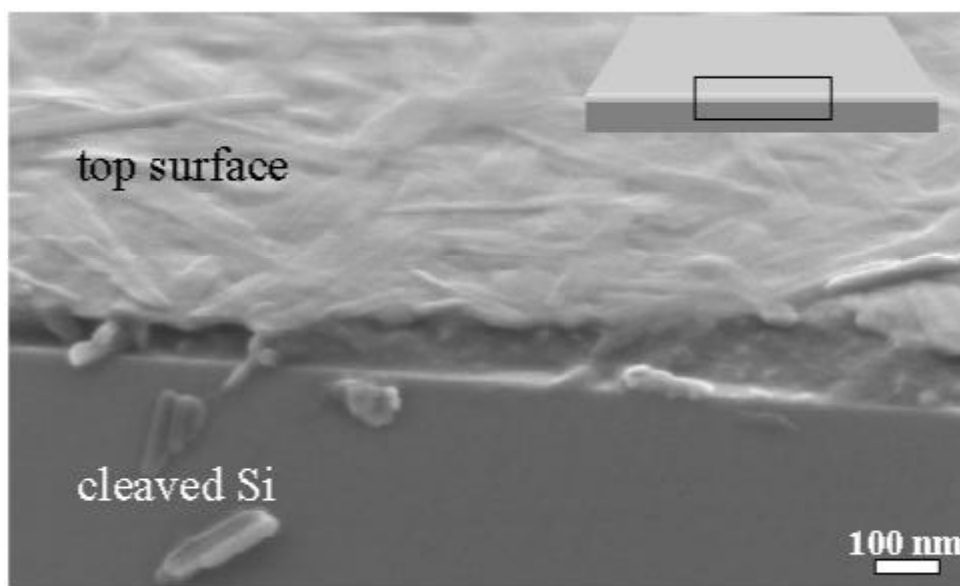


Figure 24: **Field emission SEM image of the HBC / perylene blend imaged with the cleaved surface tilted 15 degrees from normal to the incident electron beam**

Photodiodes formed by the evaporation of Al onto HBC-PhC₁₂ : perylene blend films spin-coated from 15 g/l chloroform solutions onto oxygen plasma-treated indium tin oxide (ITO), showed high quantum efficiencies. Figure 25 displays the external quantum efficiency (EQE) action spectra for a 40:60 HBC-PhC₁₂ : perylene device along with the solid state absorption spectra of HBC-PhC₁₂ and perylene films.

The EQE action spectra peaks above 34% near absorption bands associated with both materials demonstrating that efficient charge transfer takes place from either component.

Figure 26 depicts the current-voltage characteristics for a 40:60 blend photodiode in the dark and under 545 nm illumination.

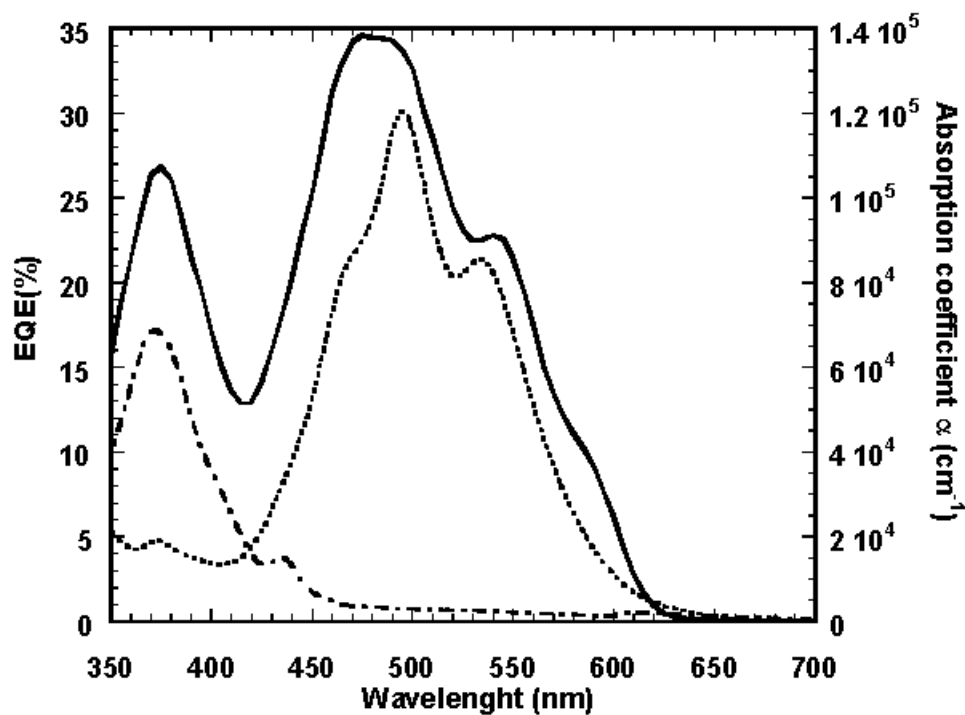


Figure 25: *External quantum efficiency (EQE) action spectra for the HBC-PhC₁₂ : perylene film*

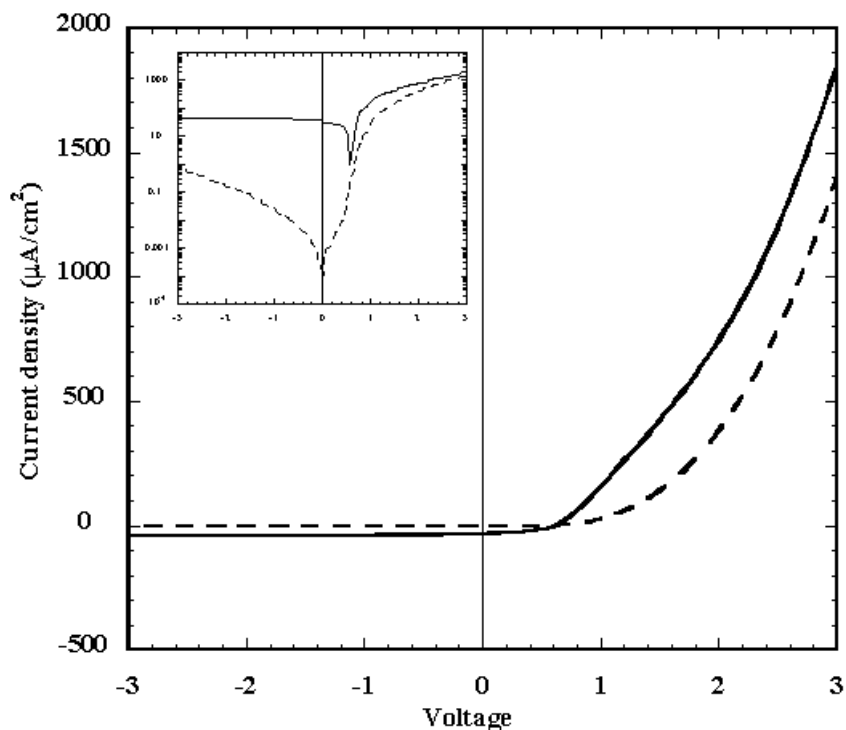


Figure 26: *Current-Voltage characteristic for the device with illumination at 545 nm*

The short circuit current and open circuit voltage under illumination were $-33.4 \mu\text{A}/\text{cm}^2$ and 0.6 V, respectively. The fill factor was 43%. The power efficiency maximum was 1.77%. It is thought that the high EQEs and open circuit voltages measured for these solution-processed devices are due to the high interfacial area within the bilayer structure suggested by the microscopic investigations presented above. The effectiveness of the vertical self-organization is supported by comparing the EQE action spectra measured for illumination from the anode and cathode side of the device. Figure 27 shows normalized EQE action spectra taken under these illumination conditions for a device with a thin cathode, corrected for absorption of the contacts and glass.

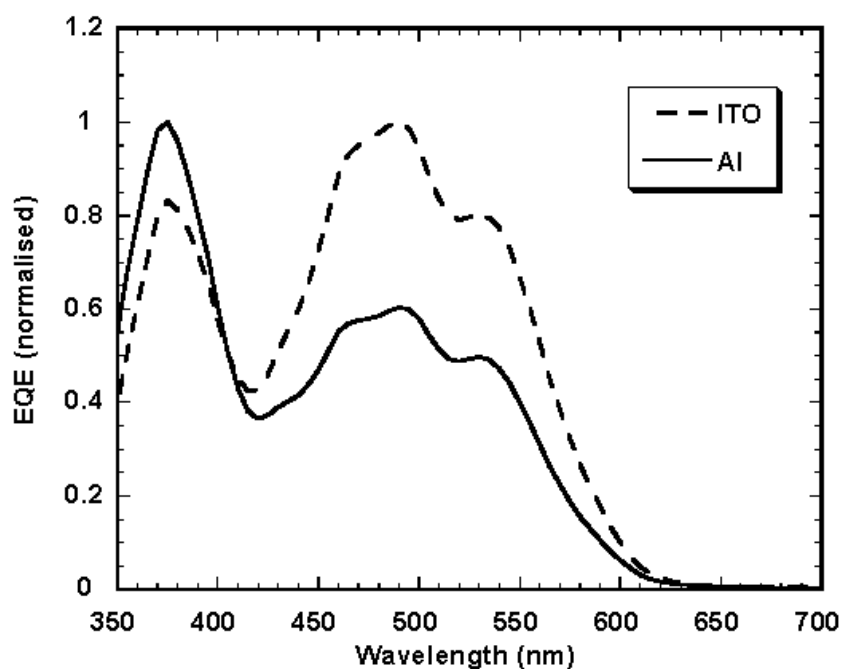


Figure 27: **Normalized EQE action spectra taken under illumination through the ITO and Aluminum electrode respectively corrected for absorption of the contacts and glass**

Illumination through the ITO electrode produces significant photoresponse for regions of the spectra corresponding to HBC and perylene absorptions due to the relative transparency of the HBC layer to longer wavelength light and the efficient dissociation of charge near the HBC – perylene interfaces. For illumination from the Al, the perylene response centered near 490 nm is reduced relative to the region of the action curve corresponding to HBC

absorption. This would be expected considering the attenuation of the longer wavelength light while traversing the perylene rich layer adjacent to the Al cathode before penetrating to the high interfacial area region where efficient photoexciton dissociation and charge collection can take place.

Two approaches have been followed to enhance charge separation in organic photovoltaic cells.^[140] The first (as applied above) is to use two-layer p-n junction devices while the second is to use a single layer of a donor-acceptor blend called a bulk D-A heterojunction. In these D-A blends, the donor moiety has a small ionization potential and good hole transport properties while the acceptor has a high electron affinity and efficient electron transport properties. Following also the first approach, Noma et al. reported the photovoltaic properties of the p-n heterojunction cell {ITO/perylene/ α -8Thiophene/Au}.^[141] This cell exhibits fairly good characteristics with a conversion efficiency of 0.6% for irradiation of white light. Similar to the discotic liquid crystalline HBC derivative utilized here, mesophase forming phthalocyanines have also been used as the electron-donor in organic solar cells.^[87] Petritsch and co-workers reported efficiencies approaching 0.5% for their phthalocyanine/perylene two-layer device. They reasoned that their device could not be further improved due to the fact that the phthalocyanine had to be annealed already at high temperatures (approximately 290°C) in order to align the sample, so that the axis of the molecule was perpendicular to the charge collecting electrodes. The results presented here, suggest that self-organization (other than alignment upon slow cooling from the isotropic liquid) can be exploited in organic photovoltaics to produce optimized structures for photoexciton dissociation and charge transport in a solution-processed materials system. This development brings together the simplicity of single step solution processing, an efficient combination of molecular materials, and multiplayer transport structure. Further optimization could prove this route to be a way towards a commercially-viable organic photovoltaic device.

3.2.7 HBC-PhC₁₂ as a semiconductor in organic field effect transistors

In Field Effect Transistors (FETs), current flows along a semiconductor path called the channel. At one end of the channel, there is an electrode called the source. At the other end of the channel, there is an electrode called the drain. The physical diameter of the channel is fixed, but its effective electrical diameter can be varied by the application of a voltage to a control electrode called the gate. The conductivity of the FET depends, at any given instant in time, on the electrical diameter of the channel. A small change in gate voltage can cause a large variation in the current from the source to the drain. This is how the FET amplifies signals. A scheme of the basic set up of a transistor is depicted in Figure 28.

A flexible transistor is one which, unlike present rigidly-structured transistors, can be successfully used in packages that can be curled up, wrapped, or bent, a quality that will enable users to - for example - have a display screen that can be rolled up.

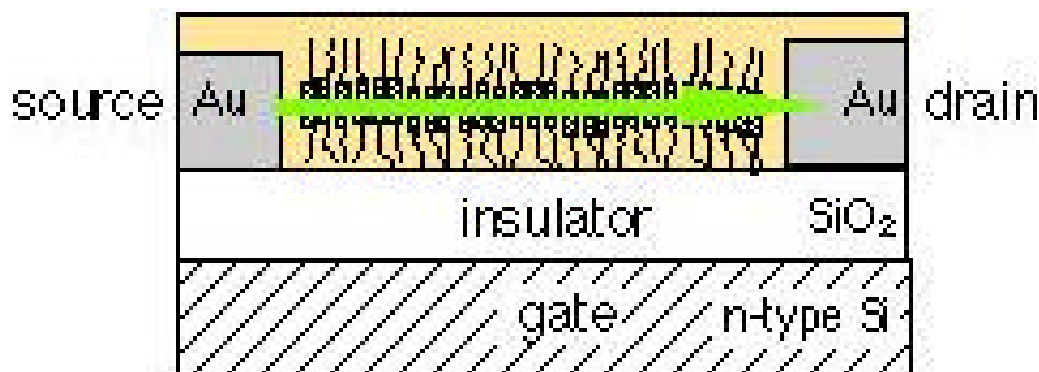


Figure 28: **Schematic view of a field effect transistor, channel length 2 – 20 μ m, channel width 3 μ m.**

Several factors have motivated engineers to conduct and continue research in organic semiconductor technology (Organic Field Effect Transistor (OFET)). One of these factors is cost. Organic materials are relatively cheap compared to silicon, but until recently, they have proven slow in terms of charge carrier mobility. Another factor that motivates research in OFET technology is handling

and application diversity. Organic materials allow easier and cheaper processing such as spin coating or printing. In applications they would permit for transistors to be fabricated on flexible surfaces, rather than on rigid materials.

A few extensive reviews on the development and principles of organic field effect transistors were recently published in the literature by Horowitz and Katz.^[142-144]

As Horowitz points out, during the build up process of a FET, the deposition of the semiconductor (polymers or organic molecules) is the determining step for the fabrication of the device. Here, solution-processed deposition, namely spin coating, is one of the most elegant ways to realize the production of a very homogeneous film. One requirement for the implementation of this technique is good solubility, which is unfortunately not present in a great number of conventional polymers.^[142] A second requirement for the utilization of the spin coating technique is a high viscosity solution, this however is not applicable to small organic molecules.^[142] From these two given points and the fact that HBC-PhC₁₂ **43** exhibits a) an extended aromatic core, b) high and constant charge carrier mobility, c) dramatically increased solubility, and d) enhanced film forming properties, i.e. liquid crystallinity at room temperature, it can be concluded that this new hexabenzocoronene derivative might be a promising candidate for implementation in OFETs. Other discotic materials such as phthalocyanines have been studied extensively for their application in organo-electronic devices.^[86, 142, 145-147] Their field-effect mobilities range between 0.0001 and 0.1 cm²/Vs.^[148-150] Although phthalocyanines have been reported to behave as both n- and p-type semiconductors, when implemented in OFETs they are all p-type. The leading problem with phthalocyanines remains their extreme sensitivity to oxygen.^[142]

In collaboration with Anick M. van de Craats in the group of Professor Friend, University of Cambridge, OFETs with HBC-PhC₁₂ **43** as the semiconducting material have been prepared and analyzed.

The performance of an FET is generally visualized by drawing its drain current I_d vs. drain voltage V_d curves for various gate voltages. This is called the output characteristic of the device. The sign of the drain current is governed by that of the majority carriers of the semiconductor. For an n-type semiconductor, I_d and

V_d are both positive, while they are negative in a p-type material. The curves can be divided into two regimes. At low drain voltage, the current follows Ohm's law and is proportional to V_d . This is the linear regime, where Equation 2.0 is valid.

$$I_d = \frac{Z}{L} C_i \mu (V_g - V_0) V_d \quad (2.0)$$

Here, Z and L are the channel width and length, C_i the capacitance of the insulator, μ the mobility of the majority carriers, V_g the gate bias and V_0 the threshold voltage. As the drain voltage increases, the device gradually enters the saturation regime where the drain current becomes independent of the drain bias. Equation 3.0 is often used to estimate the saturation current.

$$I_{dsat} = \frac{Z}{2L} C_i \mu (V_g - V_0)^2 \quad (3.0)$$

The mobility of the majority carriers is one of the most important parameters of a FET. It can be estimated from both the linear and the saturation current. The two estimations often disagree because Equation 2 relies on several assumptions that are not actually fulfilled in organic semiconductors. One of these is that the mobility is constant; that is, it does not depend on control parameters such as the gate voltage.

The transistor behavior of the apparatus built up with HBC-PhC₁₂ **43** was studied using the device structure depicted in Figure 28. HBC-PhC₁₂ performed as a p-channel transistor and operated as an accumulation-mode device. Figure 29 shows the typical source-drain current I_{sd} characteristics of an FET with HBC-PhC₁₂ as the semiconducting layer at different gate voltages. The material was deposited by spin coating onto SiO₂ and the channel length averages at 20 μm .

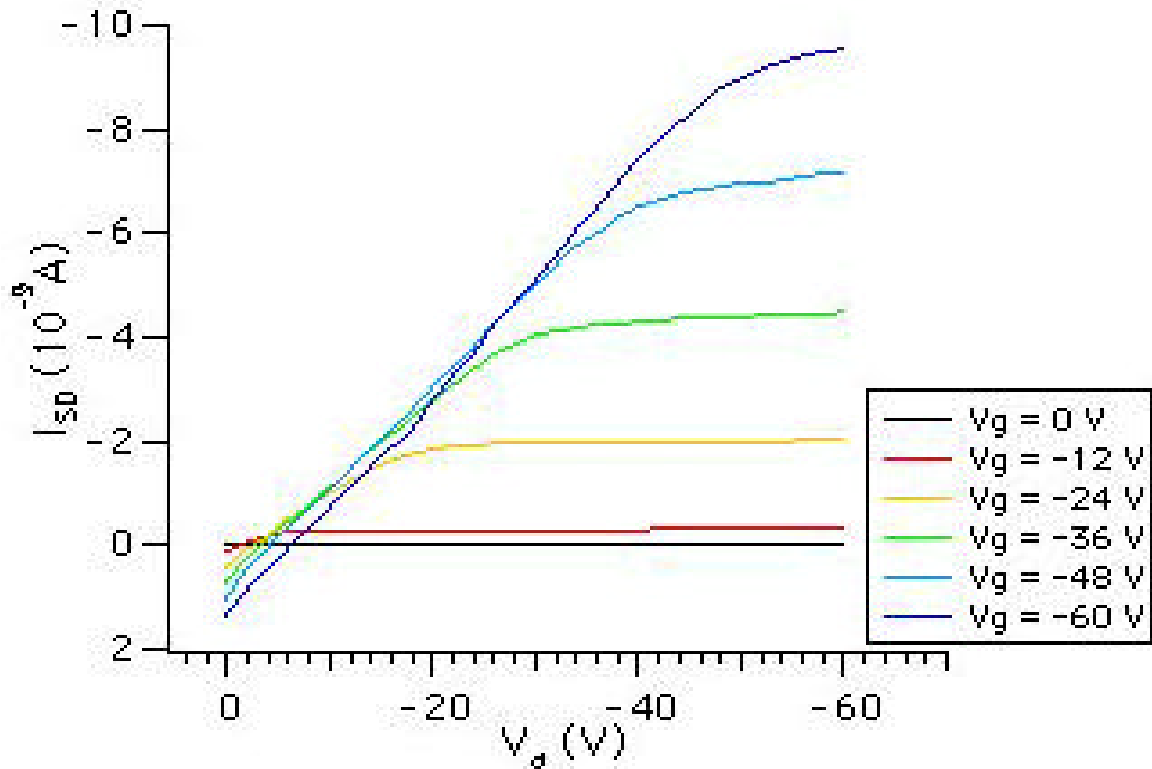


Figure 29: **The current-voltage characteristic of a FET made from HBC-PhC₁₂ with a channel length of 20 μ m and a channel width of 3 μ m operating in accumulation-mode at different gate voltages. (The FET measurements were performed by A. M. van de Craats in the group of Prof. Friend, Cavendish Laboratories, Great Britain)**

It is seen that the source–drain current increases with increasing gate voltage V_g . The device is p-channel material and works in the accumulation mode as evident from Figure 29. The field effect mobility was calculated from Equation 3.0. V_0 is the extrapolated threshold voltage and can be obtained from a plot of I_{sd} versus V_g after extrapolation of the linear region to the V_g axis as depicted in Figure 30. The determined threshold voltage is in the regime of -5 V.

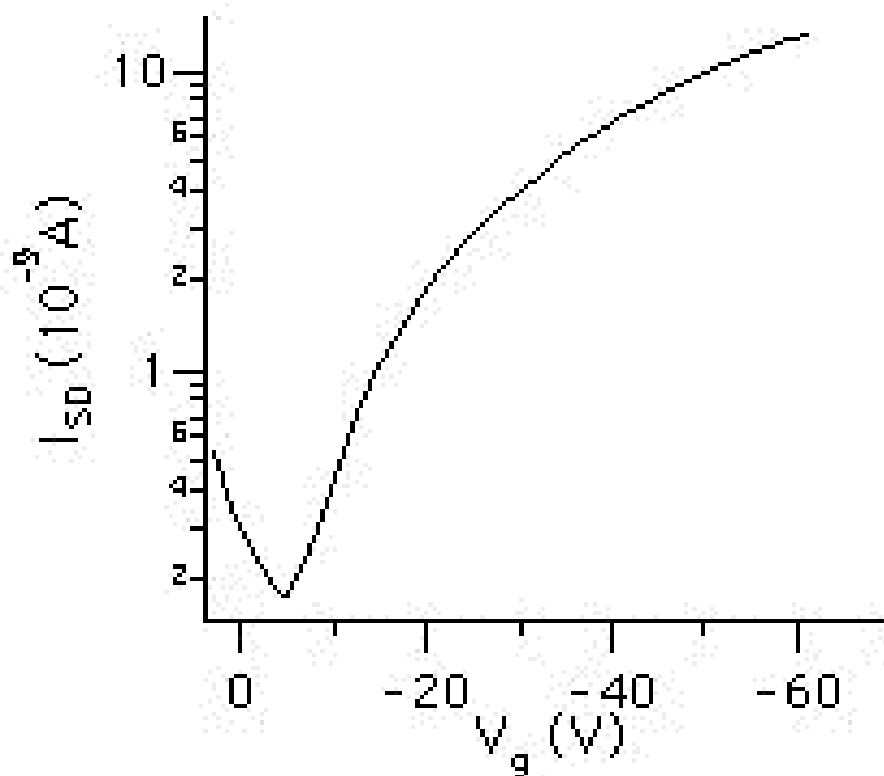


Figure 30: V_0 the extrapolated threshold voltage is obtained from a plot of I_{sd} vs. V_g after extrapolation of the linear region to the V_g axis. (The FET measurements were performed by A. M. van de Craats in the group of Prof. Friend, Cavendish Laboratories, Great Britain)

The field effect mobility calculated using Equation 3.0 is in the order of $10^{-5} \text{ cm}^2/\text{Vs}$ and can up to this point not be determined with more precision, since only a few initial measurements were conducted. However, the order of the mobilities is in the range of the ones reported for phthalocyanines.^[86, 145, 146] The high current modulation or on/off ratio was determined to be 5×10^4 this again is comparable to the results reported for discotic phthalocyanines. These initial experiments did indeed prove that HBC-Phc₁₂ has a potential relevance as a material for the utilization of discotics in organic field effect transistors. However, it is obvious that more detailed studies and further tuning of material and device fabrication have to follow.

3.3 Chiral and racemic branched-alkyl substituted HBCs – Synthesis and properties

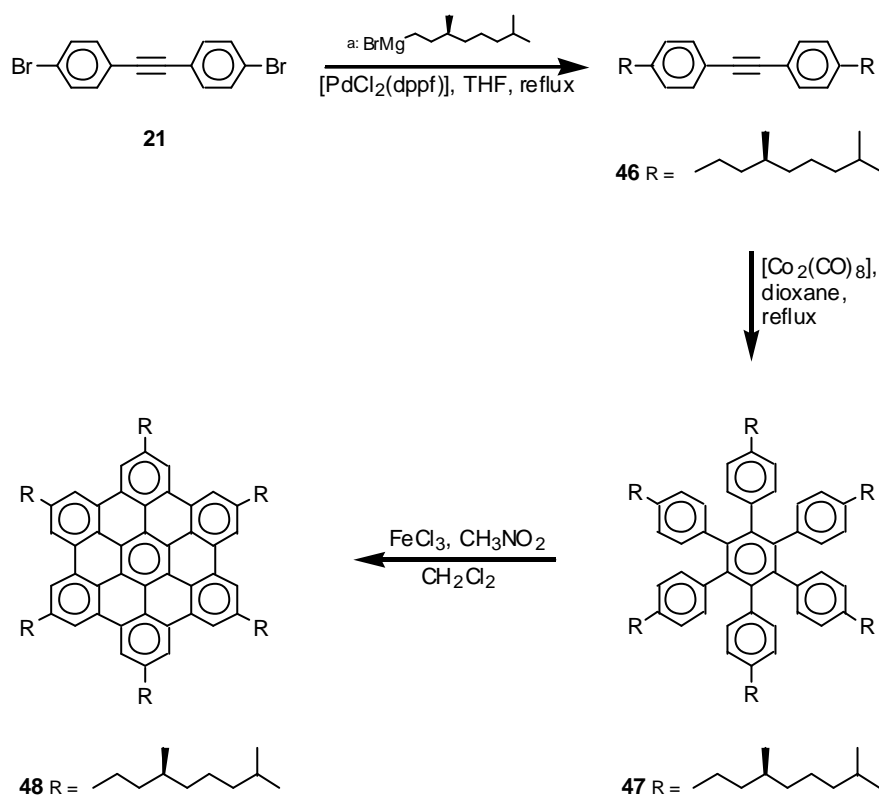
3.3.1 Synthesis and preparation of the chiral HBC-C₈*

Chirality has become one of the most important and complex topics of research in science today. The assembly and aggregation of molecules towards superstructures such as the double helix arrangement in DNA is one of the origins of life. Chirality in liquid crystals has been a focus point of interest^[151] since their first discovery by Reinitzer^[11] in 1888, where he discovered two derivatives of cholesterol which have asymmetric molecular structures, and are therefore optically active and chiral.^[151] They form chiral nematic mesophases which under certain circumstances have unusual optical properties, i.e. they can selectively reflect light. This special phase was named cholesteric mesophase. As already mentioned in the introduction the hexahexylthiotriphenylene^[45] derivative **12** exhibits a helical columnar phase and was the previous record holder for charge carrier mobilities of organic materials other than in single crystals.^[40, 45] It is generally agreed that the degree of order in an arrangement where the molecules are oriented in a helical fashion is higher than in non-helical aggregates. Since charge carrier mobilities strongly depend on order as reported for the helical phase of triphenylene derivative^[40, 45] **12**, the same “trick” was applied to the hexabenzocoronene core.

It was reported above that previous attempts^[28] to alkyl functionalize **21** under common Grignard coupling conditions using NiCl₂(dppe), NiCl₂(dppp), or Pd(PPh₃)₄ were unsatisfactory. Since the aryl-aryl coupling of **21** with two equivalents 4-*n*-dodecylphenyl-magnesiumbromide using the [PdCl₂(dppf)] catalyst gave great results, it was tried to apply this catalytic system again.^[104] The extension of this method to the coupling of alkylmagnesiumbromide species is outlined in Scheme 11. (*S*)-3,7-Dimethyloctylmagnesiumbromide is coupled with **21** under Kumada coupling conditions using [PdCl₂(dppf)]^[112] as the catalyst in THF, to yield the enantiomerically pure alkyl substituted diphenylacetylene **46** in 85% yield. This procedure is highly attractive,

especially when the group to be attached, "R", is either expensive, or must be prepared by multistep synthesis.

In a cyclotrimerization reaction under catalytic action of $\text{Co}_2(\text{CO})_8$ ^[152] **46** was transferred to the hexaphenylbenzene derivative **47**. This reaction has a yield of around 90% and the product can easily be purified using standard column chromatography. The final step for this reaction sequence is the oxidative planarization of the six pending phenyl rings in **47**, with concurrent loss of twelve hydrogens. The cyclodehydrogenation^[34, 104] is achieved by adding a solution of FeCl_3 in nitromethane to the hexaphenylbenzene precursors **47** in dichloromethane to afford the chiral alkyl substituted hexabenzocoronene (HBC- C_8^* , **48**). Isolated yields after purification using column chromatography and slow reprecipitation are of the order of 80%.



Scheme 11: **Synthesis of chiral hexaalkyl substituted hexabenzocoronene 48**

HBC **48**, substituted with chiral branched alkyl chains shows solubilities in common organic solvents more than ten times higher than HBC derivatives, substituted with n-alkyl chains, synthesized earlier by our group.^[26, 27, 31] The above introduced compounds have been characterized by ¹H- and ¹³C-NMR, UV-Vis spectroscopy, and FD-MS. As a typical example for the hexaalkyl-substituted HBCs, the ¹H-NMR spectrum of **48** is depicted in Figure 31.

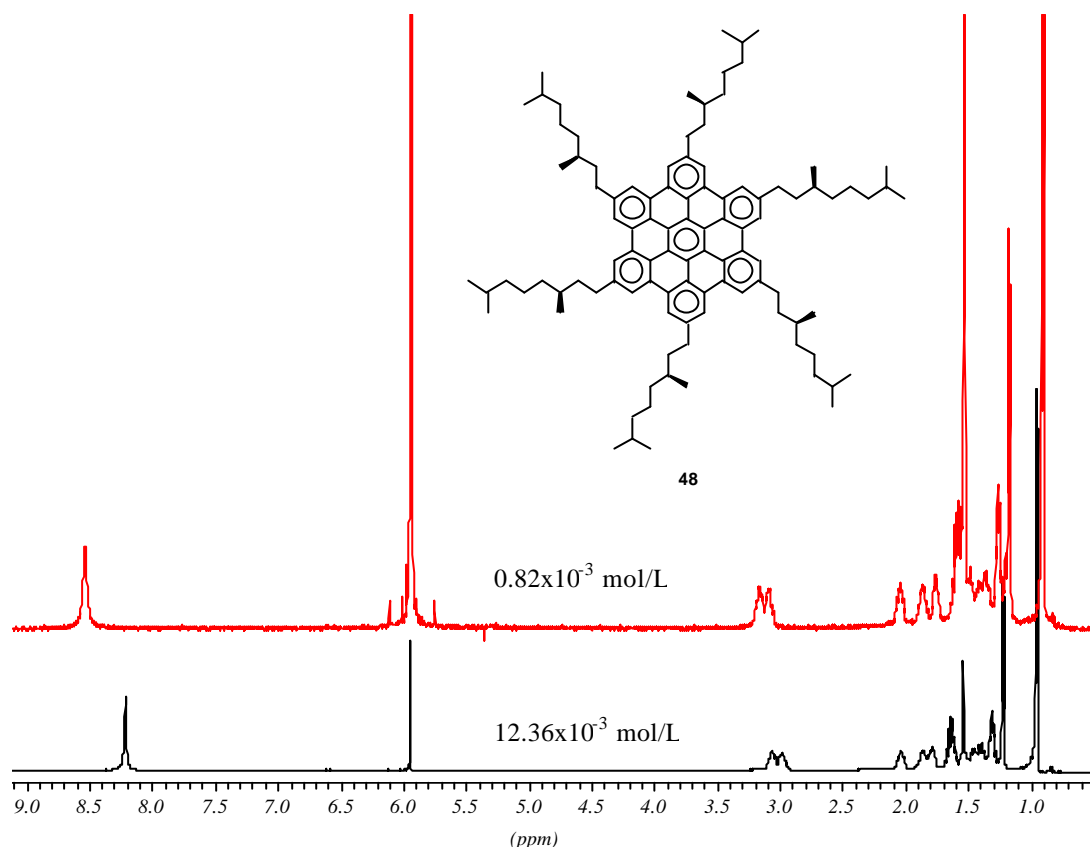


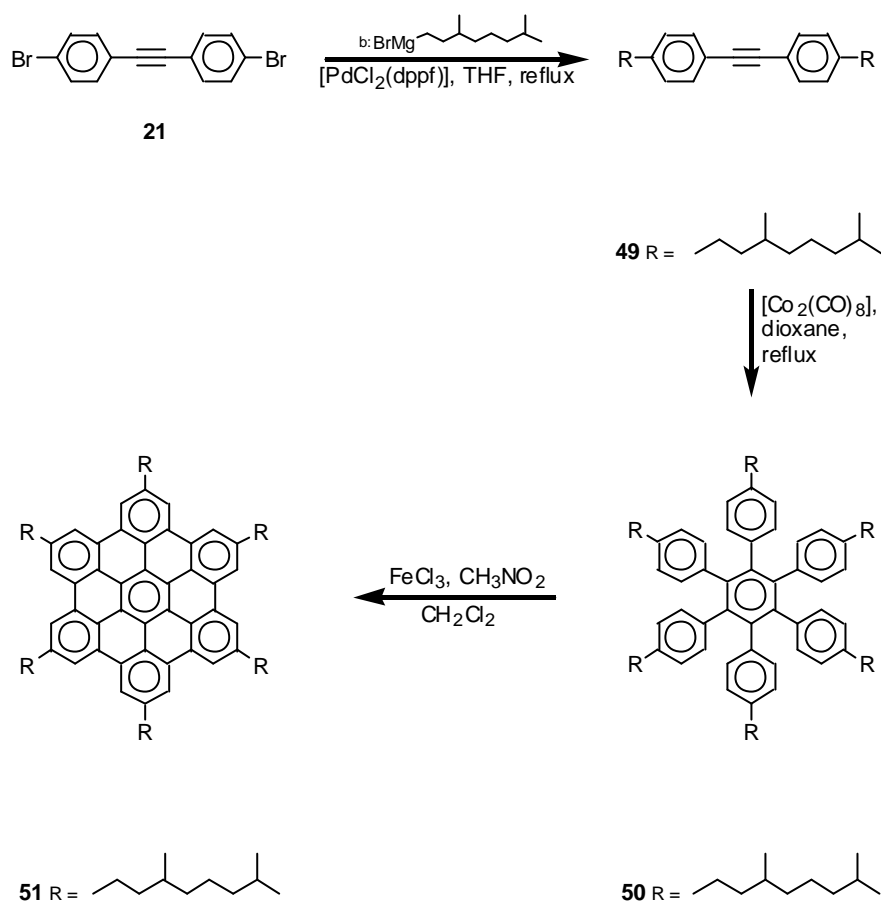
Figure 31: ¹H-NMR spectra of HBC-C₈* **48** at different concentrations (C₂D₂Cl₄, RT)

NMR spectroscopy is an important tool for investigating aromatic stacking. It has been used to investigate the π - π aggregation of phenylacetylene macrocycles^[115, 116] and columnar structures formed by hexabenzocoronene derivatives^[72] in the solid state. Here, the downfield signal at e.g. $\delta = 8.2$ ppm for the core protons of compound **48** clearly documents the diatropic character of these PAHs. These chemical shifts originate from a complex interplay of aromatic core size, perimeter type^[36] and aggregation. We have utilized ¹H-NMR spectra to qualitatively assess the strong influence that changes of

concentration have on the aggregation of these aromatic compounds in solution. As depicted in Figure 31, decreasing the concentration only from 12.36×10^{-3} mol/L to 0.82×10^{-3} mol/L results in a shift to lower field by $\Delta\delta = 0.33$ ppm for the signals arising from the core protons. A less pronounced shift to lower field can be observed for the α -CH₂ protons of the alkyl side chains. These shifts are attributed to a decrease in aggregation number with decreasing concentration, a conclusion which finds support in theoretical calculations^[83, 84] in concert with solid-state NMR measurements^[34, 80, 81, 104]. Similar shifts to lower fields are observed with increasing temperature (for a constant concentration) and when carbon disulfide (a good solvent for the aromatic core) is added. A Detailed investigation of these aggregation phenomena will be presented in Chapter 3.8.

3.3.2 Synthesis and preparation of the racemic HBC-C₈

It was demonstrated in the previous chapter that the synthesis of a hexabenzocoronene substituted with a chiral branched alkyl chain resulted in a material with promising properties. Mesophase behavior was studied by means of TGA and DSC, further phase characterization was carried out by means of X-Ray analysis of the bulk material and extruded fibers. However, the investigation whether helical superstructures are present when the HBC core is substituted with chiral side chains can only be determined with circular dichroism (CD) studies. In that respect, it was important to synthesize a non optically active version of HBC **48** namely hexabenzocoronene substituted with six racemic branched alky chains. The synthesis of the latter was carried out as depicted in Scheme 12.



Scheme 12: **Synthesis of racemic hexaalkyl substituted hexabenzocoronene 51**

Experimental details and reaction conditions were similar to the ones described earlier for HBC- C_8^* **48**. NMR spectroscopy and mass spectrometry revealed the same high purity of the obtained HBC- C_8 **51** as for the chiral derivative **48**.

3.3.3 Mesophase characterization of HBC-C₈* and HBC-C₈: TGA, DSC, and POLMIC analysis

Thermogravimetric analysis (TGA), differential scanning calorimetry (DSC) and optical polarization microscopy experiments were performed to study the phase behavior of HBCs **48** and **51**. A summary of the thermal behavior derived from these measurements is shown in Table 4.

Compound	Transition	<i>T</i> [°C]	ΔH [Jmol ⁻¹]
HBC-C₈* 48	K→Col _{ho} *	96	26
	Col _{ho} *→I	430	
HBC-C₈ 51	K→Col _{ho}	81	31
	Col _{ho} →I	420	

Table 4: *Optical, thermal, and thermodynamical data for compounds 48 and 51 (K = crystalline phase, Col_{ho} = ordered hexagonal columnar mesophase, I = isotropisation)*

At room temperature both compounds are yellow solids. Upon heating, these compounds enter the columnar discotic mesophase Col_{ho} which is of chiral nature in the case of **48**, as determined by CD spectroscopy (see next section), and therefore denoted as Col_{ho}*. For the chiral HBC **48**, a sharp endothermic peak at 96 °C (Figure 32) with a characteristic enthalpic value of 26 Jg⁻¹ indicates the transition from the solid phase into the chiral columnar mesophase. A phase transition 15 °C lower, *i.e.* 81 °C, as depicted in Figure 32, is observed for the racemic compound **51** with an enthalpic value of 31 Jg⁻¹. In the above cases, liquid crystallinity is maintained over a very large temperature range and no additional mesophase transitions were observed for any of the compounds. Thermogravimetry (TGA) revealed, as in previous cases that the beginning of decomposition starts at temperatures above 300 °C. This is again well below the isotropisation temperature of the compounds, so that annealing of the sample could not be achieved.

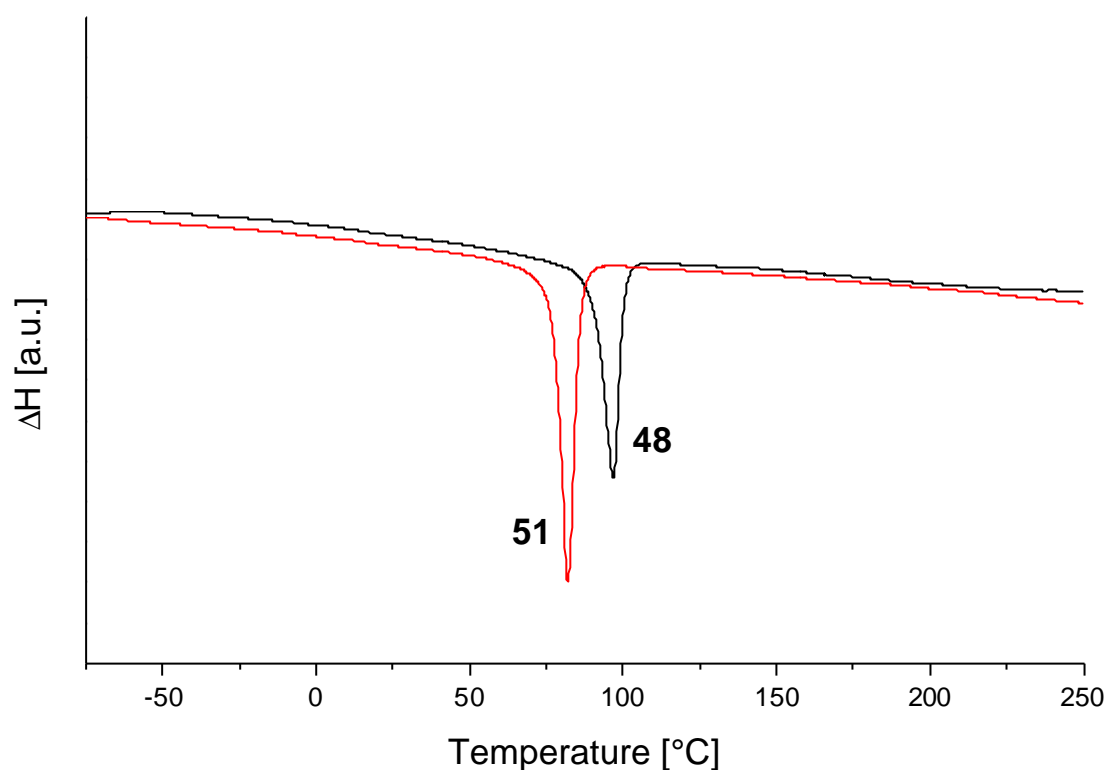


Figure 32: **Differential scanning calorimetry traces of HBC-C₈* 48 and HBC-C₈ 51**

Optical polarization microscopy studies were conducted for both the HBC derivatives introduced above, *i.e.* **48** and **51**, in order to study their thermal behavior as an addition to the DSC experiments. Drop-cast films were prepared from chloroform solutions. The films were heated at 10 K/min under a nitrogen atmosphere upon which the HBC samples changed from a crystalline to a liquid crystalline phase at temperatures reported in Table 4. The columnar hexagonal mesophases were preserved over large temperature ranges and finally entered the isotropic phase at above 400 $^{\circ}\text{C}$. Figure 33 (compound **48**) reveals textures which are typical for the columnar hexagonal mesophase formed from alkyl-substituted HBCs. These textures were observed after annealing the sample for a few minutes at the isotropisation temperature followed by cooling the sample to lower temperatures. These textures did not change until the sample temperature was decreased to the point of recrystallisation at approximately 96 $^{\circ}\text{C}$.

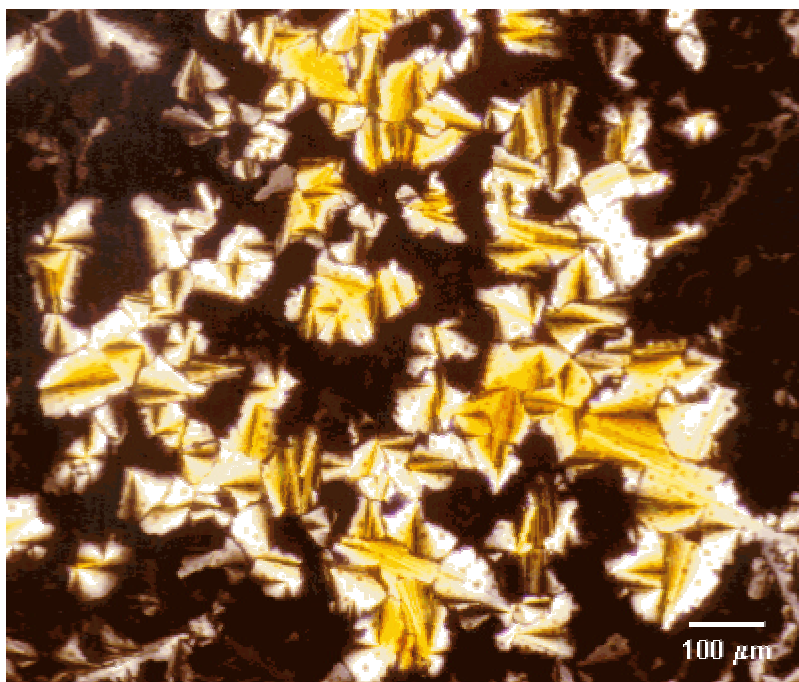


Figure 33: ***Optical textures of the hexagonal discotic mesophase of 48 observed under polarized light***

The fact that branching of the introduced alkyl chains has a positive impact on the processability of the described compounds has been demonstrated. Not only has the solubility been increased dramatically compared to HBCs substituted with *n*-alkyl chains (e.g. **6b**)^[26, 27] but also the phase transition temperature into the columnar hexagonal mesophase was reduced by up to 27 °C, without compromising the stability of the mesophase ($T_{\text{isotrop}} > 400$ °C). The synthesis of the racemic derivative **51** was important for several reasons. The mesophase formation of an optically pure material (**48**) can be documented properly only if the racemic version (**51**) of this compound is also subjected to similar characterization. DSC results showed that **48** enters the columnar hexagonal mesophase at 96 °C whereas **51** already shows a phase transition at 81 °C (Table 4).

These results are in contrast to those which van Nostrum and co-workers reported for chiral and racemic derivatives of phthalocyanines.^[15] They determined a higher phase transition temperature for the racemic than for the optically pure material, which lacks a crystalline phase, and only shows

amorphous behavior at low temperatures. This was not expected and could not be explained in the course of their experiments. In the case presented here, the results seem to be more in agreement with what one would expect. The optically pure HBC-C₈* **48** exhibits a higher order in the crystalline phase (see X-Ray results below) and thus it takes more energy, i.e. higher temperatures, to transfer the material from the crystalline phase to the mesophase compared to the racemic HBC-C₈.

3.3.4 Characterization of the chiral superstructure exhibited by HBC-C₈* **48**

Structural information for an optically active compound such as **48** can be obtained from circular dichroism (CD) spectroscopy which is an important method to study e.g. the helical orientation of discotic liquid crystalline aggregates^[151] such as triphenylenes^[153] and phthalocyanines^[15, 90, 154].

CD spectra can either be recorded from solution or films *i.e.* Langmuir-Blodgett or spincoated films. Here, thin films of the chiral HBC derivative **48** and the racemic **51**, prepared by spincoating concentrated solutions of **48** and **51** on quartz substrates were studied. These samples were investigated by means of CD spectroscopy at room temperature and the resulting spectra are given in Figure 34.

As expected, the racemic HBC derivative **51** did not show any CD effect at room temperature or after annealing in the mesophase at 90 °C. Under the same experimental conditions, the *all* chiral HBC derivative **48** showed two very strong, characteristic CD signals. A signal was observed at a wavelength of $\lambda = 361$ nm, with a positive Cotton-effect in the CD spectra as depicted in Figure 34. However, the most dominant signal in the spectra (Figure 34) is a so-called CD-couplet which traverses the baseline at $\lambda = 229$ nm. A CD-couplet is defined as the direct succession of two intensive Cotton-effects with reversed signs. Within this CD-couplet, compound **48** exhibits a positive Cotton-effect at higher wavelength and a negative one at lower wavelength.

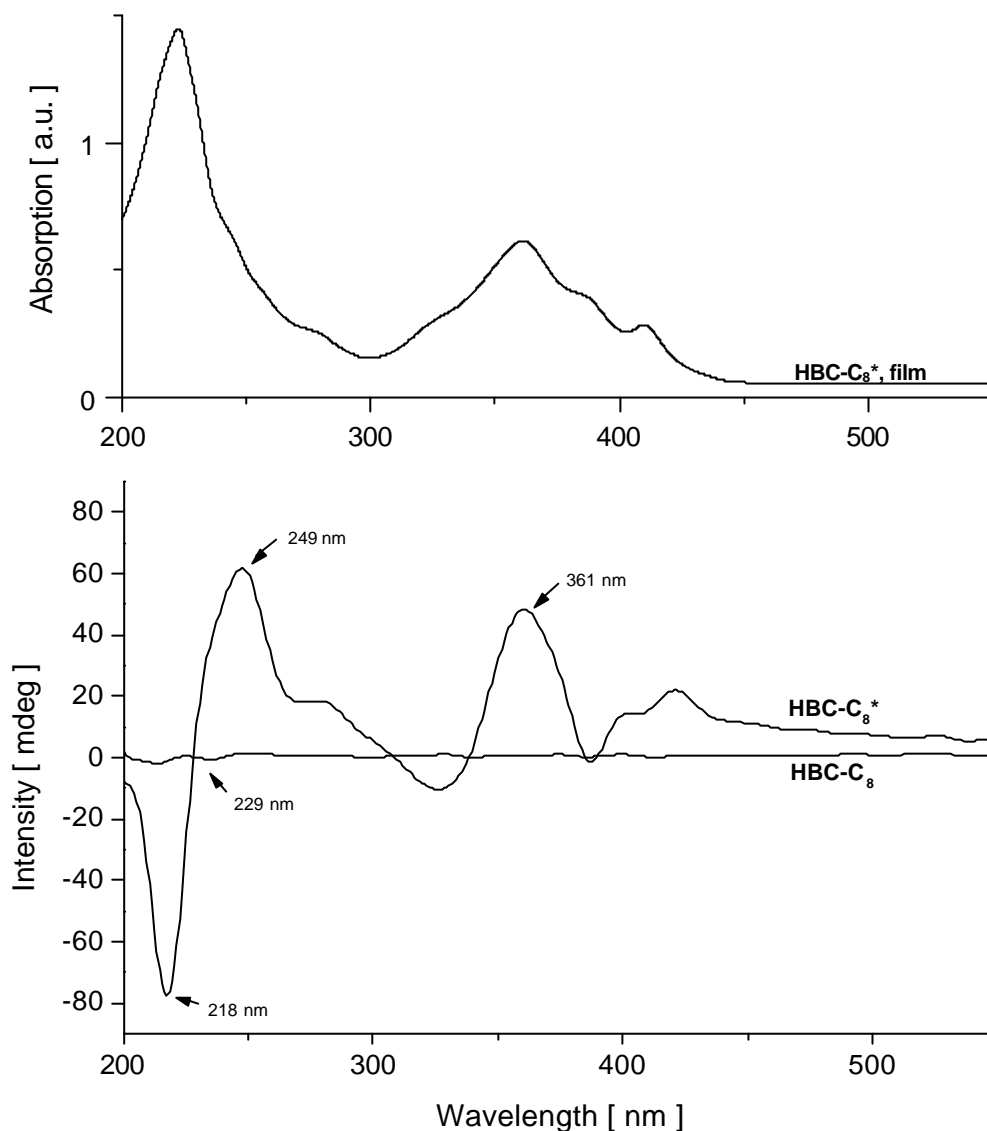


Figure 34: **UV-Vis and Circular dichroism spectra of HBC-C₈^{*} 48 and HBC-C₈ 51 recorded from spincoated films**

In contrast to optically active phthalocyanine derivatives,^[89, 90, 154] the prepared films of **48** did not have to be annealed at higher temperatures to achieve optical activity which is probably an indication of a very high degree of preorientation of the HBC discs before or during the preparation of the films. However, artifacts due to linear dichroism can be excluded, since the identical spectrum was obtained from the same sample after rotating by 90° in the plane normal to the incident light.

As depicted in Figure 34, spincoated films of **48** give very strong signals during CD measurements even without annealing whereas spincoated films of **51** do not show any signal (as expected). In a similar experiment, films of chiral phthalocyanines had to be annealed before CD signals could be recorded.^[15] In that case, identical alkyl chains were utilized, which were separated from the core by an oxygen (ether linkage) spacer. This not only increased the distance between the core and the stereogenic center, but also the added rotational freedom associated with an ether linkage may serve to further diminish the effect of the optically active center on the packing behavior of the core. In the case of the HBC **48**, the stereogenic center is very close to the center and therefore has a stronger, more direct influence on the packing behavior. The reported signals in the CD spectra (Figure 34) can be assigned as follows: Since compound **48** is per definition chiral, with six alkyl chains, each carrying a stereogenic center, the signal at $\lambda = 361$ nm results from the individual discotic molecule **48**. A similar signal is observed by UV/Vis spectroscopy, also at $\lambda = 361$ nm, assigned as the β -band according to Clar's nomenclature^[38, 155]. The presence of a CD-couplet as depicted in Figure 34 is an indication for the co-existence of two electronic excited states with individual transition dipole moments. These two dipole moments are assigned to two HBC-C₈* monomers. A splitting of the energy levels occurs, since the antiparallel orientation of dipole moments is energetically preferred. This gives rise to the two absorptions at different wavelengths ($\lambda = 249$ nm and 218 nm) in the CD-spectra. The energy difference is calculated to be $\Delta\lambda = 31$ nm (249 nm – 218 nm). This phenomena is commonly addressed as exciton-coupling or Davydov-coupling.^[156] This coupling occurs at a wave length where the UV/Vis spectra shows a presumed aggregation band, suggesting that the columnar superstructure formed by the individual HBC-C₈* molecules (compound **48**) might have a helical orientation. At this point these assumptions were made in analogy to the conclusions drawn from detailed experiments with triphenylenes^[157] and phthalocyanines^[15] but will be substantiated and strengthened by X-Ray diffraction studies conducted below.

Further, temperature dependent CD measurements on thin films as displayed in Figure 35 were conducted to probe the stability of the chiral superstructures.

Here, the temperature was increased in steps of 20 K from $-10\text{ }^{\circ}\text{C}$ up to $70\text{ }^{\circ}\text{C}$. The recorded CD signals lost intensity on the order of 20% during the course of heating, but never faded completely. However, upon increasing the temperature by an additional 20 K to $90\text{ }^{\circ}\text{C}$, the CD signal changed dramatically. The algebraic sign changed from a positive deflection to a negative one and lost intensity by around 80%. An increase of temperature by another 10 degrees shifted the signal slightly but further heating of the film by an additional 10 degrees did not result in a change of signal. Subsequent cooling of the sample back to room temperature surprisingly did not result in a change of signal back to the original.

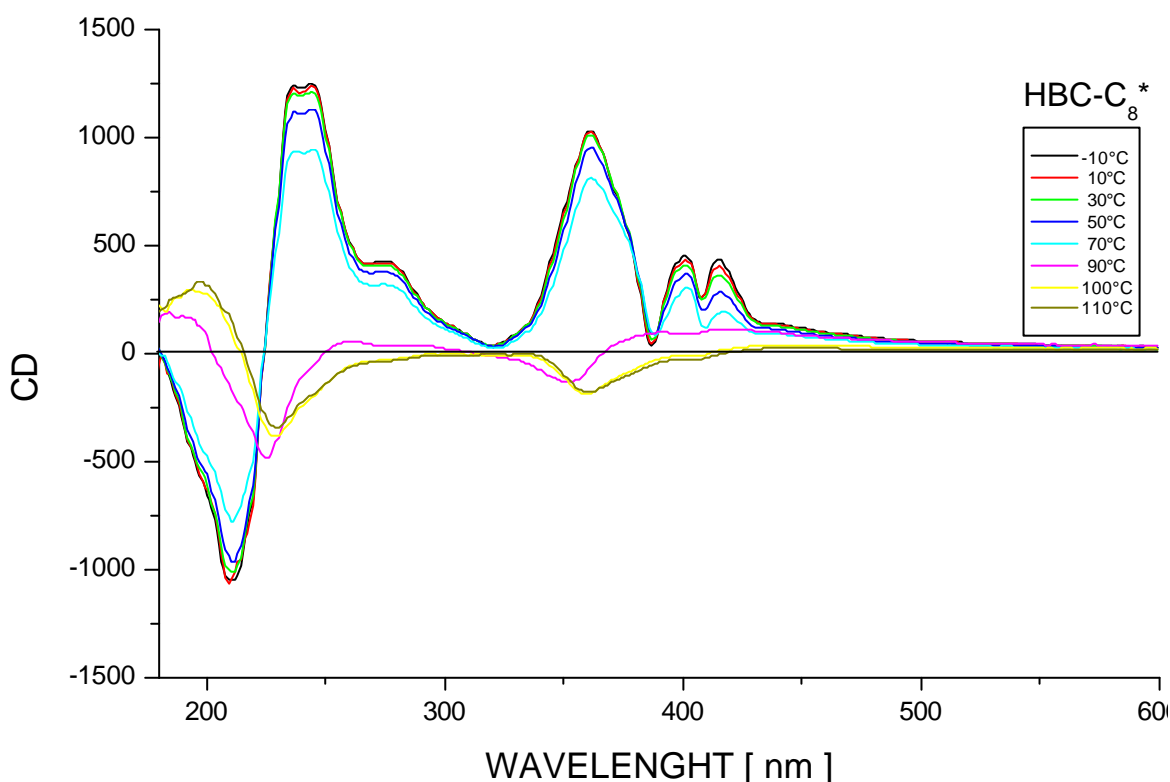


Figure 35: **Temperature dependence of optical activity for HBC-C₈***

From the initial temperature-dependent CD experiments, it can be concluded that the chiral aggregates formed must be relatively stable up to $70\text{ }^{\circ}\text{C}$ since the intensity only dropped by a factor of 20% when the temperature was raised from $-10\text{ }^{\circ}\text{C}$ up to $70\text{ }^{\circ}\text{C}$. The loss of intensity is attributed to higher mobility of the alkyl side-chains leading to the formation of more mobile, but still chiral,

aggregates. However, on heating the sample up to 90 °C, close to the entry into the discotic mesophase at 96 °C, the uni-axial rotation should drastically increase, which might change the overall orientation of the helical arrangement of the molecules resulting in a drastic change of the CD signal.

The above described phenomenon could be caused by the fact that in the temperature regime between –10 °C and 70 °C the chiral hexabenzocoronene **48** is in the crystalline phase, as demonstrated in Chapter 3.3.3. In the crystalline phase it is most likely that the HBC cores are oriented in a typical herringbone fashion as demonstrated for HBC **6b** (Figure 36, left).^[31, 34, 81] When the sample reaches the phase transition temperature at around 90 °C, reorientation into the columnar phase takes place (Figure 36, right). This reorientation would naturally cause a change of the CD signal depicted in Figure 35. On cooling back the sample to room temperature no further change of the CD signal was observed. This could be explained by the presence of a frozen-in or supercooled columnar orientation.

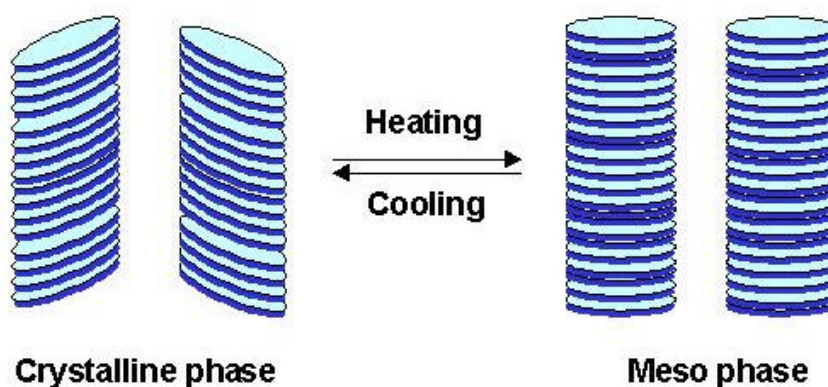


Figure 36: *Temperature dependent transition from the “Herringbone” (left) to the columnar orientation (right)*

An extensive prediction of this reorientation process of the HBC discs, leading to the drastic change of the CD signal, cannot be made without temperature dependant X-Ray characterization. These X-Ray measurements were conducted on oriented samples of HBC-C₈* **48**. Orientation was achieved by drawing fibers from an extruder which was kept at a constant temperature of 60 C. The obtained fibers were approximately 1mm in diameter and between 1

and 2 cm long. The experimental setup for the X-Ray analysis of the obtained fibers is depicted in Figure 37.

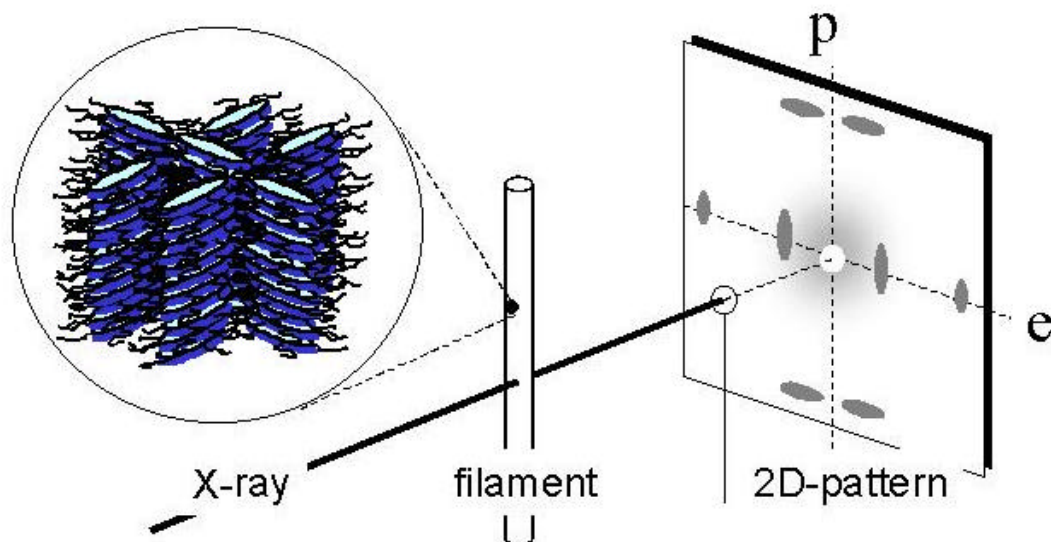


Figure 37: **Experimental setup for the X-Ray analysis of extruded filaments**

The high degree of order is revealed by their X-Ray diffraction diagrams as shown in Figure 39. When the sample was heated to 130°C, i.e. HBC-C₈* **48** has entered the mesophase, the equatorial reflections indicate the columns standing parallel to the stretching direction having a slight tilt with respect to the column axis as indicated by the splitting in the meridional reflections. In other words, the HBC discs are aligned along the fiber axis in a two-dimensional hexagonal lattice as demonstrated in Figure 38 (left).

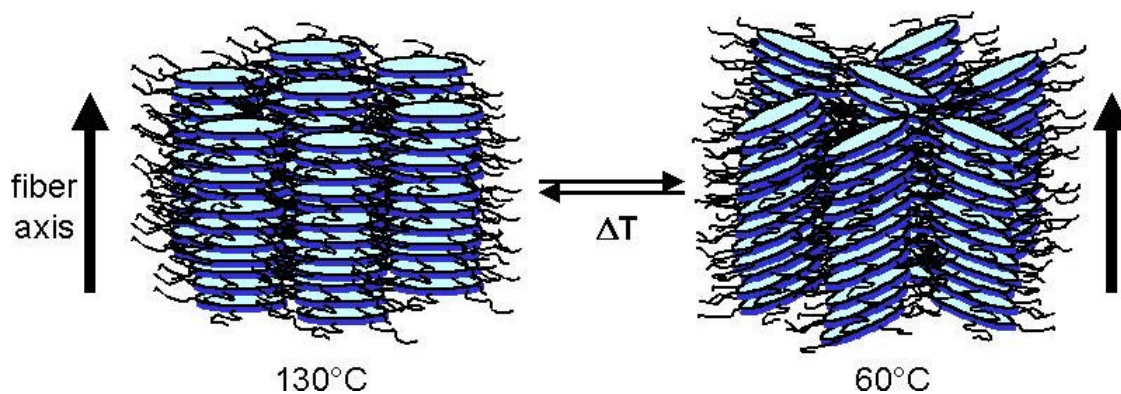


Figure 38: **Temperature dependent transition from the mesophase 130°C (left) to the crystalline phase 60°C (right)**

On the meridian the observed scattering intensity stems from the discotic subunits stacked parallel to each other with a mean distance of around 3.68 Å between the HBC sheets. The intercolumnar distance was calculated to be 26.4 Å. These findings correspond well with earlier measurements on a variety of different HBC derivatives.^[28] Crystallization of the fiber below the phase transition temperature at 96°C affects the orientational order dramatically. To guarantee that the material has completely crystallized these X-Ray measurements were conducted at 60°C, i.e. 36°C below the transition temperature.

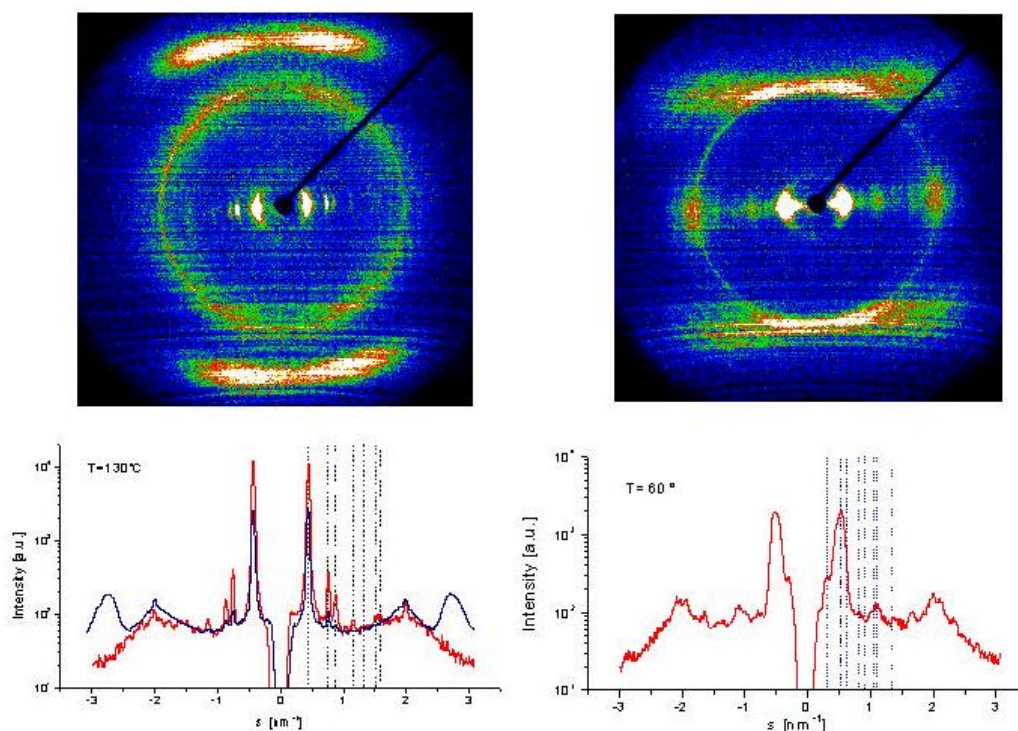


Figure 39: *X-Ray diffraction pattern of an extruded fiber of HBC-C₈* 48 at 130°C (left) and 60°C (right)*

As can be seen from Figure 39, the discs are no longer oriented parallel to the fiber axis but have adopted a tilted “Herringbone” fashion with a tilt angle of around 30° with respect to the filament axis as depicted in Figure 38 (right). It is also obvious that the discs are now stacked with a greater distance between the individual HBC sheets. Here, a periodicity h along the fiber axis is deduced with $h = 5\text{nm}$. The mean intercolumnar distance was calculated to be 37.8 Å. However, what is drastically different from other HBC derivatives investigated^[28]

earlier and in particular the racemic version of HBC-C₈* **48**, namely HBC-C₈ **51**, is the scattering in the corners of the X-Ray diffractogram depicted in Figure 39 (right). This pattern is more clearly demonstrated by the schematic representation in Figure 40. Here, (a) and (b) mark the common Bragg reflections by the columnar lattice (a) and the diffuse ring scattering by the aliphatic side chains (b). Quite different from other HBCs (c) marks the interference between HBC discs belonging to the same columns.

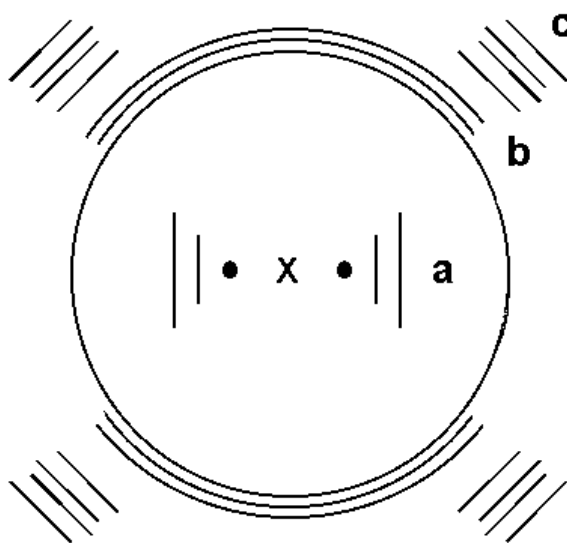


Figure 40: **Schematic representation of the X-Ray diffractogram of HBC-C₈* **48** at 80°C (Figure 39); (a) Bragg reflections by the columnar lattice, (b) diffuse ring scattering by the aliphatic side chains, (c) interference between HBC discs belonging to the same columns**

A very similar X-Ray pattern was reported by Levelut and co-workers^[158] for a discotic triphenylene derivative that was substituted with chiral alkoxy side chains. Here, a chiral superstructure was assigned to the aggregates after careful analysis of the X-Ray diffractograms.^[158] Several years later, Heiney and Jeu also confirmed helical intracolumnar order in oriented strands of a hexahexylthiotriphenylene, these were investigated by X-Ray diffraction studies.^[159] The supramolecular structure that was proposed for this triphenylene derivative is depicted in Figure 41, C. In this case adjacent molecules along a column minimize steric hinderance via a relative rotation of roughly 45°.^[159] From this,

the helical pitch P was determined to be $P = 7.92$, i.e. after approximately 8 molecules the helical motif is repeated.^[159]

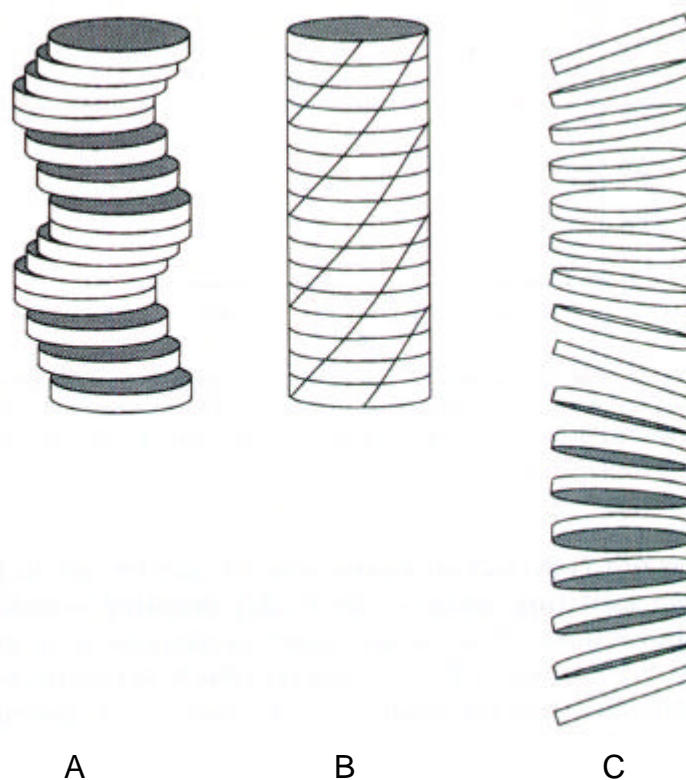


Figure 41: **Schematic representation of the three possible helical arrangements for discotic liquid crystals, reproduced from van Nostrum et.al.**^[15]

The structure and physical properties of an optically active, metal-free phthalocyanine derivative were investigated by van Nostrum and co-workers.^[15] Here, different from the previously described chiral triphenylene derivatives, X-Ray diffraction and circular dichroism studies indicated that the molecules are stacked in columns which have a hexagonal arrangement and a left handed helical superstructure. This structure is, according to van Nostrum and co-workers, best represented by column C in Figure 41.

The findings of this investigation also lead to the conclusion that the discs of HBC-C₈* **48** are arranged in a helical fashion as depicted in Figure 41, C. The following facts rule out arrangements A and B for HBC-C₈*: if the stacking pattern in the crystalline phase would follow motif B, the distance of the

individual HBC sheets along the columnar axis would be the same for all HBC discs in a column and very similar to the distance found in the columnar mesophase at 130°C. That the distance varies along the columnar axis in the crystalline phase can be derived from the scattering recorded in the X-Ray diffractogram pointed out in Figure 40, area c). The same holds true for arrangement A, further the intercolumnar distance in case A is expected to be larger due to the horizontal shift of the sheets along the column. Therefore, the third superstructure, C, is proposed for HBC-C₈* **48**. The molecules are slightly tilted and, along the columnar axis, the normal of the HBC-plane gradually rotates around the columnar axis forming a helical superstructure.

3.4 Combination of branched-alkyl chain substitution and phenyl-ring insertion – Two new HBC derivatives with C₆-symmetry

3.4.1 Synthesis and preparation of the chiral HBC-PhC₈* **61** and the racemic HBC-PhC₈ **62**

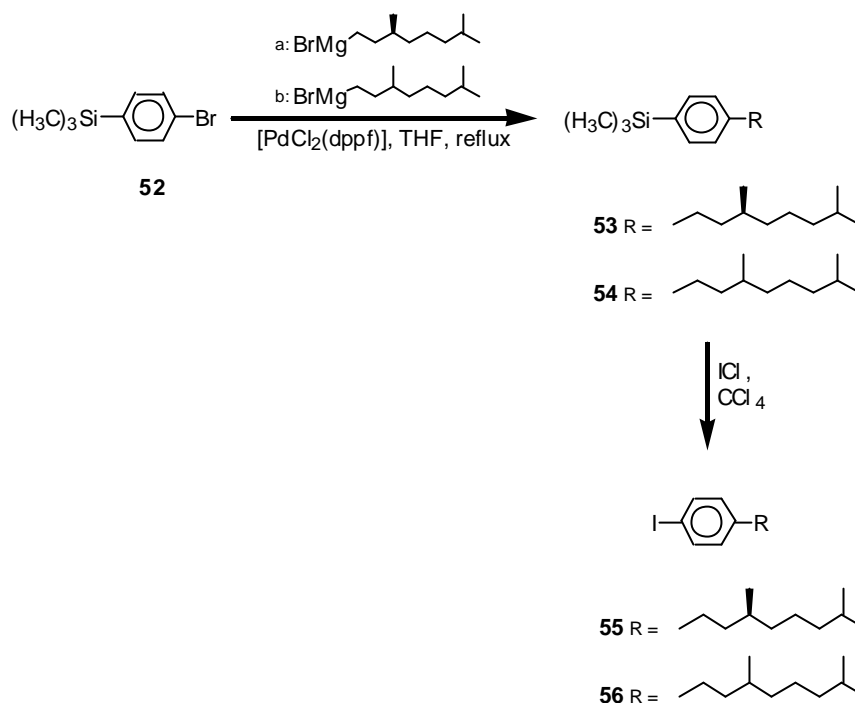
From the elucidations of the previous chapters the following can be directly deduced:

- Insertion of a phenyl ring between the aromatic HBC core and the six pending alkyl chains increased intracolumnar order,
- Liquid crystallinity at room temperature was observed for HBC-PhC₁₂ **43** resulting in a constant charge carrier mobility over a large temperature range,
- Substitution of the aromatic HBC core with six branched alkyl chains increased solubility and processability dramatically,
- Introduction of a chiral branched alkyl chain resulted in the formation of chiral aggregates with a helical superstructure.

Thus, it is desirable to combine the two advantageous properties discussed above: a) insertion of a phenyl ring and b) substitution with a branched alkyl chain. The resulting hexabenzocoronene should combine room temperature liquid crystallinity, highly oriented columnar discotic mesophases (possibly even helical), and enhanced solubility and processability.

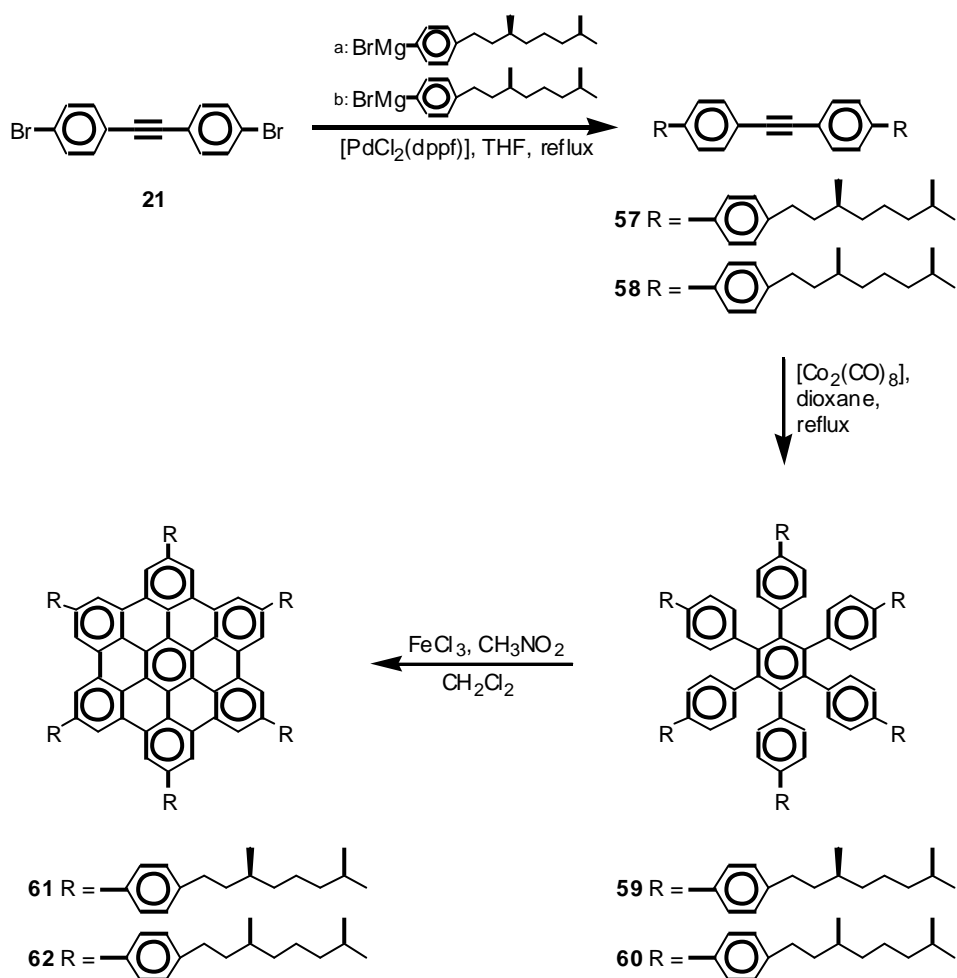
The synthesis of the starting compounds (**55** and **56**) for this endeavor is depicted in Scheme 13. In the first step, the commercially available 1-bromo-4-trimethylsilylbenzene (**52**) was alkylated under common Kumada-coupling condition with a chiral and a racemic side chain to afford **53** and **54**, respectively.^[104, 112] The trimethylsilyl-substituted alkyl-benzenes **53** and **54** were converted to the iodine-functionalized derivatives **55** and **56** via

electrophilic substitution^[160] using iodine monochloride in carbon tetrachloride as outlined in Scheme 13.^[106]



Scheme 13: **Synthesis of phenyl-alkyl precursors 55 and 56**

The aryl-aryl coupling of two equivalents of **55** or **56** with 4,4'-dibromodiphenylacetylene (**21**) was carried out under the same conditions described earlier^[37, 104], to yield the chiral biphenyl acetylene **57** and its racemic derivative **58** (Scheme 14).^[106] In a cyclotrimerization reaction in dioxane under catalytic action of Co₂(CO)₈, **57** and **58** were both transferred to the hexabiphenylbenzene derivatives **59** and **60** respectively. The cyclodehydrogenation^[34] (Scheme 14) was carried out by adding a solution of FeCl₃ in nitromethane to the precursors **59** and **60** to afford the hexabenzocoronenes HBC-PhC₈* **61** and HBC-PhC₈ **62**. Isolated yields after purification using column chromatography and slow re-precipitation were of the order of 80%.^[106]



Scheme 14: **Synthesis and preparation of the chiral HBC-PhC₈* 61 and the racemic HBC-PhC₈ 62**

All materials reported here were fully characterized by NMR spectroscopy, mass spectrometry, and UV/Vis spectroscopy. The NMR spectra show the expected number of signals, but the chemical shifts in the ¹H-NMR spectra were again strongly concentration dependent as already observed and reported for HBC-PhC₁₂ **43**. This is due to the strong π - π interactions in the aggregates which are present even at low concentrations. Figure 42 shows a characteristic ¹H-NMR of HBC-PhC₈* **61** in *p*-dichlorobenzene at 150 °C. As reported for HBC-PhC₁₂ **43**, high temperatures had to be utilized to resolve the signals of the aromatic HBC core and the pending phenyl rings.

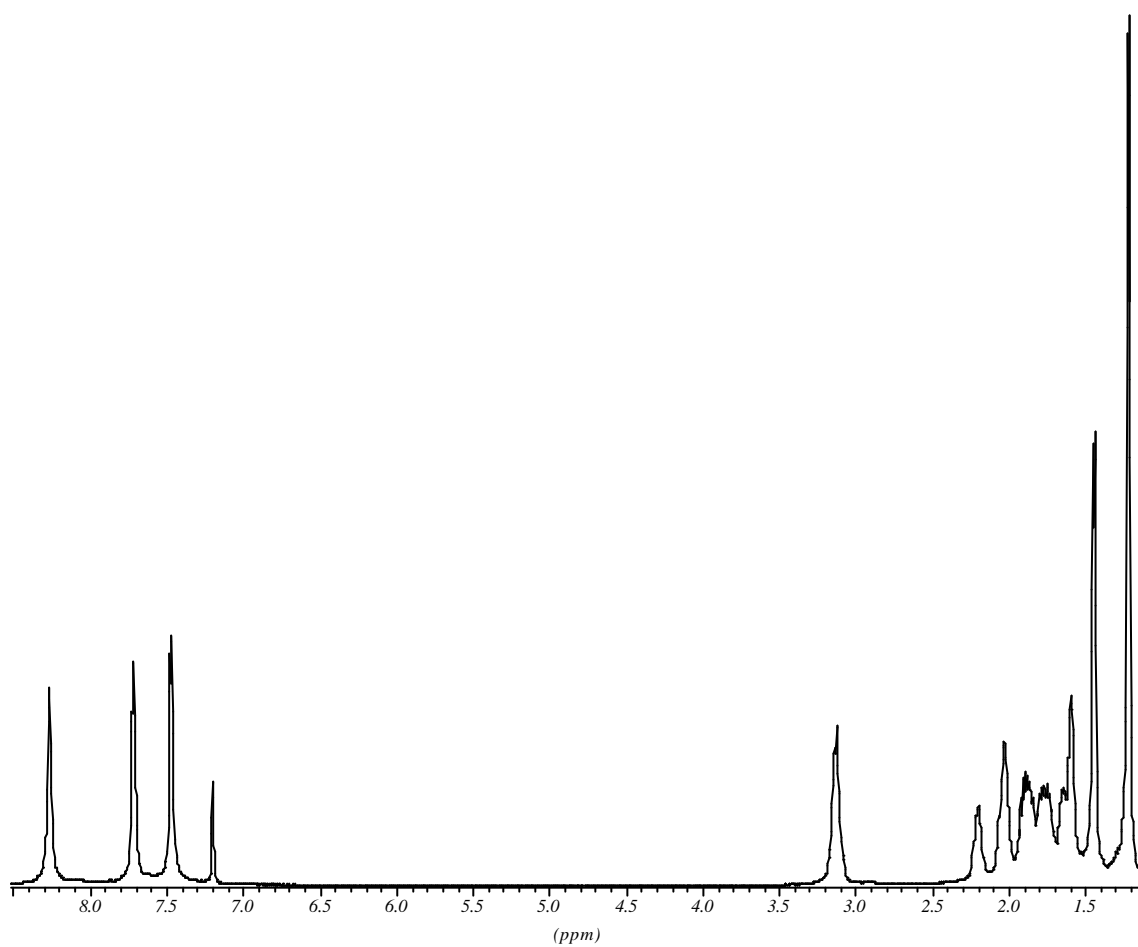


Figure 42: $^1\text{H-NMR}$ of HBC-PhC_8^* **61** in *p*-dichlorobenzene at 150 °C

As mentioned before a detailed investigation of the aggregation phenomena will be presented in Chapter 3.8.

3.4.2 Mesophase Characterization of HBC-PhC₈* **61** and HBC-PhC₈ **62**: TGA and DSC analysis

Thermogravimetric analysis (TGA), differential scanning calorimetry (DSC) and optical polarization microscopy experiments were performed to study the phase behavior of HBCs **61** and **62**. A summary of the thermal behavior derived from these measurements is shown in Table 5:

Compound	Transition	T [°C]	ΔH [Jmol ⁻¹]
HBC-PhC₈* 61	K→Col _{ho} *	< -100	
	Col _{ho} *→I	> 400	
HBC-PhC₈ 62	K→Col _{ho}	-44	3
	Col _{ho} →I	> 400	

Table 5: *Optical, thermal, and thermodynamical data for compounds 61 and 62 (K = crystalline phase, Col_{ho} = ordered hexagonal columnar mesophase, I = isotropisation)*

At room temperature, both compounds are very soft yellow solids. On heating a freshly prepared sample of HBC-PhC₈* **61**, no endothermic or exothermic peak was observed with DSC as can be seen from Figure 43. This and the presence of birefringence at room temperature, detected by means of optical microscopy, is prove of the fact that HBC-PhC₈* **61** is liquid crystalline over the entire temperature range (-100 to 250 °C) monitored with DSC.

Contrary to the chiral HBC-PhC₈* **61**, the racemic HBC derivative, namely HBC-PhC₈ **62**, depicts a phase transition from the crystalline phase to the liquid crystalline phase at – 44 °C. For both the samples, **61** and **62**, the isotropisation temperature was this time in excess of 400 °C, as monitored with optical microscopy, and thus well above the beginning of decomposition. TGA analysis revealed that the onset for decomposition starts for both HBC derivatives at around 300 °C.

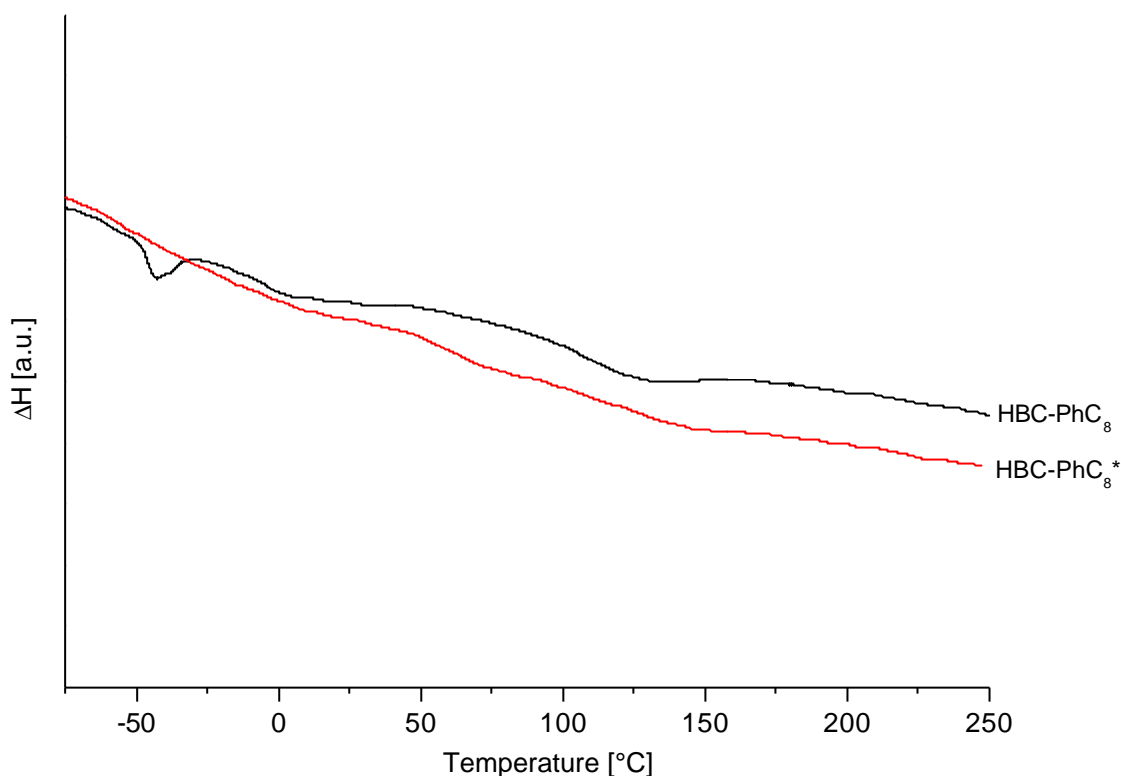


Figure 43: **Differential scanning calorimetry traces of HBC-PhC₈* 61 and HBC-PhC₈ 62**

It follows from the above that again no annealing procedure can be conducted to orient the samples as demonstrated for triphenylenes^[45, 161] and phthalocyanines^[15, 154].

3.4.3 Circular dichroism studies for HBC-PhC₈* 61

Circular dichroism (CD) spectroscopy was used to obtain detailed information related to optical activity about the superstructure present in the solid state of the material and to gain further information about the aggregates formed by HBC-PhC₈* **61** in solution. Investigations concerning the superstructure of this chiral HBC derivative were accomplished via CD spectroscopy on spincoated films. All films were prepared by spincoating a chloroform solution (15mg/mL) onto a quartz substrate. These samples were investigated at different

temperatures starting at $-10\text{ }^{\circ}\text{C}$ in 20K intervals up to $90\text{ }^{\circ}\text{C}$, the resulting spectra are shown in Figure 44.

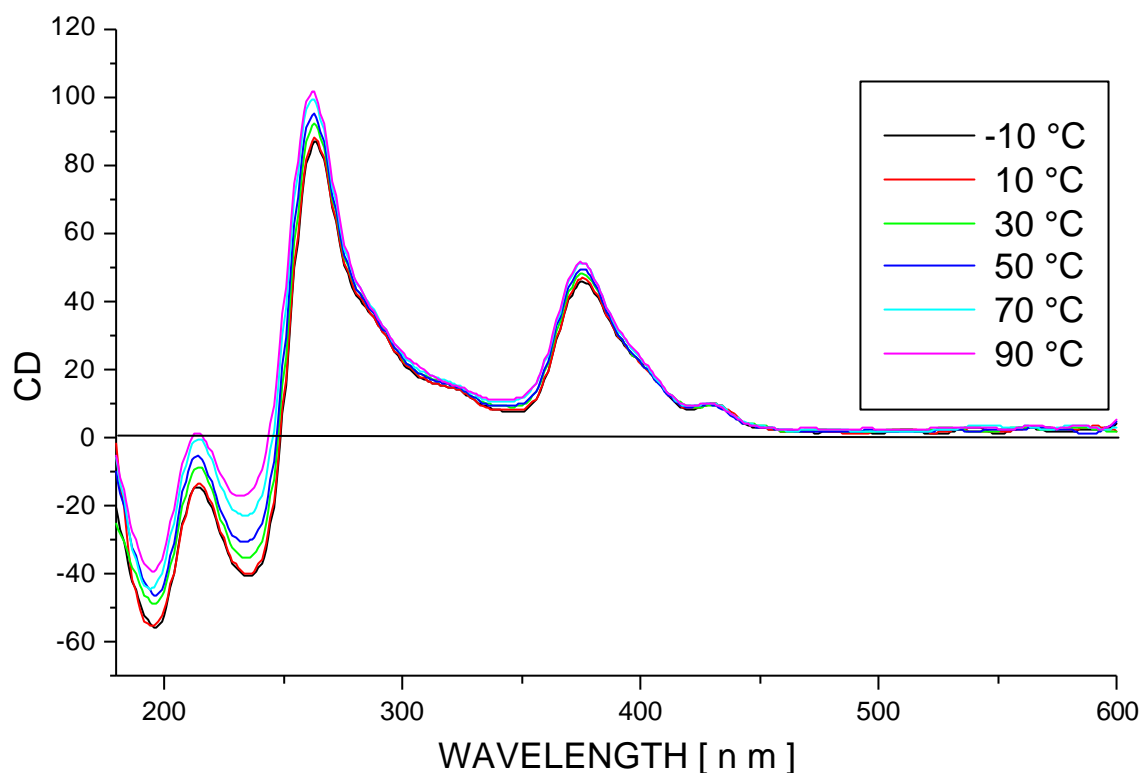


Figure 44: **Temperature dependence of optical activity for HBC-PhC₈* 61 spincoated onto a quartz substrate**

As expected, the racemic HBC derivative **62** did not show any CD effect at room temperature or at elevated temperatures. Under the same experimental conditions, the *all* chiral HBC derivative **61** showed two very strong, characteristic CD signals and two smaller ones. A signal was observed at a wavelength of $\lambda = 375\text{ nm}$, with a positive Cotton-effect in the CD spectra as depicted in Figure 44. However, the most dominant signal in the spectra also with a positive Cotton-effect (Figure 44) has its maximum at $\lambda = 263\text{ nm}$. The two weaker signals, both with a negative Cotton effect were observed at $\lambda = 235\text{ nm}$ and $\lambda = 195\text{ nm}$.

Some of the reported signals in the CD spectra (Figure 44) can be assigned as follows: Since compound **61** is per definition chiral, with six alkyl chains, each carrying a stereogenic center, the signal at $\lambda = 375\text{ nm}$ is resulting from the

individual discotic molecule **61**. A similar signal is observed by UV/Vis spectroscopy, also at $\lambda = 375$ nm, assigned as the β -band according to Clar's nomenclature^[38, 155]. The most prominent signal at $\lambda = 263$ nm is in the region where the pending phenyl rings also show an absorption maximum in the UV/Vis spectrum. This is in a way self explaining since the chiral alkyl chains are directly attached to the phenyl rings and thus experience the strongest influence from the nearby stereogenic center resulting in the most dominant signal at $\lambda = 263$ nm.

When the sample was subsequently heated from -10 °C to 90 °C, the CD activity increased by 15 % of magnitude. However, in contrast to the temperature dependant studies carried out with HBC-C₈* **48**, the CD signal did not change its algebraic sign but increased intensity upon heating. DSC analysis revealed that between -100 °C and 250 °C, no phase transition occurred, i.e. HBC-PhC₈* preserves the columnar hexagonal superstructure over a temperature range of 350 K. Therefore, upon heating the sample and observing the CD signal, no drastic change was monitored other than for HBC-C₈* **48** where a strong change was reported when the material entered the mesophase at 96 °C.

The concentration-dependent shift of the signals in the ¹H-NMR spectra of HBC-PhC₈* **61** were attributed to the formation of aggregates in solution resulting from the strong π - π interaction of the aromatic HBC cores. This aggregation behavior was also investigated by means of temperature-dependent CD spectroscopy. Dilute solutions of HBC-PhC₈* **61** and HBC-PhC₈ **62** in chloroform were prepared, then the temperature was increased in steps of 10 K from -10 °C up to 60 °C. Again, the racemic HBC derivative **62** did not show any CD effect. The recorded CD signals lost intensity on the order of 60% during the course of heating, but never faded completely as depicted in Figure 45. Due to the low concentration of the solution the resolution of the recorded signals is very poor but still interpretable.

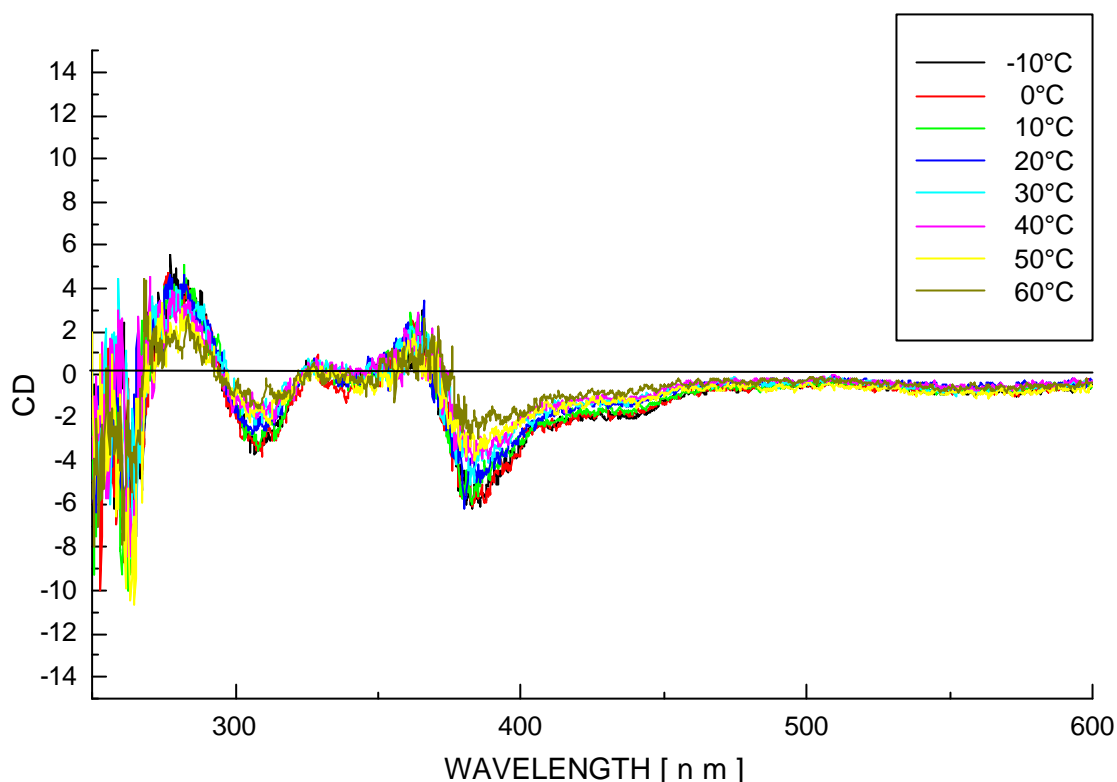


Figure 45: **Temperature dependence of optical activity for HBC-PhC₈* 61 measured in a chloroform solution**

Similar to the CD spectra recorded when the HBC derivative was spincoated onto a quartz substrate (Figure 44), the strongest CD signal (Figure 45) was observed at $\lambda = 278$ nm. This is again in the region where the pending phenyl rings absorb in the UV/Vis spectrum giving rise to the conclusion that the phenyl rings really exhibit the strongest influence of the attached chiral side chains.

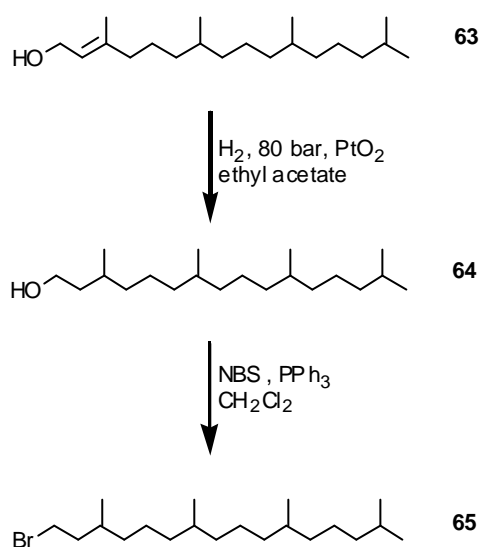
Van Nostrum and co-workers reported that chiral phthalocyanines did not show any optical activity in solution but only displayed CD activity on annealed Langmuir-Blodgett (LB) films.^[15] This hints at the fact that HBCs form stronger aggregates even at low concentrations as a direct consequence of their large aromatic core which is three times the size of triphenylene.

3.5 HBC-C₁₆: A room temperature liquid crystal with a lowered isotropization temperature

3.5.1 Synthesis and preparation of HBC-C₁₆

In order to obtain more information about the influence of the hydrocarbon side chains that are attached to the HBC core (e.g. HBCs **6a-d** or HBC-C₈* **48** and HBC-C₈ **51**) on the mesophase characteristics, a new HBC derivative substituted with six long branched alkyl chain was synthesized. A number of research groups have recently demonstrated that when branching points are introduced into the aliphatic side chains of discotic liquid crystals, the temperature range over which the columnar mesophase is stable, is widened.^[89, 162] However, the type of mesophase formed was not affected by the introduction of the branching points. An additional effect of this structural modification was the lowering of the isotropization temperature. Schouten and co-workers reported that for discotic phthalocyanines, the temperatures for the transitions from the discotic mesophase to the isotropic liquid were reduced by 175 °C upon changing the alkyl substitution from a pentoxy to a branched dodecaoxy chain.^[90] As already mentioned in the previous chapters, for any alkyl or phenyl alky substituted HBC, it was so far not possible to observe the transition into the isotropic melt without reaching the beginning of decomposition first. Stimulated by the drastic decrease of the melting point in the case of phthalocyanines^[90] substituted with long branched alky chains, the same `trick` was played for HBC. A literature survey revealed that the longest alkyl chain utilized for the decoration of triphenylenes^[163] and phthalocyanines^[164, 165] was hexadecyl. Herein the above two cases, isotropization temperatures of 322 and 196 °C were reported.^[163-165] Considering the fact that branching of alkyl chains demonstrably^[89] stabilizes the mesophase without altering the superstructure, a branched hexadecyl alkyl chain was selected for the peripheral decoration of HBC. These chains are derived from phytol **63** (Scheme 15) which is universally distributed in green plants as a component of the chlorophyll molecule, in which it is present in ester combination, and as a component part of phylloquinone (Vitamine K₁) and

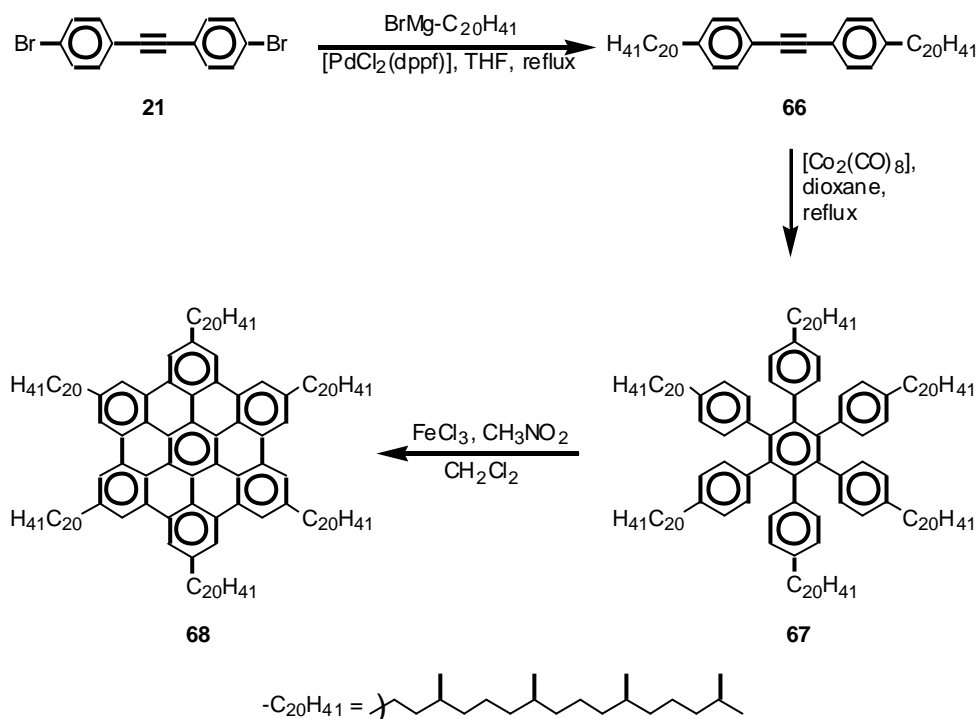
tocopherols (Vitamine E).^[166] Commercially available phytol, 3,7,11,15-tetramethyl-hexadec-2-ene-1-ol (**63**) was hydrogenated according to a modified procedure of Gramatica^[166] reported earlier in this work to yield compound **63** as demonstrated in Scheme 15.^[37] Replacement of the hydroxyl group by a bromine atom was carried out using N-bromosuccinimide and triphenylphosphine in methylene chloride (Scheme 15).^[167]



Scheme 15: **Hydrogenation and bromination of phytol 63 resulting in alkyl chain 65**

The following steps, leading to the substituted HBC-C₁₆ **68** as depicted in Scheme 16, were carried out according to procedures used before by our group.^[37, 104] 3,7,11,15-tetramethyl-hexadecylmagnesiumbromide was coupled with **21** under Kumada coupling conditions using [PdCl₂(dppf)]^[112] as the catalyst in THF to yield the alkyl substituted diphenylacetylene **66** as a colorless oil in 50% yield. In a subsequent cyclotrimerization reaction under catalytic action of Co₂(CO)₈^[152] **66** was transferred to the hexaphenylbenzene derivative **67** with 85 % yield. The resulting crude product was easily purified using standard column chromatography. The final step for this reaction sequence was the oxidative planarization of the six pending phenyl rings in **67**, with concurrent loss of twelve hydrogens. The cyclodehydrogenation^[34, 104] was carried out by adding a solution of FeCl₃ in nitromethane to the hexaphenylbenzene precursors **67** in dichloromethane to afford the alkyl substituted

hexabenzocoronene **68**. Isolated yields after purification using column chromatography and slow re-precipitation were of the order of 80%.



Scheme 16: **Synthetic pathway leading to HBC-C₁₆ 68**

The resulting HBC derivative contains six alkyl chains with sixteen carbon atoms and four branching methyl groups, and is henceforth referred to as HBC-C₁₆ **68**. The optical appearance is very much like that of a resin. The bulk material has a dark yellow color and is malleable at room temperature.

3.5.2 Mesomorphic properties: DSC and optical microscopy of HBC-C₁₆ 68

In order to detect phase transitions and to determine the corresponding transition temperatures and enthalpies, differential scanning calorimetry (DSC) was performed on HBC-C₁₆. The heating and cooling rates were 10 K/min. Figure 46 shows the recorded DSC curve for compound **68**. The peak onset in the DSC is defined as the transition temperature. During the first heating run, the sample gave rise to two exothermic peaks; subsequent cooling and heating showed both peaks to be reversible. Figure 46 only shows the third heating run,

here the peak at $-36\text{ }^{\circ}\text{C}$ is related to the crystalline to mesophase transition ($\text{K}\rightarrow\text{Col}$). When heating HBC-C_{16} , the peak at $231\text{ }^{\circ}\text{C}$ corresponds to the mesophase to isotropic phase transition ($\text{Col}\rightarrow\text{I}$). The isotropic phase lasts until $300\text{ }^{\circ}\text{C}$; above this temperature the HBC derivative **68** starts to decompose as determined by thermogravimetric analysis.

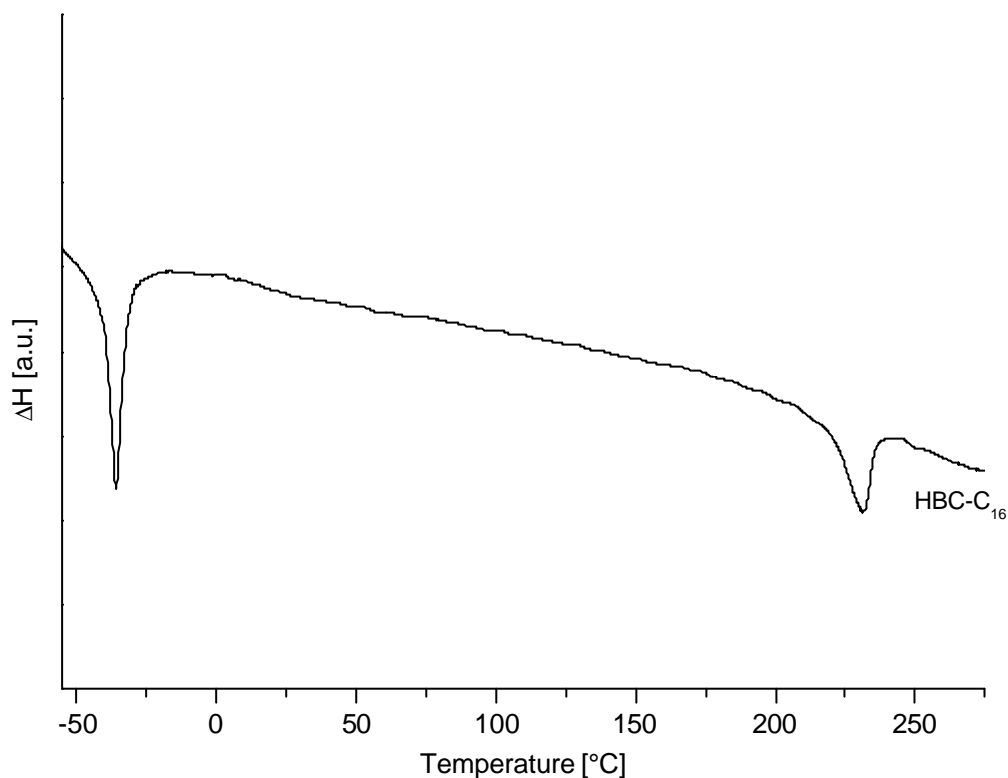


Figure 46: **Differential scanning calorimetry traces of HBC-C₁₆ 68**

This is the first time that thermodynamically stable isotropic phases have been obtained for mesomorphic hexabenzocoronenes which are peripherally substituted with nonfunctionalized alkyl chains.

Table 6 shows the DSC data, together with data obtained earlier in our group^[26, 27, 34, 37] for hexabenzocoronenes substituted with unbranched (HBCs **6a-c**) and branched (HBCs **48, 51, 68**) alkyl chains.

Compound	T [°C]	
	K→Col	Col→I
HBC-C ₁₀ 6a	124	>420
HBC-C ₁₂ 6b	107	417
HBC-C ₁₄ 6c	114	>420
HBC-C ₈ 48	96	~430
HBC-C ₈ 51	81	~420
HBC-C ₁₆ 68	-36	231

Table 6: *Phase transition temperatures of peripherally hexasubstituted hexabenzocoronenes with branched and unbranched alkyl chains*

The reduction of the melting point by branching and lengthening the attached alkyl chain is thought to be related to additional steric crowding by neighboring chains as a consequence of the latter, and to more conformational disorder in the vicinity of the branch. This causes the aliphatic chains to melt at lower temperatures, thus reducing the transition temperature to the liquid crystalline state.

When a sample of HBC-C₁₆ **68** is placed between two glass slides at room temperature, the dark yellow, spreadable substance is found to be birefringent. No definite texture can be observed under the crossed polarizers, possibly due to the mechanical distortion. However, it seems certain that this HBC derivative exhibits permanent liquid crystalline behavior even below room temperature. Upon heating, a highly fluid isotropic liquid appears above 231 °C. Upon slow cooling, a fan-shaped texture appears at 225 °C as depicted in Figure 47. This texture is characteristic for a hexagonal columnar mesophase.^[89]

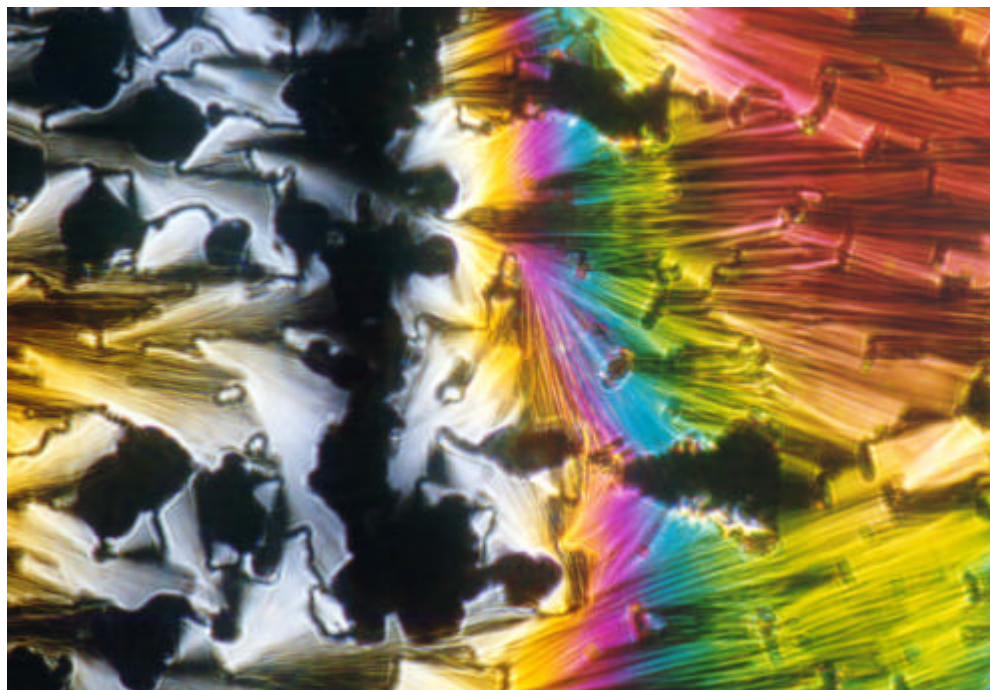


Figure 47: *Optical textures of the discotic mesophase of 68 observed under polarized light*

By means of the introduction of a long alkyl chain with four branching points it was possible to reduce the K→Col transition temperature to such an extent, that a columnar mesophase was observed even below room temperature for HBC-C₁₆ **68**. Furthermore and even more important, it was possible to reach the thermodynamically stable isotropic phase. Both facts conclude to a stable columnar mesophase width of over 267 °C for HBC-C₁₆.

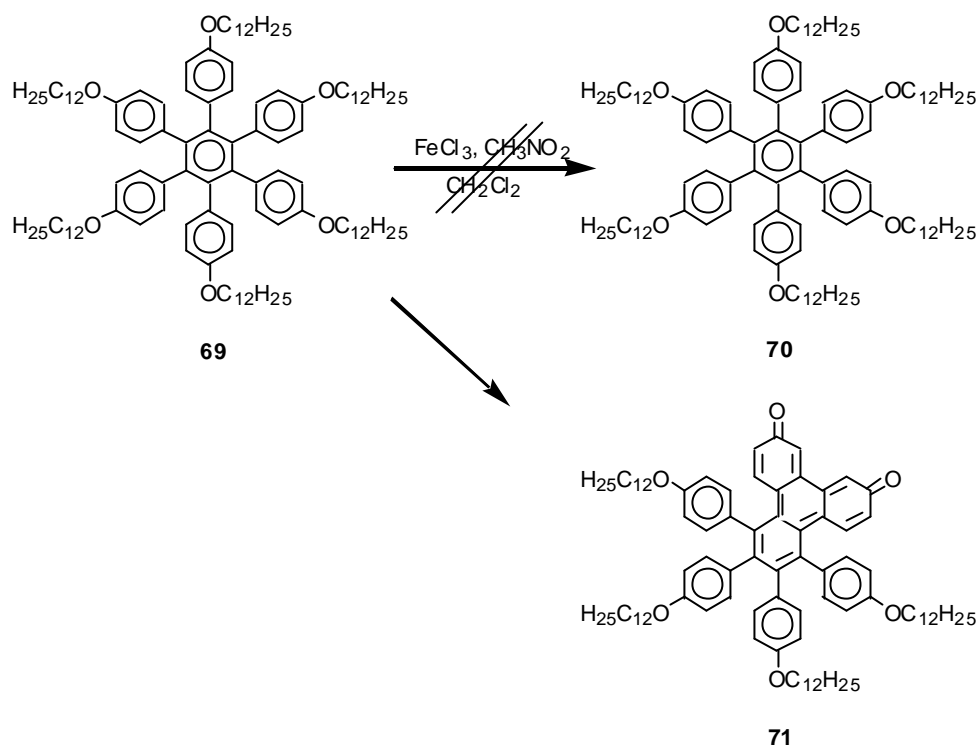
3.6 The influence of heteroatoms on liquid crystals

The relationship between the molecular structure and the resulting mesomorphic properties of a liquid crystal is important for the elucidation of effects that determine the overall behavior of a material.^[168] For this purpose, heteroatoms have been repeatedly investigated as the constituent element other than carbon atoms in liquid crystalline molecules.^[169] For example, the oxygen effect is noteworthy, because the aryl-O-R structure unit is present in many liquid crystals such as triphenylenes and phthalocyanines. Here, the oxygen stabilizes the phase width and lowers the transition temperatures.^[89, 90, 170] Incorporation of oxygen in the three positions (β -positions) of the lateral *n*-alkanoyl chains of discotic benzene hexaalkanoates and triphenylene hexaalkanoates also leads to a significant stabilization of the columnar mesophases. This effect was termed the " β -oxygen effect".^[168, 169] A similar stabilizing effect as demonstrated for oxygen was reported for the incorporation of sulfur in the side chains for a series of disc-like molecules: hexaesters of benzenes, cyclohexanes and triphenylenes.^[162] The effect was highly dependant on the position of the heteroatom but generally both transition temperatures, K \rightarrow Col and Col \rightarrow I, were depressed relative to the *n*-alkyl analogues.^[162]

The incorporation of heteroatoms can not only have strong influences on the mesophase behavior but also on the two and three dimensional crystal packing of organic materials.^[171-173]

These intriguing results prompted the group of Professor Müllen to investigate the influence that heteroatoms such as oxygen or sulfur might have on the mesomorphic properties of discotic liquid crystalline hexabenzocoronene. Brand and co-workers reported the synthesis and characterization of substituted HBC derivatives with up to six alkyl groups terminally functionalized with carboxylic ester, carboxylic acid, and hydroxy groups.^[172, 174] However, since the heteroatom functionality was not in close proximity to the aromatic core, the influence on the phase transition temperatures, i.e. lowering the Col \rightarrow I

transition below the beginning of decomposition, was very minor. It was for this reason that the synthesis of an alkoxy substituted HBC, i.e. derivative **70**, was attempted (Scheme 17).^[175]

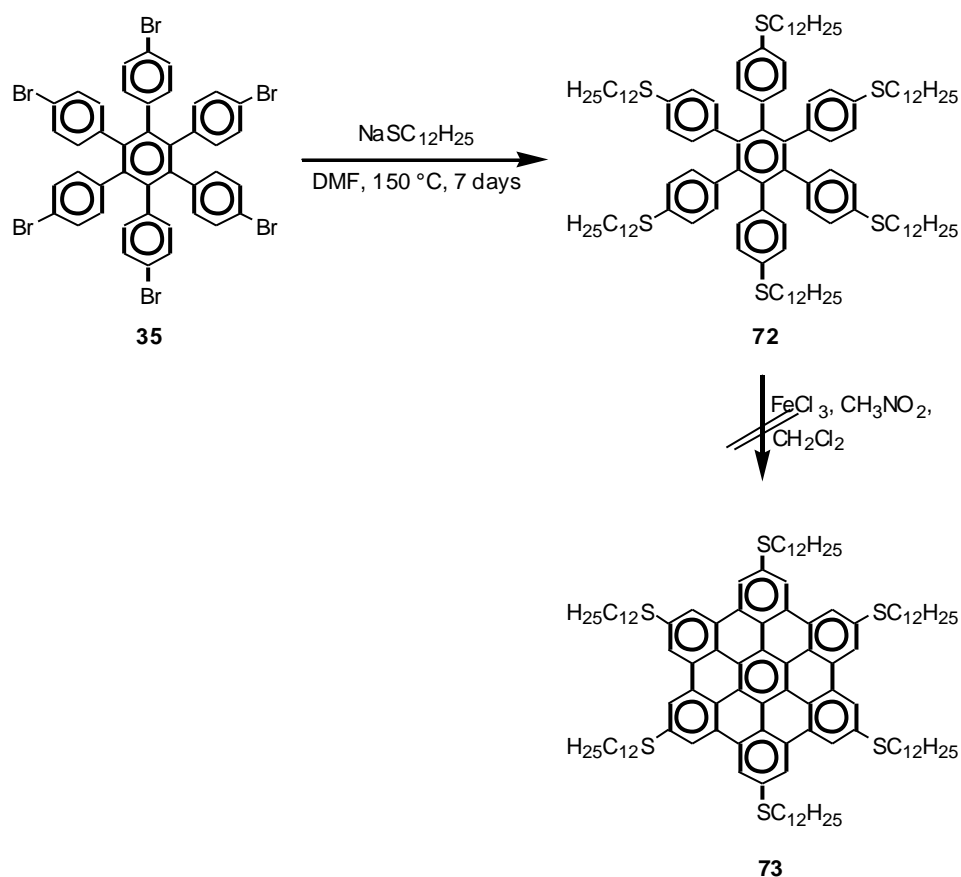


Scheme 17: **Attempted synthesis of alkoxy substituted HBC derivative 70**

The key step on the path to HBC **70** was the oxidative cyclodehydrogenation of the oligophenylene precursor **69**. Optimization of the appropriate cyclization conditions finally proved FeCl₃ to be superior to all other Lewis acids on the way to hexaalkyl-substituted HBCs.^[34, 73, 104] However, in a typical cyclization experiment the precursor **69** was dissolved in dichloromethane, and a solution of FeCl₃ in nitromethane was added dropwise at room temperature. After the starting material had disappeared the mixture was precipitated in methanol. In the case of **69** this synthetic protocol did not give the desired compound **70** but the quinone **71** (Scheme 17) in 96 % yield.^[175] Oxidative dealkylation and dehydrogenation lead to an extended quinonoid system which also incorporates the central aromatic ring.^[175] It is well known that compounds such as **69** undergo reactions in the presence of Lewis acids which involve both ether cleavage and oxidation to quinonoid aromatic structures as well as formation of new carbon-carbon bonds between adjacent phenyl rings.^[21, 176]

Since the incorporation of oxygen in the aliphatic side chain of the hexaphenylbenzene precursor **69** prevented the oxidative planarization and thus the possibility to investigate the influence of heteroatoms on the phase behavior of HBC, Dötz discovered a new strategy to modify the substitution pattern of HBC.^[73] In the case of triphenylenes, the replacement of oxygen by sulfur in the α -position to the aromatic core and its impact on the mesophase behavior as well as its influence on the charge carrier mobility is documented in the literature in great detail.^[39, 40, 45, 46, 85, 177] Especially in view of Lewis acid stability, thioether substituted hexaphenylbenzenes should be more suitable considering the fact that the sulfur-carbon bond is known to be more resistant to strong acids such as hydrobromic acid than the oxygen-carbon bond.^[73, 178, 179]

This project was tackled in a way depicted in Scheme 18. The unsuccessful attempt to functionalize 4,4'-dibromodiphenylacetylene (**21**) with thioalkyl substituents was reported by Dötz in the early stages of this endeavor. Thus, the routine procedure to build up substituted hexaphenylbenzenes via the cyclotrimerization route was impossible.^[73] However, in this case the direct hexa-functionalization of hexakis-(4-bromophen-1-yl)benzene (**35**) was successful and thioalkyl substituted compound **72** was obtained in good yields (Scheme 18).^[73] Unfortunately, it was again the crucial and product determining step of the oxidative cyclodehydrogenation that did not yield the desired hexabenzocoronene derivative **73** as depicted in Scheme 18.^[73]



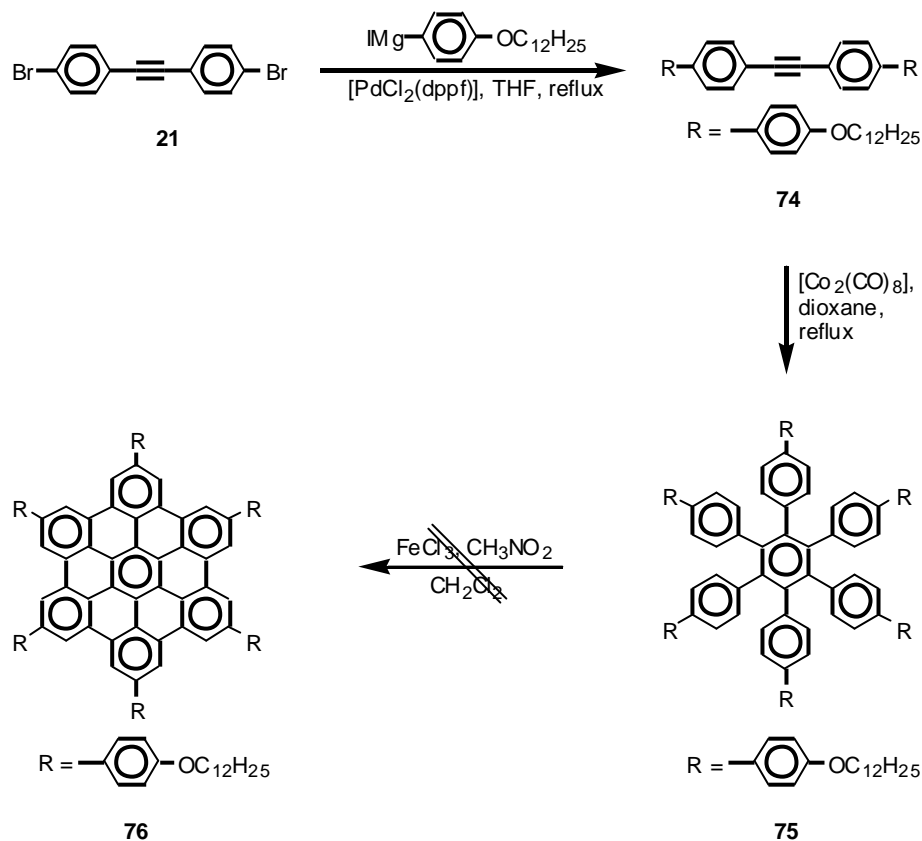
Scheme 18: **Synthesis of thioalkyl substituted hexaphenylbenzene and attempted cyclodehydrogenation**

From both the unsuccessful attempts to planarize hexaphenylbenzenes substituted in the 4-positions either by oxygen or sulfur, it can be reasoned that a different substitution pattern will have to be introduced to close the six pending phenyl rings.

To reduce the influence of the heteroatoms on the electronic structure of the HBC precursor molecules such as **69**, the distance of oxygen to the six pending phenyl rings in **69** had to be increased. This endeavor was best targeted with the insertion of an additional phenyl ring to the system. The incorporation of an extra phenyl group to the HBC precursor had many beneficial effects as already demonstrated for HBC-PhC₁₂ **43**. The starting material for this synthesis was 1-dodecyloxy-4-iodobenzene which was already utilized as a precursor for compound **69**, and was here synthesized according to literature procedure.^[175]

The synthetic sequence that was designed to yield the desired HBC derivative

with a spacer group between the aromatic center and the alkoxy side chains is demonstrated in Scheme 19.

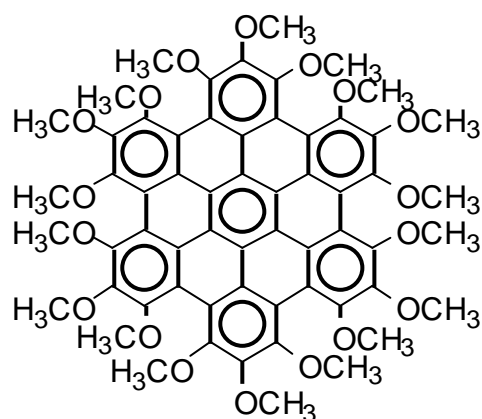


Scheme 19: **Synthetic pathway to phenylalkoxy precursor 75 and attempted cyclodehydrogenation**

The synthesis was carried out as follows: First, in a Kumada-type coupling reaction catalyzed with [PdCl₂(dppf)]^[112], 4,4'-dibromotoluene (**21**) reacts with 4-dodecyloxyphenylmagnesiumbromide and di(4-dodecyloxybiphenyl) acetylene (**74**) was obtained with a yield of 78%. Cyclotrimerization of **74**, catalyzed by [Co₂(CO)₈], in dioxane then afforded hexa(4-dodecyloxybiphenyl)benzene (**75**) with 75% yield after workup and purification using column chromatography. The key step for the synthesis of HBCs was again the oxidative cyclodehydrogenation. Here, hexa(4-dodecyloxybiphenyl)benzene (**75**) was dissolved in CH₂Cl₂ and flushed with argon for several minutes, before adding FeCl₃ dissolved in CH₃NO₂. Precipitation with MeOH after 45 minutes and workup using standard procedures produced a yellow material with a high degree of solubility. Unfortunately, mass spectrometry revealed that the desired

HBC **76** was not obtained but a number of partially cyclized products were observed. Analysis of the mass spectrum revealed that no ether cleavage had taken place or any other side products had formed. Therefore, the reaction conditions were slightly changed. First, the reaction time was increased to eight hours, with mass spectrometry analysis every 30 minutes. In this case, after eight hours the loss of six, eight and ten hydrogenatoms was observed. At all times during the reaction a mixture of different cyclodehydrogenation stages was seen. Even reaction times in excess of 24 hours did not bring the desired result. Since long reaction times did not seem to be the key to success, the excess of cyclodehydrogenation agent (FeCl_3) was increased. However, this also did not result in the formation of clean HBC **76**.

The unsuccessful outcome of the cyclodehydrogenation attempts of HBC precursors **69**, **72**, and **75** was a great disappointment for the proposed investigation of heteroatom substituted hexabenzocoronene cores. Nevertheless, further research activities of Dötz resulted in the development of a octadecamethoxy substituted hexaphenylbenzene which finally lead to a HBC derivative **77** with direct heteroatom substitution of the core (Figure 48).^[73] Investigations concerning the phase behavior and surface interaction are currently under way.^[73]



77

Figure 48: *Octadecamethoxy substituted HBC 77*

3.7 STM investigations of HBCs with C₆ symmetry

The results in this section origin from a long and productive collaboration with Dr. P. Samori in the group of Prof. Rabe, Berlin.

The self-assembly of nanometer-sized building blocks into targeted molecular architectures at surfaces represents one of the major goals of supramolecular chemistry and material science, given the perspective of the potential applications of these systems in nanotechnology, e.g. for molecular information storage devices or functional surfaces.^[180] This requires an accurate control of the molecular arrangements over a wide range of length scales, spanning from micrometers down to the molecular size. Non-covalent intermolecular forces have been used to engineer highly ordered three-dimensional (macro)molecular architectures where the single building blocks are held together by specific interactions, such as metal-ligand bonding^[181-183], hydrogen bonding^[184-186], or π - π stacking^[187]. On the other hand, the self-assembly at the solid-liquid interface has been successfully used to control the molecular arrangement in two dimensions.^[185, 188-194]

Polycyclic aromatic hydrocarbons (PAHs), which can be regarded as two-dimensional sub-sections of graphite, are well-defined nanoobjects^[26-28, 30, 37, 39, 45, 46, 52, 63, 82, 94, 95, 97, 104, 195-202] with interesting electronic properties.^[26, 30, 45, 94, 201] During the last years, soluble derivatives, namely hexa-*peri*-hexabenzocoronenes (HBCs), and larger analogues have been synthesized and characterized as already partly discussed in previous chapters. From a synthetic point of view, they are extremely versatile compounds that are able to bear different chemical functionalities in their periphery.^[26-29, 37, 82, 95, 104]

Scanning Tunneling Microscopy (STM) is a technique which allows the investigation of physisorbed layers of PAHs both at the graphite-solution interface^[26, 28, 52, 94, 201, 202] and in dry thin films on conductive substrates^[95] with molecular resolution. The first type of PAH which has been explored were triphenylene derivatives^[52, 201], which possess 18 carbon atoms in the aromatic core. Following the recent achievements in the synthesis of larger and larger PAHs, the packing at surfaces of compounds with 42^[26, 28, 95] and 60 carbons^[94] in the conjugated core has been also studied. These systems have been found

to form two-dimensional crystals where the disc-like molecules lie flat on the basal plane of the conductive substrate. Recently it has been reported that the self-assembly of a series of triphenylene derivatives with increasing lengths of the alkyl side substituents can be extended to the third (*z*) dimension in the region near the substrate, and the observed structures have been explained with a frustrated Ising net model.^[52]

In a previous report it has been shown that HBC-C₁₂ (**6b**) can crystallize in monolayers at the solution-graphite interface with the conjugated cores lying equally flat on the basal plane of the HOPG.^[26] STM and STS have been used to study the molecular structure and electronic properties of the monolayer on the molecular scale. In the latter type of analysis, a diode-like electrical behavior of the conjugated HBC core has been observed. With the aim of extending the molecular order of the physisorbed layers to the third dimension (*z* axis) in the region near the substrate surface, HBC derivatives symmetrically functionalized in the peripheral positions with more bulky side chains were investigated, which, due to steric hindrances could force neighboring HBCs to acquire different positions along the *z* axis.

Here, a sub-molecularly resolved STM investigation of the self-assembly of different chiral or achiral hydrocarbon substituted HBCs (Figure 49, which have already been introduced earlier) into monolayers highly ordered in 2D and 3D at the graphite-solution interface is reported.

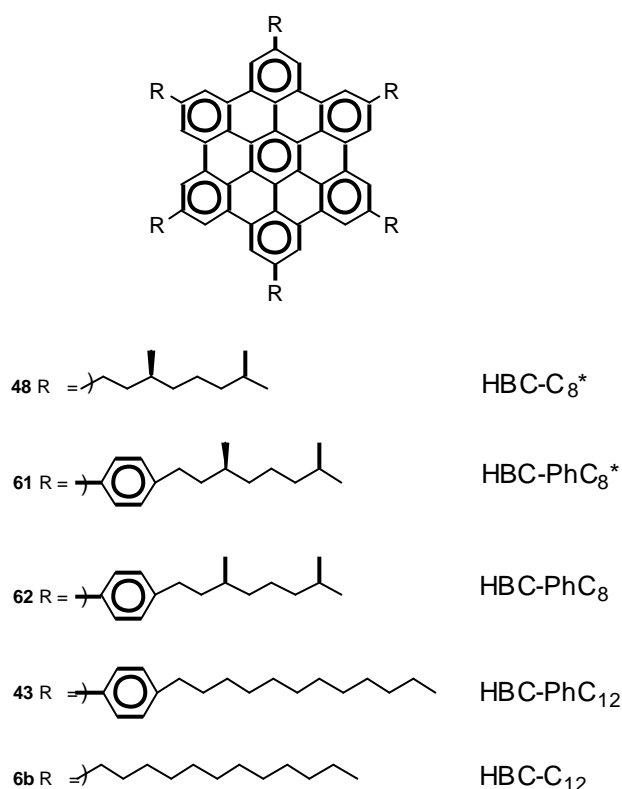


Figure 49: **Chemical structure of HBCs investigated by STM**

While **48** bears an alkyl side chain exhibiting a chiral methyl function in the 3' position and an achiral one in 7', a phenylene has been introduced in compound **61** between the HBC core and the chiral aliphatic chain in each of the six peripheral positions. In **61**, because of the repulsive interactions between ortho-protons in the phenylenes with the ones of the neighboring aromatic rings, the phenylenes are likely to be twisted with respect to the HBC core; as a consequence the whole side chains would attain a conformation which is non planar to the aromatic core. This loss of planarity of the HBC could play a role in the organization of the molecules when physisorbed into layers at the HOPG-solution interface. In addition, in order to gain insight into the role of the chirality

of the group in the 3' position, the racemic mixture of **61**, namely compound **62**, and compound **43** were also analyzed.

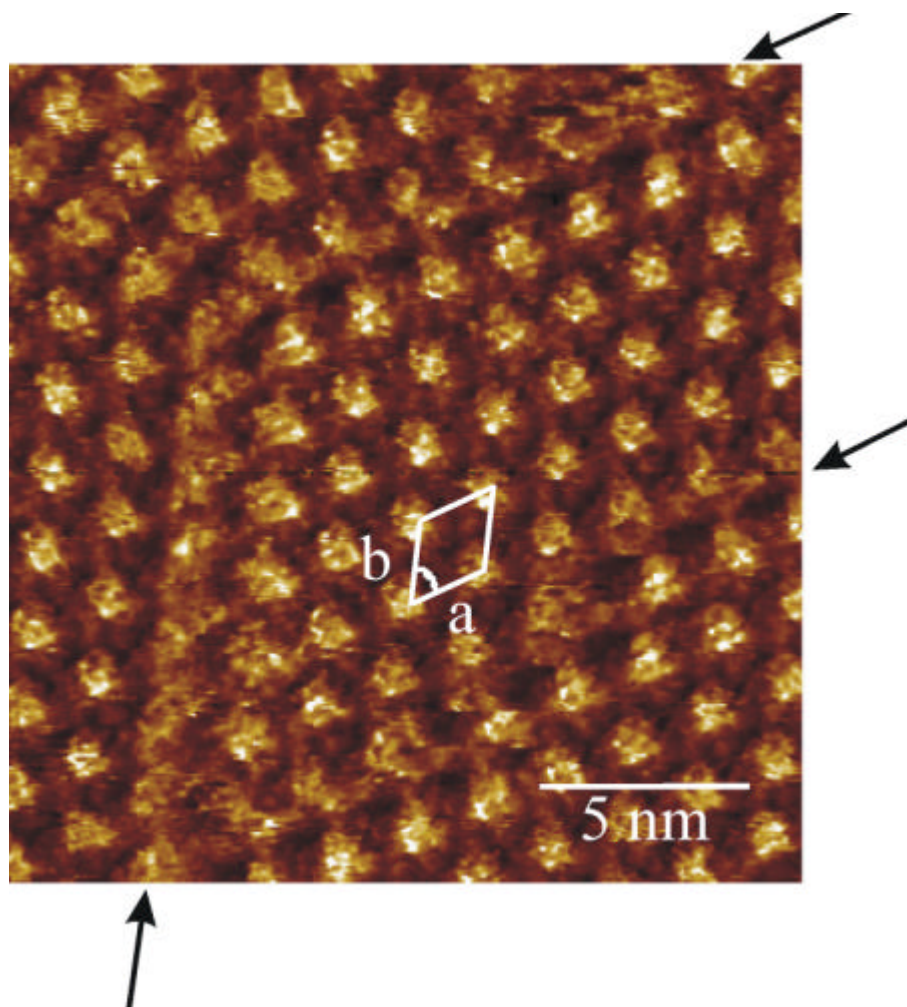


Figure 50: **Scanning Tunneling Microscopy of HBC-C₈* 48 at the solution-HOPG interface. The arrows indicate domain boundaries. Unit cell: $a=(1.86\pm0.10)$ nm; $b=(2.03\pm0.10)$ nm; $\alpha=(58\pm2)^\circ$. $U_t = 1.00$ V and average $I_t = 40$ pA.**

Figure 50 displays the STM current image of a monolayer of **48** physisorbed at the interface between an organic solution and the basal plane of highly oriented pyrolytic graphite (HOPG). It shows a polycrystalline structure with domain boundaries (indicated by the arrows in Figure 50) that are characterized by a slight translation of the crystal lattice along one of the three crystallographic axes. Inside each domain, bright spots are arranged (within experimental error) in a hexagonal motif. These bright spots are attributed to the π -conjugated

cores of the molecules, because in STM current images of alkylated aromatic molecules lying equally flat on HOPG, the aromatic moieties appear brighter (corresponding to higher currents) than the alkyl chains, due to the smaller energy difference between their frontier orbitals and the Fermi level of the substrate.^[203] This assignment is consistent with the fact that the area of the unit cell corresponds to the area within the van der Waals contour of a single molecule lying flat on the surface. Since the contrast in STM depends to a great extent also on the spatial overlap of the electronic states of the adsorbate and the substrate, molecules which are placed at variable distances from the substrate can be expected to exhibit different contrast in the STM current images. Consequently, the distribution of contrasts attained in the STM image in Figure 50 suggests that the aromatic cores are located at equal positions relative to the substrate. The high conformational mobility of the side chains at the surface, which occurs on a time scale faster than the scanning frequency, did not allow us to resolve their structures.

Starting from HBC-C₁₂ **6b**, the introduction of a phenylene ring between the aromatic core and the aliphatic side chains in all the six peripheral positions leads to a dramatic change in the supramolecular structure on the solid surface. Figure 51 displays the STM image of a monolayer of the achiral phenylene-alkyl substituted HBC-PhC₁₂ **43** physisorbed on HOPG.

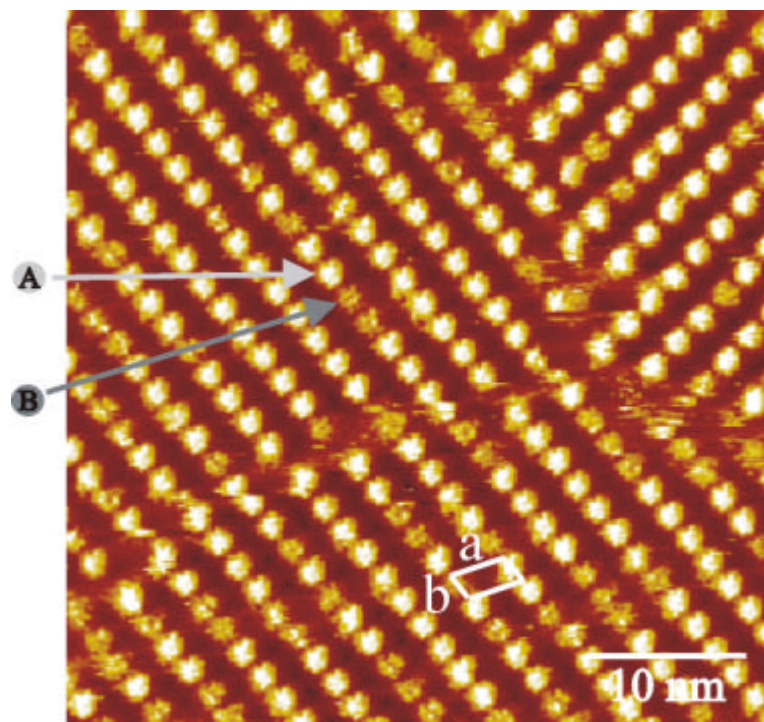


Figure 51: **Scanning Tunneling Microscopy of HBC-PhC₁₂ 43 at the solution-HOPG interface. An adsorbed molecule with brighter contrast (A) is marked with light gray arrows while a molecule with darker contrast (B) is labeled in dark gray. Unit cell: $a=(3.10\pm0.10)$ nm; $b=(2.00\pm0.10)$ nm; $\alpha=(78\pm3)^\circ$. $U_t=1.17$ V; average $I_t=251$ pA.**

Similar to the case of **6b**, the 2D unit cell of the monolayer is oblique. In contrast to **6b**, however, two different types of contrast of the aromatic core have been recorded here, as marked in the image by A (brighter) and B (darker). It is noteworthy that their spatial distribution does not follow a periodical motif. A similar contrast behavior has been observed for the other achiral phenylene-alkyl functionalized HBC, i.e. compound **62** (image not shown). However, in the latter case, the 2D unit cell is nearly hexagonal ($a=(2.41\pm0.12)$ nm; $b=(2.21\pm0.12)$ nm; $\alpha=(62\pm4)^\circ$).

The STM image of the chiral phenylene-alkyl substituted HBC derivative, HBC-PhC₈ **61**, self-assembled at the solution-HOPG interface is displayed in Figure 52. Although the 2D packing in the xy plane is almost hexagonal, similar to that of compounds **48** and **62**, the conjugated cores exhibit three different contrasts distributed in a periodical motif across the plane.

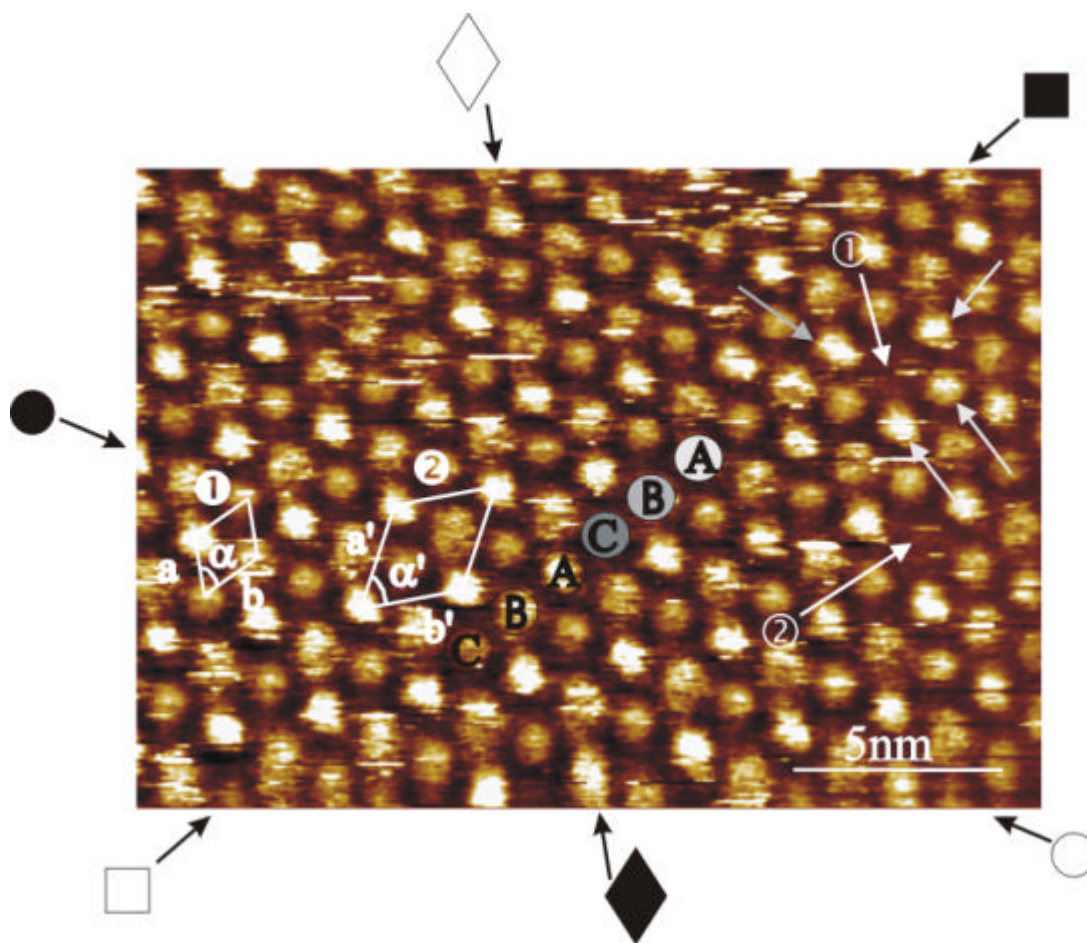


Figure 52: **Scanning Tunneling Microscopy of HBC-PhC₈* 61 at the solution-HOPG interface. A,B,C types of molecules are characterized by a different contrast. The two white arrows indicate vacancies in the crystal structure. Around the vacancy ① it is possible to notice the presence of 3 neighboring (labeled with light gray arrows) + 1 (dark gray arrow) A type of molecules. Unit cell of the 2D structure ①: $a=(2.55\pm 0.10)$ nm; $b=(2.44\pm 0.10)$ nm; $\alpha=(58\pm 3)^\circ$. Unit cell of the superstructure ②: $a'=(4.28\pm 0.17)$ nm; $b'=(4.28\pm 0.17)$ nm; $\alpha'=(58\pm 3)^\circ$. $U_t=1$ V; average $I_t=50$ pA.**

In Figure 52, the different cores are marked with A, B and C, where A exhibits the brightest contrast, and C the lowest. Assuming the unit cell of the aromatic cores to be exactly hexagonal, molecules exhibiting the same contrast form a $\sqrt{3}\times\sqrt{3}$ R30° superstructure.

In order to quantify the contrasts in the STM current images, the images have been processed. In Figure 52 the average brightness and its standard deviation

have been measured for each bright spot. It was determined from a circular area with a diameter of 1.1 nm centered on the middle of the spot. The evolution of these values along the three lattice axes are plotted vs. the position number in Figure 53.

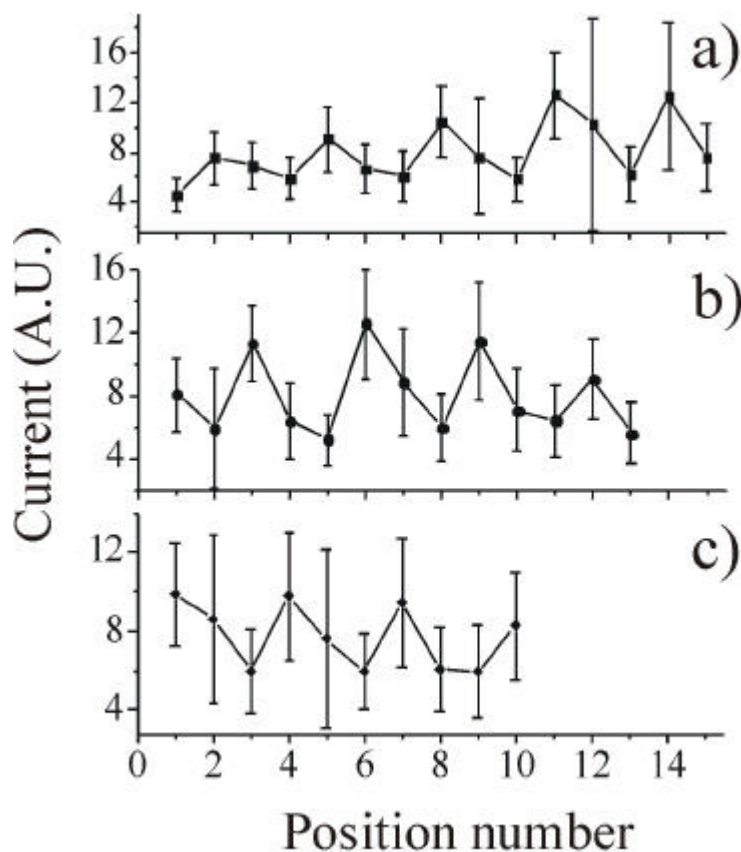


Figure 53: **Profiles of the contrast in the STM image shown in Figure 52 vs. the position number, i.e. each unit in the x-axis correspond to one disc. a) Profiles from ■ to □ ; b) from ● to ○; c) from ◆ to ◆.**

In all the three profiles in Figure 53, there is a periodicity due to 3 neighboring contrasts (A, B, C), although, due to a non perfect flattening of the image, the absolute values vary across the image.

Molecule	Unit cell in xy	Contrasts of the conjugated cores in the STM image
HBC-C₈ 48	Hexagonal	1 contrast
HBC-PhC₈ 61	Hexagonal	3 contrasts periodically distributed: "Staircase"
HBC-PhC₈ 62	Hexagonal	2 contrast randomly distributed
HBC-PhC₁₂ 43	Oblique	2 contrasts randomly distributed
HBC-C₁₂ 6b	Oblique	1 contrast

Table 7: ***Unit cell and contrasts of the conjugated cores in the STM images of functionalized HBCs.***

The different contrasts, observed in the STM images of the molecules with the phenylene-containing side chains **61**, **62** and **43** (Table 7), could be due to four main effects:

- 1 defects of the molecular packing at surface;
- 2 different number of HBCs in a stack filling the tunneling gap between tip and substrate;
- 3 different conformation of the molecule;
- 4 different position of the molecule in the gap tip-substrate.

The spatially random distribution of two different contrasts for compound **43** (Figure 51) and **62** on single crystalline domains physisorbed on HOPG could be explained with effect 1, which can be due to: (a) defects in the HOPG lattice and/or (b) impurity of the synthetic material. While (a) can be neglected since the freshly cleaved surface of HOPG in the last decade has been proven with STM to be almost defect free in the micrometer scale, (b) can be ruled out since all the compounds which have been used are analytically pure (as determined by NMR and mass spectrometry).

Assuming 2, the contrast A in Figure 52 could correspond to three stacked discs, B to two, and C to one disc filling the gap tip-substrate since a stack of aromatic cores should exhibit a better electron transfer than the solvent molecules. However, observing carefully the molecular packing in the proximity

of lattice defects such as a missing molecule (indicated with white arrows 1 and 2 in Figure 52), one can note that these defects are located where one of the darker discs should be placed, albeit it is desorbed. The desorption of a C type molecule is very unlikely, since among the three types it is the one which is better coupled with the substrate, hence more strongly physisorbed on it. This observation does not support the effect 2.

Phenylene groups which are directly attached to the molecular core are common to derivatives **61**, **62** and **43**. In order to minimize the steric interactions of the ortho-protons with those of the neighboring aromatic core, they are likely to arrange in a non-planar conformation giving rise to a non-planarity of the whole system.^[30, 104] The variation of the conformation (effect 3), from planar to non-planar, can induce a change in the electronic properties of the HBCs, causing different contrasts in the STM current image.

According to the interpretation 4, the aromatic cores may be "frozen" at different positions ("staircase") in the tunneling gap tip-substrate, as sketched in the cartoon in Figure 54.

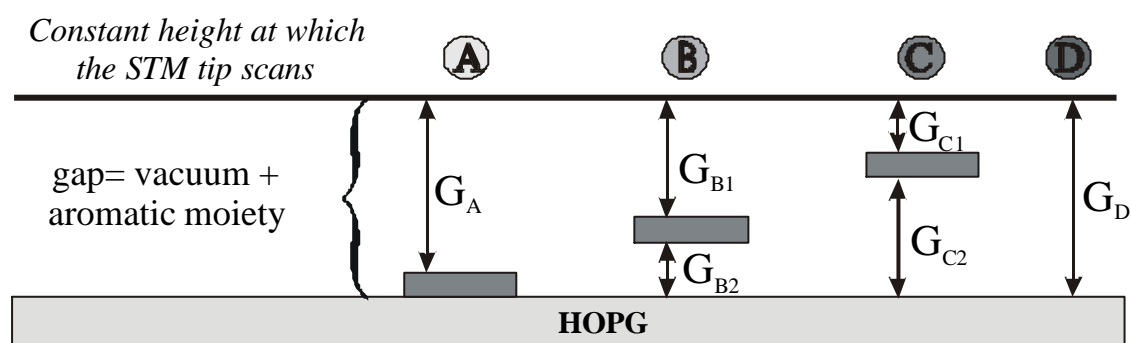


Figure 54: **Schematic cartoon of STM constant height investigation. The molecule can be localized in different z locations within the gap tip-substrate. In all three cases (A,B,C) the size of the not filled gap, which can be considered as vacuum, is equal: $G_A = G_{B1} + G_{B2} = G_{C1} + G_{C2}$. In the extreme case (D) the gap consist of vacuum where $G_A < G_D$.**

In this model, the asymmetric position of the molecule within the gap tip-substrate has an influence on the contrast in STM current images, according to a resonant tunneling contribution.^[204] In the case of the STM images of **61**, which are characterized by three different contrasts, the brighter discs (A) would

be better coupled to the substrate, while B and C would appear more and more dark because of their increasing distance from the substrate, and consequently lower coupling (Figure 54). The extreme case would be characterized by the absence of the molecule in the gap (case D), which leads to the smallest current in the STM image, like at vacancies in the 2D lattice (indicated by the white arrows 1 and 2 in Figure 52). This model is also in accordance with the observation of a missing molecule (white arrows in Figure 52) of type C, which can desorb more easily since it is located further away from the substrate.

Therefore, it can be concluded that either 3 or 4, or both of them, cause the different contrast observed in Figure 51 and Figure 52.

The observation that **61** self-assembles at the solid-liquid interface not only in two dimensions but also in three dimensions is particularly interesting. In addition to the role played by the phenylene groups attached to the molecular core (effect 3) inducing a loss of planarity of the whole system, a contribution of the aliphatic side chains for the supramolecular arrangement is likely to be relevant. The branched substitutions themselves, being chiral, also induce well-defined and periodical losses of planarity. We believe that both these chemical functionalities are required in order to attain the self-assembly into a staircase architecture of **61**.

On the other hand, the mere existence of the first of the two forces in the case of compound **43**, namely the presence of a phenylene function directly attached to the HBC core, induces a loss of planarity of the system in the non-adsorbed state, that upon physisorption at a surface leads to a molecular pattern with a degree of order only in the *xy* plane, while the molecules are located randomly, i.e. in a non periodical fashion, in the third dimension in any of two distinct positions. In the absence of the phenylene attached directly to the aromatic core, the molecules tend to physisorb equally flat on the basal plane of graphite, as has also been observed for several other symmetrically functionalized PAHs.^[26, 94]

Focussing again on the missing molecules in Figure 52, one can notice that the superstructure is lost in their vicinity. For example, a total of four A-type molecules in the vicinity of the vacancy ① in Figure 52 can be recognized:

Three neighboring ones are marked with light gray arrows and another one is labeled with a dark gray arrow. The free space provided by the missing molecule enables the neighboring moieties to attain a position which is nearer to the substrate if compared to the standard location it would usually assume. This indicates once again that the steric hindrances (intermolecular interactions) are essential in order to achieve this type of 3D arrangement. Remarkably, these vacancies are rather stable features with a life time of several minutes.

A similar supramolecular nanostructure like that of **61** at the solution-HOPG interface has been detected on triphenylenes bearing long aliphatic side-chains by Charra and Cousty.^[52] These authors have observed the appearance of a superlattice in hexagonally packed monolayers with increasing lengths of the side chains, where every third molecule appears brighter, according to a $\sqrt{3} \times \sqrt{3} R30^\circ$ superstructure. They explained this phenomenon in the light of an antiferromagnetic triangular Ising net. However, this model cannot be applied to our data because (1) it cannot be used to describe a structure consisting of more than two contrasts, e.g. the staircase built up with **61**; (2) it is limited to polymolecular structures having a hexagonal lattice in the two dimensions; and (3) it cannot be used to describe the case of randomly distributed contrasts as the ones observed for compounds **43** and **62**.

Drawing the attention to the symmetry of the molecular arrangement in 2D (Table 7), compounds **48** and **61** exhibit a 2D hexagonal unit cell while for **43** it is oblique. In the latter case, the steric hindrance of the non branched, i.e. linear, aliphatic side chains is smaller, giving rise to a larger flexibility of the molecular system. This allows **43** to pack according to a two-fold symmetry, similarly to HBC-C₁₂ (**6b**).^[26] This packing is favored since the area per unit cell is minimized, hence the enthalpy gain upon adsorption at the surface (interfacial interaction) is maximized.^[205] Instead, in the first three cases **48**, **61** and **62**, due to a larger steric hindrance of the non-conjugated bulky peripheral groups, and consequently a smaller flexibility of the system, the HBCs cannot arrange in a two-fold symmetry, thus adopting an almost hexagonal structure, that is reminiscent of columnar mesophases. Indeed, this class of compounds exhibits liquid crystalline phases which exist over a wide range of temperatures.^[27, 30, 104]

In summary, the chemical functionalization of HBCs with phenylene-alkyl chiral side chains allowed to extend the established two dimensional molecular self-assembly at the solid-liquid interface to the third dimension in the region near the substrate. The formation of the staircase architecture finds its origin in the interplay between intramolecular as well as intermolecular and interfacial interactions; a key role is played by the steric hindrance suffered by the side chains. This latter effect can also play a role inducing the molecules to adopt different conformations allowing the minimization of the intermolecular repulsive interactions. The staircase architecture appears to be an ideal candidate for scanning tunneling spectroscopy studies of equal conjugated molecules possessing different electronic properties due to their variable overlap with the substrate. Furthermore, it is possible to envisage new interesting experiments manipulating a single HBC in the xy plane from the near-vacancy to the vacancy: Depending on the final location that the manipulated molecule spontaneously adopts along the z axis, the HBC layer might exhibit properties of a molecular level machine^[205] where the stimulated switch between two different positions with respect to the substrate is controlled by intermolecular interactions.

3.8 $^1\text{H-NMR}$ investigation of the aromatic π -stacking of hexabenzocoronene in solution

3.8.1 Introduction and previous work

A major obstacle in the NMR-spectroscopic description of PAHs, related to the limited solubility, is the strong tendency of the disc-type structures to form aggregates in solution,^[115, 116] which causes significant line broadening and shielding. The shielding in this case is of course intermolecular, versus the diatropic effects^[117] which are normally considered when looking at single aromatic molecules. Figure 15 shows, however, that by increasing the temperature from 298 K to 450 K one can obtain $^1\text{H-NMR}$ signals with sufficiently narrow line widths.^[104] In a more detailed study, one can observe the strong influence that changes of temperature and concentration have on the π - π interaction of these aromatic compounds. The shifts of the aromatic ^1H resonance frequencies dependent on changes in temperature are depicted in Figure 55, and on concentration in Figure 56.^[72]

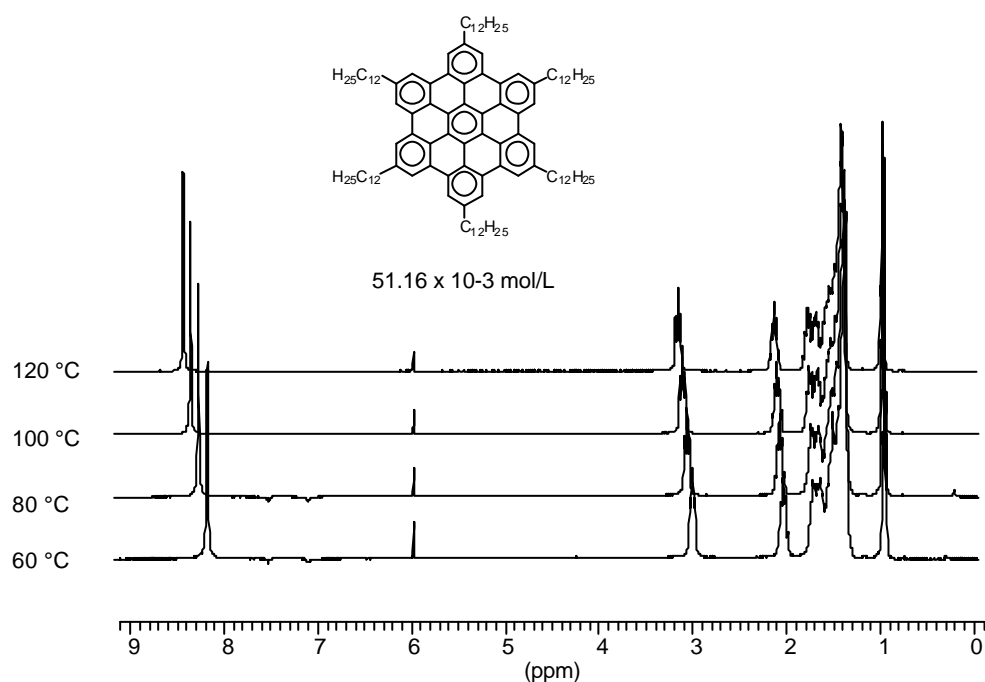


Figure 55: *Temperature dependent $^1\text{H-NMR}$ spectra of HBC- C_{12} 6b in $\text{C}_2\text{D}_2\text{Cl}_4$ at temperatures between 60 °C and 120 °C*

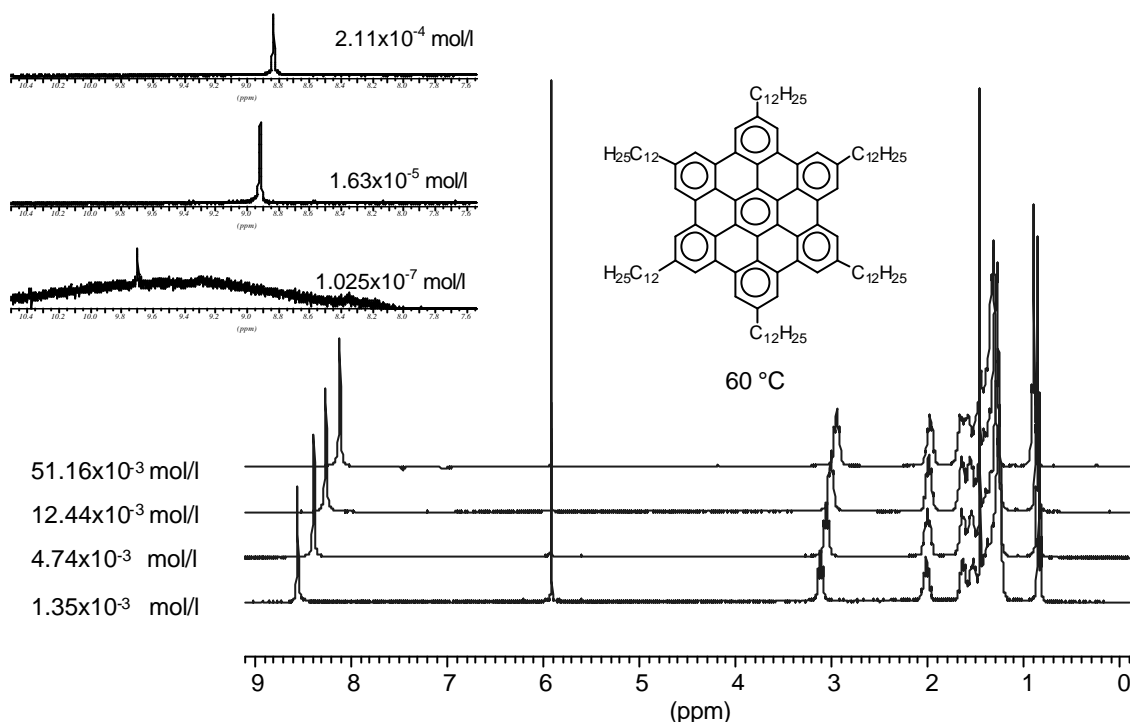


Figure 56: **Concentration dependent $^1\text{H-NMR}$ spectra of HBC- C_{12} 6b in $\text{C}_2\text{D}_2\text{Cl}_4$ at 60°C**

As can be seen in Figure 55, on heating in a temperature range between 60°C and 120°C , the relevant aromatic signals experience a downfield shift of $\Delta\delta = 0.26$, from $\delta = 8.11$ ppm to $\delta = 8.37$ ppm. A somewhat less pronounced shift to low fields can be observed for the $\alpha\text{-CH}_2$ protons of the alkyl side chains. Likewise, decreasing the concentration (at a constant temperature of 60°C) from 51.2×10^{-3} mol/L to 1.4×10^{-3} mol/L results in a shift to low fields by almost 0.5 ppm. Again, a less pronounced shift to low fields can be observed for the $\alpha\text{-CH}_2$ protons of the alkyl side chains. It can be summarized that increasing temperature and decreasing concentration affect the solution behavior in a way that smaller aggregates are formed. This results in a shift of the aromatic proton signal towards lower fields which is in accordance with the theoretical value calculated for an isolated molecule.^[83, 84] On the other hand, it was, until now, not experimentally possible to reach concentrations low enough to measure isolated HBC molecules in solution, which would make it possible to determine association constants and ring current parameters.

In a similar approach, the aggregation of phenylacetylene macrocycles in solution has been studied with $^1\text{H-NMR}$ spectroscopy.^[115, 116] The association constant for dimerisation, K_{assoc} , was determined by curve fitting the concentration dependence of the proton chemical shift to a model for monomer-dimer equilibrium. The results obtained from NMR studies, *e.g.* aggregation constants and aggregate size, have independently been verified by vapor pressure osmometry experiments. It has been further well documented in the literature that aryl groups tend to associate in either a face-to-face or an edge-to-face orientation.^[206, 207] In the phenylacetylene macrocyclic systems, it was possible to assign a face-to-face π -stacking arrangement to the macrocycles in solution.^[115, 116] However, the nature of the forces that cause these self-association phenomena are still not totally clarified, quadrupole-quadrupole and/or van der Waals interactions are being discussed in the literature.^[208, 209] These aromatic π - π interactions are suppressed when the periphery of the macrocycle is substituted with bulky *tert*-butyl groups which prevent the molecules from approaching each other.^[72, 81]

3.8.2 Application of self-association models to experimental data

The experimental data of NMR shift as a function of the concentration of HBC were used in self-association models in order to determine the association constant, as described by Martin, 1996.^[210] These models deal with equilibrium or thermodynamics and describe equilibrium constants of the self-association process using different assumptions. Several models described by Martin were used in this work, and the results are presented in this section. These models and the underlying equations involved are described in detail by Martin, only the main features of the models and the results are mentioned here. Experimentally, NMR samples of HBC- C_{12} **6b** in tetrachlorethane were prepared for a concentration range of 0.17 to 5.1×10^{-8} mol/L. All NMR experiments were conducted at a constant temperature of 60°C. In the case of very low concentrations, a large number of scans was needed to achieve resolution of the aromatic core proton above the noise level. For all of the measurements, a

Bruker DRX 500 NMR spectrometer was used and the number of scans that was utilized in the case of the lowest concentration was in the order of 40000 which translates to three days of experiment time.

3.8.3 Models using nearest neighbors:

In order to apply self-association models to NMR data, it is assumed that the chemical shift of a molecule (P) is given by

$$P = \alpha P_{\alpha} + \lambda P_{\lambda} + \xi P_{\xi}$$

where α , λ and ξ are the mole fractions of the monomer, molecule at the end of a stack and molecule within a stack respectively, and P_{α} , P_{λ} and P_{ξ} are their NMR shifts. It is assumed that the NMR shift of a molecule at the end of a stack can be expressed in terms of the NMR shifts of the monomer and of a molecule within a stack by means of a factor f , i.e.

$$P_{\lambda} = f P_{\xi} + (1-f) P_{\alpha}$$

where a setting of $f = 0.5$ means that a molecule at the end of a stack experiences half the effect of one inside the stack. This treatment leads to three unknowns which need to be determined, P_{α} , P_{ξ} and f .

Equal K (EK) Model:

In the simplest Equal K (EK) model, it is assumed that the addition of a molecule to a stack occurs with identical free energy and equilibrium constant (K_E) as for the addition of previous molecules. This model can be refined by allowing the equilibrium constant for dimer formation to differ from the value of the equilibrium constant for subsequent additions (by a factor ρ , i.e. $K_2 = K_E / \rho$). Thus, 2 more unknowns, K_E and ρ , need to be determined.

Attenuated K (AK) Model:

In the Attenuated K (AK) model, it is accounted for that successive additions become less probable and less favored entropically, and thus successive

equilibrium constants taper off. Thus, the equilibrium constant for dimer formation is given by $K_2 = K_A/2$, that of trimer formation is $K_3 = K_A/3$, etc. Similar to the EK model, it is also possible to allow the equilibrium constant for dimer formation to not follow this pattern using a factor $\tau = 2 K_2/K_A$. Thus, for this model, the additional unknowns are τ and K_A .

3.8.4 Models using next nearest neighbors:

In the above models, it was assumed that only nearest-neighbor interactions produce chemical shifts. It is also possible to consider the interactions of next nearest neighbors in vertical stacks. Let the nearest-neighbor effect producing an NMR shift be n and the next-nearest-neighbor effect be t , with the ratio $r = t/n$. A high value of t indicates a high influence of the next-nearest-neighbors. Thus, instead of the variable f in the models where only the nearest-neighbor interactions are considered, the variable t needs to be determined.

Equal K Model considering next-nearest-neighbors (EKNN):

This model is similar to the EK model, i.e. K_E and ρ need to be determined.

Attenuated K Model considering next-nearest-neighbors (AKNN):

This model is similar to the AK model, i.e. K_A and τ need to be determined.

3.8.5 Results of experimental data and applied models

The four models introduced above (EK, AK, EKNN and AKNN) were used along with the experimental data, which at this point were measured even at very low concentrations (as low as 5.122×10^{-8} mol/L) as listed in Table 8. Since the equations governing these models are nonlinear, a nonlinear least squares analysis was carried out in order to fit the parameters of the models to experimental data. For e.g., in case of the EK model, the equilibrium constant (K_E), the factor distinguishing dimer formation from other polymers (ρ), the monomer shift (P_α), the shift of a molecule within a stack (P_ξ), and the factor

relating the shift of a molecule at the end of a stack to those of the monomer and within a stack (f) were the parameters that were changed in order to achieve a good fit for the experimental data (Table 8).

c [mol / L]	δ [ppm]
0.1651	7.975
0.0917	8.049
0.0532	8.109
0.0423	8.140
0.0301	8.177
0.0191	8.238
0.0102	8.315
0.0063	8.378
0.0018	8.542
8.265×10^{-4}	8.666
4.894×10^{-4}	8.716
3.263×10^{-4}	8.785
2.114×10^{-4}	8.831
1.631×10^{-5}	8.915
1.025×10^{-6}	9.014
1.025×10^{-7}	9.699
5.122×10^{-8}	9.699

Table 8: **Experimental data; ^1H chemical shift of the aromatic core protons of HBC- C_{12} 6b in $\text{C}_2\text{D}_2\text{Cl}_4$ at 60°C**

The first results presented do not use the entire set of experimental data. The last two points were at first neglected as the errors at such high dilution values can be large. Table 9 shows the parameters of the different models for this set of experimental data. Figure 57 shows the graphical fit using this set of parameters.

EK model	AK model	EKNN model	AKNN model
$K_E = 188.68 \text{ L/mol}$	$K_A = 457.32 \text{ L/mol}$	$K_E = 188.66 \text{ L/mol}$	$K_A = 457.39 \text{ L/mol}$
$\rho = 4.485$	$\tau = 3.834$	$\rho = 4.485$	$\tau = 3.834$
$f = 0.4970$	$f = 0.3773$	$r = 0.005954$	$r = 0.3253$
$P_\alpha = 8.977 \text{ ppm}$	$P_\alpha = 8.978 \text{ ppm}$	$P_\alpha = 8.977 \text{ ppm}$	$P_\alpha = 8.978 \text{ ppm}$
$P_\xi = 7.641 \text{ ppm}$	$P_\xi = 7.239 \text{ ppm}$	$P_\xi = 7.641 \text{ ppm}$	$P_\xi = 7.239 \text{ ppm}$

Table 9: *Parameters for the different models neglecting the last two experimental data points*

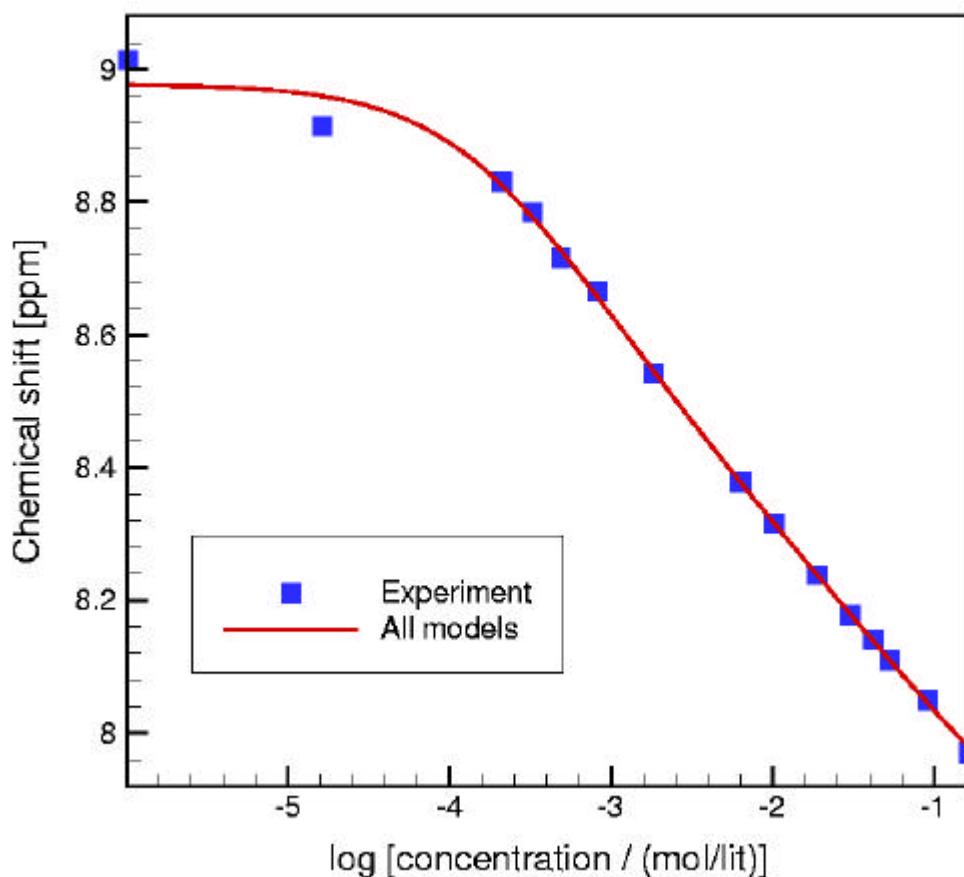


Figure 57: *Comparison between experimental data and models for the experimental data neglecting the last two experimental data points.*

As can be seen from the graphical fit in Figure 57 the experimental data (neglecting the last two data points) match well with the calculations. Association constants calculated for the different models are in the range of 188 to 457 L/mol. However, considering that aggregation is present even at low concentrations this seems rather low. The graph crosses the y-axis at around 8.9 ppm which is below the determined chemical shift for the lowest concentration used in these calculations. The graph suggests a constant decrease of aggregate size due to the leveling out towards 8.9 ppm.

In the next set of results, all the data points were used. The NMR shift of the monomer (P_α) was kept constant at 9.699 ppm, i.e. at the value of the data point with the highest dilution. Table 10 shows the parameters of the different models for this set of experimental data and Figure 58 shows the graphical fit using this set of parameters.

EK model	AK model	EKNN model	AKNN model
$K_E = 24675.5$ L/mol	$K_A = 58473.8$ L/mol	$K_E = 24695.3$ L/mol	$K_A = 58236.3$ L/mol
$\rho = 57.097$	$\tau = 49.442$	$\rho = 57.10$	$\tau = 49.61$
$f = 0.4451$	$f = 0.3365$	$r = 0.1234$	$r = 0.4861$
$P_\xi = 7.766$ ppm	$P_\xi = 7.178$ ppm	$P_\xi = 7.766$ ppm	$P_\xi = 7.176$ ppm

Table 10: **Parameters for the different models using the entire set of experimental data (Chemical shift of the monomer is constant at 9.699 ppm)**

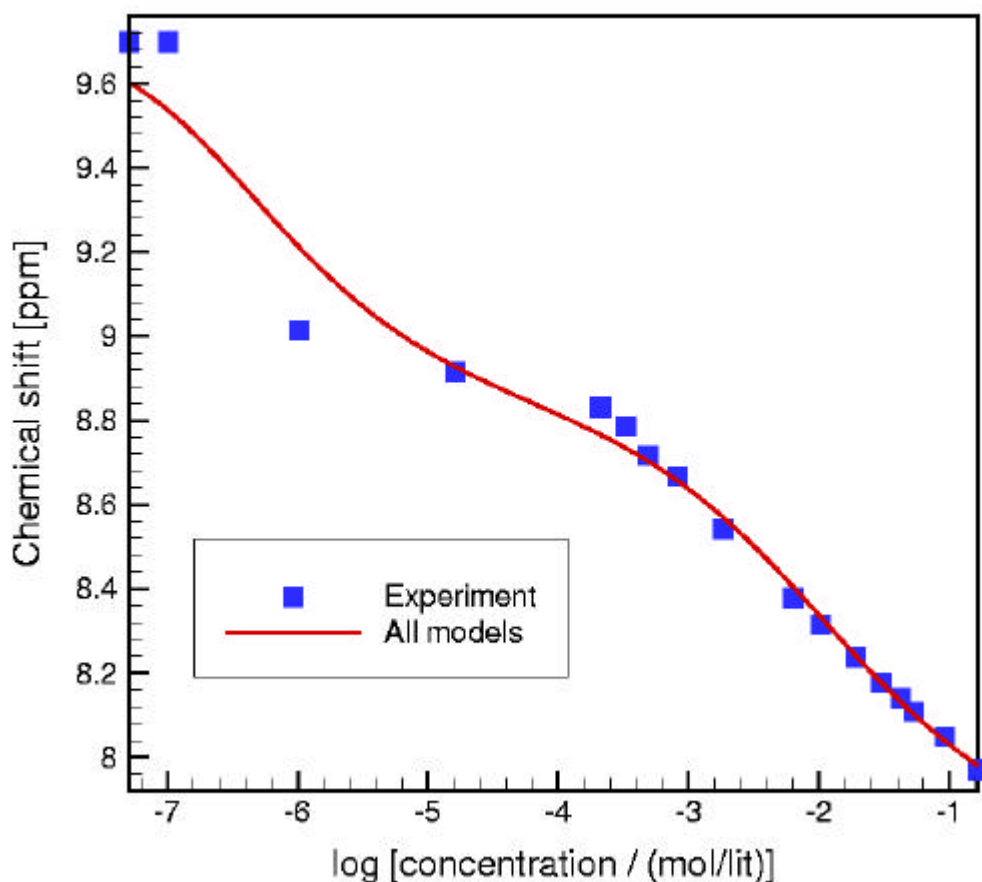


Figure 58: **Comparison between experimental data and models using the entire set of experimental data (Chemical shift of the monomer is constant at 9.699 ppm).**

When all data points are used the association constants are in the range of 25000 L/mol and 58000 L/mol. These values are by a factor of about 1000 higher than the ones calculated previously. The shape of the curve in this case is different to that observed in the previous case. Here, a shoulder emerges at concentrations of around 2.1×10^{-4} mol/L. This could be an indication of a two step aggregation process. At first, an equilibrium between dimers and multimers is present whereas at lower concentrations ($< 2.1 \times 10^{-4}$ mol/L) an equilibrium between dimers and monomers is observed. This would also explain the drastic change of the value for the chemical shift reported in Table 8, i.e. when decreasing the concentration from 1.025×10^{-6} to 1.025×10^{-7} mol/L the δ number jumped from 9.014 to 9.699 ppm. After this, the chemical shift was independent of the concentration and remained constant at 9.699 ppm.

The experimentally found value of 9.699 ppm for the chemical shift for a HBC-C₁₂ monomer is consistent with the calculated data obtained by quantum *chemical ab initio* studies. Here, Ochsenfeld and co-workers determined the chemical shift of a HBC monomer to be 9.7 ppm.^[83, 84] The conformity of both experimental data and theoretical calculations is a validation for the proof of the conducted studies. The high dilution that was necessary to reach the point where no aggregation of HBC discs was observed is an impressive demonstration for the strong π - π interactions that are responsible for the self-assembly of the investigated systems.

The distribution of HBC discs in the solution as depicted in Figure 59, i.e. the number of discs in a stack at a given concentration can be estimated using the parameters calculated from the EK, EKNN, AK and AKNN methods.

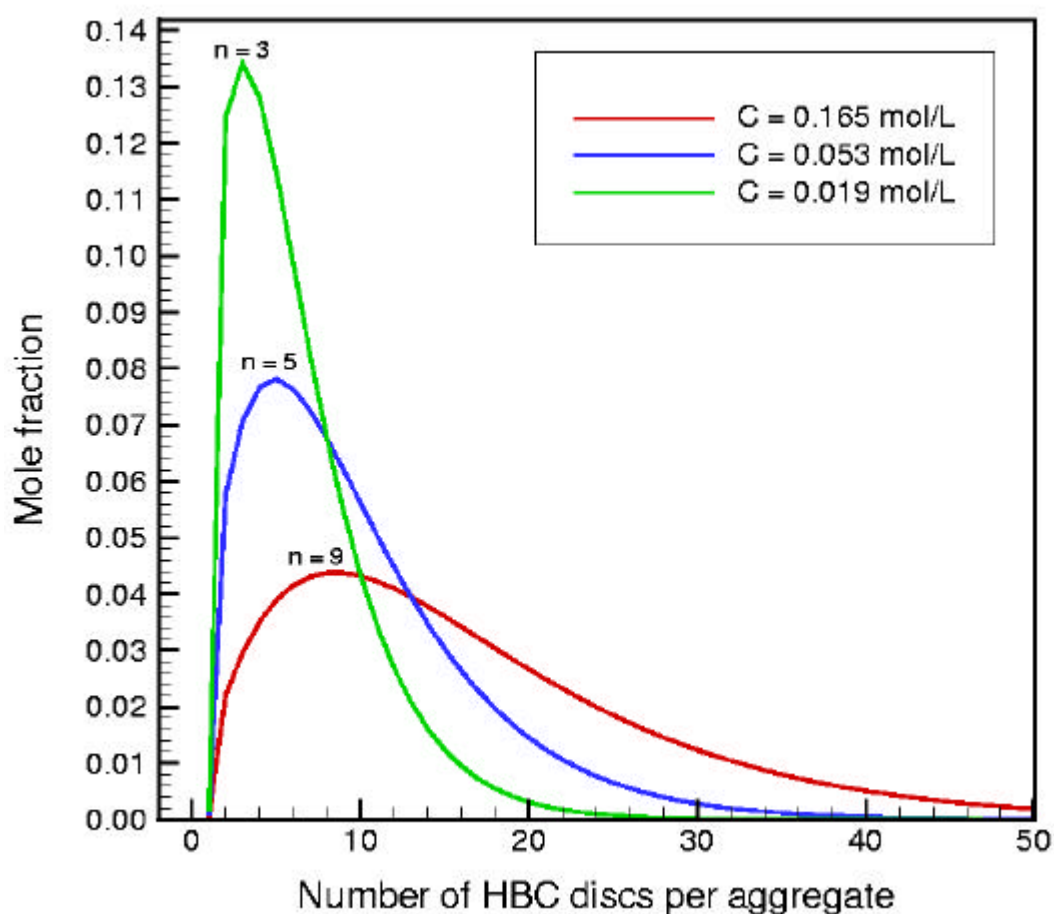


Figure 59: **Number of discs aggregated at given concentrations**

For the EK and EKNN methods, the mole fraction of the higher n -mers can be calculated using

$$a_i = r i a^i (K_E C)^{i-1}; \quad \text{with } i \geq 2$$

where C is the total concentration.

while for the AK and AKNN methods, it is given by

$$a_i = \frac{t a^i (K_A C)^{i-1}}{(i-1)!}; \quad \text{with } i \geq 2$$

The mole fractions of the number of discs in a stack for degrees one (monomer) to 50 are plotted in Figure 1 for three different total concentrations. For C = 0.019 mol/L, a maximum is attained at $n = 3$, i.e. about 13% trimers exist; for C = 0.053 mol/L, a maximum is attained at $n = 5$; and at the highest concentration of C = 0.165 mol/L, a maximum is attained at $n = 9$.

The aggregation behavior of discotic liquid crystalline phthalocyanines was investigated in a similar approach by Schutte and co-workers.^[211] Here, the absorption spectra of a metal free phthalocyanine derivative in dodecane were analyzed in terms of monomer-dimer-trimer equilibria.^[211] The aggregation in dodecane was studied in a concentration range of 10^{-2} to 10^{-7} M at room temperature. In this concentration range, the phthalocyanines were found to mainly consist of dimers with an association constant of $K_A = 1.50 \times 10^6 \text{ M}^{-1}$. These results compare to the findings of this investigation. For HBC-C₁₂ the association constant for dimers was determined to be $K_A = 5.8 \times 10^4 \text{ M}^{-1}$ when using the AKNN model. The difference in magnitude (by a factor of 100 lower for the HBCs) certainly results from the elevated temperature utilized in these experiments according to van't Hoff's law and due to the highly simplified model used by Schutte where higher aggregates (> 3) are neglected. It is not only the association constants for the discotic phthalocyanine investigated by Schutte and the HBC derivative studied here that show similar behavior. The number of phthalocyanine discs assembled in aggregates was reported to be between two

and six depending on the concentration. In the study conducted here, it was possible to further extend the investigation of disc-like HBCs, i.e. monomers as well as aggregates with an average of nine molecules in a stack were found.

Nomenclature:

EK: Equal K model

EKNN: EK considering next nearest neighbors

AK: Attenuated K model

AKNN: AK considering next nearest neighbors

K_E : Equilibrium constant

K_A : Association constant

ρ : factor by which dimer formation differs from other polymer formation in EK models ($K_2 = \rho K_E$)

τ : factor by which dimer formation differs from other polymer formation in AK models ($K_2 = \tau K_A/2$)

f : factor relating shift of end molecule to that of the monomer and the interior molecule ($P_\lambda = (1-f)P_\alpha + f P_\xi$)

r : factor indicating importance of next-nearest-neighbor

P_α : NMR shift of monomer

P_ξ : NMR shift of interior molecule

3.8.6 Concentration dependant UV/Vis measurements

In a similar approach to the above described $^1\text{H-NMR}$ experiments, UV/Vis concentration dependant measurements were conducted. Three different solutions of HBC- C_{12} **6b** in a concentration range of 6.07×10^{-3} to 6.07×10^{-5} mol/L were prepared in CHCl_3 . Here, the main HBC absorption band at 373 nm, corresponding to a $\pi\text{-}\pi^*$ transition, was monitored. It was attempted to reproduce and verify the association constants determined in the previous chapter, by fitting the shift of the UV/Vis absorption bands to the self-association

model developed by Martin^[210]. However, as apparent from Figure 60 no shift in the UV/Vis spectra was observed. No bathochromic or hypsochromic shift could be monitored for the main β -band nor for the para- (p) band. Not even the bandwidth or the overall shape of the different UV/Vis spectra changed (Figure 60).

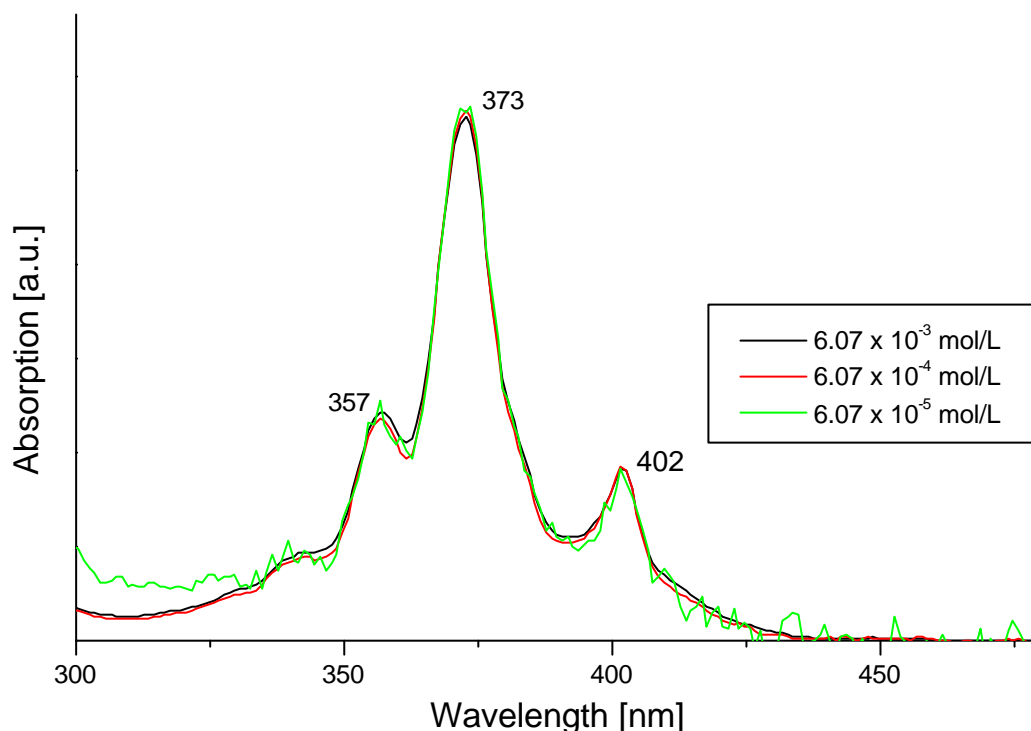


Figure 60: **Concentration dependent UV/Vis spectra of HBC-C₁₂ 6b at room temperature in chloroform**

An explanation for this phenomenon is the concentration independence of the monitored β - and para-band. A different behavior might be observed for the absorption band which is present at around 250 nm as observed for spincoated films of HBC (Figure 34). However, this band can not be monitored due to the absorption of the solvent in this region when conducting UV/Vis measurements in chloroform. A solvent that would be suited much better for this approach would be heptane. In heptane, measurements could be conducted even in the small wavelength region down to 200 nm further, aggregation would be much stronger in this non-polar solvent. However, the limiting factor in this case is the very low to non existing solubility of HBC-C₁₂ in heptane at room temperature.

Other solvents as THF or chloroform will not permit UV studies at room temperature. Thus, it can be concluded that the determination of association constants utilizing UV/Vis spectroscopy is not the method of choice. Other experiments that also reveal concentration dependent behavior are light scattering and vapor pressure osmometry (VPO). These methods will be used in the future to further investigate the aggregation behavior of HBCs in solution.

4 Functionalized HBC derivatives

4.1 Introduction

The production of materials on a large scale becomes more and more important when the targeted compound is being tested for possible device applications. The availability of hexaalkyl-substituted HBCs on a multi gram scale has become more facile with the incorporation of $[\text{PdCl}_2(\text{dppf})]$ ^[112] for the alkyl functionalization of 4,4'-dibromodiphenylacetylene **21**.^[37, 104] However, the $\text{Co}_2(\text{CO})_8$ catalyzed cyclotrimerization of a functionalized diphenylacetylene only gives access to molecules with C_6 symmetry. It has the advantage of a fast and easy access to soluble alkylated HBCs, but the disadvantage of not providing single site functionalization or break of symmetry in any controlled manner. Alternately, Ito *et al.* presented a synthetic strategy that allows *mono*-, *ortho*-di-, and *para*-di-functionalization of the hexabenzocoronene discs (HBCs **7**, **8** and **9** respectively) as already demonstrated in the Introduction.^[28] The sp^2 C-Br bond of bromo-functionalized HBCs served as a reactive site for coupling reactions leading to a number of new functionalized HBCs.^[28] By benzene-analogous transition-metal catalyzed chemistry, HBC derivatives with cyano, ether, ester, amino, etc. functionality were prepared. These syntheses met with varying levels of success, which were no doubt limited in some cases by unsuccessful coupling conditions or by low solubility.

The mesoscopic behavior as well as the packing in two and three dimensions was studied especially for functionalized HBCs. The direct visualization of two-dimensional crystals and liquid crystals of hexabenzocoronene derivatives on surfaces such as HOPG (highly oriented pyrolytic graphite) and molybdenum sulfide was achieved by STM techniques.^[26, 28, 29, 94]

The *mono* bromo-substituted HBC **7** was also used as a starting material for a surface active HBC with a tethered carboxylic acid group.^[174] This derivative was then complexed with amino functionalized polysiloxane and polyethyleneimine resulting in remarkably long columns essentially free of

defects.^[32, 33] The surface activity of the HBC with a tethered carboxylic acid group was exploited to prepare LB films at the air-water interface.^[99]

These few examples taken together with the already existing vast number of triphenylene, dibenzopyrene and phthalocyanine derivatives emphasize the wide horizon facing the field of discotic liquid crystalline PAHs. However, considering the enormous number of publications dealing with triphenylenes that have been published since 1945, namely 545, only 20 deal with unsymmetrically substituted triphenylenes.^[201, 212-230] The same holds true for phthalocyanines, here 8269 articles have been published since 1945, whereas only 109 target the topic of unsymmetrical substitution, summarized in a review article by de laTorre et.al.^[231]

Nevertheless, the ample variety of functions, properties and applications that were utilized in the development of new and improved triphenylenes, dibenzopyrenes and phthalocyanines provided impetus for the syntheses of some of the functionalized HBC derivatives presented below.

4.2 Towards single columns of HBC

The columnar structure of discotic liquid crystals has been shown to be well suited for charge transport parallel to the columnar axis. To tailor the long range order, i.e. the gross structure of the supramolecular assembly as well as the mesophase behavior and processibility of such materials discotic oligomers, polymers and networks are required.

Brand and co-workers in the group of Prof. Müllen reported that the thermal polymerization of HBC derivatives containing acryloyl or methacryloyl functions at the terminal positions of all six alkyl chains had been achieved in the liquid crystalline phase. Hereby, a network was obtained in which the columnar hexagonal superstructure of the liquid crystalline phase was preserved and reported to be stable between $-100\text{ }^{\circ}\text{C}$ and $300\text{ }^{\circ}\text{C}$.^[174] Attempts to polymerize functionalized HBC derivatives in the main or in the side chain failed so far due to solubility reasons. However, copolymers from HBC precursors (hexaphenylbenzene derivatives) with relatively high molecular weights ($M_w = 1 \times 10^6$) have been prepared and analyzed.^[232] However, attempts of oxidative

cyclodehydrogenation using FeCl_3 in order to convert them into more conjugated HBC groups failed.^[232]

Liquid crystalline polymers with triphenylenes both in the main and in the side chain have been prepared and analyzed.^[21, 54-56, 157, 233]

Side group liquid crystal polymers (SGLCP) of e.g. triphenylenes^[222] consist of three distinct structural components: a polymer backbone, a liquid crystal group and connecting these, a flexible spacer which is most commonly an alkyl spacer. The role of the flexible spacer is to decouple, to some extent, the opposing tendencies of the polymer backbone to adopt a random coil conformation from those of the liquid crystal groups to self-assemble into an ordered mesophase. This decoupling endows the polymers with a unique duality of properties; they exhibit macromolecular characteristics such as enhanced processibility and glassy behavior combined with, for example, the electro-optic properties of conventional low molar mass liquid crystalline discotics. This combination of polymeric and low molar mass mesogenic properties is the basis of the considerable application potential of liquid crystalline polymers in a range of advanced electro optical applications.^[222]

The pioneering synthesis of liquid crystalline polymers by Ringsdorf and co-workers^[54] produced a mixture of products, was limited by scale, and more importantly, produced a mixture of inseparable isomers of ill-defined structure.^[234]

In this work attempts towards main chain polymers with HBC derivatives, i.e. isolated columns of HBC, will be presented. Figure 61 shows the basic concept for the realization of single columns of HBC.

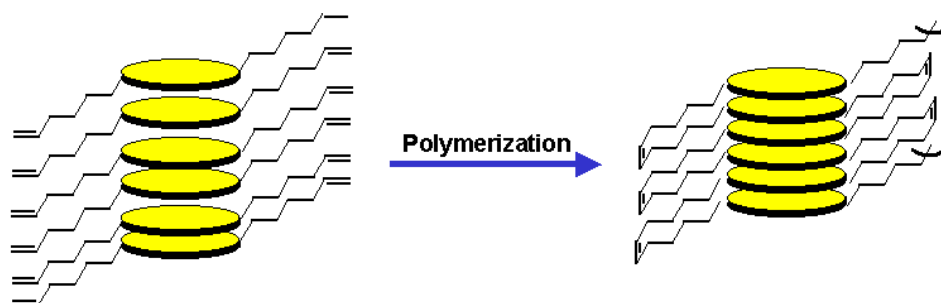
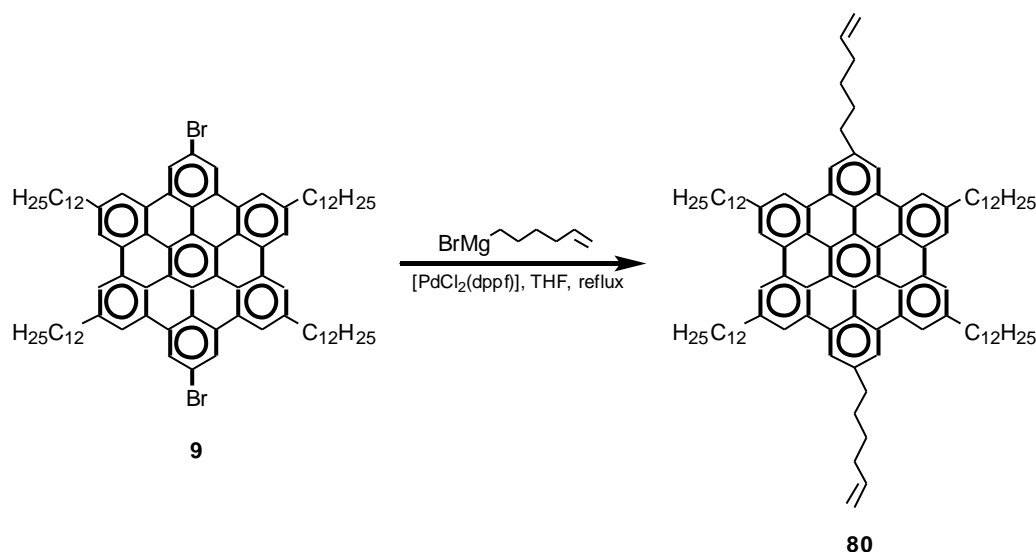


Figure 61: **Schematic representation of a single column consisting of HBC molecules**

Here, the intramolecular function is attached to the HBC core via an alkyl spacer which may allow control of orientation and/or induction of supramolecular (columnar) structures by covalent interactions with complementary components.

As indicated in Figure 61, it was planned to utilize alkyl chains with terminal double bonds for the polymerization of the HBC discs. Several advantages were implied with this design: a) all-alkyl hexabenzocoronenes such as **80** show higher solubilities than their *para* di-bromo substituted analog (HBC **9**), thus ensuring higher molecular weights, b) the alkyl spacer will permit a certain flexibility of the system, and c) olefin metathesis^[235, 236] is a transition metal catalyzed reaction which polymerizes even sterically demanding olefins under mild reaction conditions.^[237]

The synthesis of the dibromo substituted hexa-*peri*-hexabenzocoronene (*p*-Br₂-HBC-C₁₂) **9** was carried out under the same conditions as previously published by our group and depicted in the Chapter 1.^[28] The introduction of two hexene chains to the aromatic core was achieved via Kumada coupling reaction^[112] of hex-1-enyl-6-magnesiumbromide and the bis-functionalized *p*-Br₂-HBC-C₁₂ **9** in THF, using [PdCl₂(dppf)]^[112] as the catalyst. Precipitation with methanol and work-up afforded *p*-hexene-HBC-C₁₂ **80** in 75% yield as depicted in Scheme 20.



Scheme 20: **Synthesis of bis hexene functionalized HBC 80**

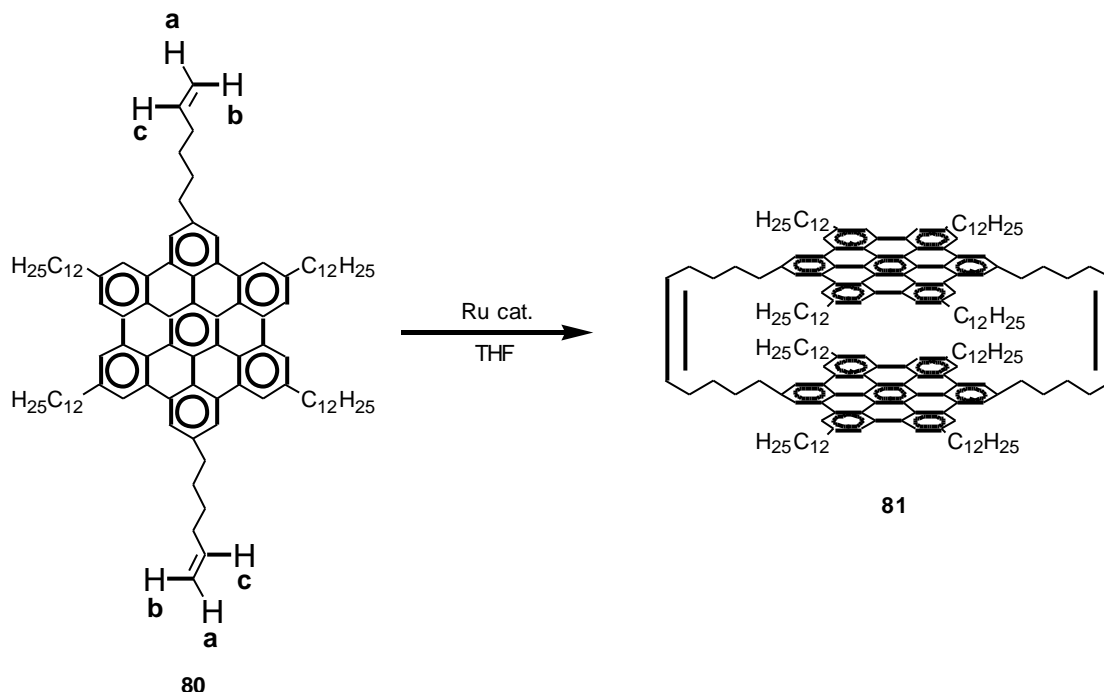
At this point it is noteworthy that the [PdCl₂(dppf)]^[112] catalyst proved to be not only excellently suited for the transition metal catalyzed functionalization of 4,4'-dibromodiphenylacetylene **21**^[37, 104] but also for the direct functionalization of bromo substituted HBCs. This is remarkable, since up till now only few reactions such as the Hagihara^[108] coupling reaction gave excess to a direct carbon-carbon bond formation with the HBC core.^[28, 174]

Differential scanning calorimetry (DSC) results revealed that *p*-hexene-HBC-C₁₂ **80** forms a discotic columnar mesophase at 121 °C.

For the endeavor of polymerization, studies conducted by Grubbs and co-workers^[235, 236] established that ruthenium carbene catalysts are very effective for the ring-closing metathesis of dienes. In their publications they disclose that the new ruthenium carbene catalyst possesses two important advantages over the common molybdenum-based reagents, i.e. a diminished sensitivity to atmospheric oxygen and moisture and an increased tolerance of most functionalities.^[235, 236] Due to these reasons, this new ruthenium-based Grubbs-catalyst was selected as the matter of choice for the ring closing polymerization of **80**.

Treatment of HBC-diene **80** with 2-4 mol % of ruthenium catalyst at room temperature in THF, as depicted in Scheme 21, did surprisingly not result in the

formation of HBC main-chain polymer or in HBC oligomers but exclusively in the formation of HBC cyclophane **81** (Scheme 21).



Scheme 21: **Outcome of ring closing metathesis of HBC-diene **80** with ruthenium-based Grubbs-catalyst**

Several attempts of varying the reaction conditions such as elevated temperature, change of solvents, and/or concentration of starting material did also not afford HBC oligomers or polymer.

Work up of the reaction mixture was performed by quenching and precipitating the product with methanol. Followed by column chromatography on silica gel using warm toluene as the eluent. HBC cyclophane **81** was obtained as a yellow crystalline powder.

Figure 62 displays the FD mass spectra that was obtained from the product after work up. Here, the two most dominant peaks (M^+ (100%) = 2663.1 and M^{2+} (35%) = 1331.6) correspond to the cyclophane product **81** (Scheme 21 and Figure 63). Further, an additional peak at M^+ (18%) = 2692.3 is apparent. This peak can be assigned to a half closed cyclophane **82** as shown in Figure 63.

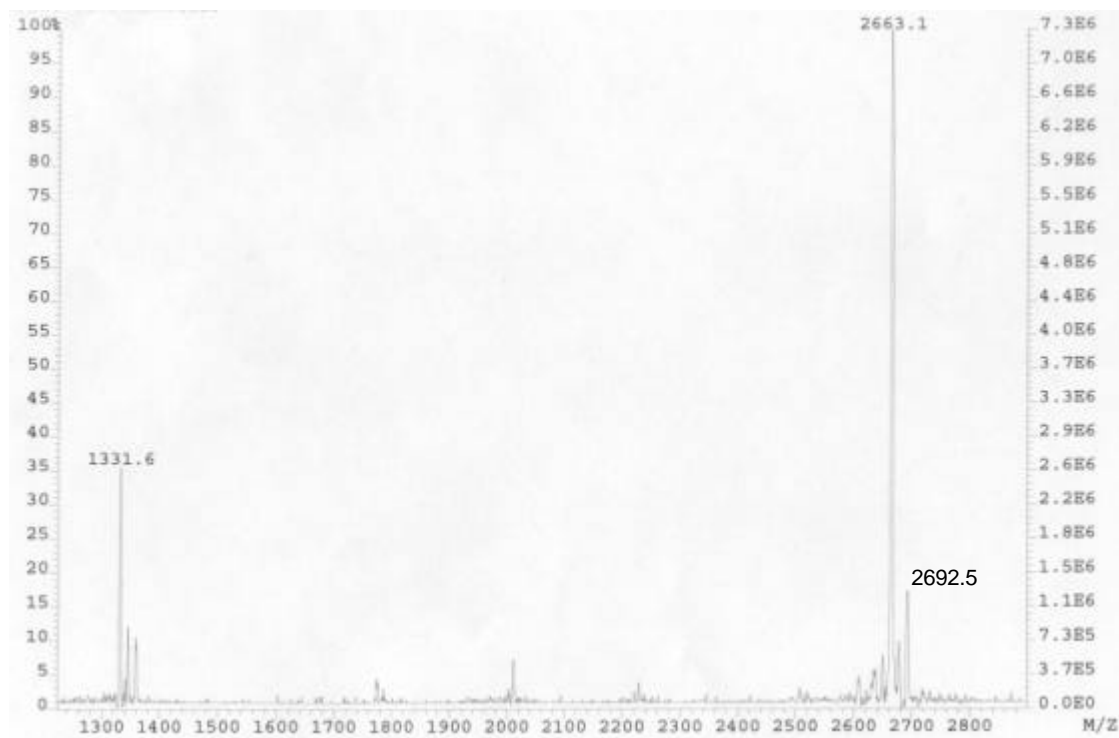


Figure 62: **FD mass spectra of cyclophane 81 after metathesis reaction**

MALDI-TOF mass spectrometry as well as GPC analysis under standard conditions of the obtained yellow product did not reveal any further oligomer derivatives or even low molecular weight polymers.

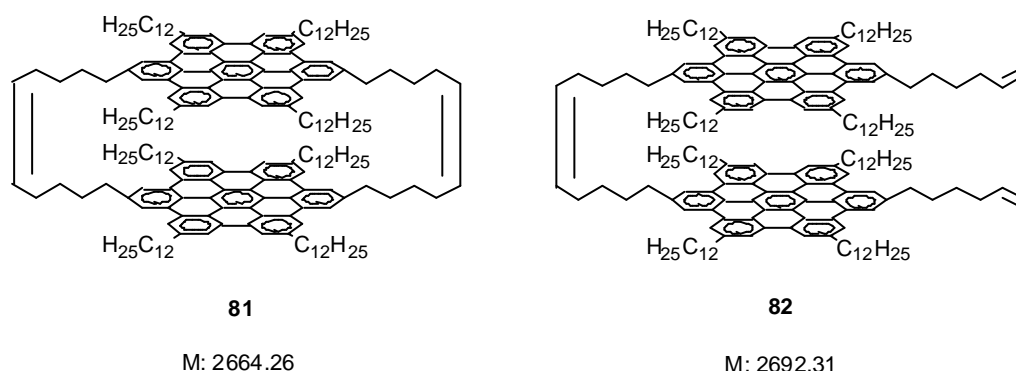


Figure 63: **HBC cyclophane 81 and partially closed derivative 82**

Literature survey revealed that in a similar experiment Ghadiri^[238] and co-workers synthesized a tricyclic peptide. Here, it was hypothesized that the hydrogen-bonded ensemble of peptides, which favors a productive orientation

of the olefinic side chain moieties, would lower the activation entropy for the intermolecular carbon-carbon bond forming olefin metathesis process.^[238] In analogy to the above, the strong π - π interactions of the HBC cores also seem to promote the formation of the cyclophane. The metathesis reaction of the peptides appeared to proceed in a stepwise fashion as judged by the transient buildup of small quantities of an intermediate dimeric species where only the first intermolecular side chain olefine bond was closed. In this case, purified samples of this intermediate, when subjected to the metathesis reaction conditions, converted to the tricyclic product.^[238]

From the displayed FD mass spectra it appears that the metathesis reaction of HBC-diene **80** to the HBC-cyclophane **81** seems to be very efficient and high yielding in terms of conversion of monomer to cyclophane. However, attempts to purify the mixture of cyclophane **81** and half closed derivative **82** by means of column chromatography and/or crystallization were not successful. Even when the mixture of products was again treated with ruthenium catalyst no defined cyclophane was obtained. Thus, no defined NMR analysis could be conducted of cyclophane **81** or its derivative **82**. Nevertheless, Figure 64 displays the ¹H-NMR spectrum of the monomer **80** (black line) and the resulting crude products **81** and **82** (red line).

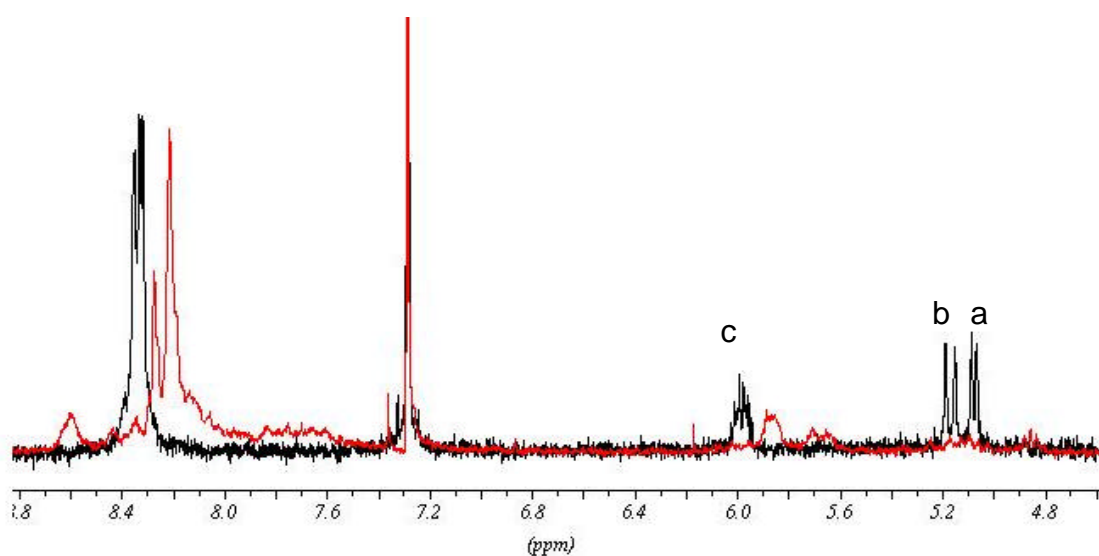


Figure 64: ¹H-NMR spectra of HBC **80** (black line) and crude products **81** and **82** (red line) in CDCl₃ at room temperature; protons a), b), and c) as outlined in Scheme 21

From this comparison it is obvious that the terminal protons **a** and **b** Scheme 21 and Figure 64 have almost disappeared and that only the internal protons **c** of the vinyl group remain. The remaining weak signals in the region of the terminal vinyl protons could be explained by the presence of unclosed double bonds as in **82**. No individual signal was observed between 5.6 and 6.1 ppm but two multiplets with different intensities. This could be an indication for the presence of cis and trans configurations of the new formed double bond in **81**. The broad signals that were recorded for the aromatic region after the metathesis reaction are also an indication for the mixture of products as depicted in Figure 63. Dr. Mark Watson in our group is currently engaged in altering the synthesis in such a way that analytically pure material will be available shortly, this includes the use of a cyclophane monomer where the solubilizing alkyl arms consists of the branched alkyl chain (as in HBC-C₈) introduced in this work.

4.3 Thiophene substituted HBCs

The beneficial effects of heteroatom inclusion on the phase behavior has already been discussed previously. Here, the substitution of HBC with thiophene moieties will be presented. There are several reasons that promote the substitution of HBC derivatives with thiophene.

For example, it is generally found in π -stacked conductors that the addition of larger chalcogenide atoms (e.g., S, Se) improves conductivity. This effect is due to an increase in the radial extension of the orbitals which increases both the delocalization (bandwidth) and carrier mobility.^[239, 240] In this context, Swager and co-workers reported the syntheses and mesomorphism of novel octaalkoxymethyl-substituted tetra-2,3-thiopheno-phorphyrazines, heterocyclic phthalocyanine analogues in which the benzene rings are replaced by thiophene rings. Among the attractive features of liquid-crystalline 2,3-thiophenophorphyrazines as compared to phthalocyanines are their lower mesomorphic and isotropic temperatures. These features have resulted in liquid crystallinity at room temperature.^[240, 241]

Additionally, it seems promising to combine the interesting semiconducting properties of thiophenes or oligothiophenes with the opto-electronic properties

of hexabenzocoronenes on the level of the respective monomers as well as further attempts to polymerize the thiophene substituted HBCs.

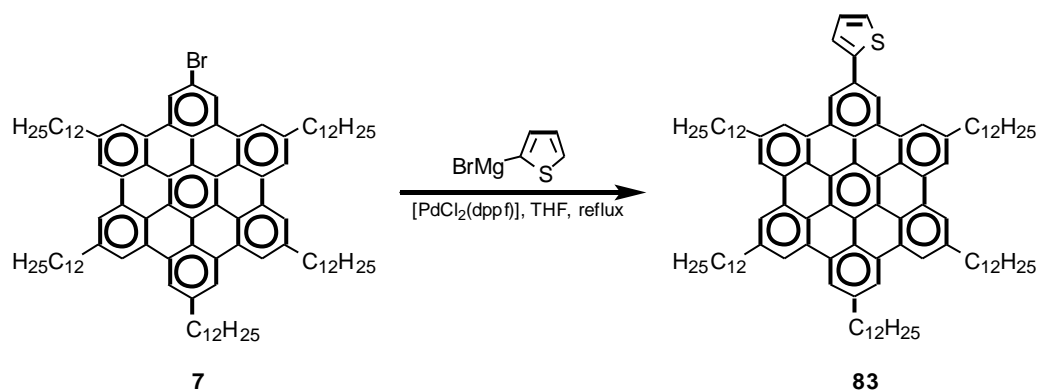
In a collaboration with Bettina Baumeister in the group of Prof. Jung (Switzerland) the self-assembly processes and the structure of monolayers of thiophene substituted HBCs on gold surfaces were intended to be studied by atomic force microscopy (AFM).

The syntheses of the different thiophene substituted HBC derivatives are presented in the following sections.

4.3.1 Synthesis and characterization of α -thiophene substituted HBCs

Over the last years, selective and high yielding syntheses involving thiophenes and oligothiophenes^[242] have gained increasing importance due to the growing interest in these materials for nanotechnology applications such as photovoltaics and field effect transistors.^[132, 142-144, 243, 244]

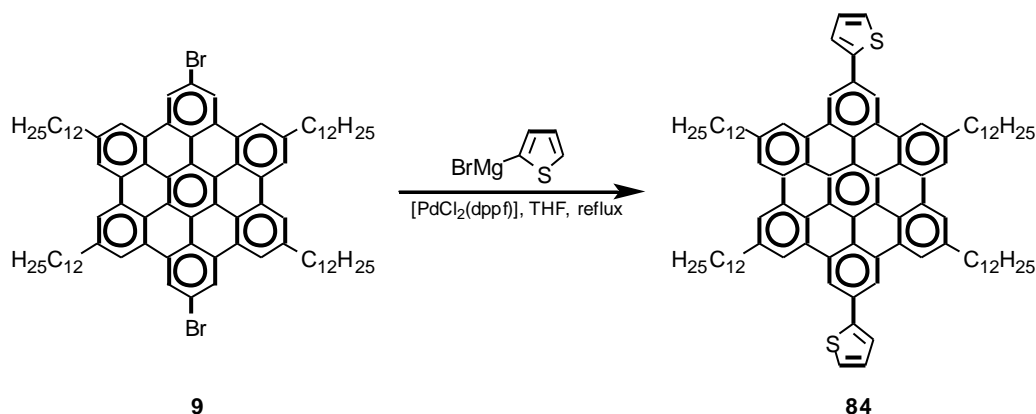
The general applicability of thiophene substitution on the HBC core was tested for the mono bromo functionalized HBC derivative **7**. One effective method for the carbon-carbon bond formation involving thiophene as one of the coupling partners is the Grignard coupling reaction.^[245] Here, commercially available 2-bromo thiophene was transferred to the corresponding thiophenylmagnesium bromide under classical Grignard conditions.^[107] The actual coupling of the metallated thiophene and the bromo functionalized HBC was carried out in THF. At first, HBC derivative **7** was dissolved in warm THF followed by addition of $[\text{PdCl}_2(\text{dppf})]$ ^[112] catalyst, then a large excess of 2-thiophenylmagnesiumbromide was added to the solution (Scheme 22). After reflux overnight, the reaction mixture was cooled down to room temperature upon which crude **83** precipitated from the solution. Reprecipitation of **83** from toluene and column chromatography on silica gel afforded α -substituted thiophene HBC derivative in good yields. HBC **83** shows good solubilities at slightly elevated temperatures in THF, chloroform and toluene.



Scheme 22: **Synthesis of mono- α -thiophene-HBC- C_{12} **83****

Compound **83** has been intensively characterized by NMR spectroscopy and has been subjected to differential scanning calorimetry (DSC) and thermo gravimetric analysis (TGA). These results will be discussed later in context with other thiophene substituted HBC materials.

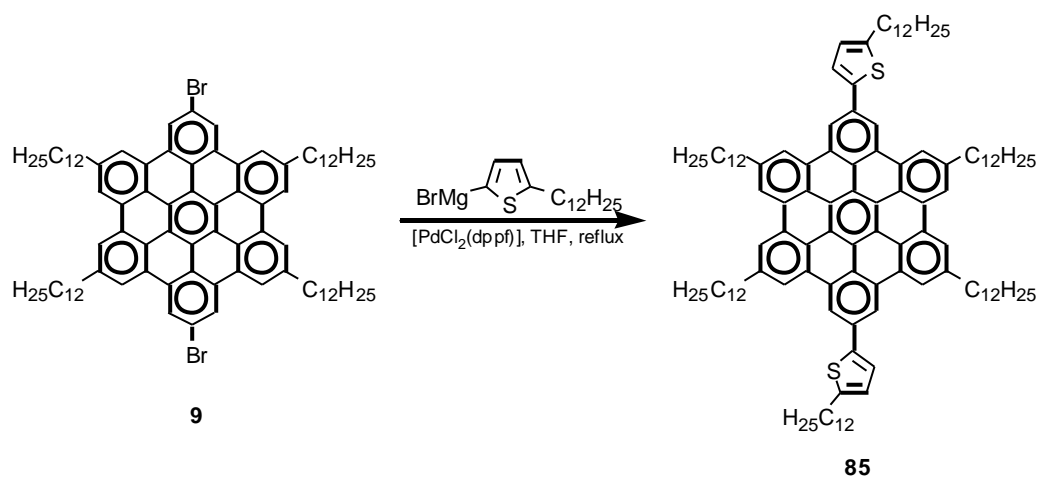
Considering HBC **83** as a model compound for the general feasibility of thiophene substitution on the HBC core, it is now important to synthesize a material that can be subjected to further reactions since **83** is, from this point of view, a dead end. Mentioned above was the idea to combine HBC and thiophene in a co-polymer. For this purpose the substitution of di-bromo HBC **9** with α -thiophene was carried out under similar conditions as elaborated for the synthesis of **83**. However, to ensure that the Kumada-type coupling reaction with $[\text{PdCl}_2(\text{dppf})]^{[112]}$ catalyst will only deliver completely substituted material an even larger excess of 2-thiophenylmagnesiumbromide was used. Scheme 23 displays this reaction sequence that afforded *para* bis- α -thiophene substituted HBC **84** in good yields.



Scheme 23: **Synthesis of para-a-thiophene-HBC-C₁₂ 84**

The work up and purification of **84** was carried out under the exact same conditions as described for **83**. NMR, DSC and TGA analysis was also carried out in this case and revealed interesting phase behavior as is discussed below. The solubility of **84** slightly decreased compared to derivative **83** but is still within tolerable limits at elevated temperatures. Polymerization of **84** was attempted with iron(III)chloride, FeCl₃, since this method is reported to be easy, suitable for large scale production, and gives high molecular weight polymers.^[246] The standard procedure for this polymerization is to suspend FeCl₃ in chloroform and then to add the monomer quickly to this solution.^[247] This, however, did not result in conversion of monomer **84** to either polymer or oligomers. Unreacted starting material was recovered after short column chromatography. Andersson^[246] and co-workers reported a slightly altered version of this polymerization. This procedure consists of adding a suspension of FeCl₃ in chloroform to the monomer which is also dissolved in chloroform. By this method, less risk of mislinkages in the polymerization, e.g. coupling in the 4-position on the thiophene ring and high molecular weights were reported.^[246] Unfortunately, also this variation of the FeCl₃-method was unsuccessful. Variation of reaction temperature and/or concentration of monomer and/or FeCl₃ also did not result in the formation of even small oligomers. The low solubility or the bulkiness of the starting material might be responsible for this outcome.

In the literature solubility problems of oligothiophenes have been reported and tackled by alkyl substitution of thiophene.^[245, 248] The same approach was utilized for the synthesis of solubilized HBC **85**. In a first step 2-bromothiophene was functionalized, according to standard literature procedures, with a *n*-dodecyl alkyl chain.^[248] In this attempt, the classical Grignard reaction in diethylether was catalyzed with $[\text{NiCl}_2\text{dppp}]$ catalyst. Next, 2-dodecylthiophene was brominated using bromine and chloroform as the solvent to afford 2-bromo-5-dodecylthiophene in good yields.^[248] The final step of this reaction sequence was the Kumada-type coupling reaction of 5-dodecylthienyl-2-magnesiumbromide with di-bromo HBC derivative **9** in THF catalyzed with $[\text{PdCl}_2(\text{dppf})]$ as depicted in Scheme 24. Here, workup and purification of the crude product by column chromatography afforded the well soluble material **85** in high yields.



Scheme 24: **Synthesis of solubilized thiophene HBC derivative 85**

The purity of the obtained product is well documented by the $^1\text{H-NMR}$ spectra depicted in Figure 65.

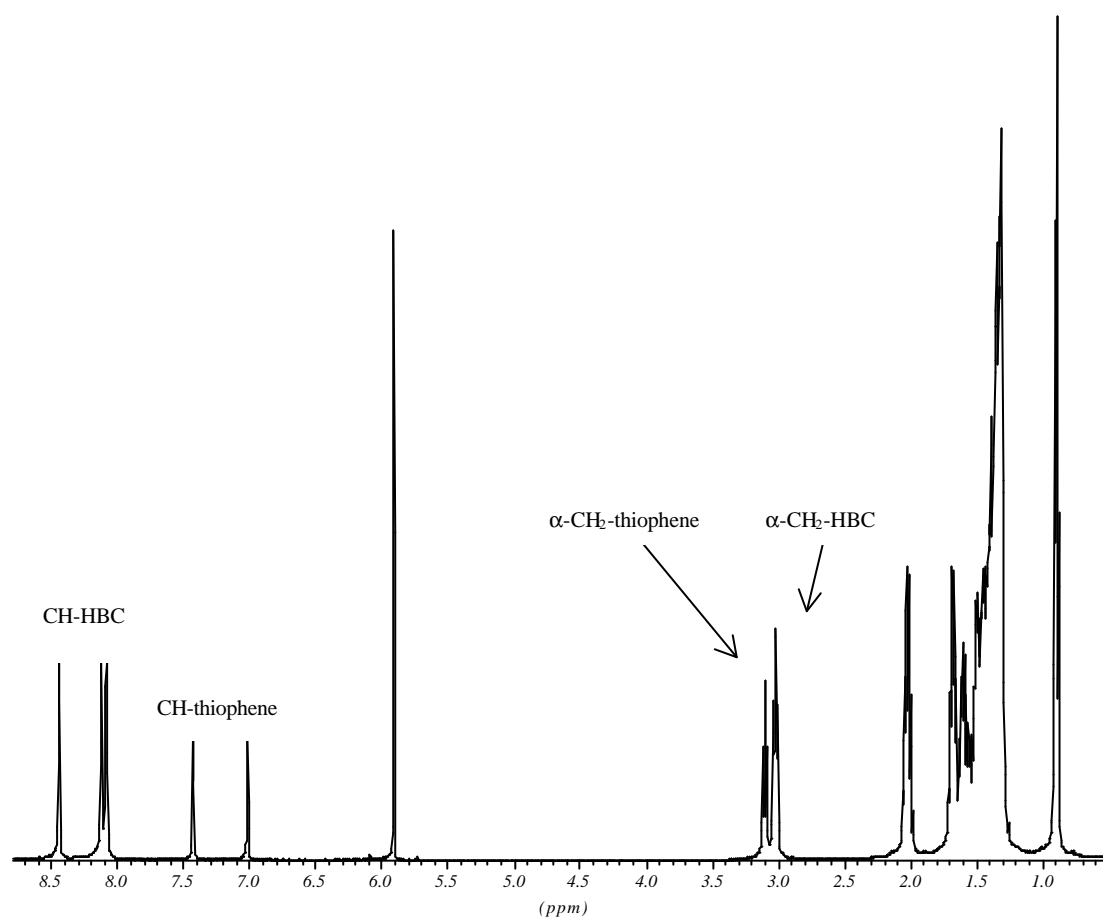


Figure 65: $^1\text{H-NMR}$ spectra of HBC 85 in $\text{C}_2\text{D}_2\text{Cl}_4$ at $100\text{ }^\circ\text{C}$

Even though the solubility was greatly enhanced in the case of HBC derivative **85**, it is not suitable for further polymerization attempts since the reactive α -positions are both locked with *n*-dodecyl alkyl chains. However, this material is of great interest for the self-assembly from solution on gold substrates and is currently investigated by means of AFM spectroscopy in the hands of Bettina Baumeister in the group of Prof. Jung (Switzerland).

4.3.2 Mesophase characterization of thiophene substituted HBC derivatives **83**, **84** and **85**

A series of hexabenzocoronenes (**83-85**) with a variety of different thiophene substitution patterns, i.e. *mono-*, *para di-*, and decorated with flexible dodecyl chains, was synthesized. Since all the above compounds are thermotropic liquid crystals, the thermal stability of these materials was first checked by thermogravimetric analysis (TGA). All other characterizations were then carried out below the decomposition temperature. The transition temperatures of compounds **83-85** were measured using differential scanning calorimetry (DSC). DSC traces and thermodynamic data are given in Figure 66 and Table 11.

In the first heating scan, **83** showed one endothermal peak at 92°C. In the second heating scan (Figure 66), the same peak was observed. The optical texture that was observed developed in a starburst shape and transformed into a texture, which was similar to some textures exhibited by columnar mesophases reported earlier.^[27, 28]

The thermal behavior of **84** is remarkably different from that of **83**. Compound **84** also formed a mesophase in a wide temperature range observed by both POM and DSC. However, in the first heating scan two endothermal maxima at 71°C and 175 °C were observed. The first cooling scan showed two exothermal peaks at 120 °C and 68 °C. The second heating scan showed similar features like the first heating scan. The peaks at 71 °C and 175 °C were attributed to the phase transition from the crystalline phase to the columnar mesophase and an inter-mesophase transition respectively.

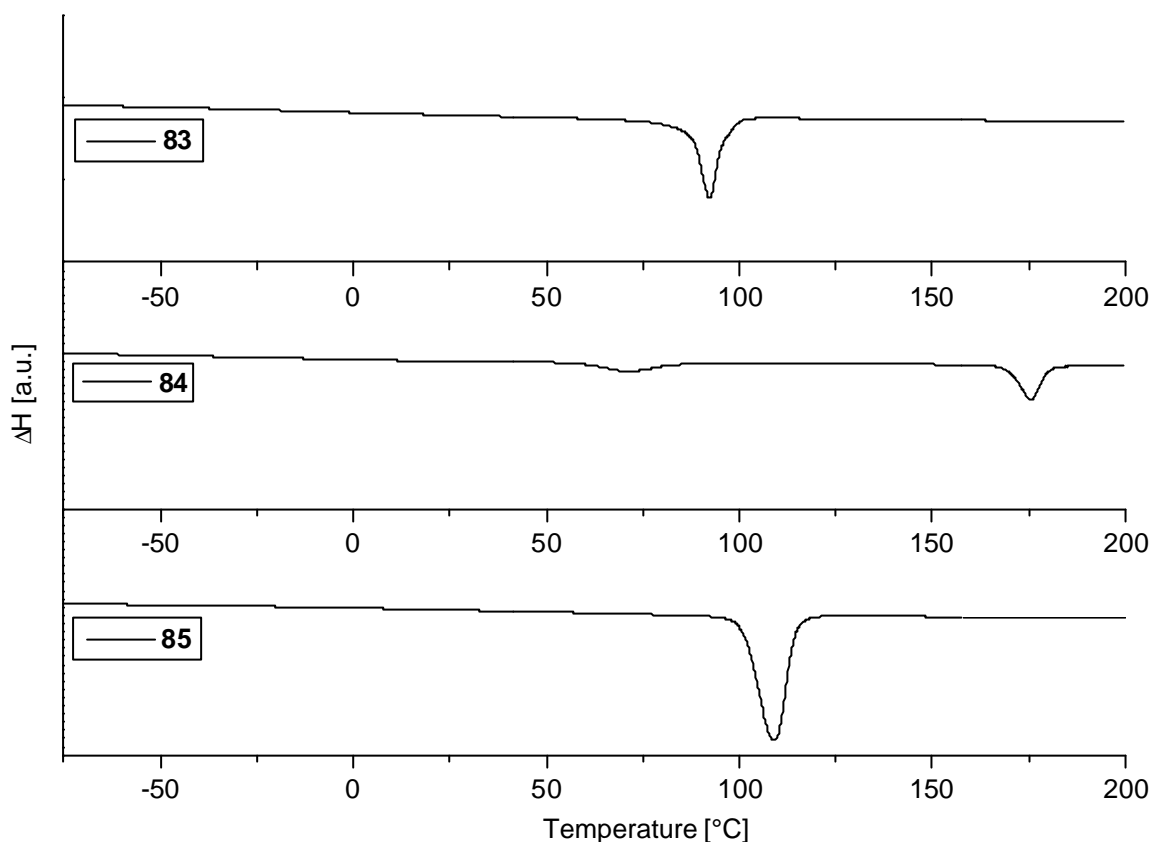


Figure 66: **Differential scanning calorimetry traces of HBC derivatives 83, 84, and 85**

Remarkably, HBC **85** exhibits the highest phase transition temperature among the thiophene substituted HBCs for the transformation of the crystalline phase to the columnar mesophase. This transition occurs at 107°C, both in the first and in the second heating scan. This is surprising since HBC **85** is decorated with two additional long flexible alkyl chains which normally ensure lower phase transition temperatures.

Table 11 summarizes optical, thermal, and thermodynamical data for compounds **83**, **84** and **85**.

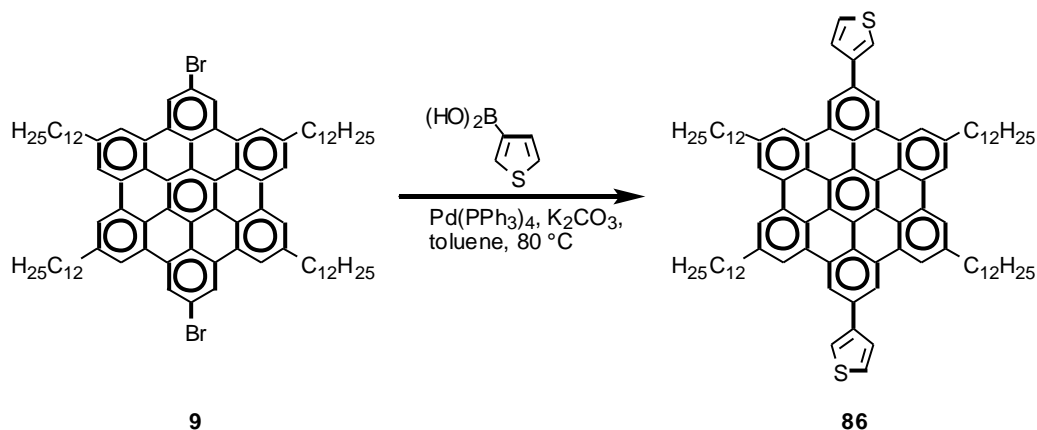
Compound	Transition	T [°C]	ΔH [Jmol ⁻¹]
83	K→Col	92	64
	Col→I	>430	
84	K→Col ₁	71	15
	Col ₁ →Col ₂	175	23
	Col→I	>430	
85	K→Col	107	134
	Col→I	>430	

Table 11: *Optical, thermal, and thermodynamical data for compounds 83, 84 and 85 (K = crystalline phase, Col_{ho} = ordered hexagonal columnar mesophase I = isotropisation)*

4.3.3 Synthesis and characterization of *b*-thiophene substituted HBC

As reported in the previous chapter, all attempts to polymerize α -thiophene substituted HBC **84** were unsuccessful. Nevertheless, in order to synthesize a polymerizable HBC derivative the synthesis of a β -thiophene substituted derivative, namely HBC **86** was attempted. In this case, both the reactive α -positions are unblocked and amenable for additional reactions. Initial efforts to synthesize **86** via Kumada-type coupling reaction of thiophenyl-3-magnesiumbromide and *para* di-bromo HBC **9** failed miserably. Alteration of reaction conditions and variation of transition metal catalyst did not result in the desired product. Thus a different coupling reaction had to be applied in this case. Other methods such as Stille or Suzuki coupling reactions involving thiophene have been reported in the literature.^[249-251] Scheme 25 displays the reaction sequence that was successfully utilized to synthesize *para* β -thiophene HBC **86**. In a Suzuki-type^[249, 251] coupling reaction catalyzed with [Pd(PPh₃)₄],

commercially available thiophene-3-boronic acid reacted with HBC **9** to yield compound **86** in good yields (75%).



Scheme 25: **Synthesis of para-b-thiophene-HBC- C_{12} 86**

Surprisingly, HBC derivative **86**, different from **84**, is almost completely insoluble in most organic solvents even at elevated temperatures. Thus, attempts to polymerize **86** with FeCl_3 were undertaken but also failed completely. Even reaction times of up to one week and/or elevated temperature did not result in the formation of dimers or oligomers.

4.4 Ultrafast excitation energy transfer in covalently linked donor-acceptor systems

The self-organization of phase separating liquid crystalline and crystalline soluble conjugated molecular materials has been reported earlier and employed to create segregated structures optimized for charge separation and transport in photovoltaic device structures. The soluble, liquid-crystalline discotic hexa-peri-hexabenzocoronene (HBC-PhC₁₂ **43**) has been combined with a soluble electron-accepting perylene diimide dye **44** to produce thin film photovoltaic cells with maximum external quantum efficiencies of over 34% near 490 nm.^[105] The high efficiencies result from efficient photoinduced charge transfer between the hexabenzocoronene and the perylene as well as effective transport of electrons and holes to the cathode and anode through segregated perylene and discotic hexabenzocoronene π -systems.

The existence of a nearly ideal, self-organized structure in which vertical segregation of charge transport layers coexists with a high interfacial area between the two charge transfer components was presented. The close ordered packing of the HBC-PhC₁₂ **43** and the perylene diimide dye **44** proved to be important for the efficiency of the fabricated photovoltaic cell. These findings directed further research towards the development of covalently connected hexabenzocoronene-perylene donor-acceptor systems.

In a similar approach Bi and co-workers^[252] reported the synthesis of a zinc phthalocyanine photosensitized donor-acceptor system for light energy conversion and for the design of photoelectrochemical molecular devices. Covalently linked phthalocyanine complexes were incorporated in bilayer lipid membranes and deposited on SnO₂ transparent electrodes. Their photovoltages were measured and compared. It was found that a more favorable orientation and closer proximity are attained in the covalently linked diad compound, between the donor (phthalocyanine)-acceptor (anthraquinone) pair, thus resulting in higher efficiencies.

Peeters et.al.^[253] recently published the synthesis, photophysical properties, and the preparation of photovoltaic devices of covalently linked oligo(p-

phenylene vinylene)(OPV)-fullerene dyads. The photophysical properties of these donor-acceptor dyads were studied as a function of the conjugation length in solvents of different polarity and as thin films. Fast singlet energy transfer occurred after photoexcitation of the OPVn moiety of the dyads towards the fullerene moiety in an apolar solvent.^[253] Here, through the link of the donor and acceptor via a covalent bond, a predefined phase segregation of nanoscopic dimension was created and gave rise to a well-ordered bicontinuous interpenetrating network of both donor and acceptor. The nanoscopic dimension of the phase separation was advantageous because the exciton diffusion length in conjugated polymers is limited to that length scale. Molecular ordering will enhance the charge carrier mobility and hence the separation of photogenerated electrons and holes. Finally, the bicontinuous network will ensure the unrestricted transport of electrons and holes to the electrodes. Each of these three factors, generation, stabilization and transport, may improve the efficiency of photovoltaic cells.^[253]

Encouraged by these findings, the synthesis and the photophysical properties of covalently linked hexabenzocoronene-perylene donor-acceptor systems will be presented below.

4.4.1 Syntheses of novel donor-acceptor systems

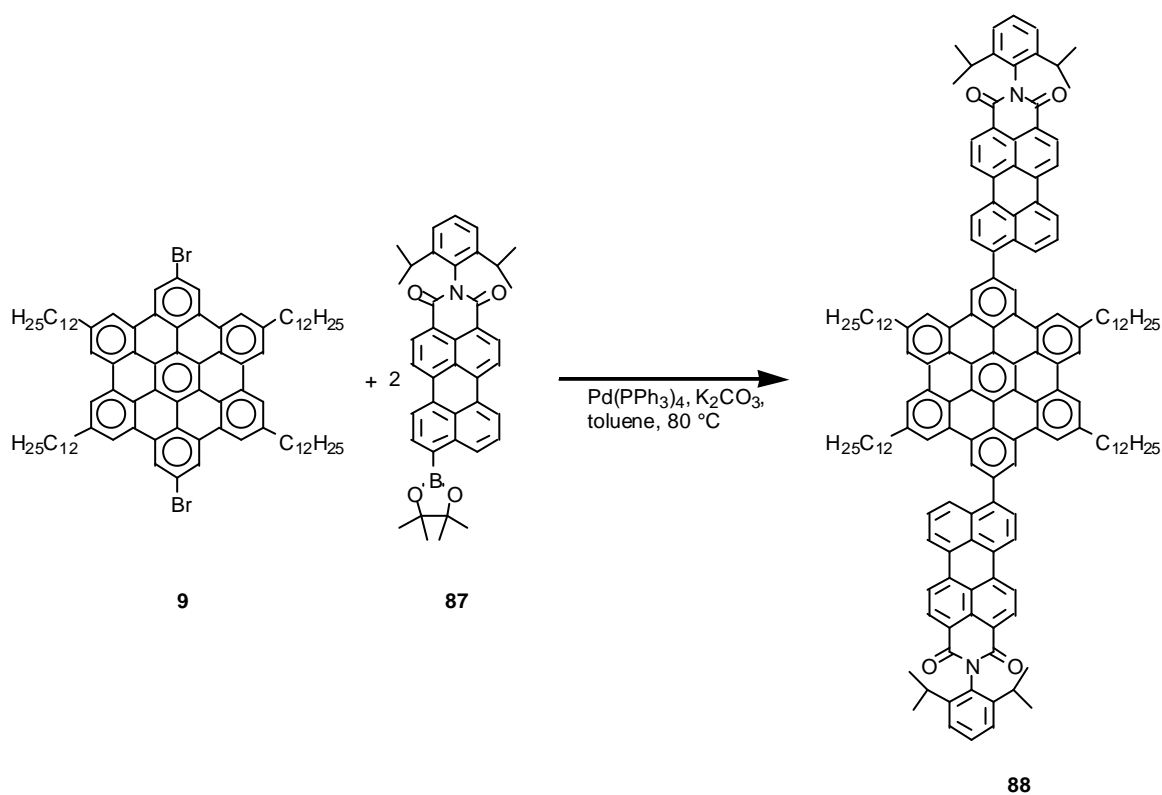
Since the above proposed endeavor combines the research interest of two of the sub-groups in the group of Prof. Müllen, the synergy of a functionalized liquid crystalline hexabenzocoronene derivative with a perylene dye was tackled together with E. Reuther.

Functionalized HBC derivative **9** has already been subjected to several transition metal catalyzed coupling reactions that have resulted in the formation of new carbon-carbon bonds. One of the most successful reactions in terms of conversion rate and yield was the Kumada-type coupling reaction.^[112] However, this method is not applicable for the connection of HBC derivative **9** with a perylene monoimide similar to **87** since the oxygen functionalities do not tolerate these conditions. Therefore, a different approach was chosen for the selective coupling of HBC with perylene dye. It was E. Reuther^[254] who successfully prepared the boronic ester derivative **87** from the mono bromo

4 Functionalized HBC derivatives

functionalized perylenemonoimide precursor. Here, the aryl boronic ester **87** was prepared in a one step procedure^[255] via a palladium catalyzed coupling reaction of the pinacol ester of diboron and the corresponding bromo substituted perylenemonoimide.^[254]

The actual Suzuki-coupling^[256] of HBC derivative **9** and the boronic ester **87** as depicted in Scheme 26 was carried out under reaction conditions reported by Ishiyama and co-workers for a large variety of aryl-aryl couplings.^[255] Compound **9** was dissolved in toluene and then peryleneboronic ester **87**, potassium carbonate (dissolved in ethanol/water (1:1)), and Pd(PPh₃)₄ were added sequentially. The resulting mixture was heated at 80 °C under argon for 16 h. Work up and purification afforded di perylenemonoimide substituted HBC **88** in 70% yield. Ishiyama^[255] reported that the reaction is accelerated in polar solvents: e.g., DMSO ≥ DMF > dioxane > toluene. In this case, use of more polar solvents than toluene, resulting in shorter reaction times, was not possible due to the extremely low solubility of HBC **9** in e.g. DMSO or DMF.^[255]



Scheme 26: **Suzuki coupling reaction of HBC derivative 9 with perylene boronic ester 87 in toluene**

The utilization of organic materials in photophysical experiments or their employment in high technology applications requires extremely high purities and thorough characterization of the respective compounds. The $^1\text{H-NMR}$ spectra depicted in Figure 67 clearly indicates the high purity of the sample.

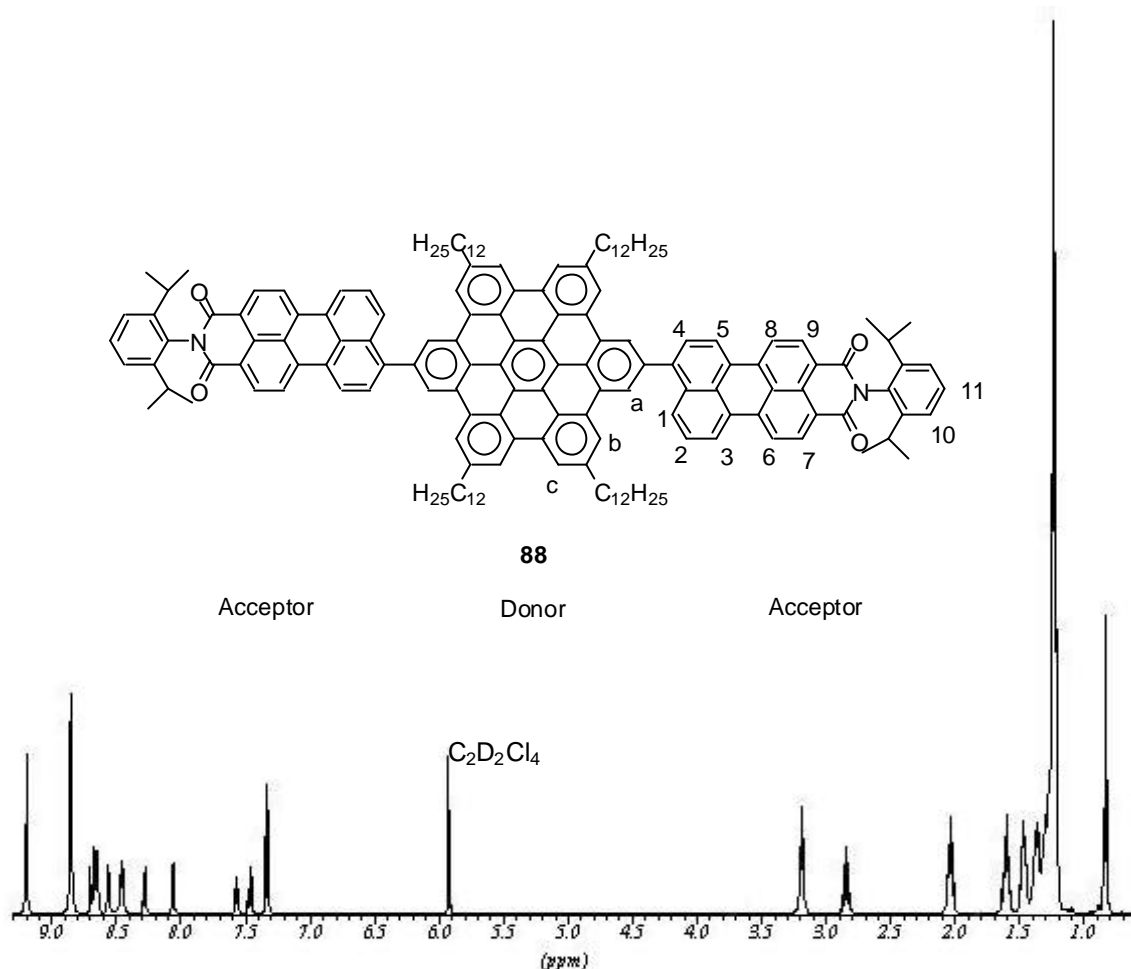


Figure 67: $^1\text{H-NMR}$ spectra of **88** in $\text{C}_2\text{D}_2\text{Cl}_4$ at 100°C and assignment of protons according to H-H cosy experiments

Using H-H cosy NMR spectroscopy, the aromatic signals of the HBC core and the two perylene substituents could be assigned as indicated in Figure 67 and Figure 68.

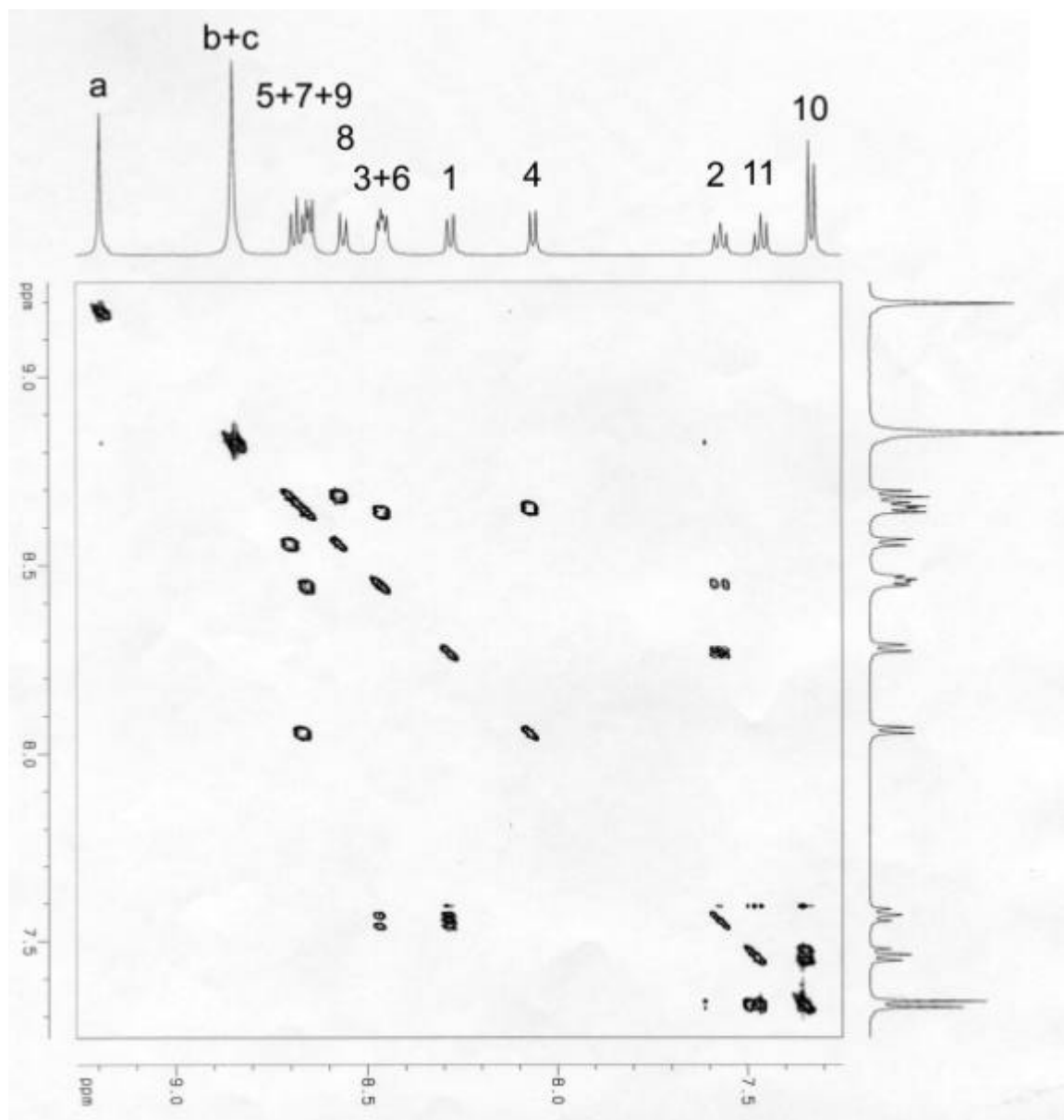
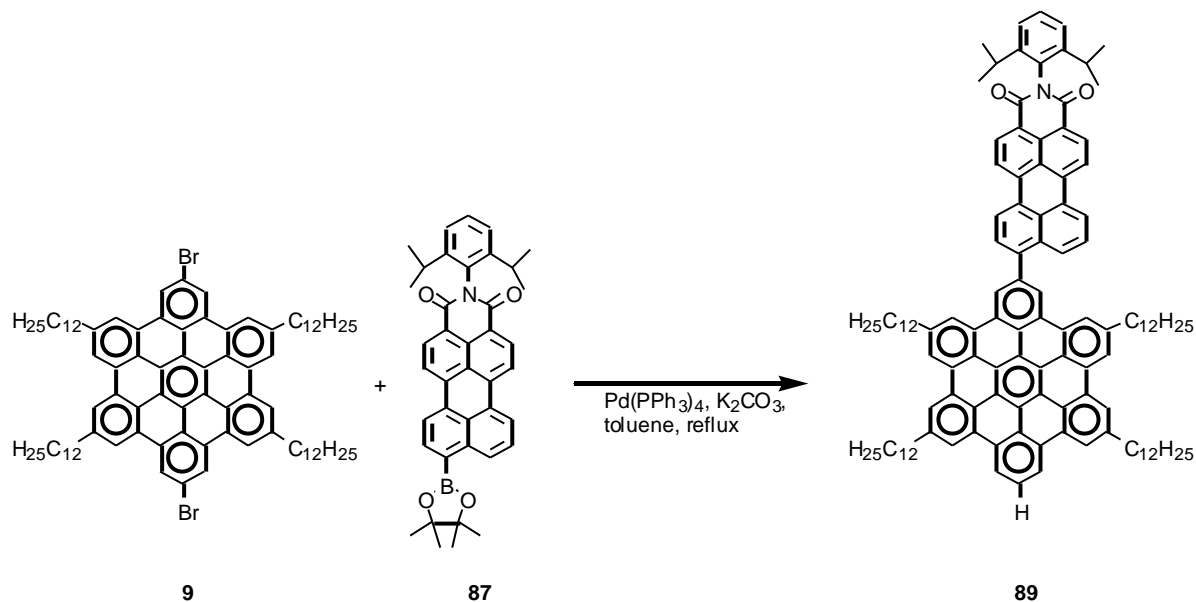


Figure 68: H-H cosy NMR spectrum of **88** in $C_2D_2Cl_4$ at $100^\circ C$

Careful analysis of the side products of this reaction, obtained from column chromatography revealed that another interesting product had been formed, i.e. approximately 5% of mono perylene substituted HBC **89**. This compound itself is interesting and important for the completion of the photophysical experiments on HBC **88** which will be discussed below. Compound **89** as depicted in Scheme 27 consists of one HBC and one perylenemoniimide moiety. Additionally, HBC precursor **9** was debrominated on the unsubstituted position during the reaction. Together with E. Reuther the reaction conditions were

altered in such a way that the former side product **89** was now obtained with 30% yield.



Scheme 27: Alternated Suzuki coupling reaction of HBC derivative **9 with perylene boronic ester **87** in refluxing toluene to yield mono substituted HBC **89****

With the new reaction conditions, only one equivalent of perylene boronic ester **87** was used and the reaction temperature was increased to reflux so that debromination of the unreacted coupling side was favored. The details of synthesis and thorough characterization of the material will be discussed by E. Reuther elsewhere.^[254]

The photophysical characterization of the above systems was carried out by Dr. S. Mitra in the laboratories of Prof. DeSchreyver (Belgium).

4.4.2 Absorption properties

The steady state spectra of the A-D-A complex **88** (Fehler! Verweisquelle konnte nicht gefunden werden.) in THF is shown in Figure 69. The absorption spectrum consists of two distinct maxima: the structured ultraviolet (UV) absorption with maxima at around 380 nm and another one at the blue edge of the spectrum (around 540 nm).

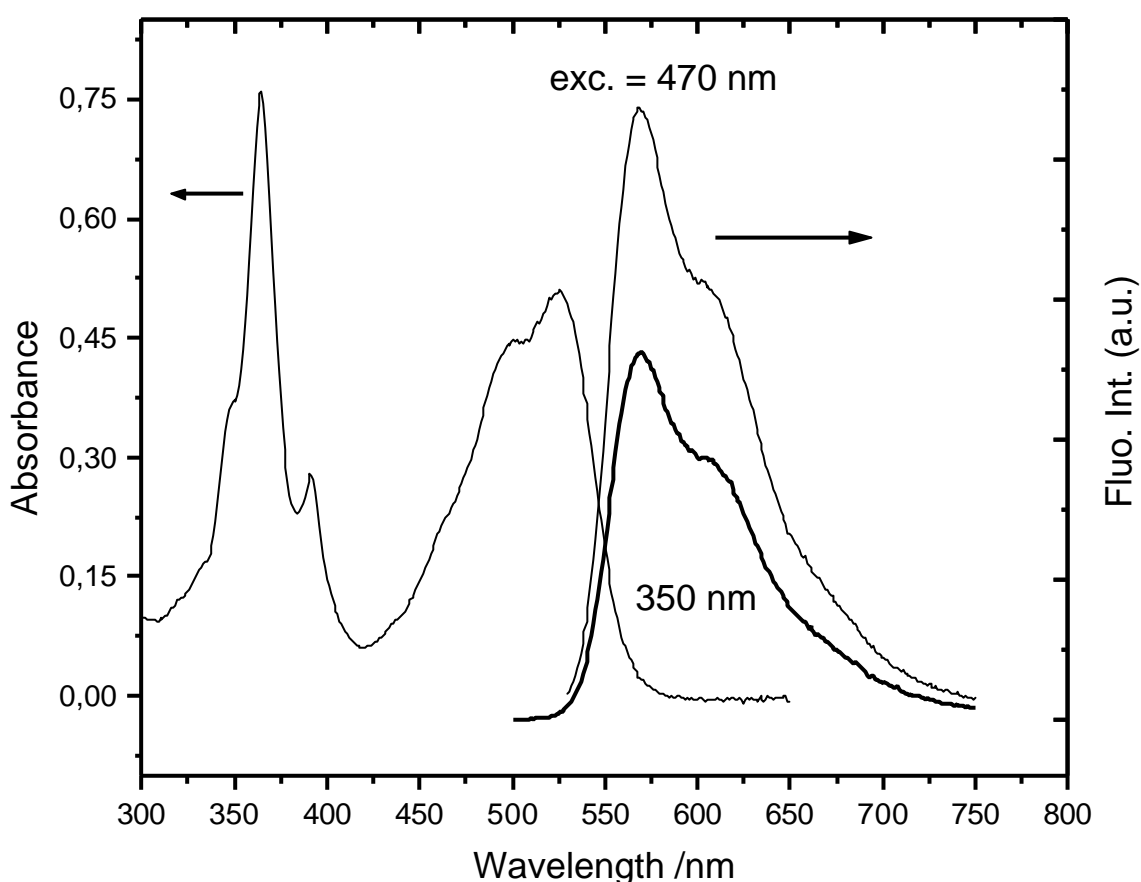


Figure 69: **Steady state absorption and fluorescence emission spectra of A-D-A complex in THF. The excitation wavelengths are indicated in the figure.**

Comparison of the spectra to those of the model chromophores **6b** and **90** (Figure 70)^[257, 258] indicates that the ultraviolet absorption originates from the donor and the blue absorption band is caused by the acceptor. The fact that the individual identity of the model compounds is almost preserved in the complex ensures either very low or no interaction between the donor and acceptor

components in the ground state. The absorption properties are similar for both the 1:1 (**89**) and 1:2 (**88**) complexes both in THF and toluene.

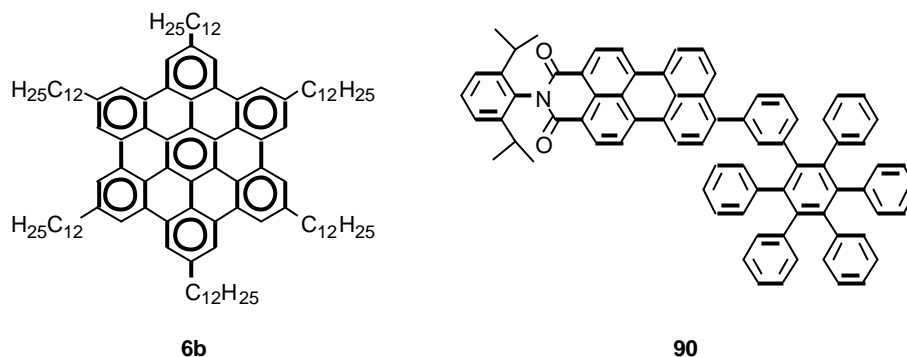


Figure 70: **Structure of the model compounds 6b and 90**

4.4.3 Fluorescence properties

Excitation at 470 nm (the acceptor absorption) gives a strong and broad yellow fluorescence in the range of 525 to 750 nm with a maximum at 568 nm and a shoulder at 608 nm. These fluorescence characteristics are identical to that of the model hexaphenylperyleneimide.^[258] The quantum yield of fluorescence is very high ($\phi_f = 0.85$).

The most interesting result is the observation of a similar emission profile even when we excite at the UV absorption band of the complex. The model HBC **6b** shows a structured fluorescence emission in the wavelength range of 450 to 520 nm with a peak at 480 nm ($\phi_f = 0.06$).^[257] However, as shown in Figure 71, no HBC emission in that wavelength range was found, instead, only identical fluorescence emission arises from the acceptor independent of the excitation wavelength. The complete quenching of the donor fluorescence points to a very efficient excitation energy transfer from the donor to the acceptor moiety in the excited state. The similarity of the fluorescence emission profile in all the excitation position indicates that the nature of the fluorescing state is same always. The quantum yield of fluorescence is about 0.54 when the complex is excited at the donor absorption band. The fluorescence excitation spectrum of this emission is similar to the absorption spectrum of the complex (Figure 71).

The fluorescence behavior is similar for both 1:1 and 1:2 complexes in both THF and toluene.

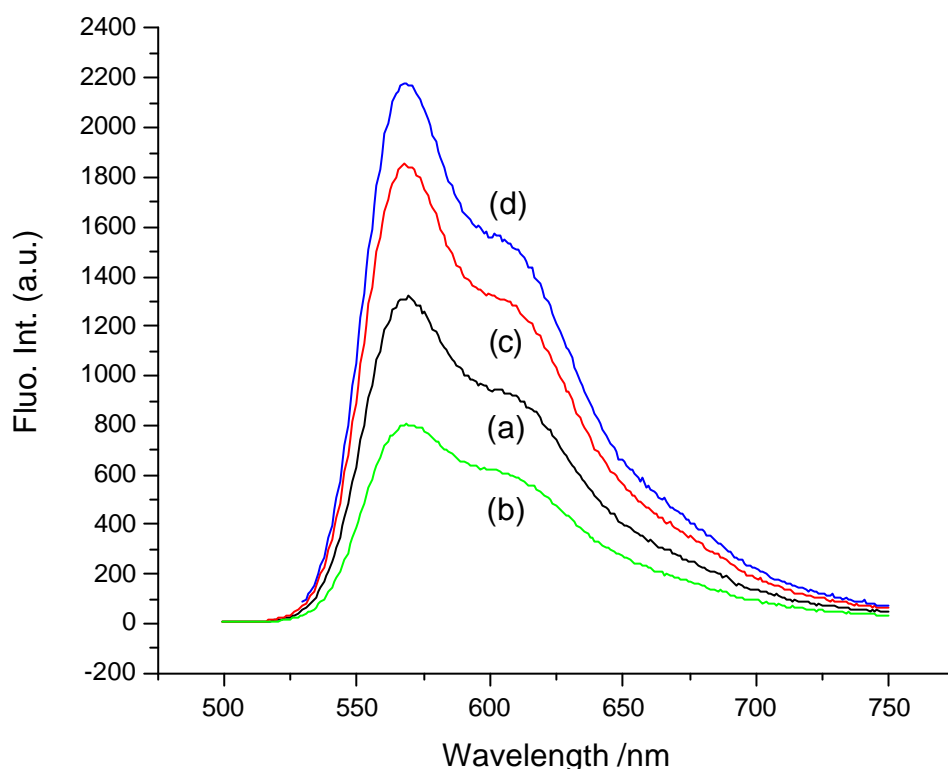


Figure 71: **The fluorescence emission of 1:2 A-D-A complex in toluene at different excitation wavelengths. The wavelength of excitation is 350(a), 400(b), 470(c) and 500(d) nm.**

4.4.4 Time resolved fluorescence experiments

To identify the nature of the fluorescing states and the dynamics of the excitation transfer process, excited state decay time measurements were conducted using picosecond time correlated single photon counting technique. All the fluorescence decay traces could be fitted well with a single exponential decay function. The fluorescence decay parameters of the complexes measured both in THF and toluene are given in Table 11 along with the corresponding values for the model compounds. For complexes, the excitation was done in both the donor and acceptor absorption (for example at 377 and 543 nm, respectively) and the fluorescence was detected at the two different

wavelengths of 570 and 610 nm. From Table 12 it can be seen that in either THF or toluene, fluorescence decay times are not dependent upon the excitation and detection wavelengths. This further indicates that the nature of the fluorescing state is the same for both excitation conditions. However, the excitation energy transfer is too fast to be measured with a time resolution of ca. 20 ps in this TCSPC set-up.

System			1:2 ^b	1:1 ^c	Model ^d
Solvent	λ_{exc} (nm)	λ_{det} (nm)	τ (ns)	τ (ns)	τ (ns)
THF	543	570	3.50	3.90	4.45
		610	3.54	3.95	4.44
	377	570	3.50	3.75	
		610	3.52	3.82	
Toluene	543	570	2.99	3.21	4.0
		610	3.10	3.24	4.1
	377	570	2.94	3.12	
		610	3.11	3.17	

Table 12: **Fluorescence Decay parameters for 1:1 and 2:1 (acceptor/donor) complexes in solution^a**

^aFor model donor (HBC), fluorescence decay times are 55ns (86%) and 15ns(14%) in hexane ($\lambda_{\text{exc}}= 365$ nm and $\lambda_{\text{det}}= 480$ nm)^[257]

^bdi-perylenemonoimide HBC; ^cmono perylenemonoimide HBC; ^dhexaphenyl perylenemonoimide

4.5 Synthesis and characterization of aryl amine substituted HBC derivatives and attempted oxidation towards diimines

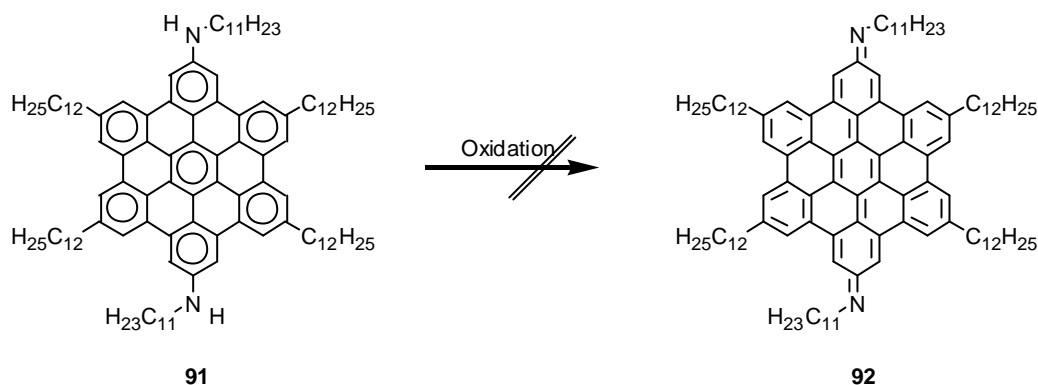
Aromatic amines play a key role in a number of fields, such as pharmaceuticals, agrochemicals, pigments and electronic materials.^[259] Organic hole transport materials find applications in organic light-emitting diodes (LEDs), where they substantially increase device performance if placed as a hole transport layer (HTL) between the anode and the luminescent layer. An organic material is a potential hole transporter if it can reversibly form radical cations, e.g., if it can accept and donate positive charges without decomposition. The triarylamine functionality is known to fulfill this requirement and constitutes a key feature of many organic hole transport materials.^[260]

Over the years, a number of cleverly designed and extremely useful methods for aryl C-N bond formation have been reported. Among those, the Buchwald coupling reaction is up to now the one that has been utilized most frequently in the literature.^[259, 261]

4.5.1 Synthesis of dodecylaniline substituted HBCs

It was M. Wehmeier in the group of Prof. Müllen who reported the synthesis of primary and secondary amines in previous studies.^[28, 262] Here, it was possible to cross-couple undecylamine with monobromo HBC **7** and dibromo HBC **9** (compound **91** in Scheme 28) in good yields under classical Buchwald^[259, 261] conditions catalyzed with Pd₂(dba)₃ and BINAP in the presence of sodium *tert*-butanolate.^[28] Furthermore, it was attempted to observe intermolecular interactions such as hydrogen bonds which are likely to be present in the case of the amino functionalized HBC derivatives; the STM image at the solid-liquid interface revealed rows of dimers. Experimental data, however, showed that the distance between the amino groups of neighboring molecules was presumably too large for intermolecular hydrogen bonding. Taking into account that the given data for the unit cell has a reasonably large error margin, hydrogen bonds could not completely be excluded.^[28] Further studies conducted by

Wehmeier^[262] also involved the attempts to chemically oxidize undecylamine substituted HBC derivative **91**.



Scheme 28: **Attempted oxidation of para undecylamino substituted HBC 91**

In this attempt, the proposed bisimine structure **92** was supposed to exhibit dramatically different current-voltage characteristics in the STM investigations.^[262] The history and scientific developments involving quinoid diimine structures such as **93** and **94** (Figure 72) have been described in great detail elsewhere.^[262] However, the formation of a quinoid diimide structure based on terphenyl (such as **95**) has not yet been reported in the literature.

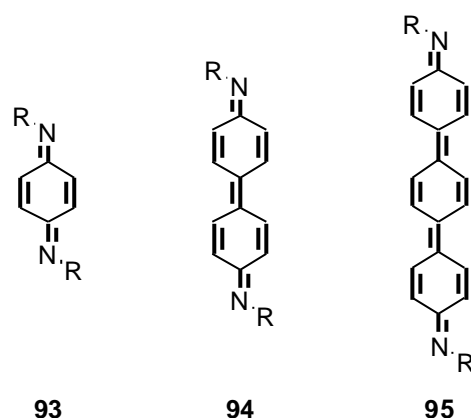


Figure 72: **Quinoid diimide structures based on benzene 93 and biphenyl 94; terphenyl based diimides such as 95 have not been reported yet**

As reported by Wehmeier^[262], the attempt to transfer bisamine substituted HBC derivative **91** via chemical oxidation to the quinoid system **92** was unsuccessful. During this endeavor, several oxidizing agents such as benzoylperoxide^[263],

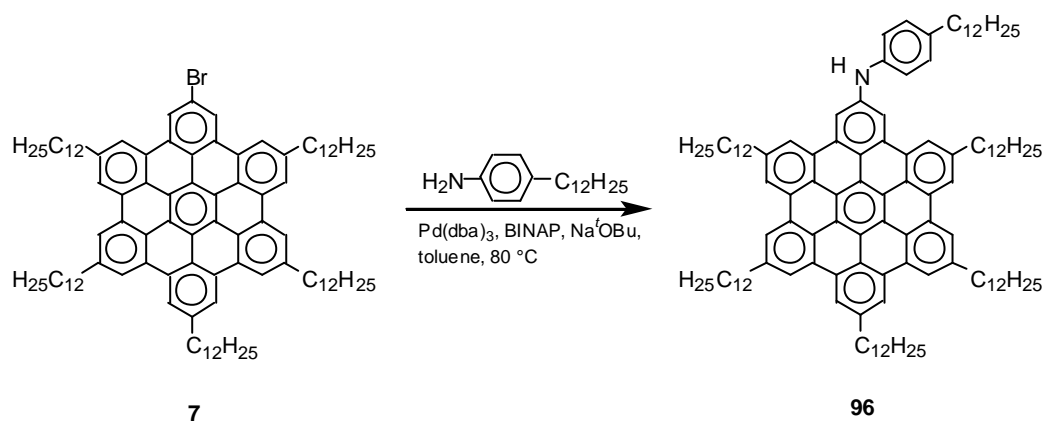
4 Functionalized HBC derivatives

silver(I)oxide^[264], lead dioxide and mercury oxide^[265] failed to produce the desired structure.

One of the drawbacks in the attempts of Wehmeier certainly was the utilization of alkyl amino substituted HBC derivatives such as **91** for the subject to oxidizing agents. It was already in 1956 when Hughes^[265] and co-workers reported the enhanced stability of N,N'-diphenyl-quinoid structure (**93**, R = phenyl) over alkyl substituted quinoid systems.

When Wehmeier^[262] tried to utilize this concept for amine substituted HBCs, he reported the unsuccessful attempts to synthesize dodecylaniline substituted HBC using **9** as the starting material and standard Buchwald^[259, 261] cross-coupling conditions.

To verify and/or cross-check the results reported earlier,^[262] monobromo substituted HBC **7** and a large excess of dodecylaniline were subjected to the Buchwald^[259, 261] reaction catalyzed with Pd₂(dba)₃ and BINAP in the presence of sodium *tert.*-butanolate as depicted in Scheme 29. Work-up by precipitation from methanol followed by filtration over a short pad of silica gel afforded arylamine substituted HBC derivative **96** in high yields (88%).



Scheme 29: **Cross-coupling reaction of monobromo HBC 7 and dodecylaniline under Buchwald conditions**

The material was obtained as a bright yellow powder which was reasonably soluble in THF, chloroform and toluene.

The purity of the material was determined by $^1\text{H-NMR}$ spectroscopy of **96** in $\text{C}_2\text{D}_2\text{Cl}_4$ at $100\text{ }^\circ\text{C}$. From Figure 73, it is unequivocal that the dodecylphenylamine substituted HBC derivative was obtained with great purity. The NMR spectra in Figure 73 only depicts the aromatic region of the compound. Here, six well resolved signals are visible for the aromatic core protons of HBC in the region between $\delta = 8.5$ and 8.0 ppm. The expected two doublets for the phenyl amine moiety are merged to one singlet at $\delta = 7.25$ ppm, whereas, the signal for the proton attached to the nitrogen is visible at $\delta = 5.8$ ppm.

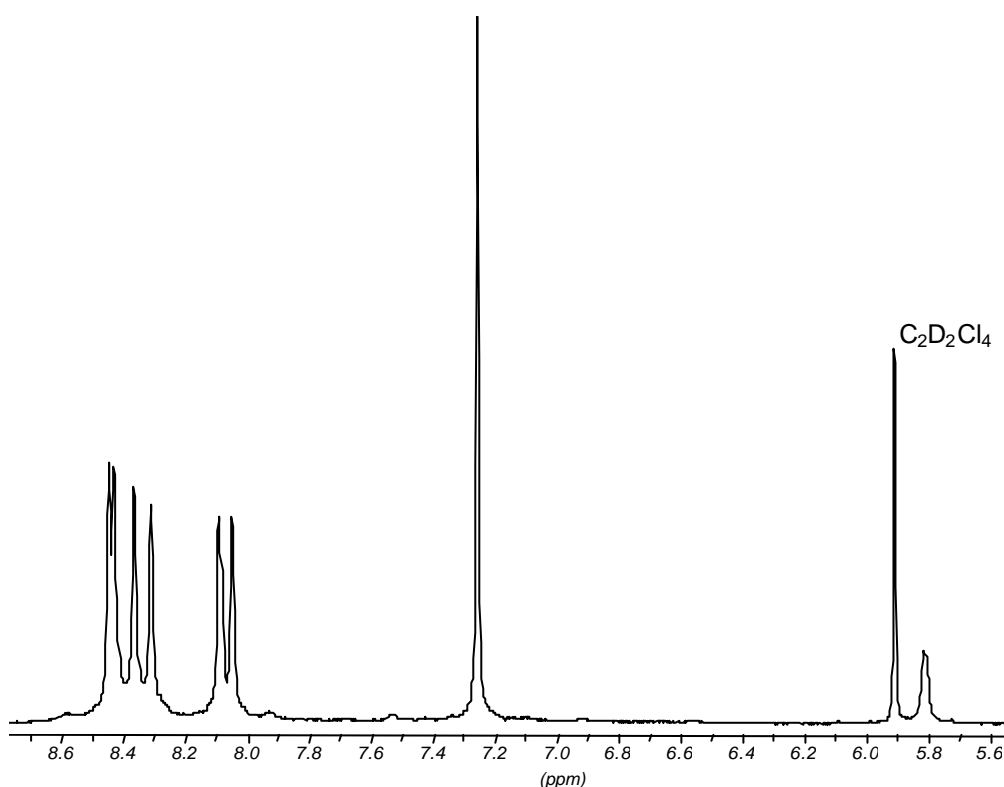
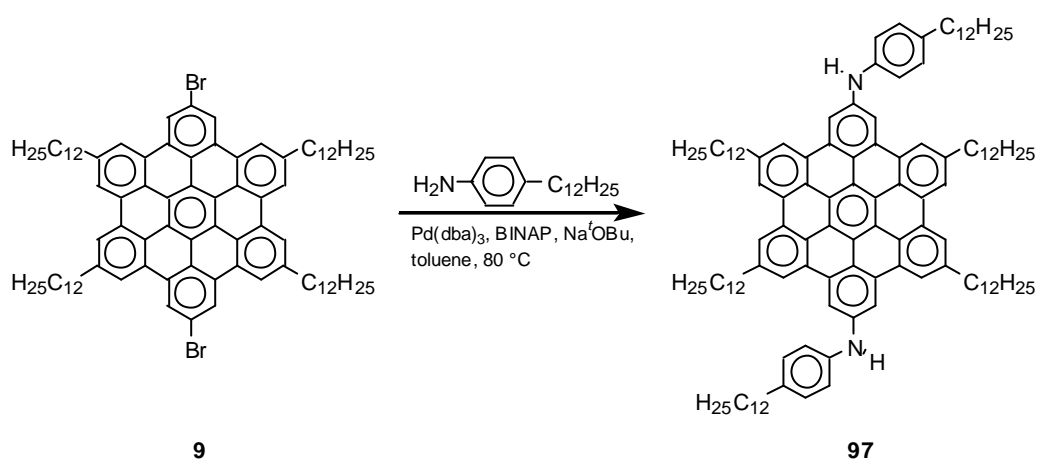


Figure 73: $^1\text{H-NMR}$ (only aromatic region) of **96** in $\text{C}_2\text{D}_2\text{Cl}_4$ at 100°C

As demonstrated above, it was possible to subject monobromo HBC **7** to a cross-coupling reaction under Buchwald conditions with dodecylaniline as the reaction partner.

Encouraged by these results, it was now again attempted to apply these conditions to the corresponding reaction with dibromo substituted HBC **9** as previously investigated by Venmeier in our group.

Scheme 30 displays the reaction pathway for the synthesis of para dodecylaniline substituted HBC **97**. In a two-fold Buchwald cross-coupling reaction under catalytic action of $\text{Pd}_2(\text{dba})_3$ and BINAP in the presence of sodium *tert*-butanolate, HBC derivative **9** reacted with a large excess of dodecylaniline so that the desired compound **97** was obtained in high yields (89%) after workup and purification. Contrary to earlier findings, it was found possible to synthesize para arylamine substituted HBCs such as **97** with good yields and high purities.



Scheme 30: **Cross-coupling reaction of dibromo HBC **9** and dodecylaniline under Buchwald conditions**

Figure 74 displays the ^1H -NMR spectra (only the aromatic region) for compound **97**. The signal to noise ratio in this case is quite poor due to low concentration of the sample. As mentioned earlier, HBC discs tend to stack on top of each other resulting in large aggregates which reduce the resolution of the NMR signal. Thus lower concentrations had to be used for HBC **97**. Higher temperatures as utilized for HBC derivative **96** were not applicable since the solubility of **97** is very low in $\text{C}_2\text{D}_2\text{Cl}_4$ but reasonably good in d_8 -THF.

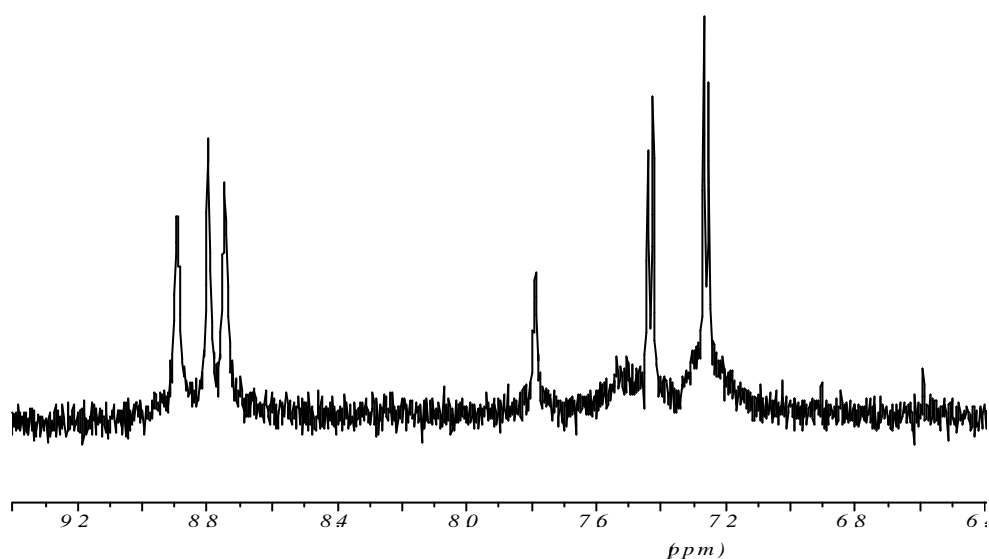


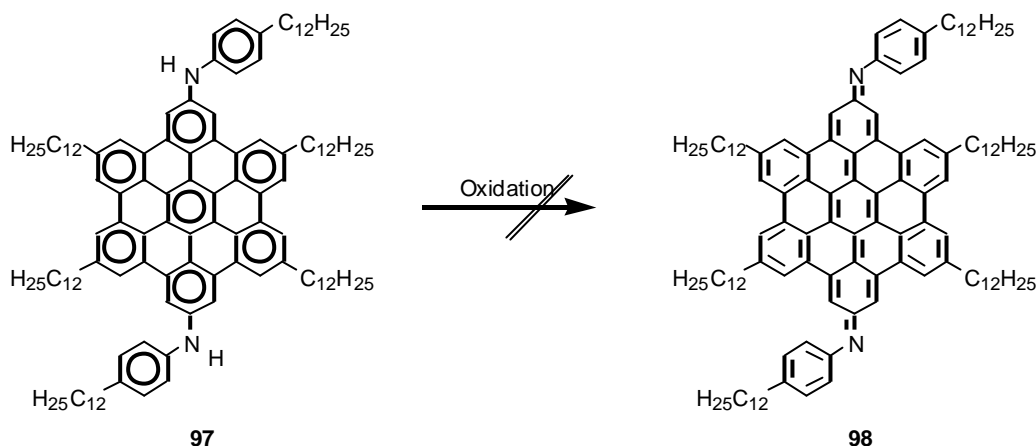
Figure 74: $^1\text{H-NMR}$ (only aromatic region) of **97** in THF at 35°C

Here, due to the increased symmetry of the molecule compared to mono substituted HBC **96**, only three signals for the aromatic HBC core are present between 9.0 and 8.9 ppm. Also the expected set of doublets for the phenyl amine are visible and well resolved at 7.4 and 7.25 ppm. As a consequence of a different solvent, lower concentration and lower temperature, the N-H proton signal emerges now at around $\delta = 7.8$ ppm, thus experiencing a shift of approximately 2 ppm compared to HBC **96**.

4.5.2 Attempt to oxidize amino substituted HBC **97** to the quinoid diimine

After having successfully synthesized and characterized the aryl amino functionalized HBC derivative **97** efforts were made to transform this compound into the corresponding quinoid diimine structure **98**. In a similar attempt, Hughes^[265] and co-workers reported the successful synthesis of N,N'-diphenyl-p-phenylenediimine via oxidation of N,N'-diphenyl-p-phenylenediamine with mercuryoxide in refluxing benzene. However, in the case of HBC diamine **97**, these conditions did not yield the desired product **98**. The reaction mixture turned slightly brown but UV/Vis analysis (Figure 75) revealed that no product

had formed after one hour, since no shift of the main HBC absorption band at $\lambda = 373$ nm occurred in comparison to the starting material **97**. Longer reaction times, even reaction overnight and/or elevated temperatures did not result in the formation of diimine **98**. The loss of the fine structure compared to the UV/Vis spectra of untreated **97**, i.e. the α - and para-band according to the Clar^[38, 63, 155] nomenclature, is attributed to the presence of oxidizing agent and not optimized UV/Vis concentrations.



Scheme 31: **Attempted oxidation of para diamine substituted HBC 97**

Further efforts to oxidize diamine system **97** with silver(I)oxide^[264] in diethyl ether also failed.

The use of more drastic conditions, i.e. deployment of stronger oxidizing agents, resulted in darker colored reaction mixtures, but also not in the desired product. Lead dioxide in combination with lead acetate gave the same unsuccessful results as the previous attempts.

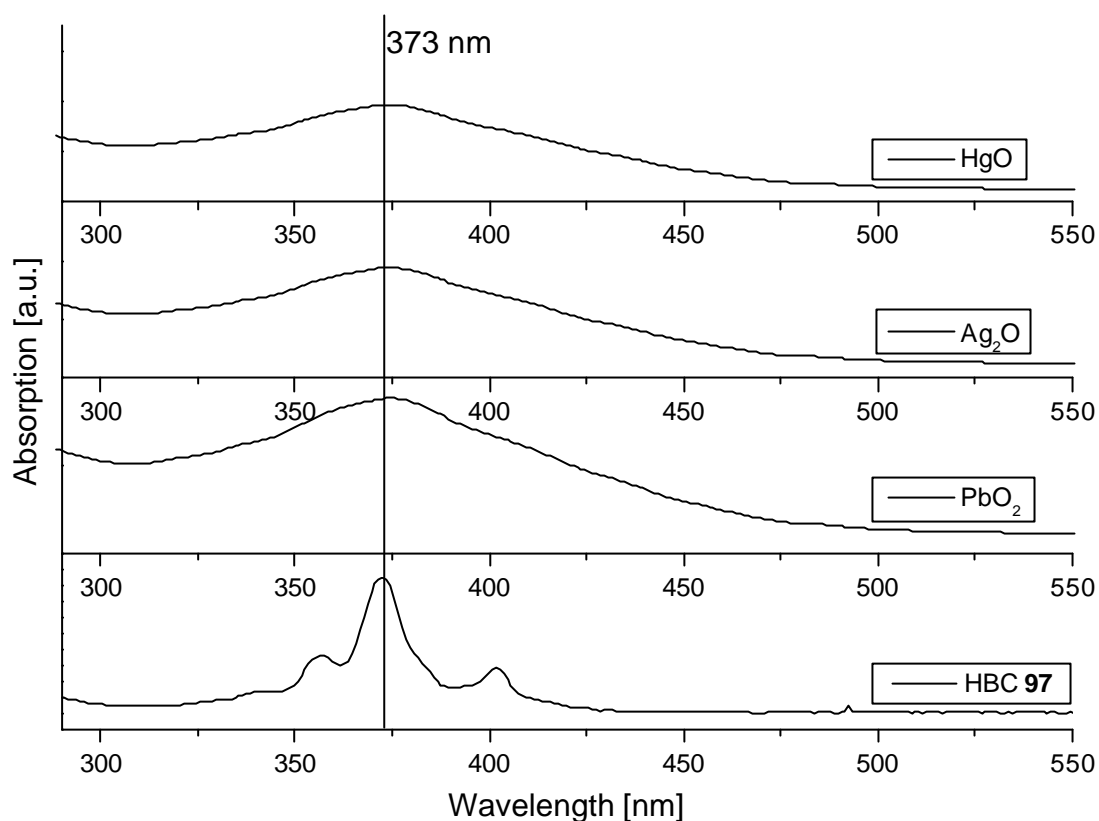


Figure 75: *UV/Vis spectra of HBC 97 before and after treatment with oxidizing agents*

It can be reasoned that the unsuccessful attempts to synthesize a diimine structure based on the HBC moiety as presented here and earlier by Wehmeier^[262] in our group is most probably not due to the instability of the proposed product **98**, since all the reactions were conducted under an inert atmosphere with the use of dry solvents, but due to a high energy barrier for the internal benzene rings of the HBC core to transform into the quinoid structure. Further studies included the transformation of HBC amine **97** to a di-anion via treatment with an excess of a strong base. In a first experiment the di-amine **97** was treated with an excess of sodium tert.-butylate in dry D₈-THF under an inert atmosphere. As can be seen from the ¹H-NMR spectra in Figure 76 the N-H protons were only partly abstracted by the base. The partly negatively charged species caused the line broadening most eminent in the resulting spectrum (Figure 76, red line). Quenching of the negatively charged HBC amine with methyl iodine was conducted to investigate the ratio of dianion and mono

anion. FD mass spectrometry revealed that 75% of mono methylated species had formed and only 25% of the di methylated were recorded.

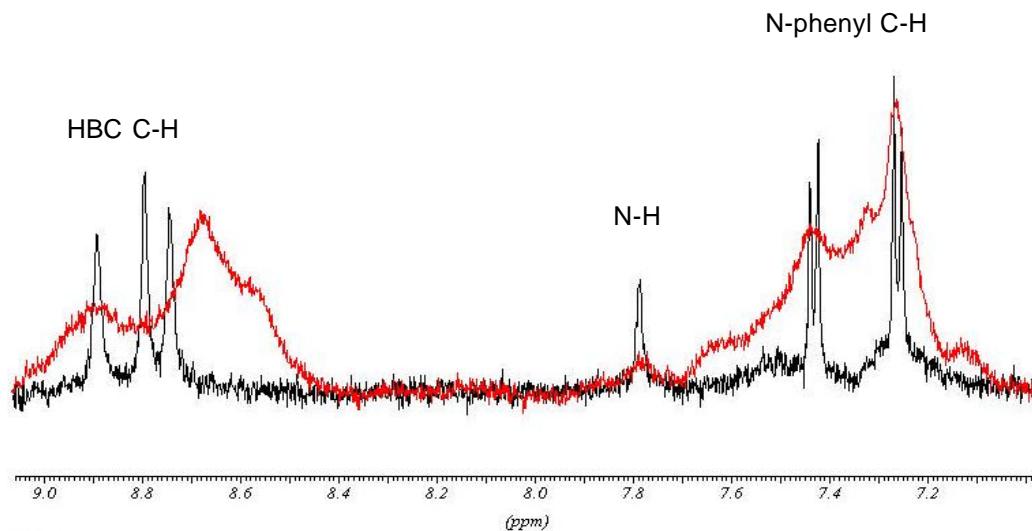


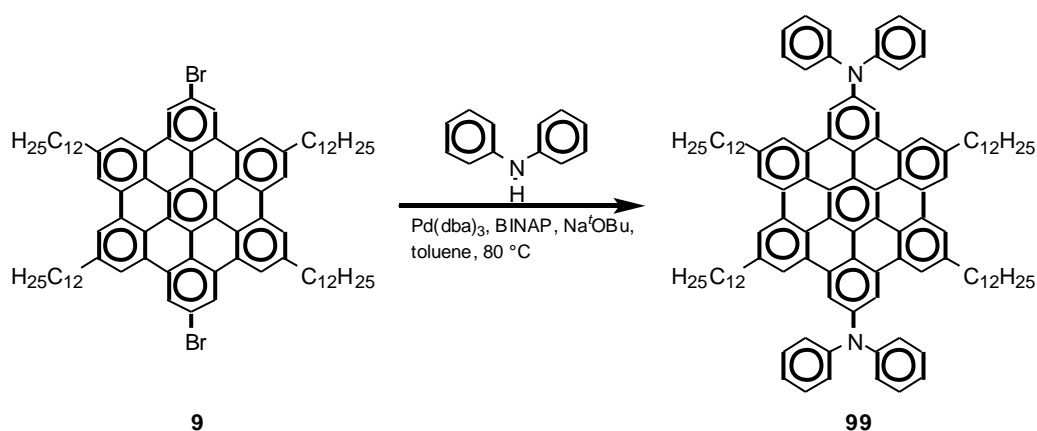
Figure 76: $^1\text{H-NMR}$ spectra of HBC 97 in THF at room temperature (only aromatic region) before (black line) and after treatment with base (red line)

This could either be an indication for the higher stability of a mono anion or it could be due to the fact that the utilized base was not strong enough. Therefore, a tert.-butyl lithium was used as the base in a second experiment. The resulting NMR spectrum after treatment with the stronger base was very similar to the one depicted in Figure 76. Here, again quenching of the anion resulted mainly in the formation of a mono methylated species and only a small portion of the analyzed material was di methylated. Thus it can be concluded that even with very strong organic bases di-anion formation of HBC 97 is suppressed.

4.5.3 A novel HBC derivative with a triarylamine moiety

Organic light emitting devices (OLEDs)^[266] have attracted a great deal of attention due to their potential use in a wide range of lighting as well as high- and low-resolution display applications. One of the principal failure modes in OLEDs involves thermal instability in molecular thin films. Currently, one of the most widely used hole transport layer (HTL) materials in OLEDs is TPD (4,4-bis(phenyl-m-tolylamino)biphenyl).^[267-273] TPD fulfills many requirements for an HTL, such as providing devices with excellent EL efficiencies and low turn-on voltages; however, the thermal stability is poor. The main objective for developing new HTL materials is to improve the thermal properties while maintaining the desired properties exhibited by TPD. A wide variety of approaches has been used in the endeavor to fulfill these requirements. For example, “starburst” molecules having a triphenylamine core have demonstrated improved thermal stability.^[274, 275]

Here, the synthesis of diphenylamine substituted HBC **99** is presented. Similar to previously described procedures, in a two-fold Buchwald cross-coupling reaction under catalytic action of $\text{Pd}_2(\text{dba})_3$ and BINAP in the presence of sodium *tert.*-butanolate, HBC derivative **9** reacted with a large excess of diphenylamine. Work up and purification afforded the desired compound **99** in high yields (89%).



Scheme 32: **Cross-coupling reaction of dibromo HBC 9 and diphenylamine under Buchwald conditions**

Similar to HBC **97**, derivative **99** has C_2 symmetry, thus only three signals are present for the aromatic protons of the HBC core as depicted in the 1H -NMR spectra displayed in Figure 77. The two typical multiplets for the phenyl amine moiety are visible between $\delta = 7.0$ and 7.5 ppm. Further, the α - CH_2 and β - CH_2 are well resolved at $\delta = 3.1$ and 1.9 ppm, respectively.

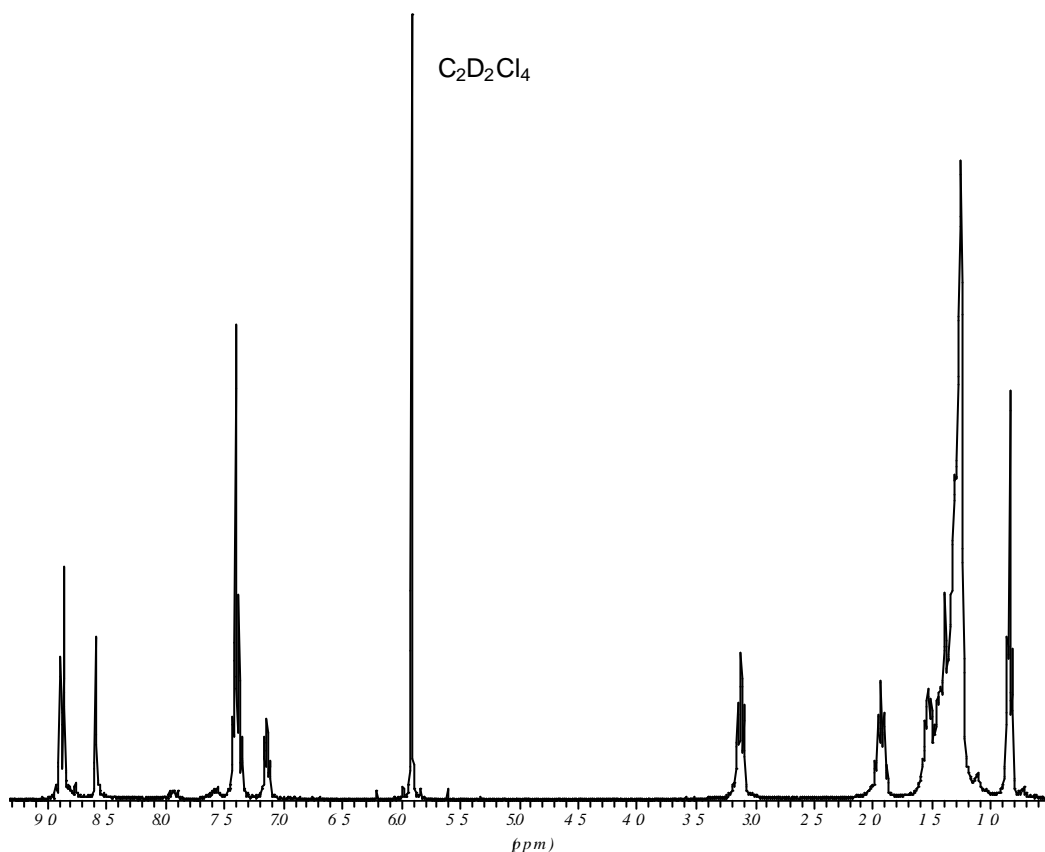


Figure 77: 1H -NMR of **99** in $C_2D_2Cl_4$ at $100^\circ C$

Thermogravimetric analysis (TGA), differential scanning calorimetry (DSC) and optical polarization microscopy experiments were performed to study the phase behavior of HBC **99**. TGA analysis revealed that the diphenylamine substituted HBC **99** is thermally stable up to $250^\circ C$ as can be seen from Figure 78. With this one of the main objectives for developing new HTL materials, i.e. to improve the thermal properties has been fulfilled.

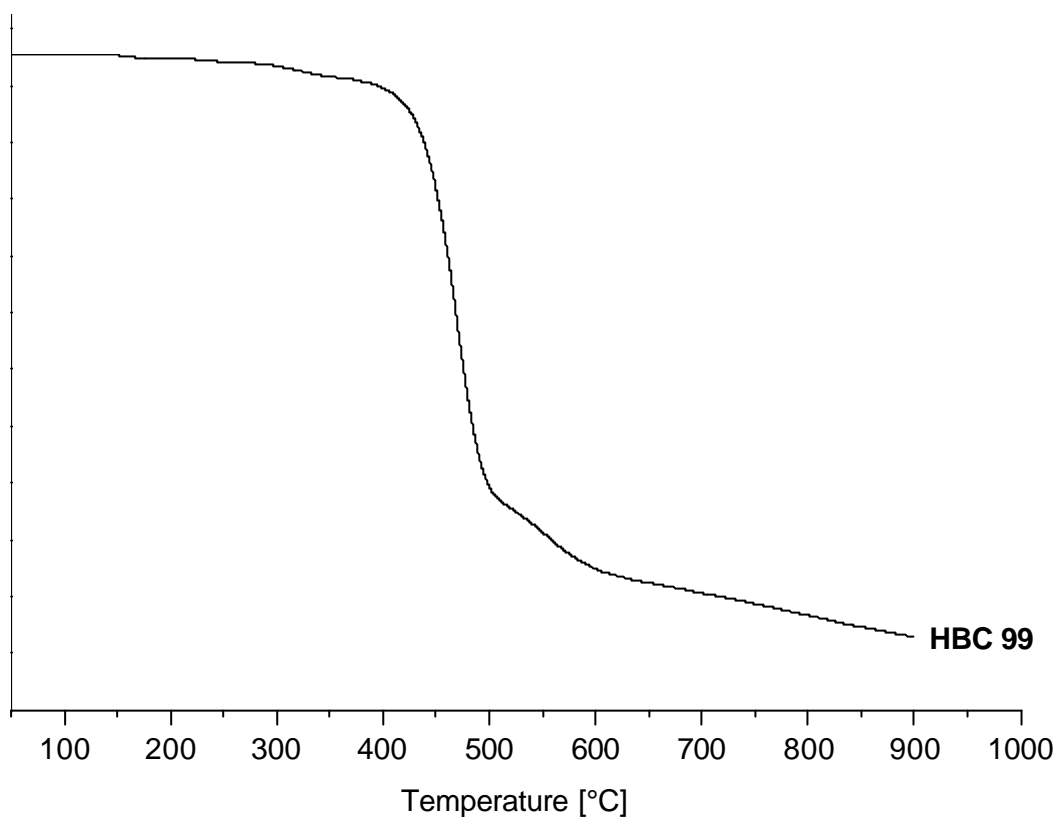


Figure 78: **TGA analysis of HBC 99**

DSC analysis revealed that HBC **99** also depicts a columnar mesophase. The phase transition from the crystalline phase to the mesophase was found to be at 157 °C. The fact that the present material also arranges in highly ordered columnar structures is a promising prerequisite for the deployment as a hole transporting material in organic light emitting devices.

4.6 HBC as a building block for supramolecular chemistry

Rapid growth and recent breakthroughs in the field of molecular manufacturing have resulted in the development of an entirely new synthetic strategy for the preparation of organized nano-structures. This strategy is based on molecular self-assembly, a phenomenon in which the individual subunits are quickly driven together and held in place by multiple, accurately positioned non-covalent interactions.^[276, 277] The use of transition metals and coordination-based design allows the formation of a variety of self-organized nanosystems in a few highly convergent synthetic steps. Molecular architecture utilizes the large diversity of available transition metals and their co-ordination chemistry to create complex geometric shapes. The challenge facing the future of modern nanotechnology is molecular manufacturing, a process that is designed to synthesize advanced materials with specific properties and functions. These are determined by controlling the form, shape and distribution of each individual building block and their precise placement. Such intermolecular control imposes strict requirements on the nature, type and directionality of the bonding forces that operate within the entire aggregated structure. The chemical bonding of the subunits must be relatively weak, thermodynamically stable, yet kinetically labile to allow the self-rearrangement of the subunits within the entire structure, thereby enabling the self-correction of possible defects. A simple and general concept for generating ordered structures is based on the recognition-driven spontaneous assembly of complementary subunits. Since transition metals have co-ordination sites with specific geometries that depend upon their electronic structure they can serve as acceptor subunits. These can be linked together *via* donor building blocks that form the rigid frame of the assembled entity. Both of these types of subunits must possess specific geometries and remain multidentate or at least bidentate, i.e. they must have at least two co-ordination sites that cannot be capped, to form the desired cyclic structure. From the above considerations it is obvious that these units can be nitrogen-containing heteroaryls, or cyano-substituted aromatic molecules.^[276, 277]

The construction of almost any entity that contains a transition metal requires the assessment of the angles between the binding sites of each donor and acceptor subunit. Hence, the subunits can be classified into two types based on the value of this angle: linear subunits that possess these reactive sites with a 180° orientation relative to each other and angular subunits that have other, smaller angles. For example a molecular square can be assembled in several different ways, either by combining four linear with four angular building blocks, or by combining two different angular subunits as depicted in Figure 79.^[276, 277]

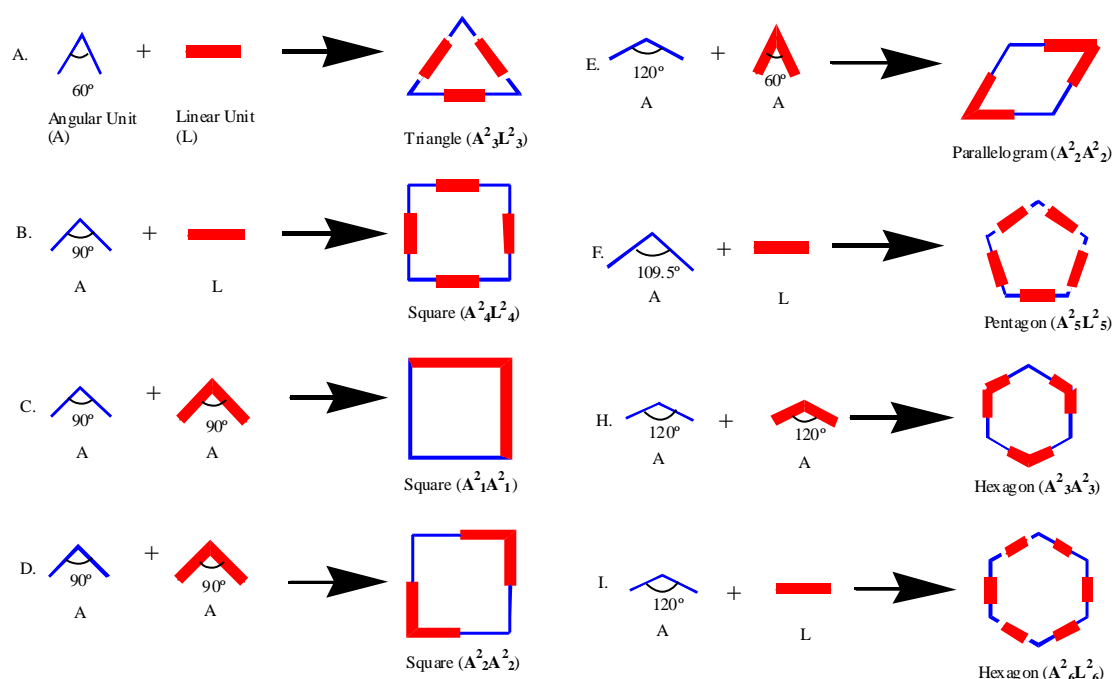


Figure 79: **Combinatorial library of cyclic molecular polygons**

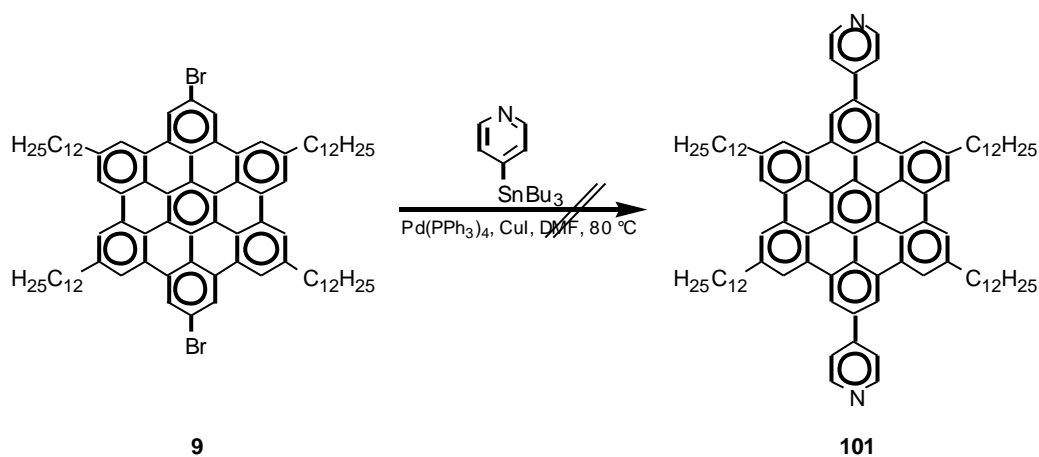
Previous attempts to utilize large polyaromatic molecules in coordination chemistry involved diazapyrene^[278], diazaperylene^[278], and porphyrin^[279] to yield molecular squares.

Drain and Lehn^[279] prepared tetranuclear assemblies by two different methods. One of them involved the *cis*-[Pt(PhCN)₂Cl₂] complex as an angular building block which, when combined with the linear porphyrin resulted in the molecular square.

4 Functionalized HBC derivatives

Here, in a similar approach, an effort was made to synthesize a HBC derivative that was suitable for the above described combinatorial approach towards supramolecular assemblies.

In a first attempt, 4-(tri-n-butyltin)pyridine was synthesized and subjected to Stille^[280, 281] coupling conditions with dibromo substituted HBC **9** (Scheme 33).



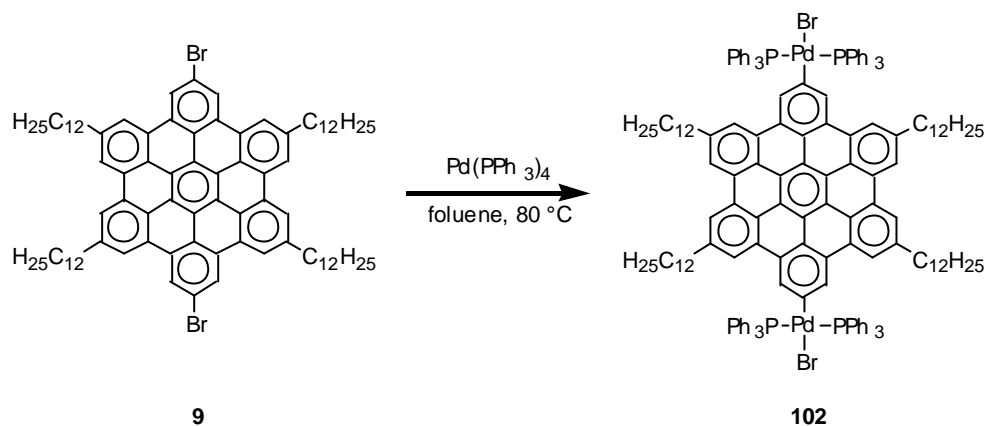
Scheme 33: **Attempted synthesis of pyridyl substituted HBC 101**

Unfortunately, all approaches towards the coupling of pyridine substituents to the HBC core failed. These attempts included variations of the Stille coupling as well as reactions of 4-bromopyridine and HBC **9** under Grignard or Kumada type coupling conditions.

Since the synthesis of a HBC as the building block carrying the donor (pyridine) site of the proposed supramolecular assembly failed, a new strategy was designed to lead to the desired structure. The synthesis of HBC containing the acceptor side was carried out by twofold oxidative addition of Pd(PPh₃)₄ into the bromo-HBC bond at 80°C in toluene as depicted in Scheme 34.

Workup by reducing the volume of toluene, followed by precipitating the crude product with hexane and subsequent short column chromatography afforded HBC **102** in moderate yields (50%). Most evident for this compound was the dramatically increased solubility compared to, for e.g. the starting material of this reaction sequence. The very bulky and space-demanding triphenylphosphine groups (PPh₃) seem to prevent aggregation of the HBC

discs **102** which results in good solubility at room temperatures even in diethylether.



Scheme 34: **Insertion of $\text{Pd}(\text{PPh}_3)_4$ into the carbon-bromine bond of HBC**

An impressive demonstration of the reduced packing behavior and the enhanced solubility of **102** is given in the ^1H -NMR spectrum of this HBC derivative (Figure 80).

The spectrum was recorded at room temperature in CD_2Cl_2 . As can be seen in Figure 80, all three expected proton signals for the aromatic HBC core are well resolved at room temperature. This behavior for other HBCs with C_2 symmetry was only observed at elevated temperatures of around 100°C . Further, integration of the signals reveals the correct relation of aromatic HBC protons to phenyl protons of the inserted palladium phosphine.

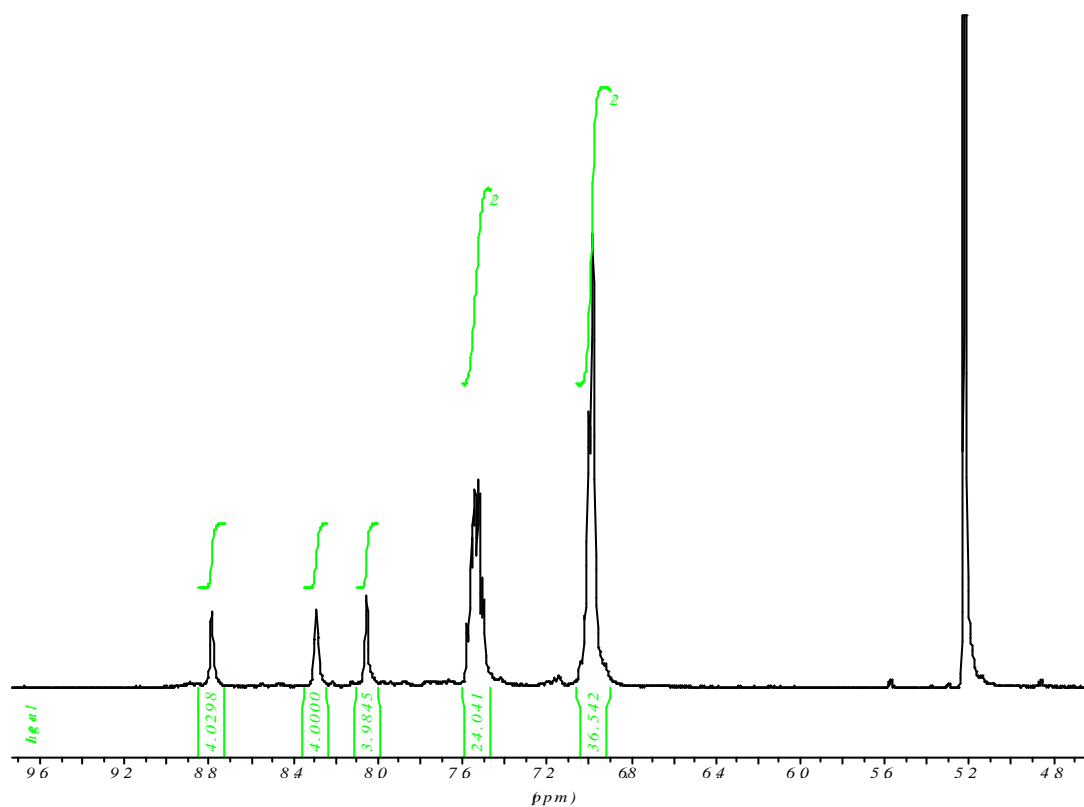


Figure 80: $^1\text{H-NMR}$ spectrum of transition metal substituted HBC 102 in CD_2Cl_2 at RT

Additional proof for the described molecule can be obtained from the phosphorus NMR spectrum of HBC **102**. In this case only one signal was recorded for the four phosphine moieties present in the material. All phosphine atoms are equivalent and thus show only one signal in the corresponding NMR spectrum as evident from Figure 81.

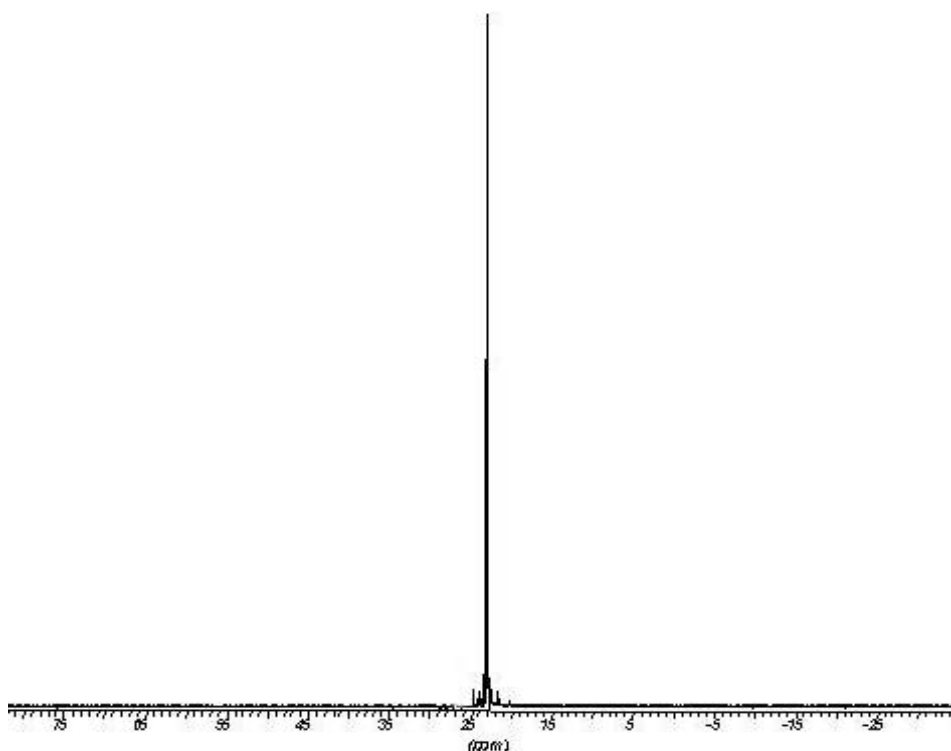


Figure 81: ³¹P-NMR spectrum of HBC 102 in CD₂Cl₂ at room temperature

Encouraged by the successful oxidative insertion of Pd(PPh₃)₄ into the carbon-bromine bond of HBC **9**, further research, investigating the utilization of HBC **102** for the self-assembly into molecular squares such as **100** is currently underway in the group of Prof. Stang (USA).

The applicability of the transition metal-mediated self-assembly process, employing coordination as the motif, allows the manipulation of the macroscopic properties of materials at the nanoscopic level and the creation of future supramolecular species and nanoscale-sized devices with specific, precisely tuned properties, functions and microenvironments. Here, a small door has been opened towards the future utilization of HBC in this field.

4.7 Towards hexa anthracene substituted HBC

Scanning tunneling microscopy (STM) is an important and powerful tool for the better understanding of the supramolecular behavior and the packing phenomena of two dimensional graphite subunits such as HBC and its higher homologues as already impressively demonstrated in earlier Chapters. Polyaromatic hydrocarbons (PAHs) larger than HBC such as the supernaphthalene **26** and the superbiphenyl **28** have also been investigated by means of STM spectroscopy.^[29, 94] The size of the resulting molecular objects became a key feature, with the opportunity of single-molecule investigations as an important consequence. Self-assembly at the interface between the basal plane of graphite and an organic solution allowed crystallization of **28** epitaxially in different 2D modifications.^[29]

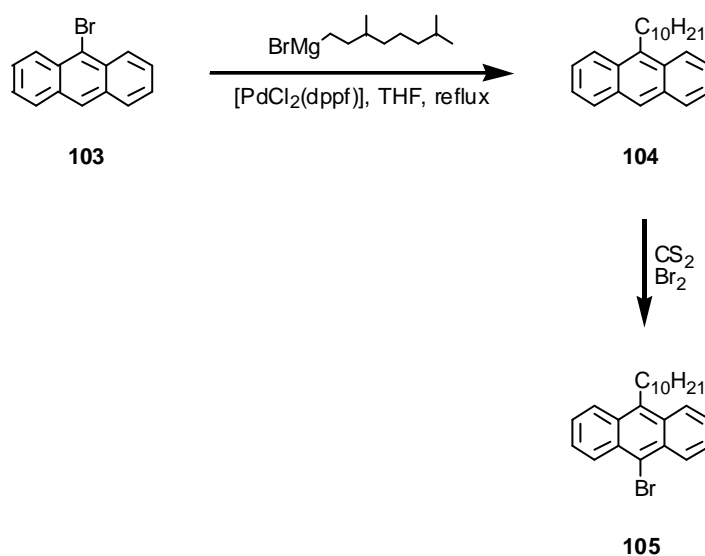
In the following section, the main focus is not directed towards the size of the desired large PAH but on a totally different topology. This new concept is based on the assumption that PAHs which exhibit free or unoccupied space in their aromatic center exhibit different contrasts in their STM images. The visualization of “holes” in a graphite lattice has been reported by Mochiji and co-workers.^[282] In this study, defects on a graphite surface were produced by single ion impact using highly charged Ar ions and then investigated by scanning tunneling microscopy and atomic force microscopy (AFM). The defects looked like a protrusion in the STM image, while they were flat in the AFM image. The average value for the defect size increased remarkably with the charge state of incident Ar ions.^[282]

Bäuerle and Mena-Osteritz reported the adsorption and self-assembling properties of macrocyclic oligothiophene-diacetylenes at the solution HOPG (highly oriented pyrolytic graphite) interface.^[283] Here, holes on graphite were not generated by an ion impact but through the arrangement of organic cyclic molecules on a graphite surface. The STM images of these macrocycles visualize a toroid structure in which the brighter colors result from the higher tunneling current through the macrocyclic π -conjugated system, whereas the interior cavity is shaded. This impressive documentation and visualization of

organic molecules with holes or cavities, described as “donut-like”,^[283] initialized part of the work reported below.

In this work, an attempt was made to synthesize a large polyaromatic compound (**109**, Scheme 36) which bears six holes in its center. These holes have the size of pyrene and thus, should be visible by means of STM spectroscopy and giving rise to intriguing current-voltage characteristics.

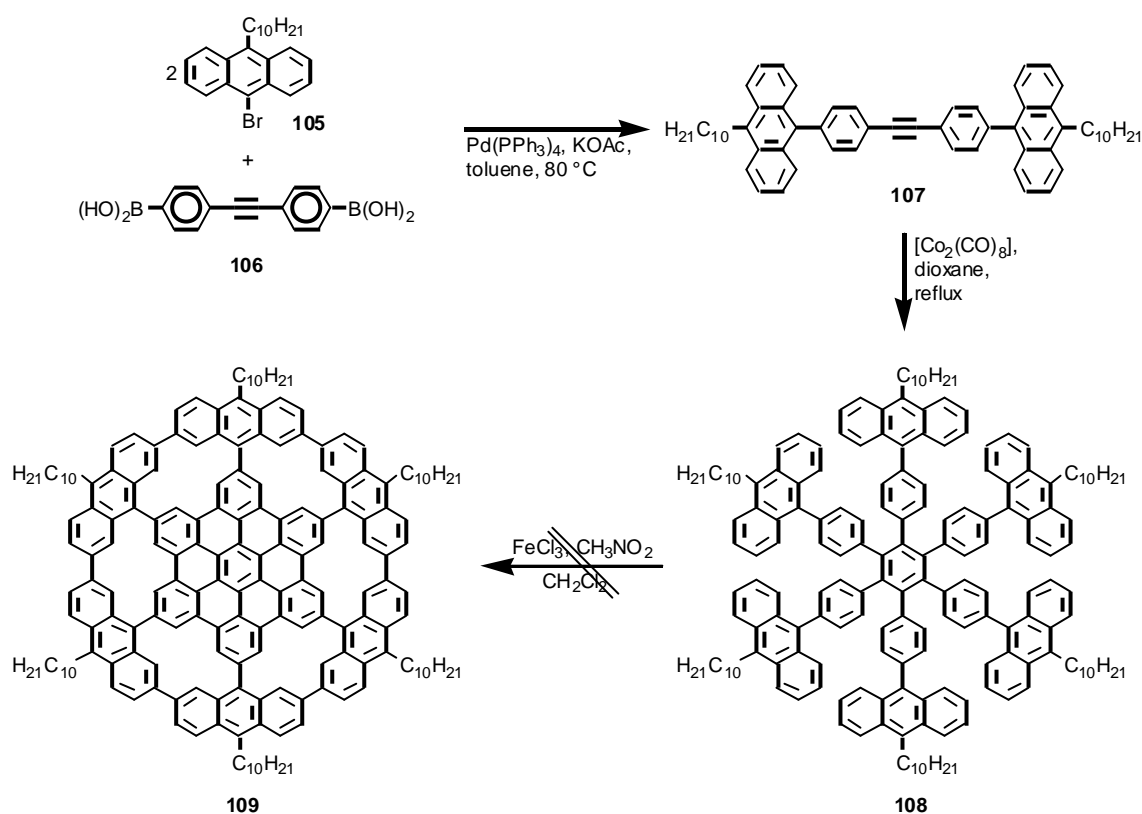
The reaction sequence was started with the design of an appropriate precursor molecule. Six anthracene moieties around a hexaphenyl benzene core, as depicted in Scheme 36, form a periphery that one might still be able to close and connect. Therefore, 9-bromo-anthracene (**103**) was decorated with a solubilizing branched alkyl chain in a Kumada-type coupling reaction to give **104** in moderate yields. Here, the same features of dramatically increased processability (as demonstrated for HBC-C₈ **51**) were utilized.^[37]



Scheme 35: Synthesis of alkyl substituted bromo-anthracene precursor

The bromination of 9-(3,7-dimethyloctanyl)anthracene (**104**) was carried out with bromine in carbon disulfide. After a very short reaction time of only 30 min., the brominated anthracene **105** was obtained as a yellow solid and purified by column chromatography. The next step of the reaction pathway was the Suzuki coupling of two equivalents 9-bromo-10-(3,7-dimethyloctanyl)anthracene (**105**) with 4,4'-diphenylacetylenediboronocacid (**106**) as depicted in Scheme 36. This

reaction was monitored by FD-mass spectrometry and after 16 hours of reaction time, no starting material was detected in the reaction mixture. Unfortunately, after purification of the crude product by means of column chromatography on silica gel, the yield of anthracene substituted tolane **107** was as low as 40%. An explanation for this could be the permanent absorption of part of the product or its decomposition on the silica gel.



Scheme 36: Cyclotrimerization and attempted cyclodehydrogenation of a large PAH with holes

It was already foreseen that the next step shown in Scheme 36, i.e. the cyclotrimerization of **107**, would be low yielding, if at all successful. This was partly attributed to the size and steric hindrance of the shielded diphenylacetylene **107**. Nevertheless, in a cyclotrimerization reaction of 4,4'-bis(10-(3,7-dimethyloctanyl)anthracen-9-yl)diphenylacetylene in dioxane using $[\text{Co}_2(\text{CO})_8]$ as the catalyst, hexaanthracene **108** was obtained in 20% yield after purification. Characteristic for **108** is good solubility in most organic solvents and a very strong fluorescence under UV light. The next, most crucial step

towards the synthesis of a large PAH with holes is the oxidative coupling of 24 aryl moieties with removal of 24 hydrogen atoms. Standard cyclodehydrogenation conditions^[34, 104], introduced earlier, were also utilized for this attempt. After a reaction time of one and two hours, samples were taken and analyzed by MALDI-Tof mass spectrometry. These spectra showed that after two hours a mixture of unreacted starting material, mono and double chlorinated products were present. The loss of a maximum of eight hydrogen atoms was only observed for the double chlorinated species. A derivative which was partly hydrogenated either on the inner hexaphenylbenzene core or on the outer anthracene perimeter was not detected. Since the utilized iron(III)chloride/nitromethane method is the mildest (and normally most successful) version of cyclodehydrogenation reactions applied to PAH precursors, this seems to be a dead end for the synthesis of a HBC derivative with holes.

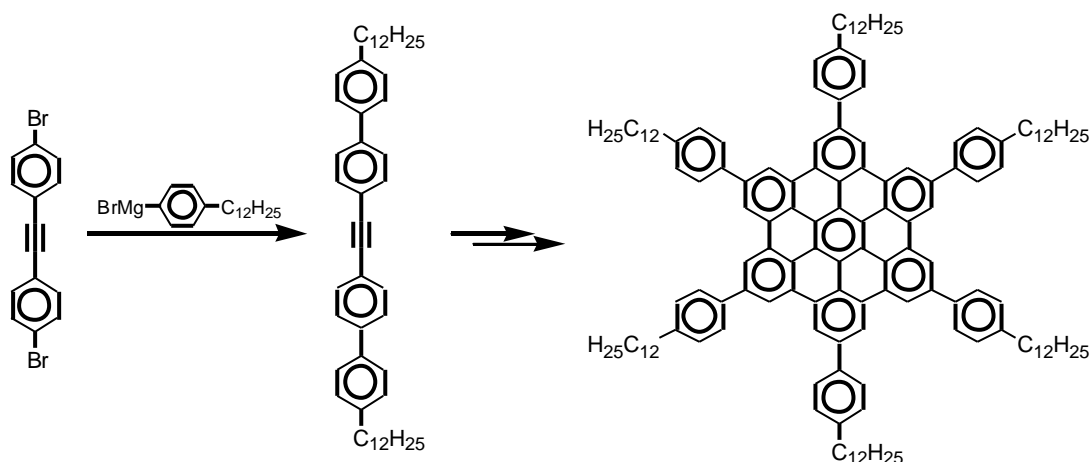
The still interesting and challenging aspect of extended aromatic molecules with holes will have to be approached in a different way.

5 Summary

The aim of the present work “Liquid Crystalline Hexabenzocoronenes as Organic Molecular Materials – Synthesis, Characterization and Application” was defined by three different topics:

1. Improvement of the synthesis leading to hexabenzocoronene derivatives with six-fold alkyl substitution,
2. Design and development of molecular materials with improved properties such as solubility and processability,
3. Implementation of the obtained molecules in optoelectronic devices such as organic solar cells and field effect transistors.

The first goal was successfully achieved by the fact that for the first time the direct functionalization of 4,4'-dibromodiphenyl acetylene was realized with a Kumada-type coupling catalyst never utilized for the synthesis of HBC precursor molecules before as displayed in Scheme 37.



Scheme 37: **Functionalization of 4,4'-dibromodiphenylacetylene and obtained HBC-PhC₁₂**

Hence, it was possible to undertake aryl-aryl and aryl-alkyl couplings very late in the reaction sequence leading to a large variety of substituted HBC derivatives. Hereby, the screening of a vast number of different substituents leading to

improved device performance became possible. The introduction of a phenyl spacer between the HBC core and the pending alkyl chains as in HBC-PhC₁₂ **43** (Scheme 37) had a number of beneficial effects on the characteristics of the new molecule. The most obvious effect was the dramatically increased solubility. HBC-PhC₁₂ became soluble even in high concentrations in common organic solvents such as dichloromethane, chloroform and THF at room temperature and in hexane or heptane at elevated temperatures. Further, the fact that this new HBC derivative was found to be liquid crystalline at room temperature ensured the formation of highly ordered films necessary for the implementation in organic molecular devices. These findings were also supported by the investigation of two-dimensional crystals of HBC-PhC₁₂ via STM techniques. By STM measurements at the solid-liquid interface highly organized 2-D structures were found and reported. Combination of increased intra-columnar order, probed by solid state NMR techniques, and almost constant charge carrier mobility over a large temperature regime (−50 to 200°C) lead to the utilization of HBC-PhC₁₂ in organic solar cells.

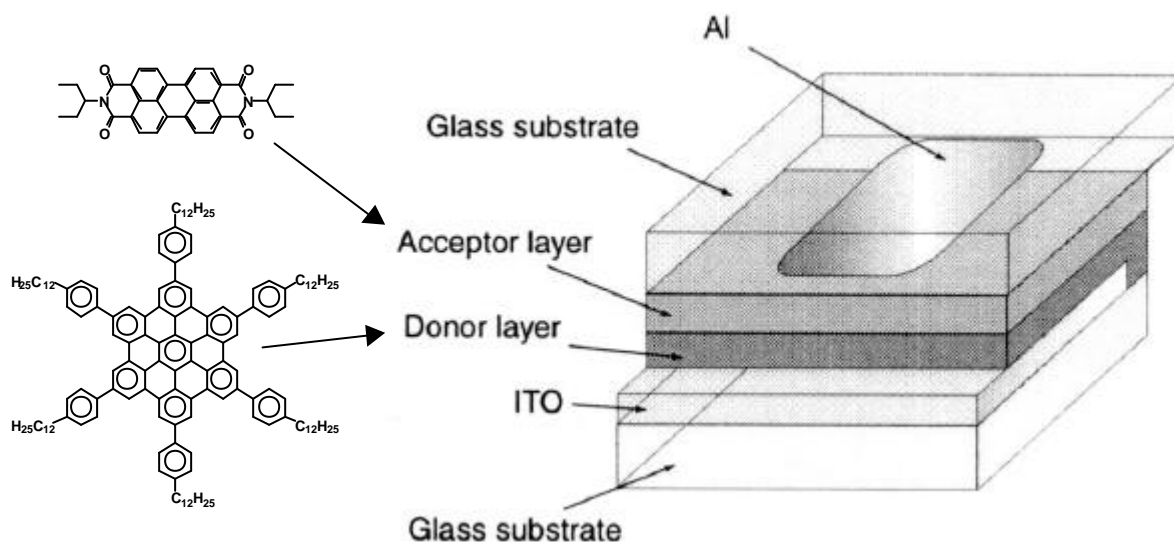


Figure 82: **Chemical structures of donor and acceptor materials and utilized device structure (image reproduced and altered from Friend et.al.^[132])**

Here, self-organization of liquid-crystalline hexabenzocoronene and crystalline conjugated perylene has been employed to create, directly from solution, thin

films with structures optimized for use in photodiodes. The discotic liquid crystalline HBC-PhC₁₂ was used in combination with a perylene dye to produce thin films with vertically-segregated perylene and hexabenzocoronene, with large interfacial surface area. When incorporated into diode structures, these films show photovoltaic response with external quantum efficiencies of >34% near 490 nm and a power efficiency of 1.77%. These efficiencies result from proficient photoinduced charge transfer between the hexabenzocoronene and perylene, as well as effective transport of charges through vertically-segregated perylene and hexabenzocoronene π -systems.

This development demonstrates that complex structures can be engineered from novel materials using simple solution-processing steps, and may enable inexpensive, high performance thin-film photovoltaic technology. In a similar approach, the above material was successfully applied in the fabrication of an organic Field Effect Transistor.

The functionalization of the hexabenzocoronene core with branched alkyl chains ensured high solubilities and gave access to a vast number of modern, transition metal catalyzed reactions which had failed earlier because of the poor solubility behavior of the HBC component. In addition to improved solubility and processability, the utilization of a branched enantiomerically pure, namely (S)-3,7-dimethyloctyl alky chain introduced chirality and highly organized helical superstructures to the HBC family.

Furthermore, this series of soluble hexabenzocoronene derivatives with the pendant optically active (S)-3,7-dimethyloctanyl and (R,S)-3,7-dimethyloctanyl (mixture of stereoisomers) hydrocarbon side chains with and without a phenylene spacer, were assembled into differently ordered arrays at the interface between a solution and the basal plane of highly ordered pyrolytic graphite (HOPG). Molecularly resolved Scanning Tunneling Microscopy (STM) images revealed that all derivatives self-assemble into oriented 2D-crystals. However, while for the alkyl substituted HBCs all the single aromatic cores within a monolayer exhibit the same contrast in the STM, the single aromatic cores with a phenylene group between the alkyl side chains and the aromatic core exhibit different contrasts within a monolayer. For the (R,S) side chains a random distribution of the two different contrasts within the 2D-crystal is

observed, while the optically active phenylene-alkyl substituted HBC exhibits a periodical distribution of three contrasts within the monolayer as displayed in Figure 83.

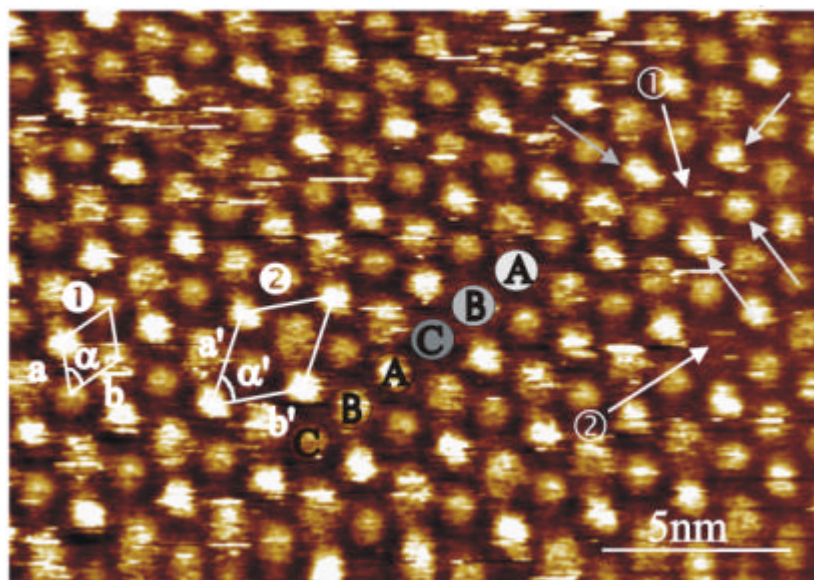


Figure 83: **Scanning Tunneling Microscopy of HBC-PhC₈* 61 at the solution-HOPG interface. A,B,C types of molecules are characterized by a different contrast**

In the case of the optically active side chains combined with the phenyl moiety, a regular superstructure with three distinctly different positions like in a staircase is attained. In the present case, the interactions can induce both the molecules to acquire distinct positions along the z axis and to adopt different conformations. The formation of the staircase architecture finds its origin in the interplay between intramolecular as well as intermolecular and interfacial interactions; a key role is played by the steric hindrance suffered by the side chains. This latter effect can also play a role inducing the molecules to adopt different conformations allowing to minimize the intermolecular repulsive interactions.

Further research in the development of improved material properties of alkyl substituted HBCs has lead to the synthesis and characterization of a hexabenzocoronene derivative substituted with six very long alkyl chains. Here, the fact that branching of alkyl chains demonstrably^[89] stabilizes the mesophase without altering the superstructure was considered and thus, a long branched

hexadecyl alkyl chain with four branching methyl groups was selected for the peripheral decoration of HBC. The resulting HBC derivative is henceforth referred to as HBC-C₁₆ **68** (Figure 84).

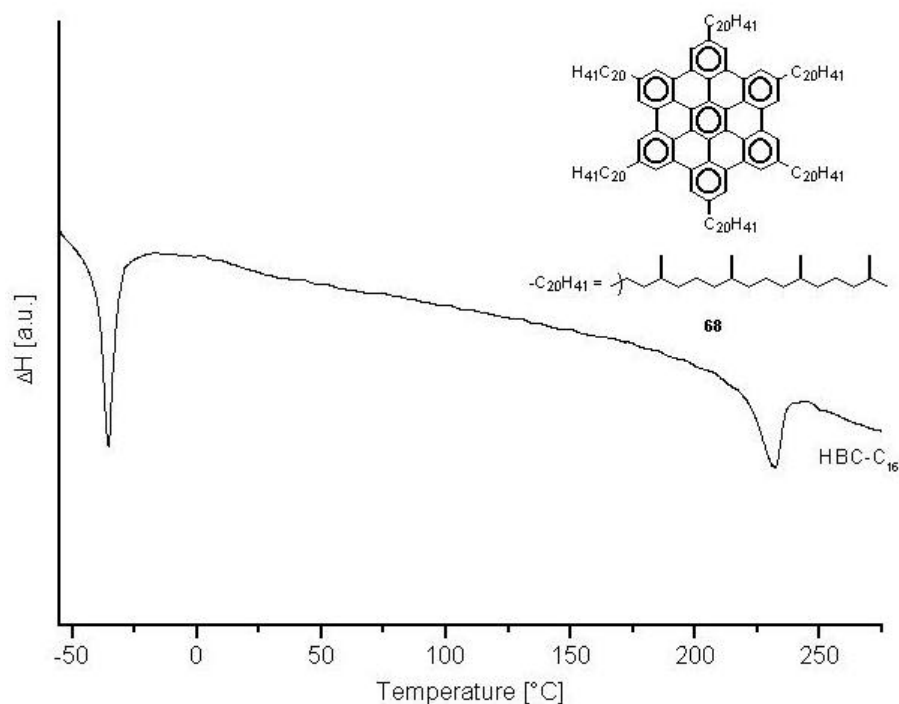


Figure 84: **Chemical structure and differential scanning calorimetry trace of HBC-C₁₆**

In addition to the fact that an enormous phase width of 267°C and liquid crystallinity at room temperature has been attained, this is the first time that thermodynamically stable isotropic phases have been obtained for mesomorphic hexabenzocoronenes which are peripherally substituted with nonfunctionalized alkyl chains.

The aggregation behavior of HBC discs without any surface interaction was investigated via concentration dependant NMR measurements in solution. Here, it was found that a total concentration of 0.165 mol/L corresponds to a maximum concentration of nine HBC molecules per stack, while a total concentration of 5.12×10^{-8} mol/L corresponds to HBC monomers in solution. In this concentration regime, the signal for the aromatic core protons experiences a downfield shift of 1.72 ppm, i.e. from 7.98 ppm for high concentrations to 9.70

ppm for the lowest one. These experimental findings match with theoretical calculations for HBC monomers.

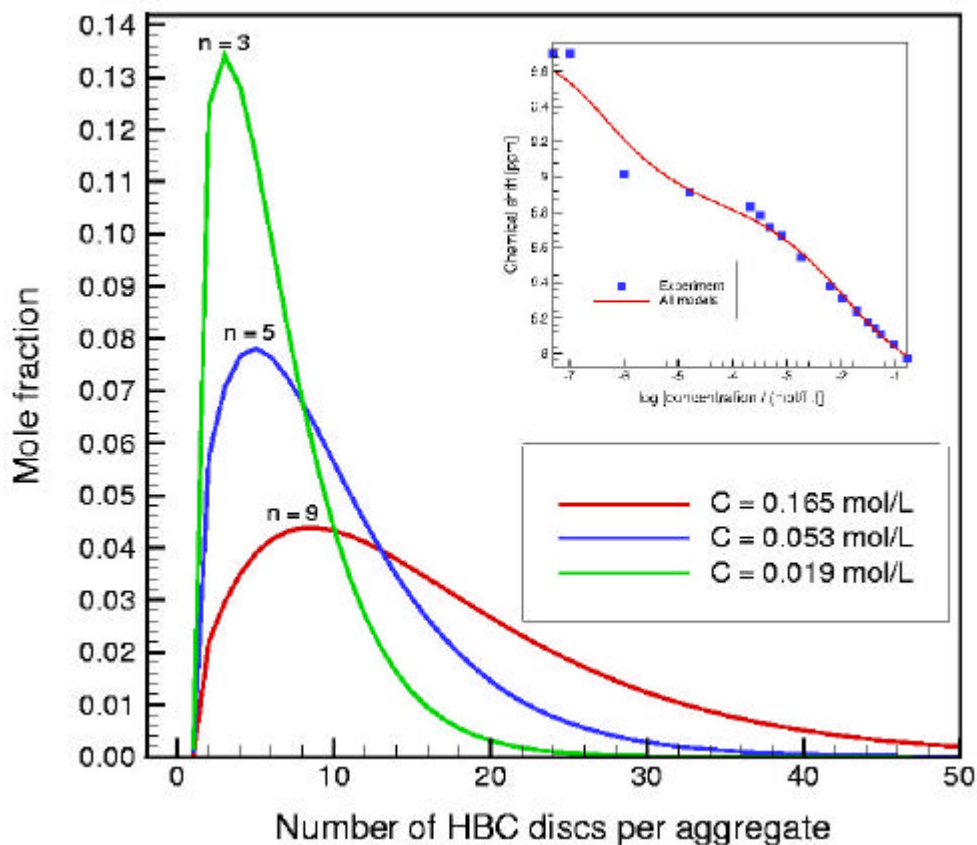


Figure 85: **Number of discs aggregated at given concentrations and comparison between experimental data and models (inset)**

In the case of the para di-bromo functionalized HBC derivative the above introduced $[\text{PdCl}_2(\text{dppf})]$ also proved to be very successful for the carbon-carbon bond formation between the HBC core and alkenyls, perylenes as well as heteroaryls. Even the hexafold substitution of hexaphenylbenzene was achieved via the Kumada-type coupling reaction utilizing this catalyst.

6 Experimental Section

6.1 General Methods

^1H -NMR and ^{13}C -NMR spectra were recorded in CD_2Cl_2 , CDCl_3 , $\text{C}_2\text{D}_2\text{Cl}_4$, and THF on a Bruker DPX 250, Bruker AMX 300 and Bruker DRX 500 with use of the solvent proton or carbon signal as internal standard. UV/Vis spectra were recorded at room temperature on Perkin-Elmer Lambda 9 or Perkin-Elmer Lambda 5 spectrometers. Infrared spectra were recorded on a Nicolet FT-IR 320 spectrophotometer as KBr pellets or as film between NaCl discs. Melting points were determined on a Büchi hot stage apparatus and are uncorrected. Mass spectra were obtained on a VG Instruments ZAB 2-SE-FPD by using FD. Elemental analysis were carried out on a Foss Heraeus Vario EL.

Differential scanning calorimetry (DSC) was measured on a Mettler DSC 30 with heating and cooling rates of 10 K/min. First order transition temperatures were reported as the minima of their endothermic peaks during heating. A Zeiss Axiophot with a nitrogen flushed Linkam THM 600 hot stage was used to characterize the polarization microscopy textures.

X-Ray diffraction experiments were performed using a Siemens D 500 Kristalloflex with a graphite-monochromatized $\text{Cu}_{\text{K}\alpha}$ X-Ray beam, emitted from a rotating Rigaku RV-300 anode. The temperature of the samples, which were directly on a copper sample holder, was measured by a bimetal sensor and calibrated by reference measurements.

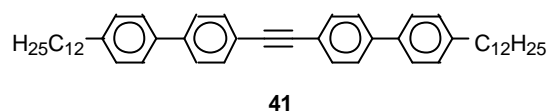
6.2 Materials

(S)-1-Bromo-3,7-dimethyloctane was synthesized according to standard literature procedure^[89] using commercially available (3S)-(+)-3,7-dimethyl-6-octene-1-ylbromide from Aldrich. 4,4'-Dibromodiphenylacetylene (2)^[114] was synthesized as previously described in the literature. $[\text{PdCl}_2(\text{dppf})]$, $\text{Pd}(\text{PPh}_3)_4$ were used as received from Strem. THF (A.C.S. reagent, Riedel-de Haen) was

refluxed over potassium and distilled freshly before use. All other materials were used as received.

6.3 Syntheses

6.3.1 4,4'-Bis(4-*n*-dodecylphen-1-yl)diphenylacetylene (**41**)



In a 250 mL Schlenk flask, 18 mL of a 1M solution of 4-dodecylphenylmagnesiumbromide was added dropwise to 1 g (3 mmol) 4,4'-dibromdiphenylacetylene (**21**) dissolved in 100 mL of dry THF. 200 mg of [PdCl₂(dppf)] catalyst was added to this solution. The resulting mixture was stirred under reflux in an inert atmosphere for 20 h. While cooling to room temperature, a white solid precipitated. The solid was then filtered and washed several times with petrol ether and methanol to yield 1.5 g (75%) of **41**.

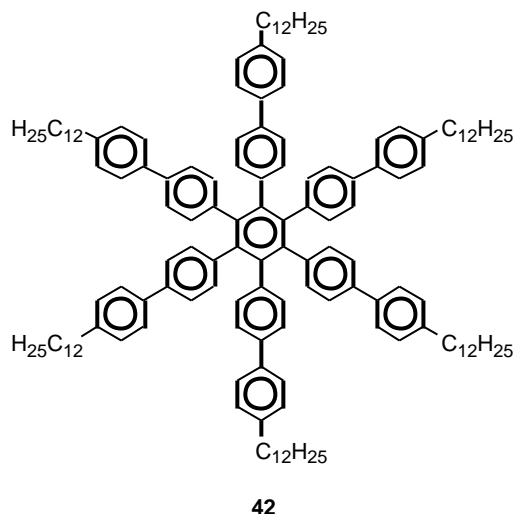
¹H-NMR (500 MHz, C₂D₂Cl₄): δ = 7.58 (s, 8H; CH), 7.51 (d, ³J(H,H) = 7 Hz, 4H; CH), 7.24 (d, ³J(H,H) = 7 Hz, 4H; CH), 2.65 (m, 4H; α-CH₂), 1.67 (m, 4H; β-CH₂), 1.25-1.45 (m, 36 H; CH₂), 0.91 (t, ³J(H,H) = 6 Hz, 6H; CH₃);

¹³C-NMR (125 MHz, C₂D₂Cl₄): δ = 143.10, 141.40, 138.0, 132.50, 129.30, 127.23, 127.17, 122.60, 90.70, 36.00, 32.30, 31.50, 30.04, 30.03, 30.00, 29.96, 29.87, 29.76, 29.67, 23.00, 14.36;

m.p.: 225 °C

EA: calcd. (%) for C₅₀H₆₆: C 90.03, H 9.97; found: C 89.40, H 10.02.

MS (FD, 8 kV): m/z (%) = 666.9 (100) [M⁺] (calcd for C₅₀H₆₆ = 666.5)

6.3.2 Hexa(4-*n*-dodecylbiphen-1-yl)benzene (**42**)

In a 100 mL round bottom flask equipped with a reflux condenser, a suspension of 1 g (1.5 mmol) di(4-*n*-dodecylbiphenyl)acetylene (**41**) and 50 mL of dioxane was degassed several times; 78 mg (0.23 mmol) $[\text{Co}_2(\text{CO})_8]$ was then added and the resulting mixture was refluxed for 3 h. The solvent was evaporated under vacuum, and was purified using column chromatography on silica with petrol ether/ CH_2Cl_2 (8/2) as the eluent, yielding 0.7 g (70%) of **42** as an off-white solid.

$^1\text{H-NMR}$ (500 MHz, $\text{C}_2\text{D}_2\text{Cl}_4$): δ = 7.31 (d, 3J (H,H) = 8 Hz, 12H; CH), 7.1 (d, 3J (H,H) = 8 Hz, 12H; CH), 7.06 (d, 3J (H,H) = 8 Hz, 12H; CH), 6.88 (d, 3J (H,H) = 8 Hz, 12H; CH), 2.51 (m, 12H; α - CH_2), 1.52 (m, 12H; β - CH_2), 1.30-1.15 (m, 108H; CH_2), 0.83 (t, 3J (H,H) = 6 Hz, 18H; CH_3);

$^{13}\text{C-NMR}$ (125 MHz, $\text{C}_2\text{D}_2\text{Cl}_4$): δ = 142.05, 140.37, 139.94, 138.10, 137.26, 132.27, 128.91, 126.83, 125.18, 35.82, 32.21, 31.76, 29.98 (2x $\underline{\text{C}}\text{H}_2$), 29.94, 29.90, 29.82, 29.70, 29.65, 23.02, 14.52;

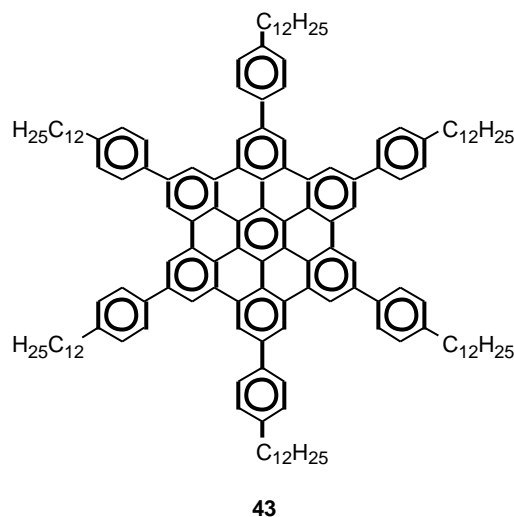
m.p.: 88 °C

EA: calcd. (%) for $\text{C}_{150}\text{H}_{198}$: C 90.03, H 9.97; found: C 90.11, H 9.82.

MS (FD, 8 kV): m/z (%) = 2002.1 (100) [M^+] (calcd for $\text{C}_{150}\text{H}_{196}$ = 2001.2)

DSC: $\text{K} \rightarrow \text{Co}|_{\text{h}_0}$ T = -66 °C, ΔH = 55.4 kJ/mol

6.3.3 Hexa(4-*n*-dodecylphen-1-yl)hexa-*peri*-hexabenzocoronene (43)



A 250 mL two necked round bottom flask was charged with 0.53 g (0.27 mmol) of hexa(4-*n*-dodecylbiphen-1-yl)benzene (**42**) and 70 mL of CH₂Cl₂. Using a glass capillary, a constant stream of argon was bubbled through the solution. Then 0.8 g (5 mmol) of FeCl₃ dissolved in CH₃NO₂ was added dropwise using a syringe. After 45 min. the mixture was quenched with MeOH and the precipitate was filtered. The resulting yellow solid was recrystallized from hot THF and dried under vacuum to yield 0.42g (80%) of **43**.

¹H-NMR (500 MHz, *p*-C₆D₄Cl₂, 160 °C): δ = 8.57 (s, 12H; CH), 7.92 (d, ³*J* (H,H) = 6.5 Hz, 12H; CH), 7.58 (d, ³*J* (H,H) = 6.5 Hz, 12H; CH), 3.18 (m, 12H; α-CH₂), 2.25 (m, 12H; β-CH₂), 1.95 (m, 12H; γ-CH₂), 1.88 (m, 12H; δ-CH₂), 1.8-1.45 (m, 84H; CH₂), 1.13 (m, 18H; CH₃);

¹³C-NMR (125 MHz, C₂D₂Cl₄, 85 °C): δ = 141.87, 140.65, 136.73, 129.83, 129.35, 128.93, 122.63, 120.31, 118.32, 37.37, 33.25, 33.22, 31.40, 31.34, 31.27, 31.21, 31.08, 30.90, 30.7, 23.91, 15.12;

UV/Vis: λ nm (log ε) = 254 (5.24), 371 (5.11);

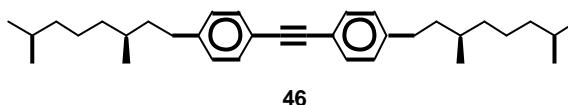
m.p.: > 300 °C

EA: anal. calcd. (%) for C₁₅₀H₁₈₆: C 90.57, H 9.43; found: C 89.62 H 9.84.

MS (MALDI-TOF): m/z (%) = 1989.1 (100) [M^+] (calcd for $C_{150}H_{186} = 1989.1$)

DSC: $K \rightarrow Col_{ho,1}$ $T = 15.3$ °C, $\Delta H = 30$ kJ/mol; $Col_{ho,1} \rightarrow Col_{ho,2}$ $T = 79.8$ °C, $\Delta H = 16.6$

6.3.4 4,4'-Bis((S)-3,7-dimethyloctanyl)diphenylacetylene (**46**)



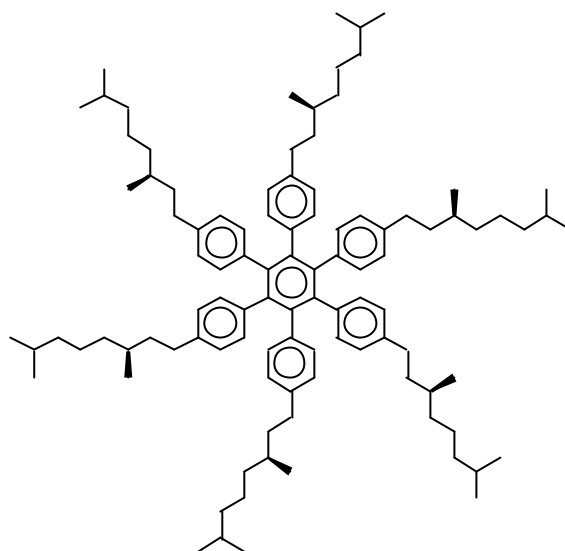
In a 250 mL two-necked round bottom flask, 60 mL of a 1M solution of (S)-3,7-dimethyloctanyl-1-magnesiumbromide (prepared immediately prior to use from (S)-1-bromo-3,7-dimethyloctane and magnesium) was added dropwise to 5 g (14.9 mmol) 4,4'-dibromodiphenylacetylene (**21**) dissolved in 150 mL of dry THF. Then, 500 mg of $[PdCl_2(dppf)]$ catalyst was added to this solution. The resulting mixture was stirred under reflux in an inert atmosphere overnight. The reaction was quenched with methanol and the solvent removed under reduced pressure. Purification using column chromatography on silica gel with petrol ether as the eluent afforded 5.8 g **46** as a colorless oil. Yield: 85%.

1H -NMR (500 MHz, $C_2D_2Cl_4$): $\delta = 7.42$ (d, 3J (H,H) = 7.9 Hz, 4H; CH), 7.15 (d, 3J (H,H) = 7.9 Hz, 4H; CH), 2.63 (m, 4H; α -CH₂), 1.63 (m, 4H; β -CH₂), 1.55 (m, 2 H; CH), 1.47 (m, 4H; CH₂), 1.37-1.24 (m, 6H; CH, CH₂), 1.81 (m, 4H; CH₂), 0.94 (d, 3J (H,H) = 6.1 Hz, 6H; CH₃) 0.91 (d, 3J (H,H) = 6.1 Hz, 12H; CH₃);

^{13}C -NMR (125 MHz, $C_2D_2Cl_4$): $\delta = 140.12, 128.11.40, 124.89, 117.35, 85.75, 35.95, 35.06, 33.76, 29.99, 29.13, 24.45, 21.17, 19.16, 19.10, 16.17$;

MS (FD, 8 kV): m/z (%) = 458.1 (100) [M^+] (calcd for $C_{34}H_{50} = 458.77$)

6.3.5 Hexa-4-((S)-3,7-dimethyloctanyl)hexaphenylbenzene (47)



47

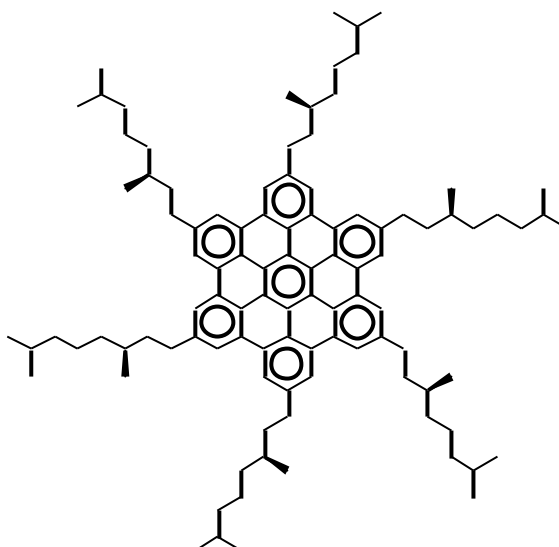
230 mg (0.68 mmol) $[\text{Co}_2(\text{CO})_8]$ was added under argon to a degassed solution of 2 g (4.36 mmol) (S)-4,4'-bis(3,7-dimethyloctanyl)diphenylacetylene (**46**) in 100 mL of dioxane in a 250 mL round bottom flask equipped with a reflux condenser. After refluxing for 3 h, the solvent was evaporated under vacuum, and the residue was purified using column chromatography on silica gel with petrol ether/ CH_2Cl_2 (9/1) as the eluent, yielding 1.8 g **47** as colorless oil. Yield: 90%.

$^1\text{H-NMR}$ (500 MHz, $\text{C}_2\text{D}_2\text{Cl}_4$): δ = 6.61 (d, $^3J(\text{H,H}) = 7.9$ Hz, 12H; CH), 6.56 (d, $^3J(\text{H,H}) = 7.9$ Hz, 12H; CH), 2.29 (m, 12H; $\alpha\text{-CH}_2$), 1.47 (m, 6H; CH), 1.35 (m, 6H; CH), 1.20 - 0.98 (m, 48H; CH_2), 0.82 (d, $^3J(\text{H,H}) = 6.7$ Hz, 36H; CH_3), 0.75 (d, $^3J(\text{H,H}) = 6.1$ Hz, 18H; CH_3);

$^{13}\text{C-NMR}$ (125 MHz, $\text{C}_2\text{D}_2\text{Cl}_4$): 136.58, 135.52, 134.91, 130.0, 122.84, 35.92, 35.24, 33.68, 29.46, 28.52, 24.49, 21.26, 19.36, 19.29, 16.22;

MS (FD, 8 kV): m/z (%) = 1377.0 (100) [M^+] (calcd for $\text{C}_{102}\text{H}_{150} = 1376.31$)

6.3.6 Hexa((S)-3,7-dimethyloctanyl)hexa-peri-hexabenzocoronene (**48**)

**48**

A 250 mL two necked round bottom flask was charged with 0.50 g (0.36 mmol) of (S)-hexa-4-(3,7-dimethyloctanyl)hexaphenylbenzene (**47**) and 100 mL of CH_2Cl_2 . Using a glass capillary, a constant stream of argon was bubbled through the solution. Then, 1.12 g (6.9 mmol) of FeCl_3 dissolved in CH_3NO_2 (13 mL) was added dropwise using a syringe. After 30 min., the mixture was quenched with a large excess of methanol and the precipitate was filtered. The resulting yellow solid was redissolved in dichloromethane and filtered through a short pad of silica gel and dried under vacuum to yield 0.39 g **48** as a yellow powder. Yield: 80%.

$^1\text{H-NMR}$ (500 MHz, $\text{C}_2\text{D}_2\text{Cl}_4$): δ = 8.09 (s, 12H; CH), 2.96 (m, 12H; $\alpha\text{-CH}_2$), 2.01 (m, 6H; CH), 1.8 (m, 12H; CH_2), 1.64 (m, 12H; CH_2), 1.54 (m, 6H; CH), 1.43 (m, 12H; CH_2), 1.33 (m, 12H; CH_2), 1.23 (d, $^3J(\text{H,H}) = 6.1$ Hz, 18H; CH_3), 0.97 (d, $^3J(\text{H,H}) = 6.7$ Hz, 36H; CH_3);

$^{13}\text{C-NMR}$ (125 MHz, $\text{C}_2\text{D}_2\text{Cl}_4$, 100 °C): δ = 140.36, 129.98, 123.41, 121.42, 119.56, 40.01, 39.96, 37.95, 35.12, 33.69, 28.42, 25.32, 23.13, 23.05, 20.36;

UV/Vis: λ nm ($\log \epsilon$) = 229 (5.22), 359 (5.34);

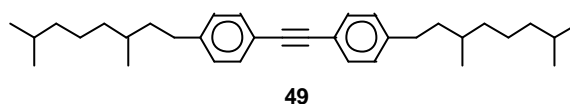
m.p. > 300 °C

EA: anal. calcd. (%) for C₁₀₂H₁₃₈: C 89.80, H 10.20; found: C 89.77 H 10.17.

MS (FD, 8 kV): m/z (%) = 1364.0 (100) [M⁺] (calcd for C₁₀₂H₁₃₈ = 1364.21)

DSC: K→Col_{h0,1} T = 96 °C, ΔH = 26 kJ/mol

6.3.7 4,4'-Bis(3,7-dimethyloctanyl)diphenylacetylene (49):



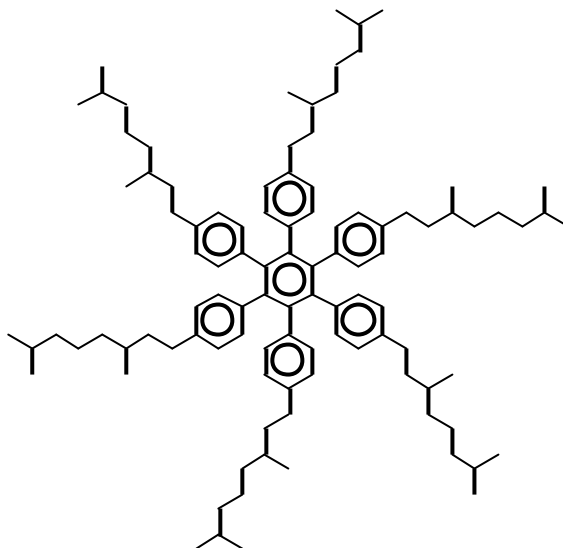
Prepared as described above for compound **46**. Colorless oil, yield: 86%.

¹H-NMR (500 MHz, C₂D₂Cl₄): δ = 7.38 (d, ³J (H,H) = 7.9 Hz, 4H; CH), 7.11 (d, ³J (H,H) = 7.9 Hz, 4H; CH), 2.54 (m, 4H; α -CH₂), 1.55 (m, 2H; CH), 1.47 (m, 2 H; CH), 1.37 (m, 4H; CH₂), 1.25 (m, 4H; CH₂), 1.11-1.05 (m, 8H; CH₂), 0.87 (d, ³J (H,H) = 6.1 Hz, 6H; CH₃) 0.82 (d, ³J (H,H) = 6.7 Hz, 12H; CH₃);

¹³C-NMR (125 MHz, C₂D₂Cl₄): δ = 143.96, 131.85, 128.75, 120.72, 89.35, 39.62, 38.98, 37.43, 33.73, 32.79, 28.25, 25.01, 23.09, 23.00, 19.94;

MS (FD, 8 kV): m/z (%) = 458.5 (100) [M⁺] (calcd for C₃₄H₅₀ = 458.77)

6.3.8 Hexa-4-(3,7-dimethyloctanyl)hexaphenylbenzene (50)



50

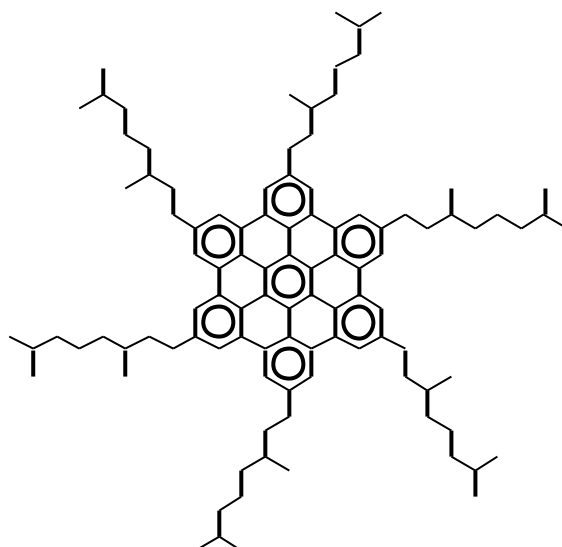
Prepared as described above for compound **47**. Colorless oil, yield: 88%.

¹H-NMR (500 MHz, C₂D₂Cl₄): δ = 6.58 (d, ³J (H,H) = 7.6 Hz, 12H; CH), 6.53 (d, ³J (H,H) = 7.9 Hz, 12H; CH), 2.26 (m, 12H; α-CH₂), 1.45 (m, 6H; CH), 1.32 (m, 6H; CH), 1.19 – 1.10 (m, 36H; CH₂), 1.05-0.97 (m, 12H; CH₂), 0.80 (d, ³J (H,H) = 6.7 Hz, 36H; CH₃), 0.73 (d, ³J (H,H) = 5.5 Hz, 18H; CH₃);

¹³C-NMR (125 MHz, C₂D₂Cl₄): 139.45, 138.41, 137.78, 130.87, 125.71, 38.79, 38.15, 36.56, 32.34, 31.34, 27.37, 24.14, 22.23, 22.16, 19.09;

MS (FD, 8 kV): m/z (%) = 1375.9 (100) [M⁺] (calcd for C₁₀₂H₁₅₀ = 1376.31)

6.3.9 Hexa(3,7-dimethyloctanyl)hexa-*peri*-hexabenzocoronene (51)



51

Prepared as described above for compound **48**. Yellow powder, yield: 83%.

¹H-NMR (500 MHz, C₂D₂Cl₄): δ = 8.26 (s, 12H; CH), 3.05 (m, 12H; α -CH₂), 2.06 (m, 6H; CH), 1.83 (m, 12H; CH₂), 1.65 (m, 12H; CH₂), 1.56-1.43 (m, 18H; CH, CH₂), 1.35 (m, 12H; CH₂), 1.23 (d, ³*J* (H,H) = 6.3 Hz, 18H; CH₃), 0.97 (d, ³*J* (H,H) = 6.6 Hz, 36H; CH₃);

¹³C-NMR (125 MHz, C₂D₂Cl₄, 100 °C): δ = 140.07, 129.68, 123.10, 121.18, 119.25, 39.93, 39.87, 37.81, 35.00, 33.57, 28.31, 25.21, 23.06, 22.97, 20.25;

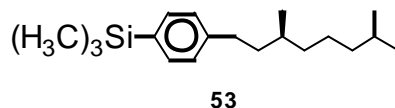
UV/Vis: λ nm (log ϵ) = 229 (5.22), 359 (5.34);

m.p. > 300 °C

EA: anal. calcd. (%) for C₁₀₂H₁₃₈: C 89.80, H 10.20; found: C 89.83 H 10.11.

MS: (FD, 8 kV): *m/z* (%) = 1363.5 (100) [M⁺] (calcd for C₁₀₂H₁₃₈ = 1364.21)

DSC: K→Col_{ho} T = 81 °C, ΔH = 31 kJ/mol

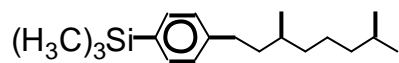
6.3.10 (S)-1-(3,7-dimethyloctanyl)-4-trimethylsilylbenzene (53)

In a 500 mL two-necked round bottom flask, 44 mL of a 1M solution of (S)-3,7-dimethyloctanyl-1-magnesiumbromide (prepared immediately prior to use from (S)-1-bromo-3,7-dimethyloctane and magnesium) was added dropwise to a solution of 5 g (22 mmol) 1-bromo-4-trimethylsilylbenzene (**52**) dissolved in 300 mL of dry THF and 500 mg of [PdCl₂(dppf)] catalyst. The resulting mixture was stirred under reflux in an inert atmosphere overnight. The reaction was quenched with methanol and the solvent removed under reduced pressure. Purification using column chromatography on silica gel with petrol ether as the eluent afforded 5.7 g **53** as a colorless oil. Yield: 90%.

¹H-NMR (500 MHz, C₂D₂Cl₄): δ = 7.41 (d, ³J (H,H) = 6.7 Hz, 2H; CH), 7.16 (d, ³J (H,H) = 7.3 Hz, 2H; CH), 2.56 (m, 2H; α-CH₂), 1.62-1.60 (m, 2H; β-CH₂), 1.59-1.35 (m, 4H; CH, CH₂), 1.30-1.10 (m, 2H; CH₂), 0.92 (d, ³J (H,H) = 6.1 Hz, 3H; CH₃) 0.86 (d, ³J (H,H) = 6.7 Hz, 6H; CH₃) 0.24 (s, 9H; CH₃);

¹³C-NMR (125 MHz, C₂D₂Cl₄): δ = 144.1, 137.2, 133.7, 128.2, 39.7, 39.1, 37.5, 33.8, 33.0, 28.3, 25.0, 23.1, 23.0, 20.0, -0.6;

MS (FD, 8 kV): m/z (%) = 291.2 (100) [M⁺] (calcd for C₁₉H₃₄Si = 290.56)

6.3.11 1-(3,7-dimethyloctanyl)-4-trimethylsilybenzene (54)

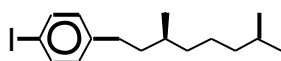
54

Prepared as described above for compound **53**. Colorless oil, yield: 88%.

¹H-NMR (500 MHz, C₂D₂Cl₄): δ = 7.48 (d, ³J (H,H) = 7.3 Hz, 2H; CH), 7.23 (d, ³J (H,H) = 7.3 Hz, 2H; CH), 2.67 (m, 2H; α-CH₂), 1.72 (m, 1H; CH), 1.62-1.54 (m, 3H; CH, CH₂), 1.34 (m, 4H; CH₂), 1.24 (m, 2H; CH₂), 1.01 (d, ³J (H,H) = 5.5 Hz, 3H; CH₃) 0.95 (d, ³J (H,H) = 6.7 Hz, 6H; CH₃) 0.33 (s, 9H; CH₃);

¹³C-NMR (125 MHz, C₂D₂Cl₄): δ = 144.0, 137.3, 133.7, 128.2, 39.7, 39.0, 37.5, 33.8, 33.0, 28.3, 27.8, 23.1, 23.0, 20.0, -0.6;

MS (FD, 8 kV): m/z (%) = 290.1 (100) [M⁺] (calcd for C₁₉H₃₄Si = 290.56)

6.3.12 (S)-1-(3,7-dimethyloctanyl)-4-iodobenzene (55)

55

A 250 mL two necked round bottom flask was charged with 6.4 g (22 mmol) of (S)-1-(3,7-dimethyloctanyl)-4-trimethylsilybenzene (**53**) dissolved in 175 mL of CCl₄. After the solution was cooled down to 0 °C, 23 mL (23 mmol) of a one molar solution of iodine monochloride were added dropwise with a syringe. The reaction mixture was stirred at this temperature for one hour, poured into an aqueous sodium thiosulfate solution, and extracted with dichloromethane. The combined organic layers were dried over anhydrous magnesium sulfate, and

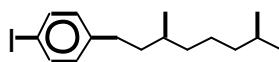
the solvent was removed at reduced pressure to provide 6.4 g (85 %) of **55** as a colorless oil.

¹H-NMR (500 MHz, C₂D₂Cl₄): δ = 7.56 (d, ³*J* (H,H) = 7.9 Hz, 2H; CH), 6.91 (d, ³*J* (H,H) = 7.9 Hz, 2H; CH), 2.53 (m, 2H; α -CH₂), 1.61-1.49 (m, 2H; β -CH₂), 1.41 (m, 2H; CH₂), 1.32-1.22 (m, 3H; CH, CH₂), 1.16 (m, 3H; CH, CH₂), 0.91 (d, ³*J* (H,H) = 6.7 Hz, 3H; CH₃) 0.87 (d, ³*J* (H,H) = 6.7 Hz, 6H; CH₃);

¹³C-NMR (125 MHz, C₂D₂Cl₄): δ = 143.2, 137.6, 130.7, 90.7, 39.6, 38.8, 37.4, 33.2, 32.8, 28.2, 24.9, 22.9, 22.8, 19.9;

MS (FD, 8 kV): *m/z* (%) = 344.7 (100) [*M*⁺] (calcd for C₁₆H₂₅I = 344.27)

6.3.13 1-(3,7-dimethyloctanyl)-4-iodobenzene (**56**)



56

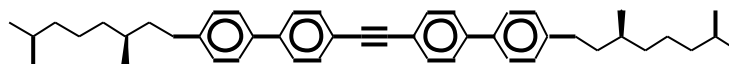
Prepared as described above for compound **55**. Colorless oil, yield: 87%.

¹H-NMR (250 MHz, C₂D₂Cl₄): δ = 7.61 (d, ³*J* (H,H) = 8.2 Hz, 2H; CH), 6.97 (d, ³*J* (H,H) = 8.4 Hz, 2H; CH), 2.58 (m, 2H; α -CH₂), 1.56 (m, 2H; β -CH₂), 1.36-1.24 (m, 4H; CH, CH₂), 1.19 (m, 2H; CH₂), 0.95 (d, ³*J* (H,H) = 6.2 Hz, 3H; CH₃) 0.91 (d, ³*J* (H,H) = 6.5 Hz, 6H; CH₃);

¹³C-NMR (62.5 MHz, C₂D₂Cl₄): δ = 144.1, 138.5, 131.8, 91.8, 40.6, 39.9, 38.4, 34.2, 33.7, 28.2, 29.2, 25.9, 23.9, 20.9;

MS (FD, 8 kV): *m/z* (%) = 343.8 (100) [*M*⁺] (calcd for C₁₆H₂₅I = 344.27)

6.3.14 Bis((S)-4-(3,7-dimethyloctanyl)biphenyl)acetylene (**57**)

**57**

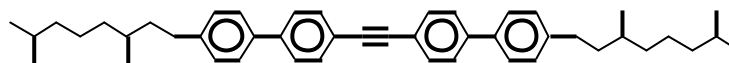
In a 250 mL Schlenk flask, 15 mL of a 1M solution of (S)-1-(3,7-dimethyloctanyl)benzene-4-magnesiumiodide (**55**) was added dropwise to 1.2 g (3.6 mmol) 4,4'-dibromodiphenylacetylene (**21**) dissolved in 100 mL of dry THF. 200 mg of [PdCl₂(dppf)] catalyst were added to this solution. The resulting mixture was stirred under reflux in an inert atmosphere for 20 h. The reaction was quenched with methanol and the solvent removed under reduced pressure. Purification using column chromatography on silica gel with petrol ether as the eluent afforded 0.92 g **57** as an off-white solid. Yield: 45%.

¹H-NMR (500 MHz, C₂D₂Cl₄): δ = 7.56 (d, ³J (H,H) = 8.5 Hz, 4H; CH), 9.1 (d, ³J (H,H) = 7 Hz, 4H; CH), 7.48 (d, ³J (H,H) = 7.9 Hz, 4H; CH), 7.22 (d, ³J (H,H) = 8.5 Hz, 4H; CH), 2.66-2.52 (m, 4H; α-CH₂), 1.60 (m, 2H; CH), 1.50-1.40 (m, 8 H; CH₂), 1.28-1.21 (m, 4H; CH₂), 1.1 (m, 6H; CH, CH₂), 0.89 (d, ³J (H,H) = 6.1 Hz, 6H; CH₃) 0.82 (d, ³J (H,H) = 6.7 Hz, 12H; CH₃);

¹³C-NMR (125 MHz, C₂D₂Cl₄): δ = 142.3, 140.0, 136.5, 131.3, 128.2, 126.1, 126.0, 121.0, 89.4, 38.6, 38.1, 36.4, 32.4, 31.9, 27.2, 24.0, 22.1, 22.0, 19.0;

MS (FD, 8 kV): m/z (%) = 611.3 (100) [M⁺] (calcd for C₄₆H₅₈ = 610.96)

6.3.15 Bis(4-(3,7-dimethyloctanyl)biphenyl)acetylene (58)



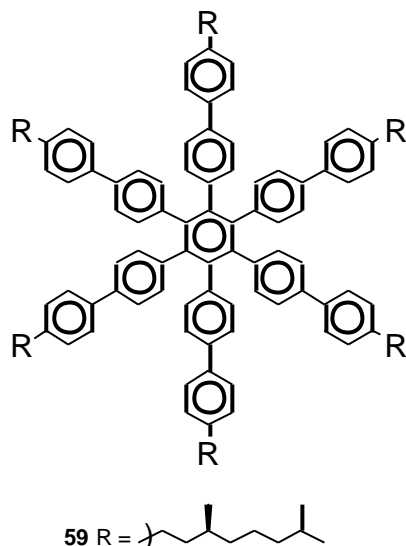
58

Prepared as described above for compound **57**. Off-white crystals, yield: 51%.

¹H-NMR (500 MHz, C₂D₂Cl₄): δ = 7.57 (m, 8H; CH), 7.50 (d, ³J (H,H) = 8.5 Hz, 4H; CH), 7.24 (d, ³J (H,H) = 8.6 Hz, 4H; CH), 2.62 (m, 4H; α -CH₂), 1.64 (m, 2H; CH), 1.54-1.45 (m, 6H; CH, CH₂), 1.32 (m, 4H; CH₂), 1.14 (m, 8H CH₂), 0.93 (d, ³J (H,H) = 6.7 Hz, 6H; CH₃) 0.86 (d, ³J (H,H) = 6.7 Hz, 12H; CH₃);

¹³C-NMR (125 MHz, C₂D₂Cl₄): δ = 143.3, 141.1, 137.7, 132.3, 129.2, 127.1, 127.0, 122.2, 90.5, 39.6, 39.0, 37.5, 33.4, 32.9, 28.2, 24.9, 23.0, 22.9, 20.0;

MS (FD, 8 kV): m/z (%) = 610.6 (100) [M⁺] (calcd for C₄₆H₅₈ = 610.96)

6.3.16 Hexa((S)-4-(3,7-dimethyloctanyl)biphenyl)benzene (**59**)

In a 100 mL round bottom flask equipped with a reflux condenser, a solution of 0.6 g (0.98 mmol) bis((S)-4-(3,7-dimethyloctanyl)biphenyl)acetylene (**57**) in 30 mL of dioxane was degassed several times; 78 mg (0.23 mmol) $[\text{Co}_2(\text{CO})_8]$ was then added and the resulting mixture was refluxed for 5 h. The solvent was evaporated under vacuum, and the crude product was purified using column chromatography on silica with petrol ether/ CH_2Cl_2 (8/2) as the eluent, yielding 0.4 g (70%) of **59** as an off-white solid.

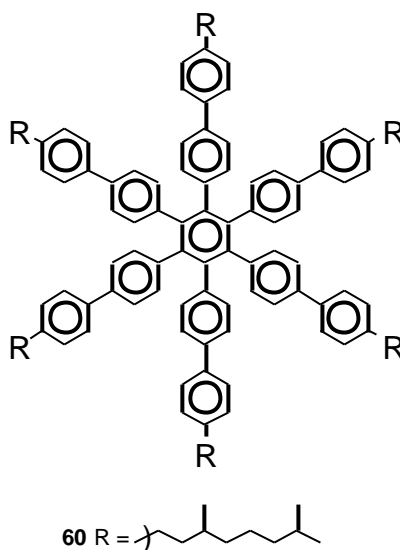
$^1\text{H-NMR}$ (500 MHz, $\text{C}_2\text{D}_2\text{Cl}_4$): δ = 7.32 (d, 3J (H,H) = 7.9 Hz, 12H; CH), 7.1 (d, 3J (H,H) = 8.5 Hz, 12H; CH), 7.07 (d, 3J (H,H) = 8.5 Hz, 12H; CH), 6.88 (d, 3J (H,H) = 7.9 Hz, 12H; CH), 2.50 (m, 12H; $\alpha\text{-CH}_2$), 1.55-1.42 (m, 6H; CH), 1.41 (m, 12H; CH_2) 1.24-1.17 (m, 18H; CH, CH_2) 1.07 (m, 24H, CH_2) 0.85 (d, 3J (H,H) = 6.1 Hz, 18H; CH_3) 0.80 (d, 3J (H,H) = 6.7 Hz, 36H; CH_3);

$^{13}\text{C-NMR}$ (125 MHz, $\text{C}_2\text{D}_2\text{Cl}_4$): 142.3, 140.3, 139.9, 138.1, 137.2, 132.3, 128.9, 126.9, 125.2, 39.6, 39.2, 37.4, 33.3, 32.8, 28.2, 24.9, 23.1, 23.0, 19.9 ;

m.p.: 217 °C

MS (FD, 8 kV): m/z (%) = 1833.2 (100) [M^+] (calcd for $\text{C}_{138}\text{H}_{174}$ = 1832.89)

6.3.17 Hexa(4-(3,7-dimethyloctanyl)biphenyl)benzene (60)



Prepared as described above for compound **59**. Off-white solid, yield: 74%.

¹H-NMR (500 MHz, CD₂Cl₂): δ = 7.24 (d, 3J (H,H) = 8.1 Hz, 12H; CH), 7.08 (d, 3J (H,H) = 8.4 Hz, 12H; CH), 7.03 (d, 3J (H,H) = 8.1 Hz, 12H; CH), 6.91 (d, 3J (H,H) = 8.2 Hz, 12H; CH), 2.48 (m, 12H; α -CH₂), 1.53-1.38 (m, 6H; CH), 1.31 (m, 12H; CH₂) 1.30-1.13 (m, 18H; CH, CH₂) 1.05 (m, 24H, CH₂) 0.81 (d, 3J (H,H) = 6.1 Hz, 18H; CH₃) 0.76 (d, 3J (H,H) = 6.5 Hz, 36H; CH₃);

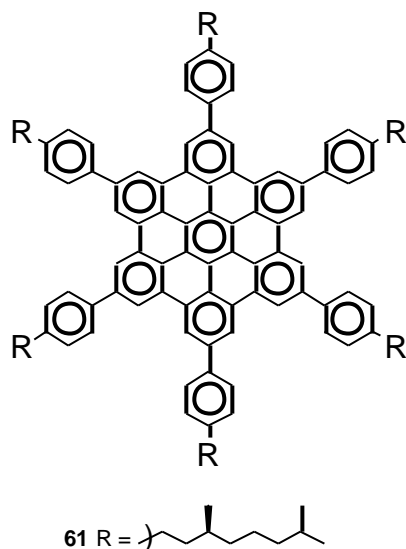
¹³C-NMR (125 MHz, CD₂Cl₂): 143.0, 141.1, 140.4, 138.5, 138.4, 132.7, 129.3, 127.2, 125.7, 40.1, 39.7, 37.9, 33.7, 33.3, 28.7, 25.4, 23.2, 23.1, 20.1 ;

m.p.: 214 °C

EA: anal. calcd. (%) for C₁₃₈H₁₇₄: C 90.43, H 9.57; found: C 90.48 H 9.59.

MS (FD, 8 kV): m/z (%) = 1834.2 (100) [M⁺] (calcd for C₁₃₈H₁₇₄ = 1832.89)

6.3.18 Hexa((S)-4-(3,7-dimethyloctanyl)phenyl)hexa-peri-hexabenzocoronene (**61**)



A 250 mL two necked round bottom flask was charged with 0.4 g (0.21 mmol) of hexa((S)-4-(3,7-dimethyloctanyl)biphenyl)benzene **59** and 60 mL of CH₂Cl₂. Using a glass capillary, a constant stream of argon was bubbled through the solution. Then, 0.7 g (4 mmol) of FeCl₃ dissolved in CH₃NO₂ (8 mL) was added dropwise using a syringe. After 45 min., the mixture was quenched with a large excess of methanol and the precipitate was filtered. The resulting yellow solid was redissolved in dichloromethane and filtered through a short pad of silica gel and dried under vacuum to yield 0.31 g **61** as a yellow solid. Yield: 80%.

¹H-NMR (500 MHz, *p*-C₆D₄Cl₂, 150 °C): δ = 8.27 (s, 12H; CH), 7.72 (d, ³J (H,H) = 6.1 Hz, 12H; CH), 7.47 (d, ³J (H,H) = 6.1 Hz, 12H; CH), 3.13 (m, 12H; α-CH₂), 2.20 (m, 6H; CH), 2.03 (m, 12H; β-CH₂), 1.90 (m, 12H; CH₂), 1.75 (m, 12H; CH₂), 1.66-1.60 (m, 18H; CH, CH₂), 1.45 (d, ³J (H,H) = 6.1 Hz, 18H; CH₃) 1.22 (d, ³J (H,H) = 5.5 Hz, 36H; CH₃);

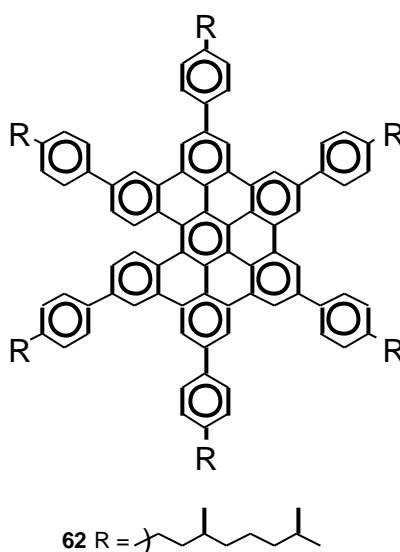
¹³C-NMR (125 MHz, *p*-C₆D₄Cl₂, 150 °C): δ = 136.8, 134.8, 127.9, 124.1, 1231, 117.9, 114.6, 113.4, 99.4 35.1, 34.7, 33.0, 29.0, 28.7, 23.5, 20.4, 17.9, 17.8, 15.3;

UV/Vis: λ nm (log ε) = 255 (5.23), 372 (5.16);

m.p.: > 300 °C

MS (FD, 8 kV): m/z (%) = 1819.5 (100) [M^+] (calcd for $C_{138}H_{162}$ = 1820.80)

6.3.19 Hexa(4-(3,7-dimethyloctanyl)phenyl)hexa-*peri*-hexabenzocoronene (**62**)



Prepared as described above for compound **61**. Yellow solid, yield: 79%.

1H -NMR (500 MHz, p - $C_6D_4Cl_2$, 180 °C): δ = 8.81 (s, 12H; CH), 8.01 (m, 12H; CH), 7.58 (m, 12H; CH), 3.13 (m, 12H; α - CH_2), 2.19 (m, 6H; CH), 2.00 (m, 12H; β - CH_2), 1.83-1.72 (m, 24H; CH_2), 1.39 (m, 18H; CH, CH_2), 1.39 (m, 18H; CH_3) 1.17 (m, 36H; CH_3);

^{13}C -NMR (125 MHz, p - $C_6D_4Cl_2$, 80 °C): δ = 142.7, 140.6, 137.7, 133.2, 129.1, 126.1, 123.6, 120.7, 119.4, 40.8, 38.7, 34.8, 34.3, 31.5, 29.2, 26.2, 23.9, 23.8, 21.0;

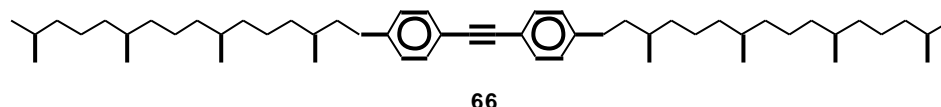
UV/Vis: λ nm ($\log \epsilon$) = 254 (5.05), 374 (4.69);

m.p.: > 300 °C

MS (FD, 8 kV): m/z (%) = 1821.3 (100) [M^+] (calcd for $C_{138}H_{162}$ = 1820.80)

HRMS (MALDI-TOF): m/z (%) = 1820.3064 (100) [M^+] (calcd for $C_{138}H_{162}$ = 1820.80)

6.3.20 4,4'-Bis(3,7,11,15-tetramethylhexadecenyl)diphenylacetylene (**66**)



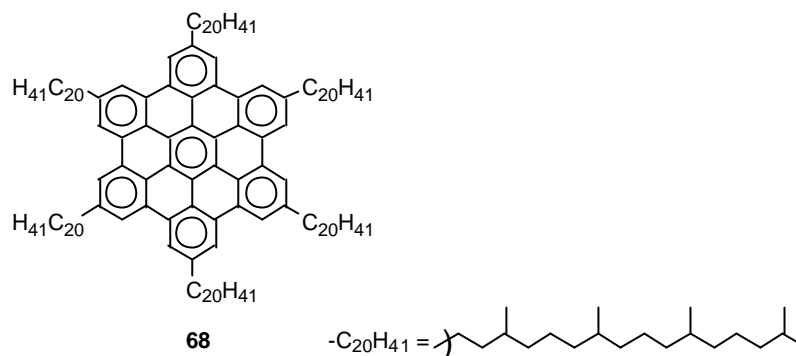
In a 250 mL two-necked round bottom flask, 60 mL of a 1M solution of 3,7,11,15-tetramethylhexadecenyl-1-magnesiumbromide (prepared immediately prior to use from 1-bromo-3,7,11,15-tetramethylhexadecane and magnesium) was added dropwise to a solution of 5 g (14.9 mmol) 4,4'-dibromodiphenylacetylene (**21**) dissolved in 150 mL of dry THF and 1 g of $[PdCl_2(dppf)]$ catalyst. The resulting mixture was stirred under reflux in an inert atmosphere overnight. The reaction was quenched with methanol and the solvent removed under reduced pressure. Purification using column chromatography on silica gel with petrol ether as the eluent afforded 5.5 g **66** as a colorless oil. Yield: 50%.

1H -NMR (500 MHz, $C_2D_2Cl_4$, 80 °C): δ = 7.4 (d, 3J (H,H) = 8.5 Hz, 4H; CH_2), 7.14 (d, 3J (H,H) = 8.5 Hz, 4H; CH_2), 2.61 (m, 4H; α - CH_2), 1.63 (m, 2H; CH), 1.52 (m, 2H; CH), 1.45 (m, 4H; 2xCH), 1.26 (m, 24H; 6x CH_2), 1.15 (m, 8H; 2x CH_2), 1.09 (m, 8H; 2x CH_2), 0.92 (m, 6H; CH_3) 0.78 (m, 24H; 4x CH_3);

^{13}C -NMR (125 MHz, $C_2D_2Cl_4$): δ = 144.0, 131.9, 128.8, 120.8, 89.4, 39.7, 39.0, 38.9, 37.8, 37.7, 37.6, 33.8, 33.1, 33.0, 32.8, 28.3, 25.1, 24.82, 24.80, 24.7, 23.1, 23.0, 20.14, 20.11, 20.08, 20.00, 19.9;

MS (FD, 8 kV): m/z (%) = 738.9 (100) [M^+] (calcd for $C_{54}H_{90}$ = 739.29)

6.3.22 Hexa-(3,7,11,15-tetramethylhexadecanyl)hexa-*peri*-hexabenzocoronene (**68**)



A 250 mL two necked round bottom flask was charged with 0.5 g (0.23 mmol) of hexakis(4-(3,7,11,15-tetramethylhexadecenyl)phen-1-yl)benzene (**67**) and 80 mL of CH_2Cl_2 . Using a glass capillary, a constant stream of argon was bubbled through the solution. Then 0.7 g (4.3 mmol) of $FeCl_3$ dissolved in 8 mL CH_3NO_2 was added dropwise using a syringe. After 30 min. the mixture was quenched with methanol and the precipitate was filtered. The resulting yellow solid was reprecipitated from THF and methanol and dried under vacuum to yield 0.41g (81%) of **68**.

1H -NMR (500 MHz, $C_2D_2Cl_4$, 120 °C): δ = 8.92 (s, 12H; CH), 3.28 (m, 12H; α - CH_2), 2.12 (m, 6H; CH), 1.96 (m, 6H; CH), 1.81 (m, 6H; CH), 1.60 (m, 6H; CH), 1.55-1.47 (m, 24H; CH_2), 1.30-1.26 (m, 60H; CH_2), 1.19 (d, 3J (H,H) = 6.1 Hz, 18H; CH_3), 1.15-1.07 (m, 36H; CH_2), 0.92 (d, 3J (H,H) = 6.1 Hz, 18H; CH_3), 0.85 (m, 54H; CH_3);

^{13}C -NMR (75 MHz, $C_2D_2Cl_4$, 80 °C): δ = 140.7, 130.1, 123.5, 121.6, 119.7, 40.0, 39.7, 38.00, 37.9, 37.79, 37.77, 37.69, 37.62, 35.0, 33.5, 28.1, 25.0, 24.8, 22.9, 22.8, 20.22, 20.17, 20.13, 20.02, 19.97;

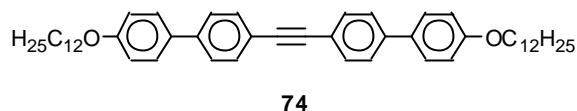
m.p.: 231 °C

MS (FD, 8 kV): m/z (%) = 2206.7 (100) [M^+] (calcd for $C_{162}H_{258}$ = 2205.83)

EA: calcd. (%) for $C_{162}H_{258}$: C 88.21, H 11.79; found: C 88.56 H 11.91.

DSC: $K \rightarrow \text{CoI}_{\text{ho}}$ $T = -36 \text{ }^\circ\text{C}$, $\Delta H = 13.5 \text{ kJ/mol}$

6.3.23 4,4'-Bis(4-*n*-dodecyloxyphen-1-yl)diphenylacetylene (**74**)



In a 250 mL round bottom flask, 15 mL of a 1M solution of 4-dodecyloxyphenylmagnesiumiodide was added dropwise to 0.5 g (1.5 mmol) 4,4'-dibromotoluene (**21**) dissolved in 75 mL of dry THF. 100 mg of [PdCl₂(dppf)] catalyst was added to this solution. The resulting mixture was stirred under reflux in an inert atmosphere for 16 h. While cooling to room temperature, a white solid precipitated. The solid was then filtered and washed several times with petrol ether and methanol to yield 0.81 g (78%) of **74**.

¹H-NMR (500 MHz, *p*-C₆D₄Cl₂, 160 °C): $\delta = 7.68$ (d, 3J (H,H) = 8.2 Hz, 4H; CH), 7.59 (m, 8H; CH), 7.06 (d, 3J (H,H) = 8.5 Hz, 4H; CH), 4.11 (m, 4H; α -CH₂), 1.92 (m, 4H; β -CH₂), 1.63 (m, 4H; CH₂), 1.55-1.35 (m, 32 H; CH₂), 1.03 (t, 3J (H,H) = 6.1 Hz, 6H; CH₃);

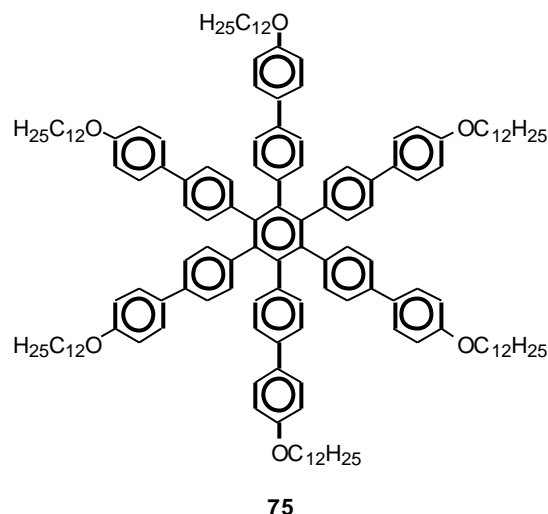
¹³C-NMR (125 MHz, C₂D₂Cl₄): $\delta = 159.6, 141.0, 133.1, 132.2, 128.2, 126.7, 122.1, 115.8, 90.4, 68.9, 32.0, 29.8, 29.7, 29.69, 29.63, 29.5, 29.4, 29.3, 26.3, 22.7, 14.0$;

m.p.: 240 °C

EA: calcd. (%) for C₅₀H₆₆O₂: C 85.91, H 9.52; found: C 85.56 H 9.43.

MS (FD, 8 kV): m/z (%) = 700.7 (100) [M^+] (calcd for C₅₀H₆₆O₂ = 699.07)

6.3.24 Hexa(4-*n*-dodecyloxybiphenyl)benzene (**75**)



In a 50 mL round bottom flask equipped with a reflux condenser, a suspension of 0.4 g (0.57 mmol) di(4-*n*-dodecyloxybiphenyl)acetylene (**74**) and 20 mL of dioxane was degassed several times; 39 mg (0.12 mmol) $[\text{Co}_2(\text{CO})_8]$ was then added and the resulting mixture was heated to reflux. After 3 h additional 20 mg (0.06 mmol) $[\text{Co}_2(\text{CO})_8]$ was added and reflux was maintained for 2 h. The solvent was evaporated under vacuum, and the crude product was purified using column chromatography on silica with petrol ether/ CH_2Cl_2 (7/3) as the eluent, yielding 0.3 g (75%) of **75** as an off-white solid.

$^1\text{H-NMR}$ (500 MHz, $\text{C}_2\text{D}_2\text{Cl}_4$, 110 °C): δ = 7.31 (d, 3J (H,H) = 8.6 Hz, 12H; CH), 7.09 (d, 3J (H,H) = 7.9 Hz, 12H; CH), 6.94 (d, 3J (H,H) = 8.5 Hz, 12H; CH), 6.82 (d, 3J (H,H) = 8.6 Hz, 12H; CH), 3.93 (m, 12H; $\alpha\text{-CH}_2$), 1.74 (m, 12H; $\beta\text{-CH}_2$), 1.43 (m, 12H; CH_2), 1.40-1.20 (m, 96H; CH_2), 0.89 (t, 3J (H,H) = 6.7 Hz, 18H; CH_3);

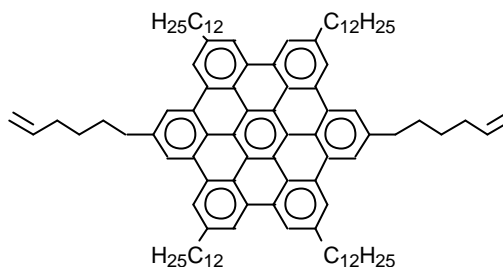
$^{13}\text{C-NMR}$ (125 MHz, $\text{C}_2\text{D}_2\text{Cl}_4$): δ = 159.0, 140.6, 139.7, 137.7, 133.9, 132.2, 128.0, 124.9, 115.4, 68.9, 32.0, 29.7, 29.69, 29.68, 29.66, 29.64, 29.61, 29.4, 26.2, 22.7, 14.0;

m.p.: 134 °C

EA: calcd. (%) for $\text{C}_{150}\text{H}_{198}$: C 85.91, H 9.52; found: C 85.97 H 9.67.

MS (FD, 8 kV): m/z (%) = 2097.2 (100) [M^+] (calcd for $C_{150}H_{198}O_6 = 2097.21$)

6.3.25 2,11-Di-(hex-5-enyl)-5,8,14,17-tetradodecyl-hexa-*peri*-hexabenzocoronene (**80**)



In a 250 mL Schlenk flask, 15 mL of a 1M solution of hex-1-enyl-6-magnesiumbromide was added dropwise to 1 g (0.75 mmol) 2,11-di-bromo-5,8,14,17-tetradodecyl-hexa-*peri*-hexabenzocoronene **9**) dissolved in 100 mL of dry THF. 200 mg of $[PdCl_2(dppf)]$ catalyst was added to this solution. The resulting mixture was stirred under reflux in an inert atmosphere for 16 h. While cooling to room temperature, a yellow solid precipitated. The solid was then filtered and washed several times with petrol ether and methanol followed by reprecipitation from THF to yield 0.87 g (75%) of **80**.

1H -NMR (500 MHz, $CDCl_3$): δ = 8.35 (s, 4H; CH), 8.33 (s, 4H; CH), 8.32 (s, 4H; CH), 5.98 (m, 2H; CH), 5.17 (d, 3J (H,H) = 17.7 Hz, 2H; CH_2), 5.08 (d, 3J (H,H) = 9.8 Hz, 2H; CH_2) 3.01 (m, 8H; α - CH_2 (dodecyl)), 2.32 (m, 4H; α - CH_2 (hexenyl)), 1.99 (m, 8H; β - CH_2 (dodecyl)), 1.74 (m, 4H; β - CH_2 (hexenyl)), 1.66 (m, 8H, CH_2), 1.47-1.32 (m, 74 H; CH_2), 0.91 (t, 3J (H,H) = 6.4 Hz, 12H; CH_3);

^{13}C -NMR (125 MHz, $C_2D_2Cl_4$): δ = 139.8, 139.5, 138.9, 129.6, 123.1, 121.0, 119.4, 114.6, 99.0, 37.3, 37.0, 34.0, 32.5, 32.0, 31.8, 31.1, 30.0, 29.93, 29.87, 29.79, 29.5, 29.2, 22.7, 14.1;

UV/Vis: λ nm ($\log \epsilon$) = 228 (5.30), 358 (5.23);

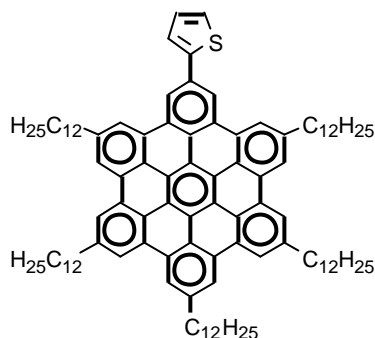
m.p.: > 300 °C

EA: anal. calcd. (%) for C₁₀₂H₁₃₄: C 90.07, H 9.93; found: C 90.41 H 10.17.

MS (FD, 8 kV): m/z (%) = 1359.1 (100) [M⁺] (calcd for C₁₀₂H₁₃₄ = 1360.18)

DSC: K→Col_{h0} T = 121 °C, ΔH = 91 kJ/mol

6.3.26 2-(Thien-2-yl)-5,8,14,11,17-pentadodecyl-hexa-*peri*-hexabenzocoronene (83)



A 250 mL two-necked round bottom flask was charged with 0.20 g (0.14 mmol) 2-bromo-5,8,11,14,17-pentadodecyl-hexa-*peri*-hexabenzocoronene (**7**) dissolved in 100 mL of dry THF and 10 mg of [PdCl₂(dppf)] catalyst was added. Then 1 mL of a 1M solution of thienyl-2-magnesiumbromide was added dropwise to this solution. The resulting mixture was stirred under reflux in an inert atmosphere for 16 h. While cooling to room temperature, a yellow solid precipitated. The solid was then filtered and washed several times with petrol ether and methanol followed by re-precipitation from THF to yield 0.13 g (65%) of **83**.

¹H-NMR (500 MHz, C₂D₂Cl₄, 100 °C): δ = 8.69 (s, 2H; CH), 8.48 (s, 2H; CH), 8.46 (s, 2H; CH), 8.39 (s, 2H; CH), 8.36 (s, 4H; CH), 7.66 (m, 1H; CH_{thiophene}), 7.55 (m, 1H; CH_{thiophene}), 7.37 (m, 1H; CH_{thiophene}), 3.11 (m, 10H; α-CH₂), 2.09 (m, 10H; β-CH₂), 1.70 (m, 10H, CH₂), 1.62 (m, 10H, CH₂), 1.52-1.33 (m, 70 H; CH₂), 0.91 (m, 15H; CH₃);

6 Experimental Section

$^{13}\text{C-NMR}$ (125 MHz, $\text{C}_2\text{D}_2\text{Cl}_4$, 130 °C): $\delta = 140.3, 131.6, 130.3, 130.1, 129.9, 129.6, 128.4, 125.2, 123.9, 123.3, 121.7, 121.5, 119.6, 118.9, 37.4, 37.3, 32.1, 31.9, 30.2, 30.0, 29.9, 29.8, 29.5, 29.2, 22.7, 14.0$;

UV/Vis: λ nm ($\log \epsilon$) = 226 (6.12), 362 (6.11);

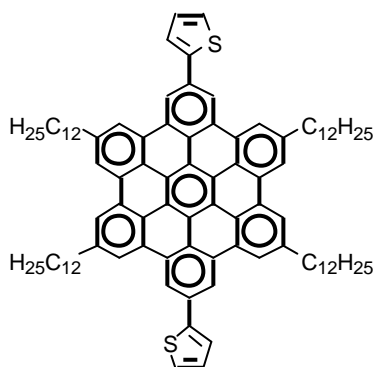
m.p.: > 300 °C

EA: anal. calcd. (%) for $\text{C}_{106}\text{H}_{140}\text{S}$: C 88.03, H 9.76, S 2.22; found: C 87.67 H 9.97.

MS (FD, 8 kV): m/z (%) = 1446.1 (100) [M^+] (calcd for $\text{C}_{106}\text{H}_{140}\text{S} = 1446.33$)

DSC: $\text{K} \rightarrow \text{Co}$ $h_{0,1}$ $T = 92$ °C, $\Delta H = 64.1$ kJ/mol

6.3.27 2,11-Di-(thien-2-yl)-5,8,14,17-tetradodecyl-hexa-*peri*-hexabenzocoronene (84)



A 250 mL two-necked round bottom flask was charged with 0.25 g (0.19 mmol) 2,11-di-bromo-5,8,14,17-tetradodecyl-hexa-*peri*-hexabenzocoronene (**9**) dissolved in 100 mL of dry THF and 30 mg of $[\text{PdCl}_2(\text{dppf})]$ catalyst was added. Then 3.7 mL of a 1M solution of thienyl-2-magnesiumbromide was added dropwise to this solution. The resulting mixture was stirred under reflux in an inert atmosphere for 16 h. While cooling to room temperature, a yellow solid precipitated. The solid was then filtered and washed several times with petrol ether and methanol followed by re-precipitation from THF to yield 0.17 g (68%) of **84**.

6 Experimental Section

¹H-NMR (500 MHz, C₂D₂Cl₄, 100 °C): δ = 8.65 (s, 4H; CH), 8.29 (s, 4H; CH), 8.23 (s, 4H; CH), 7.62 (d, ³J (H,H) = 3.4 Hz, 2H; CH_{thiophene}), 7.54 (d, ³J (H,H) = 4.9 Hz, 2H; CH_{thiophene}), 7.35 (m, 2H; CH_{thiophene}), 3.03 (m, 8H; α-CH₂), 2.00 (m, 8H; β-CH₂), 1.67 (m, 8H, CH₂), , 1.57 (m, 8H, CH₂), 1.49-1.26 (m, 56 H; CH₂), 0.94 (t, ³J (H,H) = 6.4 Hz, 12H; CH₃);

¹³C-NMR (125 MHz, C₂D₂Cl₄, 130 °C): δ = 139.9, 131.4, 130.0, 129.4, 129.2, 128.4, 125.1, 123.8, 122.8, 121.4, 121.2, 119.1, 118.7, 37.3, 32.1, 31.8, 30.3, 30.1, 30.0, 29.9, 29.8, 29.5, 28.7, 22.7, 14.0;

UV/Vis: λ nm (log ε) = 230 (5.10), 363 (5.13);

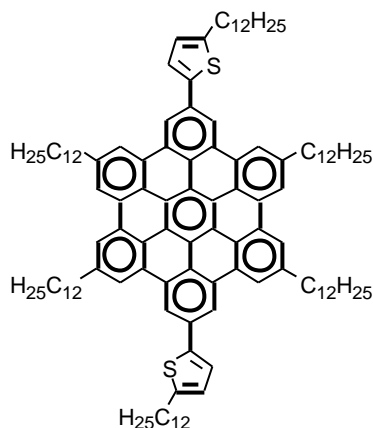
m.p.: > 300 °C

EA: anal. calcd. (%) for C₉₈H₁₁₈S₂: C 86.54, H 8.74, S 4.71; found: C 86.97 H 8.99.

MS (FD, 8 kV): m/z (%) = 1359.6 (100) [M⁺] (calcd for C₉₈H₁₁₈S₂ = 1360.13)

DSC: K→Col_{ho,1} T = 71 °C, ΔH = 14.9 kJ/mol, Col_{ho,1}→Col_{ho,2} T = 175 °C, ΔH = 23.4 kJ/mol

6.3.28 2-Di-(5-dodecyl-thien-2-yl)-5,8,14,17-tetradodecyl-hexa-*peri*-hexabenzocoronene (**85**)



A 250 mL two-necked round bottom flask was charged with 0.20 g (0.19 mmol) 2,11-di-bromo-5,8,14,17-tetradodecyl-hexa-*peri*-hexabenzocoronene (**9**) dissolved in 100 mL of dry THF and 30 mg of [PdCl₂(dppf)] catalyst was added. Then 2 mL of a 1M solution of 5-dodecyl-thienyl-2-magnesiumbromide was added dropwise to this solution. The resulting mixture was stirred under reflux in an inert atmosphere for 16 h. While cooling to room temperature, a yellow solid precipitated. The solid was then filtered and washed several times with petrol ether and methanol followed by re-precipitation from THF to yield 0.21 g (67%) of **85**.

¹H-NMR (500 MHz, C₂D₂Cl₄, 100 °C): δ = 8.46 (s, 4H; CH), 8.14 (s, 4H; CH), 8.11 (s, 4H; CH), 7.45 (d, ³J (H,H) = 3.1 Hz, 2H; CH_{thiophene}), 7.04 (d, ³J (H,H) = 3.1 Hz, 2H; CH_{thiophene}), 3.12 (m, 4H; α-CH₂(thiophene-dodecyl)), 3.04 (m, 8H; α-CH₂(HBC-dodecyl)), 2.05 (m, 12H; CH₂), 1.70-1.58 (m, 24H; CH₂), 1.53-1.33 (m, 84 H; CH₂), 0.91 (m, 18H; CH₃);

¹³C-NMR (125 MHz, C₂D₂Cl₄, 130 °C): δ = 146.0, 143.4, 139.4, 131.4, 129.5, 129.0, 128.9, 125.4, 123.4, 123.3, 122.4, 121.1, 120.9, 118.6, 118.4, 118.1, 37.4, 32.3, 32.21, 32.19, 31.0, 30.6, 30.3, 30.23, 30.15, 30.09, 30.04, 30.0, 29.93, 29.9, 29.7, 29.6, 22.9, 14.3;

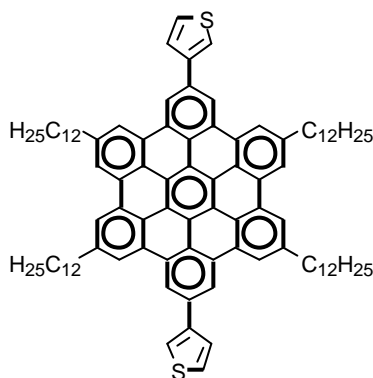
m.p.: > 300 °C

EA: anal. calcd. (%) for C₁₀₆H₁₄₀S: C 86.36, H 9.86, S 3.78; found: C 85.91 H 9.97.

MS (FD, 8 kV): m/z (%) = 1695.7 (100) [M⁺] (calcd for C₁₂₂H₁₆₆S₂ = 1696.78)

DSC: K→Col_{h0,1} T = 107 °C, ΔH = 134.3 kJ/mol

6.3.29 2,11-Di-(thien-3-yl)-5,8,14,17-tetradodecyl-hexa-*peri*-hexabenzocoronene (86)



A 100 mL two-necked round bottom flask was charged with 0.1 g (0.074 mmol) 2,11-di-bromo-5,8,14,17-tetradodecyl-hexa-*peri*-hexabenzocoronene (**9**) in 25 mL of toluene. After the mixture was degassed and purged with argon several times 1.3 g of K₂CO₃, dissolved in 5 mL EtOH/H₂O [1:1], 40 mg (0.16 mmol) of 3-thienylboronic acid, and 10 mg of [Pd(PPh₃)₄] catalyst were added. The resulting mixture was stirred at 80 °C in an inert atmosphere for 16 h. While cooling to room temperature, a yellow solid precipitated. The solid was then filtered and washed several times with petrol ether and methanol followed by reprecipitation from toluene to yield 75 mg (75%) of crude **86**.

¹H-NMR (500 MHz, C₂D₂Cl₄, 130 °C): δ = 8.68 (s, 4H; CH), 8.34 (s, 4H; CH), 8.30 (s, 4H; CH), 7.81 (m, 2H; CH_{thiophene}), 7.79 (m, 2H; CH_{thiophene}), 7.67 (m, 2H; CH_{thiophene}), 3.07 (m, 8H; α-CH₂), 2.05 (m, 8H; β-CH₂), 1.65 (m, 16H, CH₂), 1.47-1.30 (m, 56 H; CH₂), 0.91 (m, 12H; CH₃);

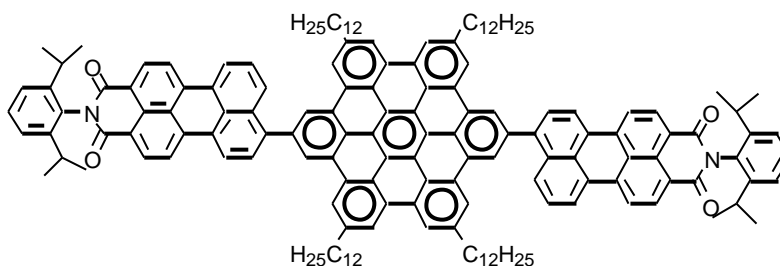
$^{13}\text{C-NMR}$ (125 MHz, $\text{C}_2\text{D}_2\text{Cl}_4$, 130 °C): δ = 139.8, 131.5, 129.9, 129.4, 129.3, 128.2, 125.0, 123.9, 122.8, 121.4, 121.3, 119.5, 118.9, 37.0, 32.1, 31.9, 30.2, 30.1, 30.05, 29.9, 29.7, 29.5, 28.6, 22.7, 13.9;

UV/Vis: λ nm ($\log \epsilon$) = 221 (4.83), 363 (4.46);

m.p.: > 300 °C

MS (FD, 8 kV): m/z (%) = 1359.5 (100) [M^+] (calcd for $\text{C}_{98}\text{H}_{118}\text{S}_2$ = 1360.13)

6.3.30 2,11-Di[*N*-(2,6-diisopropylphenyl)-perylene-9-yl-3,4-dicarboxiimide]-5,8,14,17-tetradodecyl-hexa-*peri*-hexabenzocoronene (**88**)



A 500 mL two-necked round bottom flask was charged with 0.25 g (0.185 mmol) 2,11-di-bromo-5,8,14,17-tetradodecyl-hexa-*peri*-hexabenzocoronene (**9**) and 250 mL of toluene. Then 0.6 g (0.98 mmol) peryleneboronicester, 3.5 g (25 mmol) potassium carbonate (dissolved in 25 mL ethanol/water (1:1)), and 100 mg $\text{Pd}(\text{PPh}_3)_4$ were added sequentially. The resultant mixture was heated at 80 °C under argon for 16 h. After cooling to room temperature the reaction mixture was dried under vacuum and the crude product was purified using column chromatography on silica with dichloromethane as the eluent, yielding 0.28 g (70%) of **88** as a red solid.

$^1\text{H-NMR}$ (500 MHz, $\text{C}_2\text{D}_2\text{Cl}_4$, 100 °C): δ = 9.20 (s, 4H; CH_{HBC}), 8.86 (m, 8H; CH_{HBC}), 8.69 (d, 3J (H,H) = 7.3 Hz, 2H; $\text{CH}_{\text{perylene}}$), 8.67 (d, 3J (H,H) = 4.9 Hz, 2H; $\text{CH}_{\text{perylene}}$), 8.65 (d, 3J (H,H) = 4.3 Hz, 2H; $\text{CH}_{\text{perylene}}$), 8.57 (d, 3J (H,H) = 8.6 Hz, 2H; $\text{CH}_{\text{perylene}}$), 8.47 (d, 3J (H,H) = 3.7 Hz, 2H; $\text{CH}_{\text{perylene}}$), 8.46 (d, 3J (H,H) =

6 Experimental Section

4.9 Hz, 2H; CH_{perylene}), 8.28 (d, 3J (H,H) = 8.6 Hz, 2H; CH_{perylene}), 8.07 (d, 3J (H,H) = 7.9 Hz, 2H; CH_{perylene}), 7.57 (m, 2H; CH_{perylene}), 7.47 (t, 3J (H,H) = 7.9 Hz, 2H; CH_{isopropylphenyl}), 7.34 (d, 3J (H,H) = 7.93 Hz, 4H; CH_{isopropylphenyl}), 3.19 (m, 8H; α -CH₂), 2.85 (m, 4H; CH_{isopropyl}), 2.04 (m, 8H; β -CH₂), 1.61 (m, 8H, CH₂), 1.48 (m, 8H; CH₂), 1.37 (m, 8H; CH₂), 1.31-1.22 (m, 72H; CH₂, CH₃, isopropyl), 0.84 (t, 3J (H,H) = 7.0 Hz, 12H; CH₃);

¹³C-NMR (125 MHz, C₂D₂Cl₄, 80 °C): δ = 164.04, 146.16, 144.08, 141.46, 137.86, 137.79, 137.68, 133.42, 131.76, 130.84, 130.72, 130.32, 130.08, 129.91, 129.22, 128.90, 127.64, 127.29, 124.96, 123.82, 123.77, 121.61, 120.60, 120.17, 37.42, 32.31, 32.07, 30.11, 30.00, 29.94, 29.89, 29.83, 29.51, 29.47, 24.31, 22.80, 12.22;

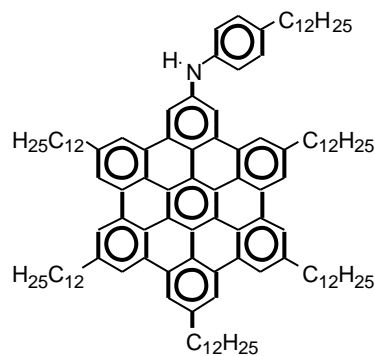
UV/Vis: λ nm (log ϵ) = 242 (5.29), 263 (4.98), 346 (4.89), 363 (5.20), 390 (4.74), 498 (4.96), 527 (5.02);

m.p.: > 300 °C

EA: calcd. (%) for C₁₅₈H₁₆₄ N₂O₄: C 88.06, H 7.67, N 1.30, O 2.97; found: C 88.74 H 7.93, N 1.45.

MS (FD, 8 kV): m/z (%) = 2155.1 (100) [M⁺] (calcd for C₁₅₈H₁₆₄N₂O₄ = 2155.05)

6.3.31 2-((4-Dodecylphenyl)amino)-5,8,11,14,17-pentadodecylhexa-*peri*-hexabenzocoronene (96)



A 100 mL flame dried and argon purged Schlenk flask was charged with 0.20 g (0.14 mmol) 2-bromo-5,8,14,11,17-pentadodecyl-hexa-*peri*-hexabenzocoronene

6 Experimental Section

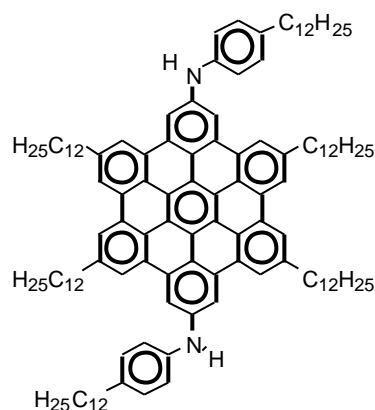
7 and 50 mL of dry toluene. Then 17.4 mg (0.028 mmol) of *rac*-2,2'-bis(diphenylphosphino)-1,1'-binaphthyl (BINAP), 25.6 mg (0.028 mmol) of tris(dibenzylideneacetone)-dipalladium(0) (Pd₂(dba)₃), and 0.92 g (3.5 mmol) of 4-dodecylphenylamine were added. After the resulting mixture was degassed several times, 0.34 g (3.5 mmol) of sodium-tert.-butanolate was added to this solution. The resulting mixture was stirred at 80 °C in an inert atmosphere for 16 h. After cooling to room temperature the reaction mixture was carefully poured into 300 mL of methanol. A yellow solid precipitated, which was then filtered and washed several times with petrol ether and methanol followed by reprecipitation from THF to yield 0.2 g (88%) of **96**.

¹H-NMR (500 MHz, C₂D₂Cl₄, 100 °C): δ = 8.47 (s, 2H; CH), 8.45 (s, 2H; CH), 8.38 (s, 2H; CH), 8.33 (s, 2H; CH), 8.11 (s, 2H; CH), 8.07 (s, 2H; CH), 7.28 (s, 4H; CH_{amino-phenyl}), 5.81 (s, 1H; NH), 3.01 (m, 6H; CH₂), 2.96 (m, 4H; CH₂), 2.73 (m, 2H; CH₂), 2.05 (m, 6H; CH₂), 1.94 (m, 4H; CH₂), 1.78 (m, 2H; CH₂), 1.60-1.33 (m, 108 H; CH₂), 0.94 (m, 18H; CH₃);

¹³C-NMR (125 MHz, C₂D₂Cl₄, 80 °C): δ = 141.9, 141.2, 140.1, 139.9, 135.9, 131.0, 129.8, 129.6, 129.2, 123.4, 123.3, 123.2, 121.3, 120.2, 119.5, 119.4, 119.0, 118.8, 117.9, 111.3, 37.5, 37.2, 35.7, 32.4, 32.2, 32.1, 31.9, 30.4, 30.3, 30.2, 30.1, 30.06, 29.97, 29.9, 29.6, 22.9, 14.3;

m.p.: > 300 °C

MS (FD, 8 kV): m/z (%) = 1623.0 (100) [M⁺] (calcd for C₁₂₀H₁₆₇N = 1623.65)

6.3.32 2,11-Di-((4-dodecylphenyl)amino)-5,8,14,17-tetradodecyl-hexa-*peri*-hexabenzocoronene (97)

A 100 mL flame dried and argon purged Schlenk flask was charged with 0.25 g (0.19 mmol) 2,11-di-bromo-5,8,14,17-tetradodecyl-hexa-*peri*-hexabenzocoronene **9** and 50 mL of dry toluene. Then, 17.4 mg (0.028 mmol) of *rac*-2,2'-bis(diphenylphosphino)-1,1'-binaphthyl (BINAP), 25.6 mg (0.028 mmol) of tris(dibenzylideneacetone)-dipalladium(0) (Pd₂(dba)₃), and 1.84 g (7 mmol) of 4-dodecylphenylamine were added. After the resulting mixture was degassed several times, 0.7 g (7 mmol) of sodium-*tert*.-butanolate was added to this solution. The resulting mixture was stirred at 80 °C in an inert atmosphere for 16 h. After cooling to room temperature the reaction mixture was carefully poured into 300 mL of methanol. A yellow solid precipitated, which was then filtered and washed several times with petrol ether and methanol followed by reprecipitation from THF to yield 0.3 g (89%) of **97**.

¹H-NMR (500 MHz, THF 30 °C): δ = 8.89 (s, 4H; CH), 8.80 (s, 4H; CH), 8.75 (s, 4H; CH), 7.79 (s, 2H; NH), 7.43 (d, ³*J* (H,H) = 8.5 Hz, 4H; CH_{amino-phenyl}), 7.26 (d, ³*J* (H,H) = 7.9 Hz, 4H; CH_{amino-phenyl}), 3.17 (m, 12H; CH₂), 2.69 (m, 12H; CH₂), 2.01 (m, 12H, CH₂), 1.59 (m, 12H, CH₂), 1.51-1.29 (m, 84 H; CH₂), 0.88 (m, 18H; CH₃);

¹³C-NMR (125 MHz, C₂D₂Cl₄, 130 °C): δ = 141.8, 140.1, 136.2, 132.9, 132.8, 132.3, 131.2, 129.6, 129.1, 129.0, 123.5, 121.5, 118.9, 118.5, 111.31, 37.24,

37.16, 35.68, 32.10, 31.94, 31.80, 30.16, 30.07, 30.03, 29.98, 29.93, 29.89, 29.85, 29.79, 29.70, 29.60, 29.51, 22.81, 22.69, 14.18, 14.09;

UV/Vis: λ nm ($\log \epsilon$) = 228 (5.44), 374 (5.22);

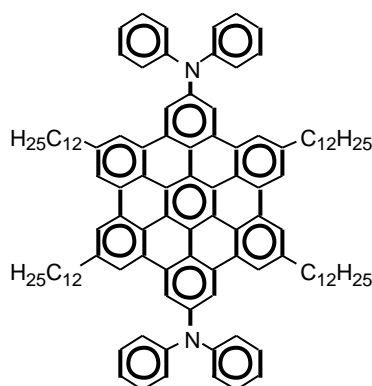
m.p.: > 300 °C

EA: anal. calcd. (%) for C₁₂₆H₁₇₂N₂: C 88.26, H 10.11, N 1.63; found: C 88.01 H 9.99.

MS (FD, 8 kV): m/z (%) = 1715.7 (100) [M⁺] (calcd for C₁₂₆H₁₇₂N₂ = 1714.76)

DSC: K→Col_{h0,1} T = 118 °C, ΔH = 24.0 kJ/mol

6.3.33 2,11-Di-(diphenylamino)-5,8,14,17-tetradodecyl-hexa-*peri*-hexabenzocoronene (99)



A 100 mL flame dried and argon purged Schlenk flask was charged with 0.2 g (0.15 mmol) 2,11-di-bromo-5,8,14,17-tetradodecyl-hexa-*peri*-hexabenzocoronene **9** and 50 mL of dry toluene. Then 17.4 mg (0.028 mmol) of *rac*-2,2'-bis(diphenylphosphino)-1,1'-binaphthyl (BINAP), 25.6 mg (0.028 mmol) of tris(dibenzylideneacetone)-dipalladium(0) (Pd₂(dba)₃), and 0.625 g (3.7 mmol) of diphenylamine were added. After the resulting mixture was degassed several times, 0.7 g (7 mmol) of sodium-tert.-butanolate was added to this solution. The resulting mixture was stirred at 80 °C in an inert atmosphere for 16 h. After cooling to room temperature the reaction mixture was carefully poured into 300 mL of methanol. A yellow solid precipitated, which was then filtered and washed

several times with petrol ether and methanol followed by reprecipitation from THF to yield 0.2 g (85%) of **99**.

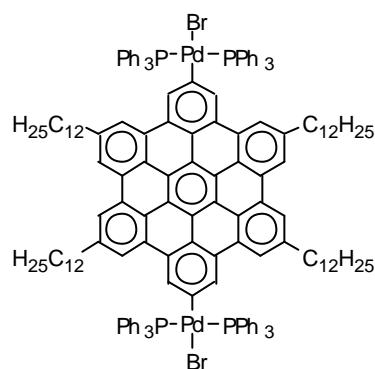
¹H-NMR (500 MHz, C₂D₂Cl₄ 100 °C): δ = 8.91 (s, 4H; CH), 8.88 (s, 4H; CH), 8.61 (s, 4H; CH), 7.42 (m, 16H; CH_{amino-phenyl}), 7.16 (m, 4H; CH_{amino-phenyl}), 3.14 (m, 8H; CH₂), 1.95 (m, 8H; CH₂), 1.55 (m, 8H; CH₂), 1.41-1.27 (m, 64 H; CH₂), 0.86 (m, 12H; CH₃);

¹³C-NMR (125 MHz, C₂D₂Cl₄, 130 °C): δ = 148.5, 146.8, 141.3, 132.1, 130.7, 130.4, 129.7, 125.0, 124.3, 123.6, 122.4, 122.3, 122.1, 120.4, 120.3, 117.9, 37.1, 32.0, 31.7, 29.9, 29.8, 29.7, 29.4, 22.7, 14.0;

m.p.: > 300 °C

MS (FD, 8 kV): m/z (%) = 1530.2 (100) [M⁺] (calcd for C₁₁₄H₁₃₂N₂ = 1530.31)

6.3.34 2,11-Di-[*trans*-Pd(PPh₃)₂-Br]-5,8,14,17-tetradodecyl-hexa-*peri*-hexabenzocoronene (**102**)



A 100 mL flame dried and argon purged Schlenk-flask was charged with 0.1 g (0.074 mmol) 2,11-di-bromo-5,8,14,17-tetradodecyl-hexa-*peri*-hexabenzocoronene (**9**) dissolved in 25 mL of dry toluene. This mixture was degassed and purged with argon three times. Then 0.18 g (0.16 mmol, 2.1 eq.) of tetrakis-(triphenyl-phosphine)-palladium(0) [(Pd(PPh₃)₄)] were added to this solution. The resulting mixture was stirred at 80 °C in an inert atmosphere for 48 h. After cooling to room temperature, the volume of the reaction mixture was

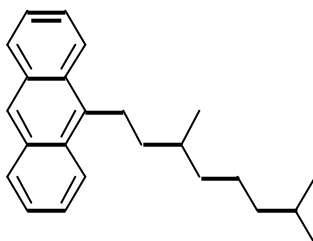
reduced by 70%, followed by adding 60 mL of dry hexane to the flask. A yellow solid precipitated, which was then filtered and washed with hexane under an argon stream several times. Drying under vacuum afforded 96 mg (50%) of **102**.

¹H-NMR (500 MHz, CD₂Cl₂): δ = 8.79 (s, 4H; CH), 8.29 (s, 4H; CH), 8.04 (s, 4H; CH), 7.53 (m, 36H; CH_{PPh₃}), 6.99 (d, ³J (H,H) = 5 Hz, 24H; CH_{PPh₃}), 3.03 (m, 8H; α-CH₂), 1.86 (m, 8H; β-CH₂), 1.46 (m, 8H, CH₂), 1.35-1.16 (m, 64 H; CH₂), 0.76 (t, ³J (H,H) = 6.4 Hz, 12H; CH₃);

³¹P-NMR (202 MHz, CD₂Cl₂): δ = 22.91;

MS (FD, 8 kV): m/z (%) = 1195.8 (100) [M⁺ - 2x [Pd(PPh₃)₂-Br]] (calcd for C₁₆₂H₁₇₂Br₂P₄Pd₂ = 2615.69)

6.3.35 9-(3,7-Dimethyloctanyl)anthracene (**104**)



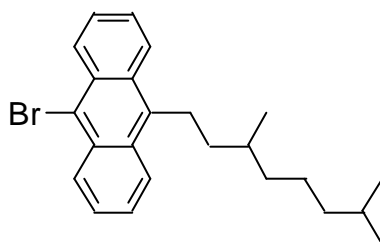
In a 250 mL two-necked round bottom flask, 78 mL of a 1M solution of 3,7-dimethyloctanyl-1-magnesiumbromide (prepared immediately prior to use from 1-bromo-3,7-dimethyloctane and magnesium) was added dropwise to 10 g (39 mmol) 9-bromoanthracene (**103**) dissolved in 150 mL of dry THF. Then, 1.4 g (5 mol%) of [PdCl₂(dppf)] catalyst was added to this solution. The resulting mixture was stirred under reflux in an inert atmosphere overnight. The reaction was quenched with methanol and the solvent removed under reduced pressure. Purification using column chromatography on silica gel with petrol ether as the eluent afforded a mixture of the desired product and anthracene. Recrystallisation from hot heptane afforded 6.2 g **104** as a yellow solid. Yield: 50%.

¹H-NMR (500 MHz, C₂D₂Cl₄): δ = 8.26 (s, 1H; CH), 8.19 (d, ³J (H,H) = 9.2 Hz, 2H; CH), 7.94 (d, ³J (H,H) = 7.9 Hz, 2H; CH), 7.47 (t, ³J (H,H) = 7.3 Hz, 2H; CH), 7.41 (t, ³J (H,H) = 7.3 Hz, 2H; CH) 3.59-3.44 (m, 2H; α-CH₂), 1.73 (m, 2H; β-CH₂), 1.55 (m, 1 H; CH), 1.48 (m, 2H; CH₂), 1.43 (m, 2H; CH₂), 1.34-1.26 (m, 3H; CH, CH₂), 1.09 (d, ³J (H,H) = 6.1 Hz, 3H; CH₃) 0.85 (d, ³J (H,H) = 6.1 Hz, 6H; CH₃);

¹³C-NMR (125 MHz, C₂D₂Cl₄): δ = 136.0, 129.7, 129.5, 128.1, 126.2, 125.2, 124.1, 120.9, 38.7, 37.6, 36.3, 33.1, 27.4, 25.3, 24.1, 22.1, 22.0, 19.1;

MS (FD, 8 kV): m/z (%) = 318.1 (100) [M⁺] (calcd for C₂₄H₃₀ = 318.5)

6.3.36 9-Bromo-10-(3,7-dimethyloctanyl)anthracene (105)



A 250 mL round bottom flask was charged with 3.51 g (11 mmol) of 9-(3,7-dimethyloctanyl)anthracene (**104**) and dissolved in 75 mL of carbondisulfide. Then 1,77 g (0.57 mL, 11.1 mmol) bromine dissolved in 10 mL of carbondisulfide were added dropwise to this solution. After stirring the reaction mixture for 30 min the solvent was evaporated under reduced pressure. The remaining crude product was purified using column chromatography on silica gel with petrol ether as the eluent to yield 3.9 g (90%) of **105** as a yellow solid.

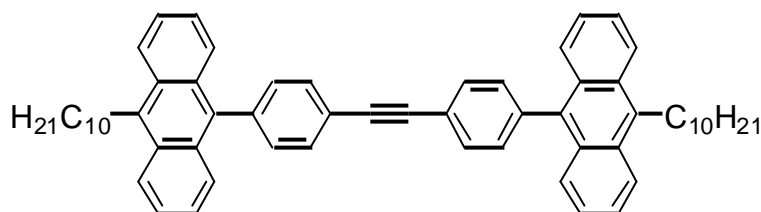
¹H-NMR (500 MHz, C₂D₂Cl₄): δ = 8.56 (d, ³J (H,H) = 9.2 Hz, 2H; CH), 8.22 (d, ³J (H,H) = 8.5 Hz, 2H; CH), 7.57 (t, ³J (H,H) = 7.3 Hz, 2H; CH), 7.52 (t, ³J (H,H) = 7.0 Hz, 2H; CH) 3.51-3.42 (m, 2H; α-CH₂), 1.76 (m, 2H; β-CH₂), 1.57 (m, 1 H;

CH), 1.47 (m, 2H; CH₂), 1.39 (m, 2H; CH₂), 1.33-1.22 (m, 3H; CH, CH₂), 1.13 (d, ³J (H,H) = 6.2 Hz, 3H; CH₃) 0.92 (d, ³J (H,H) = 6.2 Hz, 6H; CH₃);

¹³C-NMR (125 MHz, C₂D₂Cl₄): δ = 135.9, 129.6, 129.4, 127.9, 126.1, 125.1, 124.0, 120.8, 38.7, 37.6, 36.3, 33.1, 27.4, 25.3, 24.1, 22.1, 22.0, 19.1;

MS (FD, 8 kV): m/z (%) = 397.1 (100) [M⁺] (calcd for C₂₄H₂₉Br = 397.39)

6.3.37 4,4'-Bis(10-(3,7-dimethyloctanyl)anthracen-9-yl)diphenylacetylene (107)



A 250 mL two-necked round bottom flask was charged with 2.9 g (7.3 mmol) 9-bromo-10-(3,7-dimethyloctanyl)anthracene (**105**) and 125 mL of toluene. Then 0.65 g (2.45 mmol) 4,4'-diphenylacetylenediboronic acid (**106**), 1.7 g (12 mmol) potassium carbonate (dissolved in 12 mL ethanol/water (1:1)), and 150 mg Pd(PPh₃)₄ were added sequentially. The resultant mixture was heated at 80 °C under argon for 16 h. After cooling to room temperature the reaction mixture was dried under vacuum and the crude product was purified using column chromatography on silica with petrol ether/CH₂Cl₂ as the eluent, yielding 0.79 g (40%) of **107** as a yellow solid.

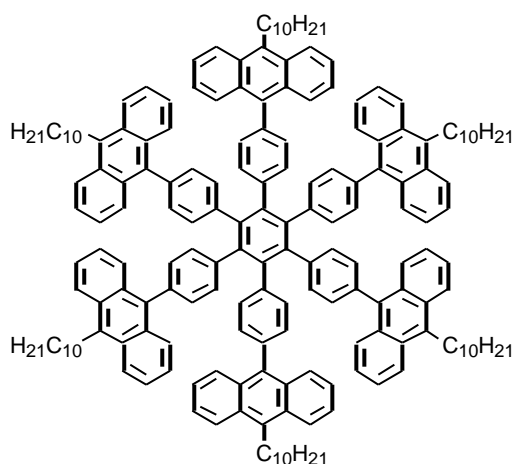
¹H-NMR (500 MHz, C₂D₂Cl₄): δ = 8.28 (d, ³J (H,H) = 9.2 Hz, 4H; CH), 7.79 (d, ³J (H,H) = 7.9 Hz, 4H; CH), 7.65 (d, ³J (H,H) = 9.2 Hz, 4H; CH), 7.49 (t, ³J (H,H) = 7.3 Hz, 4H; CH), 7.42 (d, ³J (H,H) = 7.9 Hz, 4H; CH), 7.34 (t, ³J (H,H) = 7.6 Hz, 4H; CH) 3.69-3.54 (m, 4H; α-CH₂), 1.79 (m, 4H; β-CH₂), 1.66 (m, 2H; CH), 1.50 (m, 4H; CH₂), 1.39 (m, 4H; CH₂), 1.33-1.26 (m, 6H; CH, CH₂), 1.14 (d, ³J (H,H) = 6.1 Hz, 6H; CH₃) 0.87 (d, ³J (H,H) = 6.1 Hz, 12H; CH₃);

$^{13}\text{C-NMR}$ (125 MHz, $\text{C}_2\text{D}_2\text{Cl}_4$): δ = 139.9, 136.3, 135.1, 133.9, 131.9, 130.2, 129.2, 127.8, 125.6, 125.3, 124.7, 122.4, 90.2, 39.6, 38.7, 37.4, 34.1, 28.3, 26.2, 25.1, 23.1, 23.0, 20.1;

UV/Vis: λ nm ($\log \epsilon$) = 235 (4.88), 274 (5.93), 373 (4.56), 390 (4.81), 411 (4.80);

MS (FD, 8 kV): m/z (%) = 810.7 (100) [M^+] (calcd for $\text{C}_{62}\text{H}_{66}$ = 811.19)

6.3.38 Hexakis(4-(10-(3,7-dimethyloctanyl)anthracen-9-yl)phen-1-yl)benzene (**108**)



In a 100 mL three-necked round bottom flask equipped with a reflux condenser 0.5 g (0.62 mmol) 4,4'-bis(10-(3,7-dimethyloctanyl)anthracen-9-yl)diphenylacetylene (**107**) dissolved in 25 mL of dioxane were added under argon to a degassed solution of 60 mg (0.18 mmol) $[\text{Co}_2(\text{CO})_8]$ in 25 mL of dioxane. After refluxing for 5 h, the solvent was evaporated under vacuum, and the residue was purified using column chromatography on silica gel with petrol ether/ CH_2Cl_2 (7/3) as the eluent, yielding 0.1 g **108** as colorless oil. Yield: 20%.

$^1\text{H-NMR}$ (500 MHz, $\text{C}_2\text{D}_2\text{Cl}_4$): δ = 8.19 (d, 3J (H,H) = 9.2 Hz, 12H; CH), 7.55 (d, 3J (H,H) = 7.9 Hz, 12H; CH), 7.52 (d, 3J (H,H) = 8.9 Hz, 12H; CH), 7.30 (d, 3J (H,H) = 7.9 Hz, 12H; CH), 7.15 (t, 3J (H,H) = 7.3 Hz, 12H; CH), 6.60 (t, 3J (H,H) = 7.5 Hz, 12H; CH) 3.69-3.62 (m, 12H; α - CH_2), 1.92 (m, 12H; β - CH_2), 1.80 (m, 6H; CH), 1.61-1.54 (m, 12H; CH_2), 1.36 (m, 12H; CH_2), 1.28-1.20 (m, 18H; CH,

6 Experimental Section

CH₂), 1.17 (d, ³J (H,H) = 6.1 Hz, 18H; CH₃) 0.93 (d, ³J (H,H) = 6.1 Hz, 36H; CH₃);

¹³C-NMR (125 MHz, C₂D₂Cl₄): δ = 139.9, 136.3, 135.1, 133.9, 131.9, 130.2, 129.2, 127.8, 125.6, 125.3, 124.7, 122.4, 121.2, 39.6, 38.7, 37.4, 34.1, 28.3, 26.2, 25.1, 23.1, 23.0, 20.1;

UV/Vis: λ nm (log ε) = 239 (5.50), 274 (5.82), 369 (4.93), 389 (5.15), 409 (5.10);

MS (FD, 8 kV): m/z (%) = 2433.6 (100) [M⁺] (calcd for C₁₈₆H₁₉₈ = 2433.56)

7 Literature

- [1] E. Becquerel, *Comptes Rendues* **1839**, 6, 561.
- [2] D. M. Chapin, C. S. Fuller, G. L. Pearson, *J. Appl. Phys.* **1954**, 25, 676.
- [3] J. Bardeen, W. H. Brattain, W. Shockley, *J. Chem. Phys.* **1946**, 14, 714.
- [4] W. H. Brattain, W. Shockley, *Physical Review* **1947**, 72, 345.
- [5] W. Shockley, J. Bardeen, W. H. Brattain, *Science* **1948**, 108, 678.
- [6] M. J. Cohen, J. S. Harris, *IEEE Trans. Electron Devices* **1978**, 25, 1355.
- [7] M. J. Cohen, J. S. Harris, *Appl. Phys. Lett.* **1978**, 33, 812.
- [8] M. J. Cohen, *Journal of the Electrochemical Society* **1980**, 127, C83.
- [9] H. Koezuka, A. Tsumura, *Synthetic Metals* **1989**, 28, C753.
- [10] J. Paloheimo, E. Punkka, P. Kuivalainen, H. Stubb, P. Ylilahti, *Acta Polytech. Scand.-Electr. Eng. Ser.* **1989**, 178.
- [11] F. Reinitzer, *Monatsh. Chem.* **1888**, 9, 421.
- [12] S. Chandrasekhar, B. K. Sadashiva, K. A. Suresh, *Pramana* **1977**, 7, 471.
- [13] S. Chandrasekhar, S. K. Prasad, *Contemop. Phys.* **1999**, 40, 237.
- [14] A. N. Cammidge, R. J. Busby,, (Eds.: D. Demus, J. W. Goodby, G. W. Gray, H. W. Spiess, V. Vill), Wiley-VCH, Weinheim, **1998**.
- [15] C. F. van Nostrum, A. W. Bosman, G. H. Gelinck, P. G. Schouten, J. M. Warman, A. P. M. Kentgens, M. A. C. Devillers, A. Meijerink, S. J. Picken, U. Sohling, A.-J. Schouten, R. J. M. Nolte, *Chem. Eur. J.* **1995**, 1, 171.
- [16] C. W. Struijk, A. B. Sieval, J. E. J. Dakhorst, M. van Dijk, P. Kimkes, R. B. M. Koehorst, H. Donker, T. J. Schaafsma, S. J. Picken, A. M. van de Craats, J. M. Warman, H. Zuilhof, E. J. R. Sudholter, *J. Am. Chem. Soc.* **2000**, 122, 11057.
- [17] G. R. J. Müller, C. Meiners, V. Enkelmann, Y. Geerts, K. Müllen, *J. Mater. Chem.* **1998**, 8, 61.
- [18] A. M. van de Craats, J. M. Warman, P. Schlichting, U. Rohr, Y. Geerts, K. Müllen, *Synth. Met.* **1999**, 102, 1550.
- [19] H. Eichhorn, *J. Porphyr. Phthalocya.* **2000**, 4, 88.

- [20] C. S. Frampton, D. D. MacNicol, S. J. Rowan, *J. Mol. Struct.* **1997**, *405*, 169.
- [21] P. Henderson, H. Ringsdorf, P. Schuhmacher, *Liq. Cryst.* **1995**, *18*, 191.
- [22] O. C. Musgrave, C. J. Webster, *J. Chem. Soc. (C)* **1971**, 1397.
- [23] T. Yatabe, M. Harbison, J. D. Brand, M. Wagner, K. Müllen, P. Samori, J. P. Rabe, *J. Mater. Chem.* **2000**, *10*, 1519.
- [24] H. Bock, W. Helfrich, *Liq. Cryst.* **1995**, *18*, 387.
- [25] P. Uznanski, S. Marguet, D. Markovitsi, P. Schumacher, H. Ringsdorf, *Mol. Cryst. Liq. Cryst.* **1997**, *293*, 123.
- [26] A. Stabel, P. Herwig, K. Müllen, J. P. Rabe, *Angew. Chem.* **1995**, *107*, 1768.
- [27] P. Herwig, C. W. Kayser, K. Müllen, H. W. Spiess, *Adv. Mater.* **1996**, *8*, 510.
- [28] S. Ito, M. Wehmeier, J. D. Brand, C. Kubel, R. Epsch, J. P. Rabe, K. Müllen, *Chem.-Eur. J.* **2000**, *6*, 4327.
- [29] S. Ito, P. T. Herwig, T. Böhme, J. P. Rabe, W. Rettig, K. Müllen, *J. Am. Chem. Soc.* **2000**, *122*, 7698.
- [30] A. M. van de Craats, J. M. Warman, A. Fechtenkötter, J. D. Brand, M. A. Harbison, K. Müllen, *Adv. Mater.* **1999**, *11*, 1469.
- [31] P. T. Herwig, V. Enkelmann, O. Schmelz, K. Müllen, *Chem. Eur. J.* **2000**, *6*, 1834.
- [32] A. F. Thünemann, D. Ruppelt, S. Ito, K. Müllen, *J. Mater. Chem.* **1999**, *9*, 1055.
- [33] A. F. Thünemann, D. Ruppelt, C. Burger, K. Müllen, *J. Mater. Chem.* **2000**, *10*, 1325.
- [34] S. P. Brown, I. Schnell, J. D. Brand, K. Müllen, H. W. Spiess, *J. Am. Chem. Soc.* **1999**, *121*, 6712.
- [35] A. M. van de Craats, J. M. Warman, K. Müllen, Y. Geerts, J. D. Brand, *Adv. Mater.* **1998**, *10*, 36.
- [36] F. Dötz, J. D. Brand, S. Ito, L. Gherghel, K. Müllen, *J. Am. Chem. Soc.* **2000**, *122*, 7707.
- [37] A. Fechtenkötter, N. Tchebotareva, M. D. Watson, K. Müllen, *Tetrahedron* **2001**, *57*, 3769.

- [38] M. Zander, *Polycyclische Aromaten*, Teubner, Stuttgart, **1995**.
- [39] A. M. van de Craats, J. M. Warman, M. P. de Haas, D. Adam, J. Simmerer, D. Haarer, P. Schuhmacher, *Adv. Mater.* **1996**, *8*, 823.
- [40] A. M. van de Craats, M. P. de Haas, J. M. Warman, *Synth. Met.* **1997**, *86*, 2125.
- [41] A. M. van de Craats, L. D. A. Siebbeles, I. Bleyl, D. Haarer, Y. A. Berlin, A. A. Zharikov, J. M. Warman, *J. Phys. Chem. B* **1998**, *102*, 9625.
- [42] A. Brown, F. Wilkinson, *J. Chem. Soc. Farad. T.* **1979**, *75*.
- [43] D. Markovitsi, A. Germain, P. Millie, P. Lecuyer, L. K. Gallos, P. Argyrakis, H. Bengs, H. Ringsdorf, *J. Phys. Chem.* **1995**, *99*, 1005.
- [44] D. Adam, F. Closs, T. Frey, D. Funhoff, D. Haarer, H. Ringsdorf, P. Schuhmacher, K. Siemensmeyer, *Phys. Rev. Lett.* **1993**, *70*, 457.
- [45] D. Adam, P. Schuhmacher, J. Simmerer, L. Häussling, K. Siemensmeyer, K. H. Etzbach, H. Ringsdorf, D. Haarer, *Nature* **1994**, *371*, 141.
- [46] J. Simmerer, B. Glüsen, W. Paulus, A. Kettner, P. Schuhmacher, D. Adam, K. H. Etzbach, K. Siemensmeyer, J. H. Wendorff, H. Ringsdorf, D. Haarer, *Adv. Mater.* **1996**, *8*, 815.
- [47] N. Boden, R. J. Bushby, J. Clements, B. Movaghar, K. J. Donovan, T. Kreouzis, *Phys. Rev. B* **1995**, *52*, 13247.
- [48] N. Boden, R. J. Bushby, A. N. Cammidge, J. Clements, R. Luo, *Mol. Cryst. Liq. Cryst.* **1995**, *261*, 251.
- [49] S. Kumar, P. Schuhmacher, P. Henderson, J. Rego, H. Ringsdorf, *Mol. Cryst. Liq. Cryst.* **1996**, *288*, 211.
- [50] A. Vaes, M. Van der Auweraer, F. C. De Schryver, B. Laguitton, A. Jonas, P. Henderson, H. Ringsdorf, *Langmuir* **1998**, *14*, 5250.
- [51] D. M. Walba, F. Stevens, N. A. Clark, D. C. Parks, *Acc. Chem. Res.* **1996**, *29*, 591.
- [52] F. Charra, J. Cousty, *Phys. Rev. Lett.* **1998**, *80*, 1682.
- [53] S. Ikeda, Y. Takanishi, K. Ishikawa, H. Takezoe, *Mol. Cryst. Liq. Cryst.* **1999**, *329*, 589.
- [54] W. Kreuder, H. Ringsdorf, P. Tschirner, *Macromol. Chem., Rapid Commun.* **1985**, *6*, 367.

- [55] G. Wenz, *Macromol. Chem., Rapid Commun.* **1985**, *6*, 577.
- [56] N. Boden, R. J. Bushby, P. S. Martin, S. D. Evans, R. W. Owens, D. A. Smith, *Langmuir* **1999**, *15*, 3790.
- [57] W. Kranig, B. Hüser, H. W. Spiess, W. Kreuder, H. Ringsdorf, H. Zimmermann, *Adv. Mater.* **1990**, *2*, 36.
- [58] Bachmann, Clarke, *J. Am. Chem. Soc.* **1927**, *49*, 2093.
- [59] C. Destrade, M. C. Mondon, J. Malthete, *J. Phys. Colloq.* **1979**, *C3*, 17.
- [60] N. Boden, R. C. Borner, R. J. Bushby, A. N. Cammidge, M. V. Jesudason, *Liq. Cryst.* **1993**, *15*, 851.
- [61] S. Kumar, S. K. Varshney, *Liq. Cryst.* **1999**, *26*, 1841.
- [62] H. G. Franck, J. W. Stadelhofer, *Industrielle Aromatenchemie*, Springer-Verlag, Heidelberg, **1987**.
- [63] E. Clar, *The Aromatic Sextet*, John Wiley and Sons, London, **1972**.
- [64] Halleux, e. al., *Helv. Chim. Acta.* **1958**, *41*, 1177.
- [65] J. M. Robertson, J. Trotter, *J. Chem. Soc.* **1961**, 1280.
- [66] E. Clar, C. T. Ironside, M. Zander, **1959**, 142.
- [67] E. Clar, J. F. Stephen, *Tetrahedron* **1965**, *21*, 467.
- [68] P. Kovacic, C. Wu, *J. Polym. Sci.* **1960**, *47*, 45.
- [69] P. Kovacic, A. Kyriakis, *Tetrahedron Lett.* **1962**, 467.
- [70] P. Kovacic, R. M. Lange, *J. Org. Chem.* **1963**, *28*, 968.
- [71] P. Kovacic, A. Kyriakis, *J. Am. Chem. Soc.* **1963**, *85*, 454.
- [72] J. D. Brand, Johannes Gutenberg Universität (Mainz), **1999**.
- [73] F. Dötz, Johannes Gutenberg Universität (Mainz), **2000**.
- [74] W. Hendel, Z. H. Khan, W. Schmidt, *Tetrahedron* **1986**, *42*, 1127.
- [75] S. U. Vallerien, M. Werth, F. Kremer, H. W. Spiess, *Liquid Crystals* **1990**, *8*, 889.
- [76] M. Werth, S. U. Vallerien, H. W. Spiess, *Liquid Crystals* **1991**, *10*, 759.
- [77] C. Göltner, D. Pressner, K. Müllen, H. W. Spiess, *Angew. Chem.-Int. Ed. Engl.* **1993**, *32*, 1660.
- [78] D. Goldfarb, Z. Luz, H. Zimmermann, *Journal De Physique* **1981**, *42*, 1303.
- [79] D. Goldfarb, Z. Luz, H. Zimmermann, *J. Chem. Phys.* **1983**, *78*, 7065.

- [80] S. P. Brown, I. Schnell, J. D. Brand, K. Müllen, H. W. Spiess, *Phys. Chem. Chem. Phys.* **2000**, *2*, 1735.
- [81] S. P. Brown, I. Schnell, J. D. Brand, K. Müllen, H. W. Spiess, *J. Mol. Struct.* **2000**, *521*, 179.
- [82] R. Goddard, M. Haenel, W. C. Herndon, C. Krüger, M. Zander, *J. Am. Chem. Soc.* **1995**, *117*, 30.
- [83] C. Ochsenfeld, *Phys. Chem. Chem. Phys.* **2000**, *2*, 2153.
- [84] C. Ochsenfeld, S. P. Brown, I. Schnell, J. Gauss, H. W. Spiess, *J. Am. Chem. Soc.* **2000**, *submitted*.
- [85] S. Marguet, D. Markovitsi, Millié, H. Sigal, S. Kumar, *J. Phys. Chem. B* **1998**, *102*, 4697.
- [86] Z. Bao, A. J. Lovinger, A. Dodabalapur, *Adv. Mater.* **1997**, *9*, 42.
- [87] K. Petritsch, R. H. Friend, A. Lux, G. Rozenberg, S. C. Moratti, A. B. Holmes, *Synthetic Metals* **1999**, *102*, 1776.
- [88] N. Boden, R. J. Bushby, J. Clements, B. Movaghar, *J. Mater. Chem.* **1999**, *9*, 2081.
- [89] P. G. Schouten, J. F. van der Pol, J. W. Zwikker, W. Drenth, S. J. Picken, *Mol. Cryst. Liq. Cryst.* **1991**, *195*, 291.
- [90] P. G. Schouten, J. H. Warman, M. P. de Haas, C. F. van Nostrum, G. G. Gelinck, R. J. M. Nolte, M. J. Copyn, J. W. Zwikker, M. K. Engel, M. Hanack, Y. H. Chang, W. T. Ford, *J. Am. Chem. Soc.* **1994**, *116*, 6880.
- [91] L. C. Giancarlo, G. W. Flynn, *Annu. Rev. Phys. Chem.* **1998**, *49*.
- [92] L. C. Giancarlo, G. W. Flynn, *Acc. Chem. Res.* **2000**, *33*, 491.
- [93] K. Müllen, J. P. Rabe, in *Annals of the New York Academy of Sciences Macromolecular and Supramolecular Architectures for Molecular Electronics, Vol. 852* (Eds.: A. Aviram, M. Ratner), **1998**, pp. 205.
- [94] V. S. Iyer, K. Yoshimura, V. Enkelmann, R. Epsch, J. P. Rabe, K. Müllen, *Angew. Chem. Int. Ed.* **1998**, *37*, 2696.
- [95] T. Schmitz-Hübsch, F. Sellam, R. Staub, M. Törker, T. Fritz, C. Kübel, K. Müllen, K. Leo, *Surf. Sci.* **2000**, *445*, 358.
- [96] M. Müller, J. Petersen, R. Strohmeier, C. Günther, N. Karl, K. Müllen, *Angew. Chem. Int. Ed.* **1996**, *35*, 886.
- [97] M. Müller, C. Kübel, K. Müllen, *Chem. Eur. J.* **1998**, *4*, 2099.

- [98] N. K. Zimmermann, *Surf. Sci.* **1992**, 268, 296.
- [99] N. Reitzel, T. Hassenkamp, K. Balashev, T. R. Jensen, P. B. Howes, K. Kjaer, A. Fechtenkötter, S. Ito, K. Müllen, T. Bjornholm, *Chem.-Eur. J.* **2001**, *accepted*.
- [100] R. G. Harvey, *Polycyclic Aromatic Hydrocarbons*, Wiley-VCH, New York, **1997**.
- [101] A. J. Berresheim, M. Müller, K. Müllen, *Chem. Rev.* **1999**, 99, 1747.
- [102] V. S. Iyer, M. Wehmeier, J. D. Brand, M. A. Keegstra, K. Müllen, *Angew. Chem.* **1997**, 109, 1675.
- [103] L. Przybilla, J. D. Brand, K. Yoshimura, H. J. Rader, K. Mullen, *Anal. Chem.* **2000**, 72, 4591.
- [104] A. Fechtenkötter, K. Saalwächter, M. A. Harbison, K. Müllen, H. W. Spiess, *Angew. Chem. Int. Ed.* **1999**, 38, 3039.
- [105] L. Schmidt-Mende, A. Fechtenkötter, K. Müllen, E. Moons, R. H. Friend, J. D. MacKenzie, *in preparation* **2001**.
- [106] P. Samorí, A. Fechtenkötter, T. Böhme, F. Jäckel, K. Müllen, J. P. Rabe, *in preparation* **2001**.
- [107] *Organikum, Vol. 17th ed*, VEB Deutscher Verlag der Wissenschaften, Berlin, **1988**.
- [108] S. Taskahashi, Y. Kuroyama, K. Sonogashira, N. Hagihara, *Synthesis* **1980**, 627.
- [109] W. Broser, *Chem. Ber.* **1968**, 101, 69.
- [110] M. Baumgarten, T. Yüksel, *Phys. Chem. Chem. Phys.* **1999**, 1, 1699.
- [111] L. Truce, *J. Am. Chem. Soc.* **1951**, 73, 126.
- [112] T. Hayashi, M. Konishi, Y. Kobori, M. Kumada, T. Higuchi, K. Hirotsu, *J. Am. Chem. Soc.* **1984**, 106, 158.
- [113] J. I. G. Cadogan, P. W. Inward, *J. Chem. Soc.* **1962**, 4170.
- [114] H. J. Barber, R. Slack, *J. Chem. Soc.* **1944**, 612.
- [115] A. S. Shetty, J. Zhang, J. S. Moore, *J. Am. Chem. Soc.* **1996**, 118, 1019.
- [116] A. S. Shetty, P. R. Fischer, K. F. Storck, P. W. Bohn, J. S. Moore, *J. Am. Chem. Soc.* **1996**, 118, 9409.
- [117] K. K. Laali, M. Tanaka, R. H. Mitchell, D. K. Y. Lau, *J. Org. Chem.* **1998**, 63, 3059.

- [118] J. Billard, *Liq. Cryst.* **1998**, *24*, 99.
- [119] J. Kopitzke, J. H. Wendorff, *Chem. unserer Zeit* **2000**, *34*, 4.
- [120] K. Schmidt-Rohr, H. W. Spiess, *Multidimensional Solid-State NMR and Polymers*, Academic Press, New York, **1994**.
- [121] D. Demus, J. W. Goodby, G. W. Gray, H. W. Spiess, V. Vill, *Handbook of Liquid Crystals*, Wiley-VCH, Weinheim, **1998**.
- [122] K. Saalwächter, R. Graf, H. W. Spiess, *J. Magn. Reson.* **2000**, *in press*.
- [123] H. Geen, J. J. Titman, J. Gottwald, H. W. Spiess, *Chem. Phys. Lett.* **1994**, *227*, 79.
- [124] J. Gottwald, D. E. Demco, R. Graf, H. W. Spiess, *Chem. Phys. Lett.* **1995**, *243*, 314.
- [125] K. Saalwächter, R. Graf, D. E. Demco, H. W. Spiess, *J. Magn. Reson.* **1999**, *139*, 287.
- [126] C. Filip, S. Hafner, I. Schnell, D. E. Demco, H. W. Spiess, *J. Chem. Phys.* **1999**, *110*, 423.
- [127] M. Pope, *Electronic Processes in Organic Crystals*, Oxford, Clarendon, **1982**.
- [128] M. S. Dresselhaus, G. Dresselhaus, *Adv. Phys* **1981**, *31*, 139.
- [129] P. G. Schouten, J. M. Warman, G. H. Gelinck, M. J. Coppy, *J. Phys. Chem.* **1995**, *99*, 17780.
- [130] J. J. M. Halls, C. A. Walsh, N. C. Greenham, E. A. Marseglia, R. H. Friend, S. C. Moratti, A. B. Holmes, *Nature* **1995**, *376*, 498.
- [131] G. Yu, J. Gao, J. C. Hummelen, F. Wudl, A. Heeger, J., *Science* **1995**, *270*, 1789.
- [132] M. Granström, K. Petritsch, A. C. Arias, A. Lux, M. R. Andersson, R. H. Friend, *Nature* **1998**, *395*, 257.
- [133] C. W. Tang, *Appl. Phys. Lett.* **1986**, *48*, 183.
- [134] J. J. M. Halls, K. Pichler, R. H. Friend, S. C. Moratti, A. B. Holmes, *Appl. Phys. Lett.* **1996**, *68*, 3120.
- [135] L. Chen, D. Godovsky, O. Inganäs, J. C. Hummelen, R. Janssens, M. Svensson, M. Andersson, *Adv. Mater.* **2000**, *12*, 1367.
- [136] J. H. Schön, C. Kloc, B. Batlogg, *Appl. Phys. Lett* **2000**, *77*, 3776.

- [137] J. J. Dittmer, K. Petritsch, E. A. Marseglia, R. H. Friend, H. Rost, A. B. Holmes, *Synth. Met.* **1999**, *102*, 879.
- [138] J. J. Dittmer, R. Lazzaroni, P. Leclere, P. Moretti, M. Gangström, K. Petritsch, E. A. Marseglia, R. H. Friend, J. L. Bredas, H. Rost, A. B. Holmes, *Sol. Energy Mater. Sol. Cells* **2000**, *61*, 53.
- [139] J. Mizuguchi, *J. Appl. Phys.* **1998**, *84*, 4479.
- [140] D. Fichou, *J. Mater. Chem.* **2000**, *10*, 571.
- [141] N. Noma, T. Tsuzuki, Y. J. Shirota, *Adv. Mater.* **1995**, *7*, 647.
- [142] G. Horowitz, *Adv. Mater.* **1998**, *10*, 365.
- [143] G. Horowitz, *J. Mater. Chem.* **1999**, *9*, 2021.
- [144] H. E. Katz, Z. Bao, *J. Phys. Chem. B* **2000**, *104*, 671.
- [145] F. Schauer, I. Zhivkov, S. Nespurek, *J. Non-Cryst. Solids* **2000**, 266-269, 999.
- [146] W. Hu, Y. Liu, X. Y., S. Liu, S. Zhou, D. Zhun, *Synth. Met.* **1999**, *104*, 19.
- [147] W. Hu, Y. Liu, Y. Xu, S. Liu, S. Zhou, D. Zhun, B. Xu, C. Bai, C. Wang, *Thin Solid Films* **2000**, *360*, 256.
- [148] R. Madru, G. Guillaud, M. Alsadoun, M. Maitrot, J. J. Andre, J. Simon, R. Even, *Chem. Phys. Lett.* **1988**, *145*, 343.
- [149] C. Clarisse, M. T. Riou, *J. Appl. Phys.* **1991**, *69*, 3324.
- [150] Z. Bao, A. Dodabalapur, A. J. Lovinger, *Appl. Phys. Lett.* **1996**, *69*, 4108.
- [151] J. W. Goodby, *J. Mater. Chem.* **1991**, *1*, 307.
- [152] M. Strukelj, F. Papadimitrakopoulos, T. M. Miller, L. J. Rothberg, *Science* **1995**, *267*, 1969.
- [153] K. Praefcke, A. Eckert, D. Blunk, *Liq. Cryst.* **1997**, *22*, 113.
- [154] C. F. van Nostrum, *Mol. Cryst. Liq. Cryst.* **1997**, *302*, 303.
- [155] E. Clar, *Ber. Dtsch. Chem. Ges.* **1936**, *69*, 607.
- [156] A. Rodger, B. Norden, *Circular Dichroism & Linear Dichroism*, University Press, Oxford, **1997**.
- [157] M. M. Green, H. Ringsdorf, J. Wagner, R. Wüstefeld, *Angew. Chem.* **1990**, *102*, 1525.
- [158] A. M. Levelut, P. Oswald, A. Ghanem, *J. Physique* **1984**, *45*, 745.
- [159] E. Fontes, P. A. Heiney, W. H. de Jeu, *Phys. Rev. Lett.* **1988**, *61*, 1202.

- [160] R. Wu, J. S. Schumm, D. L. Pearson, J. T. Tour, *J. Org. Chem.* **1996**, *61*, 6906.
- [161] B. Orgasinska, A. Kocot, K. Merkel, R. Wrzalik, J. Ziolo, T. Perova, J. K. Vij, *J. Mol. Struct.* **1999**, *511-512*, 271.
- [162] D. M. Collard, C. P. Lillya, *J. Am. Chem. Soc.* **1989**, *111*, 1829.
- [163] H. Bengs, O. Karthaus, H. Ringsdorf, C. Baehr, M. Ebert, J. H. Wendorff, *Liq. Cryst.* **1991**, *10*, 161.
- [164] K. E. Treacher, G. J. Clarkson, N. B. McKeown, *Mol. Cryst. Liq. Cryst.* **1995**, *260*, 255.
- [165] P. Humberstone, G. J. Clarkson, N. B. McKeown, K. E. Treacher, *J. Mater. Chem.* **1996**, *6*, 315.
- [166] P. Gramatica, P. Manitto, G. Speranza, *Tetrahedron* **1987**, *43*, 4481.
- [167] E. E. Schweizer, W. S. Creasy, K. K. Light, E. T. Shaffer, *J. Org. Chem.* **1969**, *34*, 212.
- [168] I. Tabushi, K. Yamamura, Y. Okada, *J. Org. Chem.* **1987**, *52*, 2502.
- [169] H. Budig, R. Lunchwitz, R. Paschke, C. Tschierske, U. Nütz, S. Diele, G. Pelzl, *J. Mater. Chem.* **1996**, *6*, 1283.
- [170] D. M. Collard, C. P. Lillya, *J. Org. Chem.* **1991**, *56*, 6064.
- [171] A. T. Christensen, K. O. Stromme, *Acta Crystallogr.* **1969**, *B25*, 657.
- [172] G. R. Desiraju, R. Parthasarathy, *J. Am. Chem. Soc.* **1989**, *111*, 8725.
- [173] S. L. Price, A. J. Stone, J. Lucas, R. S. Rowland, A. E. Thornley, *J. Am. Chem. Soc.* **1994**, *116*, 4910.
- [174] J. D. Brand, C. Kübel, S. Ito, K. Müllen, *Chem. Mater.* **2000**, *12*, 1638.
- [175] K. Weiss, G. Beernink, F. Dötz, A. Birkner, K. Müllen, C. H. Wöll, *Angew. Chem. Int. Ed.* **1999**, *38*, 3748.
- [176] O. C. Musgrave, *Chem. Rev.* **1969**, *69*, 499.
- [177] J. A. Rego, S. Kumar, H. Ringsdorf, *Chem. Mater.* **1996**, *8*, 1402.
- [178] S. Andersson, *Synthesis* **1985**, 437.
- [179] M. V. Bhatt, S. U. Kulkarni, *Synthesis* **1983**, 249.
- [180] J.-M. Lehn, *Supramolecular Chemistry - Concepts and Perspectives*, VCH, Weinheim, **1995**.
- [181] A. Semenov, J. P. Spatz, M. Möller, J.-M. Lehn, B. Sell, D. Schubert, C. H. Weidl, D. S. Schubert, *Angew. Chem. Int. Ed.* **1999**, *38*, 2547.

- [182] S. Guo, L. Konopny, R. Popovitz-Biro, H. Cohen, H. Porteanu, E. Lifshitz, M. J. Lahav, *J. Am. Chem. Soc.* **1999**, *121*, 9589.
- [183] D. G. Kurth, P. Lehmann, M. Schütte, *Proc. Natl. Acad. Sci. USA* **2000**, *97*, 5704.
- [184] G. R. Desiraju, *Angew. Chem. Int. Ed.* **1995**, *34*, 2328.
- [185] G. Gottarelli, S. Masiero, E. Mezzina, S. Pieraccini, J. P. Rabe, P. Samorí, G. P. Spada, *Chem.-Eur. J.* **2000**, *6*, 3242.
- [186] J. H. K. Hirschberg, L. Brunsveld, A. Ramzi, A. J. M. Vekemans, R. P. Sijbesma, E. W. Meijer, *Nature* **2000**, *407*, 167.
- [187] H. Engelkamp, S. Middelbeek, R. J. M. Nolte, *Science* **1999**, *284*, 785.
- [188] J. P. Rabe, S. Buchholz, *Science* **1991**, *253*, 424.
- [189] D. M. Cyr, B. Venkataraman, G. W. Flynn, A. Black, G. M. Whitesides, *J. Phys. Chem.* **1996**, *100*, 13747.
- [190] C. L. Claypool, F. Faglioni, W. A. Goddard, H. B. Gray, N. S. Lewis, R. A. Marcus, *J. Phys. Chem. B* **1997**, *101*, 5978.
- [191] P. Samorí, V. Francke, K. Müllen, J. P. Rabe, *Chem.-Eur. J.* **1999**, *5*, 2312.
- [192] M. E. Stawasz, D. L. Sampson, B. A. Parkinson, *Langmuir* **2000**, 2326.
- [193] X. Qiu, C. Wang, Q. Zeng, B. Xu, S. Yin, H. Wang, S. Xu, C. Bai, *J. Am. Chem. Soc.* **2000**, *122*, 5550.
- [194] A. Gesquière, M. M. S. Abdel-Mottaleb, S. D. Feyter, F. C. D. Schryver, F. Schoonbeek, J. v. Esch, R. Kellogg, B. L. Feringa, A. Calderone, R. Lazzaroni, J. L. Brédas, *Langmuir* **2000**, *16*, 10385.
- [195] E. Clar, *Aromatische Kohlenwasserstoffe - Polycyclische Systeme*, Springer, Berlin, Göttingen, Heidelberg, **1952**.
- [196] F. Diederich, Y. Rubin, *Angew. Chem. Int. Ed.* **1992**, *31*, 1101.
- [197] R. Faust, *Angew. Chem. Int. Ed.* **1995**, *34*, 1429.
- [198] D. M. Hudgins, L. J. Allamandola, *J. Phys. Chem.* **1995**, *99*, 3033.
- [199] L. T. Scott, P.-C. Cheng, M. M. Hashemi, M. S. Bratcher, D. T. Meyer, H. B. Warren, *J. Am. Chem. Soc.* **1997**, *119*, 10963.
- [200] L. Tong, H. Lau, D. M. Ho, R. A. J. Pascal, *J. Am. Chem. Soc.* **1998**, *120*, 6000.

- [201] L. Askadskaya, C. Boeffel, J. P. Rabe, *Ber. Bunsen-Ges. Phys. Chem. Chem. Phys.* **1993**, *97*, 517.
- [202] J.-C. Gabriel, N. B. Larsen, M. Larsen, N. Harrit, J. S. Pedersen, K. Schaumburg, K. Bechgaard, *Langmuir* **1996**, *12*, 1690.
- [203] R. Lazzaroni, A. Calderone, J. L. Brédas, J. P. Rabe, *J. Chem. Phys.* **1997**, *107*, 99.
- [204] W. Mizutani, M. Shigeno, K. Kajimura, M. Ono, *Ultramicroscopy* **1992**, *42-44*, 236.
- [205] V. Balzani, A. Credi, F. M. Raymo, J. F. Stoddart, *Angew. Chem. Int. Ed.* **2000**, *39*, 3348.
- [206] S. K. Burley, G. A. Petsko, *Adv. Protein. Chem.* **1988**, *39*, 125.
- [207] C. A. Hunter, J. Singh, J. M. Thornton, *J. Mol. Biol.* **1991**, *218*, 837.
- [208] N. M. D. Brown, F. L. Swinton, *J. Chem. Soc., Chem. Commun.* **1974**, 770.
- [209] J. Hernández-Trujillo, M. Costas, A. Vela, *J. Chem. Soc., Faraday Trans.* **1993**, *89*, 2441.
- [210] R. B. Martin, *Chem. Rev.* **1996**, *96*, 3043.
- [211] W. J. Schutte, M. Sluyters-Rehbach, J. H. Sluyters, *J. Phys. Chem.* **1993**, *97*, 6069.
- [212] S. Kumar, S. K. Varshney, *Synthesis* **2001**, 305.
- [213] S. Kumar, M. Manickam, S. K. Varshney, D. S. S. Rao, S. K. Prasad, *J. Mater. Chem.* **2000**, *10*, 2483.
- [214] K. Krishnan, V. S. K. Balagurusamy, *Liq. Cryst.* **2000**, *27*, 991.
- [215] R. Freudenmann, B. Behnisch, F. Lange, M. Hanack, *Synth. Met.* **2000**, *111*, 441.
- [216] S. Kumar, S. K. Varshney, *Liq. Cryst.* **1999**, *26*, 1841.
- [217] N. Boden, R. J. Bushby, A. N. Cammidge, A. El-Mansoury, P. S. Martin, Z. B. Lu, *J. Mater. Chem.* **1999**, *9*, 1391.
- [218] S. Kumar, M. Manickam, *Liq. Cryst.* **1999**, *26*, 1097.
- [219] G. Cooke, V. Sage, T. Richomme, *Synth. Commun.* **1999**, *29*, 1767.
- [220] S. Kumar, M. Manickam, *Chem. Commun.* **1998**, 1427.
- [221] S. J. Cross, J. W. Goodby, A. W. Hall, M. Hird, S. M. Kelly, K. J. Toyne, C. Wu, *Liq. Cryst.* **1998**, *25*, 1.

- [222] D. Stewart, G. S. McHattie, C. T. Imrie, *J. Mater. Chem.* **1998**, *8*, 47.
- [223] S. Kumar, M. Manickam, *Chem. Commun.* **1997**, 1615.
- [224] N. Boden, R. J. Bushby, A. N. Cammidge, P. S. Martin, *J. Mater. Chem.* **1995**, *5*, 1857.
- [225] P. Henderson, H. Ringsdorf, P. Schuhmacher, *Liq. Cryst.* **1995**, *18*, 191.
- [226] N. Boden, R. J. Bushby, A. N. Cammidge, G. Headdock, *Synthesis* **1995**, 31.
- [227] J. W. Goodby, M. Hird, K. J. Toyne, T. Watson, *J. Chem. Soc.-Chem. Commun.* **1994**, 1701.
- [228] L. C. Porter, J. R. Polam, J. Mahmoud, *Organometallics* **1994**, *13*, 2092.
- [229] N. Boden, R. J. Bushby, A. N. Cammidge, *J. Chem. Soc.-Chem. Commun.* **1994**, 465.
- [230] N. Boden, R. C. Borner, R. J. Bushby, A. N. Cammidge, M. V. Jesudason, *Liq. Cryst.* **1993**, *15*, 851.
- [231] G. de la Torre, C. G. Claessens, T. Torres, *Eur. J. Org. Chem.* **2000**, 2821.
- [232] M. Teraguchi, T. Masuda, A. Fechtenkötter, K. Müllen, *Polymer Bulletin* **2000**, *44*, 255.
- [233] W. Kranig, C. Boeffel, H. W. Spiess, *Macromolecules* **1990**, *23*.
- [234] N. Boden, R. J. Bushby, A. N. Cammidge, *J. Am. Chem. Soc.* **1995**, *117*, 924.
- [235] G. C. Fu, S. T. Nguyen, R. H. Grubbs, *J. Am. Chem. Soc.* **1993**, *115*, 9856.
- [236] S. T. Nguyen, R. H. Grubbs, *J. Am. Chem. Soc.* **1993**, *115*, 9858.
- [237] S. Blechert, M. Schuster, *Angew. Chem. Int. Ed.* **1997**, *36*, 2036.
- [238] T. D. Clark, M. R. Ghadiri, *J. Am. Chem. Soc.* **1995**, *117*, 12364.
- [239] F. Wudl, *Acc. Chem. Res.* **1984**, *17*, 227.
- [240] D. M. Knawby, T. M. Swager, *Chem. Mat.* **1997**, *9*, 535.
- [241] D. M. Knawby, T. M. Swager, *Abstr. Pap. Am. Chem. Soc.* **1995**, *210*, 487.
- [242] R. D. McCullough, *Adv. Mater.* **1998**, *10*, 93.

- [243] H. Sirringhaus, P. J. Brown, R. H. Friend, M. M. Nielson, K. Bechgaard, B. M. W. Langeveld-Voss, A. J. H. Spiering, R. A. J. Janssen, E. W. Meijer, P. Herwig, D. M. de Leeuw, *Nature* **1999**, *401*, 685.
- [244] P. K. H. Ho, J.-S. Kim, J. H. Burroughes, H. Becker, S. F. Y. Li, T. M. Brown, F. Cacialli, R. H. Friend, *Nature* **2000**, *404*, 481.
- [245] D. Delabouglise, M. Hmyene, G. Horowitz, A. Yassar, F. Garnier, *Adv. Mater.* **1992**, *4*, 107.
- [246] M. R. Andersson, D. Selse, M. Berggren, H. Järvinen, T. Hjertberg, O. Inganäs, O. Wennerström, J.-E. Österholm, *Macromolecules* **1994**, *27*, 6503.
- [247] R. Sugimoto, S. Takeda, H. B. Gu, K. Yoshino, *Chem. Express* **1986**, *1*, 635.
- [248] P. Bäuerle, F. Würthner, G. Götz, F. Effenberger, *Synthesis* **1993**, 1099.
- [249] T. Kirschbaum, R. Azumi, E. Mena-Osteritz, P. Bauerle, *New J. Chem.* **1999**, *23*, 241.
- [250] K. Davidson, A. M. Ponsonby, *Synth. Met.* **1999**, *102*, 1512.
- [251] C. A. Briehn, T. Kirschbaum, P. Bauerle, *J. Org. Chem.* **2000**, *65*, 352.
- [252] Z. C. Bi, Y. Y. Qian, X. L. Zhao, S. Y. Shen, J. Y. Yu, H. J. Xu, H. T. Tien, *Photochem. Photobiol.* **1994**, *59*, 111.
- [253] E. Peeters, P. A. van Hal, J. Knol, C. J. Brabec, N. S. Sariciftci, J. C. Hummelen, R. A. J. Janssen, *J. Phys. Chem. B* **2000**, *104*, 10174.
- [254] E. Reuther, Johannes Gutenberg Universität (Mainz), **2001**.
- [255] T. Ishiyama, M. Murata, N. Miyaura, *J. Org. Chem.* **1995**, *60*, 7508.
- [256] N. Miyaura, A. Suzuki, *Chem. Rev.* **1995**, *95*, 2457.
- [257] M. A. Biasutti, J. Rommens, A. Vaes, S. De Feyter, F. D. De Schryver, P. Herwig, K. Müllen, *Bull. Soc. Chim. Belg.* **1997**, *106*, 659.
- [258] J. Hofkens, L. Latterini, G. De Belder, T. Gensch, M. Maus, T. Vosch, Y. Karni, G. Schweitzer, F. C. De Schryver, A. Herrmann, K. Müllen, *Chem. Phys. Lett.* **1999**, *304*, 1.
- [259] J. P. Wolfe, S. Wagaw, J. F. Marcoux, S. L. Buchwald, *Accounts Chem. Res* **1998**, *31*, 805.

- [260] E. Bellmann, S. E. Shaheen, S. Thayumanavan, S. Barlow, R. H. Grubbs, S. R. Marder, B. Kippelen, N. Peyghambarian, *Chem. Mater.* **1998**, *10*, 1668.
- [261] B. H. Yang, S. L. Buchwald, *J. Organomet. Chem.* **1999**, *576*, 125.
- [262] M. Wehmeier, Johannes Gutenberg Universität (Mainz), **1999**.
- [263] C. J. Pedersen, *J. Am. Chem. Soc.* **1957**, *79*, 2295.
- [264] J. Honzl, M. Metalova, *Tetrahedron* **1969**, *25*, 3641.
- [265] G. M. K. Hughes, B. C. Saunders, *J. Chem. Soc.* **156**, 38143820.
- [266] U. Scherf, *Top. Curr. Chem.* **1999**, *201*, 163.
- [267] G. Gu, P. E. Burrows, S. Venkatesh, S. R. Forrest, M. E. Thompson, *Opt. Lett.* **1997**, *22*, 172.
- [268] P. Fenter, F. Schreiber, V. Bulovic, S. R. Forrest, *Chem. Phys. Lett.* **1997**, *277*, 521.
- [269] X. C. Li, Y. Q. Liu, M. S. Liu, A. K. Y. Jen, *Chem. Mat.* **1999**, *11*, 1568.
- [270] S. Berleb, A. G. Muckl, W. Brutting, M. Schwoerer, *Synth. Met.* **2000**, *111*, 341.
- [271] V. Fattori, M. Cocchi, P. Di Marco, G. Giro, G. Barbarella, G. Sotgiu, *Synth. Met.* **2000**, *111*, 83.
- [272] L. Chkoda, C. Heske, M. Sokolowski, E. Umbach, *Appl. Phys. Lett.* **2000**, *77*, 1093.
- [273] C. H. Lee, G. W. Kang, J. W. Jeon, W. J. Song, S. Y. Kim, C. Seoul, *Synth. Met.* **2001**, *117*, 75.
- [274] Y. J. Shirota, T. Kobata, N. Noma, *Chem. Lett.* **1989**, 1145.
- [275] E. M. Han, L. M. Do, M. Fujihira, H. Inada, Y. J. Shirota, *Appl. Phys.* **1996**, *80*, 3297.
- [276] B. Olenyuk, A. Fechtenkötter, P. J. Stang, *J. Chem. Soc.-Dalton Trans.* **1998**, 1707.
- [277] B. Olenyuk, J. A. Whiteford, A. Fechtenkötter, P. J. Stang, *Nature* **1999**, *398*, 796.
- [278] M. Fujita, J. Yazaki, K. Ogura, *J. Am. Chem. Soc.* **1990**, *112*, 5645.
- [279] C. M. Drain, J.-M. Lehn, *J. Chem. Soc., Chem. Commun.* **1994**, 2313.
- [280] B. Dominguez, B. Iglesias, A. R. de Lera, *Tetrahedron* **1999**, *55*, 15071.
- [281] J. A. Porco, *Comb. Chem. High Throughput Screen* **2000**, *3*, 93.

- [282] K. Mochiji, S. Yamamoto, H. Shimizu, S. Ohtani, T. Seguchi, N. Kobayashi, *J. Appl. Phys.* **1997**, 82, 6037.
- [283] E. Mena-Osteritz, P. Bäuerle, *Adv. Mater.* **2001**, 13, 243.

List of Publications

“Self-organized Structures for High Efficiency Organic Photovoltaic from Soluble Molecular Materials”

Schmidt-Mende, L.; Fechtenkötter, A.; Müllen, K.; Moons, E.; Friend, R. H.; MacKenzie, J. D. *Science*, **2001**, *accepted*.

“Supramolecular Staircase via Self-assembly of Disc-like Molecules at the Solid-liquid Interface”

Samorí, P.; Fechtenkötter, A.; Böhme, T.; Jäckel, F.; Müllen, K.; Rabe, J. P. *J. Am. Chem. Soc.* **2001**, *submitted*.

“Langmuir Films of Graphitic Nanowires of Amphiphilic Hexabenzocoronene. New Phase Transitions and Switchable Electronic Properties”

Reitzel, N.; Hassenkam, T.; Balashev, K.; Jensen, T. R.; Howes, P. B.; Kjaer, K.; Fechtenkötter, A.; Tchegotareva, N.; Ito, S.; Müllen, K.; Bjørnholm T. *Chem.-Eur. J.*, **2001**, *submitted*.

“Star-like Substituted Hexaarylbenzenes: Synthesis and Mesomorphic Properties”

Geng, Y.; Fechtenkötter, A.; Müllen, K. *J. Mater. Chem.*, **2001**, *11*, 1634-1641.

“Big is Beautiful – “Aromaticity” Revisited from the Viewpoint of Macromolecular and Supramolecular Benzene Chemistry“

Watson, M. D.; Fechtenkötter, A.; Müllen, K. *Chem. Rev.*, **2001**, *101*, 1267-1300.

“Discotic Liquid Crystalline Hexabenzocoronenes Carrying Chiral and Racemic Branched Alkyl Chains: Supramolecular Engineering and Improved Synthetic Methods”

Fechtenkötter, A.; Tchegotareva, N.; Watson, M. D.; Müllen, K. *Tetrahedron*, **2001**, *57*, 3769-3783.

“Synthesis and Properties of Copolymers from a Diphenyl-acetylene Having Hexaphenylbenzene Moiety”

Teraguchi, M.; Fechtenkötter, A.; Müllen, K.; Masuda, T. *Polym. Bull.*, **2000**, *44*, 255-260.

“Record Charge Carrier Mobility in a Room-Temperature Discotic Liquid-Crystalline Derivative of Hexabenzocoronene”

Van de Craats, A.; Warman, J.; Fechtenkötter, A.; Brand, J.; Harbison, M.; Müllen, K. *Adv. Mater.*, **1999**, *11*, 1469-1472.

"Highly Ordered Columnar Structures from Hexa-*peri*-hexabenzocoronenes - Synthesis, X-ray Diffraction, and Solid-state Heteronuclear Multiple-Quantum NMR Investigations"

Fechtenkötter, A; Saalwächter, K; Harbison, M.; Müllen, K.; Spiess, H. W. *Angew. Chem. Int. Ed.*, **1999**, 38, No. 20, 3039-3042, *Angew. Chem.*, **1999**, 111, No. 20, 3224-3228.

"Self-assembly of nanoscale cuboctahedra by coordination chemistry"

Olenyuk, B.; Whiteford, J.; Fechtenkötter, A; Stang, P.J. *Nature*, **1999**, 398, 796-799.

"Molecular Architecture of cyclic nanostructures: use of co-ordination chemistry in the building of supermolecules with predefined geometric shapes"

Olenyuk, B.; Fechtenkötter, A; Stang, P.J. *J. Chem. Soc., Dalton Trans.*, **1998**, 11, 1707-1924.

"An Investigation of Carbon-Fluorine Bond Functionalization. Versatile Reactivity of Tungsten(II) Fluorine Carbonyl Metallacycles with Alkynes"

Kiplinger, J. L.; King, M. A.; Fechtenkötter, A.; Atta, A.; Richmond, T. G. *Organometallics*, **1996**, 15, 5292-5301.

Acknowledgements

I would like to thank the following persons who made this work possible and supported me when needed:

Professor Dr. K. Müllen for accepting me in his research group and for giving me the opportunity to work on this interesting and challenging topic.

Special thanks is given to the many national and international research partners. Without the close collaboration with these people many of the presented results and achievements would not have been possible. From the MPI-P: Ingrid Fischbach, Dr. Kai Saalwächter and Dr. Steven Brown for the solid-state NMR experiments, Piotr Minkin and Prof. Dr. Tadeusz Pakula for all the X-Ray measurements.

Dr. Anick M. van de Craats and Lukas Schmidt-Mende from the Cavendish Laboratory in Cambridge for a very fruitful cooperation in the field of optoelectronic devices.

Dr. Paolo Samorí and Thilo Böhme, both from the HU Berlin, for great and colorful STM results.

Further Chan Im (Marburg) Niels Reitzel (Denmark), Lior Eshdat (Israel) and Dr. Jonathan N. Coleman (Ireland)

Luc Brunsfeld and Prof. Dr. E. W. Meijer for their hospitality and helpfulness in the introduction to chirality.

The HBC and Dendrimer group Roland Bauer, Cornelia Beer, Dr. Alexander J. Berresheim, Dr. Didi Brand, Dr. Florian Dötz, Dr. Yanhou Geng, Vera-Maria Graubner, Christina Hampel, Martha Harbison, Dörthe Grebel-Köhler, Dr. Gunther Mattersteig, Christopher Simpson, Dr. Vesko Sinigersky, Stefan Spang, Natalia Tchebotareva, Projektleiter Dr. Manfred Wagner, Dr. Karl Wang, Bob Wu, Dr. Mark D. Watson, Dr. Mike Wehmeier, Tanja Weil, Uwe Wiesler, as well as the "Kochstudenten" Christian Behnes and Jörn Woll and all members of the Perylene group.

My office colleagues Emma Caputo and Erik Reuther for distracting me when it was too much to type along.

Anke Rösel and Stefan Spang and Dr. Manfred Wagner for their friendship especially after working hours.

The soccer guys for many challenging games and the team that made it possible to win the "MPI-P Summer Soccer Tournament" in 2000.

My friends Dr. Uli Rohr, Dr. Peter Schlichting, Simone Pinger, Erik Reuther and Dr. Chrys Correa for numerous mountain-bike trips that kept me in physical shape.

My parents and my brother for their support and Dr. Chrys Correa for her never ending encouragement.

Curriculum vitae

ANDREAS FECHTENKÖTTER

PERSONAL DETAILS

Date of birth: 17 October 1971

Place of birth: Georgsmarienhütte

Nationality: German

Marital Status: Single

UNIVERSITY EDUCATION

May 1998 –
June 2001

PhD studies, Max-Planck-Institut für Polymerforschung,
Prof. Dr. K. Müllen

Topic: Liquid Crystalline Hexabenzocoronenes as Organic
Molecular Materials – Synthesis, Characterization and
Application

Oct 1994
April 1998

Technische Universität Braunschweig
Degree: Diplom-Chemiker, "sehr-gut"

June 1997 –

Masters thesis (Diplomarbeit), University of Utah (USA),
Department of March 1998 Chemistry, Prof. Dr. P. J. Stang:
"Preparation and Characterization of Building Blocks for the Self-
assembly of Metallacyclic Polygons and Polyhedra"

Sept 1995 -
Sept 1996

DAAD exchange program with the University of Utah (USA),
Department of Chemistry

Oct 1992 –
Oct 1994

Phillips-Universität Marburg, Department of Chemistry, Vordiplom

ARMY SERVICE

July 1991 –
June 1992

3./Panzergranadierbatallion 323, Schwanewede

SCHOOL EDUCATION

1984 – 1991

Gymnasium Carolinum Osnabrück, Abitur

1982 – 1984

Thomas-Morus-Schule Osnabrück

1978 – 1982

St. Franziskus Schule Osnabrück